Cellular and molecular characterisation of MFSD8 mutations associated with the variant late-infantile NCL CLN7

M GUEVARA-FERRER

2023

Cellular and molecular characterisation of MFSD8 mutations associated with the variant late-infantile NCL CLN7

MARTA GUEVARA-FERRER

A thesis submitted in fulfilment of the requirements of Manchester Metropolitan University for the degree of Doctor of Philosophy

Department of Life Sciences

Manchester Metropolitan University

2023

Declaration

This thesis is the result of my own work and includes nothing which is the outcome of work done in collaboration except as specified in the text and declared here:

- Immunocytochemistry imaging analysis of the neural progenitor cells (NPCs) with the treatment of tamoxifen was performed in collaboration with Prof Diego Medina (TIGEM, Naples).
- Immunocytochemistry imaging analysis of the NPCs with the treatment of AZ67 was performed in collaboration with Prof Juan P Bolaños (University of Salamanca).
- AlphaFold images of the MFSD8 structure were obtained in collaboration with Prof Sam Hay (University of Manchester).
- Mass spectrometry was conducted by the MS-Bio facilities (University of Manchester) and proteomics analysis was performed by Dr Jon Humphries (Manchester Metropolitan University).

This thesis is not substantially the same as any work that has already been submitted before for any degree or other qualification.

Acknowledgements

I would like to express my sincere gratitude to my supervisor, Prof Tristan McKay, for granting me the opportunity to pursue this PhD and contribute to significant research on Batten disease. Your trust in my abilities has been invaluable. These four years at Manchester Metropolitan University have fostered my growth as a more independent and collaborative researcher.

I extend my heartfelt thanks to all members of the McKay group. Special appreciation goes to Aseel and Alysha for guiding me through the labs and iPSC culture during my initial days as a PhD student. To Chrysa and Amita, though our time working together in the lab was brief, I am grateful for your always-wise advice. Thanks to Rhys for sharing lab techniques and engaging conversations in tissue culture, and Stu for your consistent help with lab materials and reagents. Maria and Razan, your endless support, shared meals, and coffee breaks turned rainy days into sunny ones. Sana, your positivity and joy brightened the lab environment immeasurably (thank you also for all the thoughtful gifts!).

I am particularly indebted to Dr Jon Humphries for his assistance with mass spectrometry analysis and for connecting me with the MS facilities personnel. Your time and help are truly appreciated. My gratitude also extends to Prof Sam Hay for providing the AphaFold-generated structures on different MFSD8 variants.

I would like to acknowledge the DTA University Alliance and Marie Curie Actions for funding my PhD project and organising workshops and events that provided invaluable support throughout these years. Through this programme, I've had the privilege of meeting incredibly talented and inspiring PhD students, especially Elisa, Cristina, Spyros, and Pablo, whose unconditional support and shared adventures have added extra motivation to this work.

Finally, I am profoundly grateful to my family and friends for their love, care, and understanding during this journey, particularly during challenging times. Your support has been a constant source of strength and motivation. This overall experience has been a deeply enriching educational opportunity, and I am immensely thankful for every aspect of it.

Abstract

Batten disease (BD), also known as neuronal ceroid lipofuscinoses (NCLs), is a collective group of inherited neurodegenerative disorders. NCLs are the most prevalent cause of dementia in children, and they are distinguished by a common symptomatology that includes epileptic seizures, visual impairment, and a progressive decline in cognitive and physical function that results in early mortality. There are currently 12 different NCLs genetically identified in humans (*CLN1-CLN8*, *CLN10-CLN13*), with four newly identified genes (*CLN9*, *CLN14*, *CLCN6*, and *SGSH*). This study specifically focused on the variant late-infantile NCL (vLINCL) CLN7, which is caused primarily by homozygous mutations in *CLN7/MFSD8*, a major facilitator superfamily gene. *MFSD8* encodes a multispanning integral lysosomal membrane protein with 12 transmembrane domains and has recently been described as a potential chloride channel on endosomes and lysosomes. However, there is still no cure or treatment available for CLN7 disease.

Additionally, there is strong evidence demonstrating that *MFSD8* is involved in the pathogenesis and pathobiology of other adult dementias, such as amyotrophic lateral sclerosis (ALS) and frontotemporal dementia (FTD), as well as maculopathies and retinopathies, which share common disease-causing mutations in a heterozygosity manner.

Considering the emerging relevance of the use of induced pluripotent stem cells (iPSCs) as a model for the investigation of neurodegenerative diseases, in this thesis, I studied CLN7 disease employing CLN7 patient-derived iPSCs. Specifically, two iPS cell lines were utilised, which were derived from a female patient diagnosed at the age of 2.5 years, who exhibited homozygosity for the common missense mutation p.T294K and a male patient diagnosed at the age of 4.5 years, who was also homozygous for a more severe missense mutation corresponding to p.R465W. These iPS cell lines were further differentiated into Neural Progenitor Cells (NPCs), constituting a novel approach to study the variant late-infantile NCL CLN7 and providing an opportunity to examine the disease using cell types that could more closely resemble those affected *in vivo*.

In light of previous proteomic studies conducted in CLN7 patient-derived NPCs by our group, resulting in a downregulation of several nuclear proteins and, consistent with the observation of other studies, we identify the localisation of MFSD8 in the nucleus. These findings provide evidence of the potential existence of several co-existing MFSD8 variants within the cells, suggesting that MFSD8 might exert different functions depending on the different isoform expressed and its localisation. Additionally, this work also reveals an impairment in the autophagy-lysosomal pathway and mitochondria produced by disease-causing mutations in NPCs and the

improvement of these phenotypes with the use of existing compounds. Furthermore, through the study of the post-translational modifications of MFSD8 and different protein stability assays, this work also provides more evidence of the intricacy of this protein. Therefore, further studies on the potential protein binding partners of MFSD8 were conducted to gain a deeper understanding of novel signalling pathways or molecular mechanisms in which MFSD8 might be involved.

In summary, this thesis provides significant insights into the cellular and molecular biology of MFSD8 through the use of a clinically relevant model, which sheds new light on future directions for the study of CLN7 disease. These findings can contribute to the development of significant therapeutic strategies to ameliorate CLN7 disease and, as a consequence, improve other adult neurodegenerative diseases which share the same disease-causing mutations as CLN7 disease.

Contents

List of figures

List of tables

Abbreviations

ABCA4	ATP binding cassette subfamily A member 4 gene
ACHM	Achromatopsia
Ala, A	Alanine
ALS	Amyotrophic lateral sclerosis
AMPK	Adenosine monophosphate (AMP)-activated protein kinase
ANCL	Adult onset NCL
ANOVA	Analysis of variance
APS	Ammonium persulfate
Arg, R	Arginine
ASD	Autism spectrum disorder
Asp, D	Aspartic acid
ATG	Autophagy protein
ATP	Adenosine-5'-triphosphate
ATP13A2	ATPase cation transporting 13A2
AV	Autophagic vacuole
Baf A1	Bafilomycin A1
BCA	Bicinchoninic acid
BD	Batten disease
BLBP	Brain lipid binding protein
BMP	Bis(monoacylglycero)phosphate
BSA	Bovine serum albumin
Cas9	CRISPR-associated protein 9
CAT	Catalase
cDNA	Complementary DNA
CHX	Cycloheximide
CLCN6	Chloride voltage-gated channel 6
CLN1	Neuronal ceroid lipofuscinosis type 1
CLN2	Neuronal ceroid lipofuscinosis type 2
CLN3	Neuronal ceroid lipofuscinosis type 3
CLN4	Neuronal ceroid lipofuscinosis type 4
CLN5	Neuronal ceroid lipofuscinosis type 5
CLN6	Neuronal ceroid lipofuscinosis type 6
CLN7	Neuronal ceroid lipofuscinosis type 7
CLN8	Neuronal ceroid lipofuscinosis type 8
CLN9	Neuronal ceroid lipofuscinosis type 9
CLN10	Neuronal ceroid lipofuscinosis type 10

CLN11	Neuronal ceroid lipofuscinosis type 11
CLN12	Neuronal ceroid lipofuscinosis type 12
CLN13	Neuronal ceroid lipofuscinosis type 13
CLN14	Neuronal ceroid lipofuscinosis type 14
CNS	Central nervous system
CRISPR	Clustered regularly interspaced palindromic repeats
Cys, C	Cysteine
COD	Cone dystrophy
CRD	Cone-rod dystrophy
CTSD	Cathepsin D
CTSF	Cathepsin F
DAPI	4',6-Diamidino-2-phenylindole
DARPP-32	Dopamine- and cyclic AMP-regulated phosphoprotein
ddH_2O	Double-distilled water
dH_2O	Distilled water
DMEM	Dulbecco's Modified Eagle Medium
DMSO	Dimethyl sulfoxide
DNA	Deoxyribonucleic acid
DNAJC5	DnaJ heat shock protein family (Hsp40) member C5
DPBS	Dulbecco's phosphate buffered saline
ECAT	ESC-associated transcript
EDTA	Ethylenediaminetetraacetic acid
EOSRD	Early onset severe retinal dystrophy
ER	Endoplasmic reticulum
ERG	Electroretinography
ESCs	Embryonic stem cells
EST	Expressed-sequence tag
FABP	Fatty acid-binding protein
FALS	Familial amyotrophic lateral sclerosis
FBS	Fetal bovine serum
FGF	Fibroblast growth factor
FTD	Frontotemporal dementia
FTLD	Frontotemporal lobar degeneration
Gb3	Glycosphingolipid globotriaosylceramide
Gln, Q	Glutamine
Glu, E	Glutamic acid
Gly, G	Glycine
GM2AP	GM2 activator protein
GOF	Gain-of-function
GPx	Glutathione peroxidase
GRN	Progranulin

GSLs	Glycosphingolipids
HD	Huntington's disease
HEPES	N-2-hydroxyethylpiperazine-N-2-ethane sulfonic acid
hESCs	Human embryonic stem cells
HCl	Hydrochloric acid
hiPSCs	Human induced pluripotent stem cells
His, H	Histidine
HOPS	Homotypic fusion and protein sorting
HRP	Horseradish peroxidase
HTT	Huntingtin
Ile, I	Isoleucine
iMEFs	Inactivated mouse embryonic fibroblasts
INCL	Infantile onset NCL
iPSCs	Induced pluripotent stem cells
IRD	Inherited retinal degeneration
JNCL	Juvenile onset NCL
KCl	Potassium chloride
KCTD7	Potassium channel tetramerization domain containing 7
KSR	Knockout serum replacement
LAMP1	Lysosome associated membrane protein 1
LBPA	Lysobisphophatidic acid
LC3	Protein 1A/1B-light chain 3
Leu, L	Leucine
LINCL	Late-infantile onset NCL
LMN	Lower motor neurons
LOF	Loss-of-function
LRRK2	Leucine-rich repeat kinase 2
LSD	Lysosomal storage disorder
Lys, K	Lysine
MD	Macular dystrophy
MEM	Minimum Essential Medium
Met, M	Methionine
MFS	Major facilitator superfamily
MFSD8	Major facilitator superfamily domain containing 8
MFSD9	Major facilitator superfamily domain containing 9
$MgCl_2$	Magnesium chloride
MPR	Mannose 6-phosphate receptor
mDA	Midbrain dopaminergic
MS	Mass spectrometry
mtDNA	Mitochondrial DNA
mTORC1	mTOR complex 1

NaCl	Sodium chloride
NaOH	Sodium hydroxide
NBR1	Next to BRCA1 gene 1 protein
NCL	Neuronal ceroid lipofuscinosis
NDP52	Nuclear domain 10 protein 52
NE	Neuroectoderm
NEAA	Non-essential amino acids
NEM	Neural expansion medium
NIM	Neural induction medium
NPCs	Neural progenitor cells
NSCs	Neural stem cells
OCT	Optical coherence tomography
OCT-3/4	Octamer-binding transcription factor 3/4
PBS	Phosphate buffered saline
PD	Parkinson's disease
PFA	Paraformaldehyde
PIC	Protease Inhibitor Cocktail
PINK1	PTEN-induced kinase 1
PME	Progressive myoclonic epilepsy
PMP	Protein metallophosphatase
PMSF	Phenylmethylsulfonyl fluoride
PNGase F	Peptide N-glycanase F
PPT1	Palmitoyl-protein thioesterase 1
Pro, P	Proline
PtdIns3P/PI3P	Phosphatidylinositol 3-phosphate
PtdIns(3,5)P2/PI(3,5)P_2	Phosphatidylinositol 3,5-bisphosphate
PSC	Pluripotent stem cell
RIPA	Radioimmunoprecipitation assay
RNA	Ribonucleic acid
ROS	Reactive oxygen species
RP	Retinitis pigmentosa
RPE	Retinal pigment epithelium
SALS	Sporadic amyotrophic lateral sclerosis
SAPs	Sphingolipid activator proteins
SCMAS	Subunit c of mitochondrial ATP synthase
SCNT	Somatic cell nuclear transfer
SDS	Sodium dodecyl sulfate
SDS-PAGE	Sodium dodecyl-sulfate polyacrylamide gel electrophoresis
SERCA	Sarcoplasmic/endoplasmic reticulum Ca^{2+}-ATPase
SGSH	N-sulfoglucosamine sulfohydrolase
SLC18A2	Solute carrier family 18 member 2

SLC22A18	Solute carrier family 22 member 18
SNARE	Soluble N-ethylmaleimide-sensitive factor activating protein receptor
SOD	Superoxide dismutase
SOX2	SRY box-containing gene 2
SQSTM1/p62	Sequestosome 1
SSEA-3	Stage-specific embryonic antigen-3
SSEA-4	Stage-specific embryonic antigen-4
SUMO	Small ubiquitin-like modifier
TBS	Tris-buffered saline
TBST	Tris-buffered saline with Tween® 20
TDP-43	TAR DNA-binding protein 43
TEMED	N,N,N',N'-tetramethylethylene-diamine
TETRAN	Tetracycline transporter-like protein
TGN	Trans-Golgi network
Thr, T	Threonine
TPP1	Tripeptidyl peptidase 1
Trp, W	Tryptophan
TSC2	Tuberous sclerosis 2 protein
Tyr, Y	Tyrosine
UBL	Ubiquitin-like protein
UMN	Upper motor neurons
V-ATPase	Vacuolar ATPase
vLINCL	Variant late-infantile neuronal ceroid lipofuscinosis
VPS34	Vacuolar protein sorting 34
WIPI1	WD repeat domain phosphoinositide-interacting protein 1
WIPI2	WD repeat domain phosphoinositide-interacting protein 2
WT	Wild-type

Chapter 1

Introduction

1.1 Batten disease

Batten disease (BD), also known as neuronal ceroid lipofuscinoses (NCLs), is a collective group of inherited neurodegenerative disorders. NCLs are the most prevalent cause of dementia in children, and they are distinguished by a common symptomatology that includes epileptic seizures, visual impairment, and a progressive decline in cognitive and physical function that results in early mortality (Haltia, 2003). Although the age at disease onset can range from birth to adulthood, NCLs typically appear in childhood. In adulthood, NCLs are predominantly presented clinically as dementia (Haltia, 2003). The global incidence of NCL diagnoses is 1:100,000, while the incidence in the USA and Scandinavia is 1:12,500, classifying this condition as an ultra-rare disease (Brudvig and Weimer, 2022; Santavuori, 1988). At a molecular level, NCLs are characterised by the accumulation of a lipofuscin-like lipopigment – an autofluorescent pigment stored in lysosomes – in a variety of cell types, including neurons, which leads to ongoing selective neuronal death.

NCL was first described by Otto Christian Stengel as a juvenile onset of vision loss and dementia. It was not until 1903 when Batten disease was similarly described by Frederick Batten, from whom the infant form of the disorder received the current name, Batten disease, as a result of this neuropathology study (Batten and Mayou, 1915). Subsequently, other medical researchers, such as Spielmeyer and Vogt, described the same neurodegeneration with a juvenile onset. Janský and Bielschowsky reported a late-infantile onset form and Kufs defined an adult-onset disorder with related pathological features. Almost 50 years later, Haltia and Saltavuori characterised the classic infantile (or congenital) NCL (Haltia et al., 1973; Santavuori et al., 1973). The five distinct forms of NCLs are now classified as different variants according to the age of onset: congenital (prenatal and perinatal), infantile (INCL) (6-24 months), late infantile (LINCL) (1.5-4 years), juvenile (JNCL) (5-7 years) and adult (ANCL) (more than 16 years of age) (Goebel, 1995).

Up to now, disease-causing mutations have been identified in 12 genes resulting in NCL (Arsov et al., 2011; Bras et al., 2012; Jalanko and Braulke, 2009; Kousi et al., 2012; Nosková et al., 2011a; Smith et al., 2012, 2013; Staropoli et al., 2012). These genes are *CLN1/PPT1*, *CLN2/TPP1*, *CLN3*, *CLN4/DNAJC5*, *CLN5*, *CLN6*, *CLN7/MFSD8*, *CLN8*, *CLN10/CTSD*, *CLN11/GRN*, *CLN12/ATP13A2*, *CLN13/CTSF* (https://www.ucl.ac.uk/ncl-disease/) (**Table 1.1**). Additionally, there are other four phenotypes described as more recent candidate genes belonging to the NCL diseases. These genes are the following: *CLN9*, *CLN14/KCTD7*, *CLCN6* (Pressey et al., 2010), and *SGSH* (https://www.ucl.ac.uk/ncl-disease/) (**Table 1.1**). The majority of NCLs are recessively inherited, and the disease-causing mutations are biallelic. However, there are two exceptions, including the NCL caused by mutations in *CLN4/DNAJC5*, which is a rare dominant adult type (Nosková et al., 2011b), and the homozygous inherited deletion in *CLN8* caused by a maternal isodisomy of chromosome 8 (Vantaggiato et al., 2009).

NCLs are typically described as lysosomal storage disorders (LSDs), however, for the majority of them, the specific underlying mechanisms remain unknown. In NCLs, the lysosomes accumulate ceroid lipopigments and many of the NCL proteins reside there, which is similar to what happens in LSDs (Futerman and van Meer, 2004; Kyttälä et al., 2006). In typical LSDs, an enzyme or transporter deficiency/dysfunction results in the accumulation of substrates or metabolites in lysosomes. Nonetheless, the central storage material in the subunit c of mitochondrial ATP synthase (SCMAS) or sphingolipid activator proteins (SAPs) A and D in NCLs is not mechanistically linked to disease (Elleder et al., 1997; Tyynelä et al., 1993). The SCMAS is a 75 aa short peptide that is highly hydrophobic and localises as a transmembrane α-helical hairpin in the mitochondrial inner membrane. Depending on the species, this hairpin assembles into oligomers of 8-16 units. The c-ring, which is the main structural element of the rotor, is formed by the SCMAS oligomers, which are a crucial component of the F_0 complex of the ATP synthase (Walker, 2013). The SCMAS can be found in cytosolic compartments and the plasma membrane when it accumulates uncontrollably in ceroid-lipofuscinoses (LSDs or NCLs) (Palmer, 2015; Palmer et al., 1992). Small, enzymatically inactive glycoproteins known as SAPs (or saposins) are widely distributed in lysosomes and function as co-factors to promote interactions between membrane-bound hydrophobic sphingolipids and water-soluble lysosomal hydrolases. There are five known SAPs, which are called SAP A, B, C, and D (or saposins A-D) and the fifth protein is called GM2 activator protein (GM2AP), which participates in the degradation of gangliosides GM1 and GM2. Prosaposin (pSAP) is a precursor protein that generates the highly homologous SAPs A-D, promotes neurite outgrowth, inhibits programmed cell death of neuronal cells *in vitro*, and protects neurons *in vivo* (Fürst, Machleidt and Sandhoff, 1988; Nakano *et al.*, 1989; Hiraiwa *et al.*, 1993, 1997;

Sano *et al.*, 1994). Although the precise role of the various SAPs *in vivo* is still unclear, it is known that they stimulate the lysosomal degradation of various sphingolipids (Schnabel et al., 1992).

Almost all the NCL genes encode proteins that are found in the endo/lysosomal pathways. Most of them include lysosomal enzymes and a soluble lysosomal protein (CLN1/PPT1, CLN2/TPP1, CLN5, CLN10/CTSD, CLN13/CTSF), as well as lysosomal transmembrane proteins (CLN3, CLN7/MFSD8, CLN12/ATP13A2) (**Table 1.1**). Other transmembrane proteins include CLN6 and CLN8, which are found in the endoplasmic reticulum (ER), and CLN11/GRN (progranulin), which reside in the secretory pathway (Ryan et al., 2009). The proteins that *CLN4/DNAJC5* and *CLN14/KCTD7* encode are both cytoplasmic and associated with cellular membranes (**Table 1.1**). However, the primary roles of the majority of the membrane proteins, as well as the specific substrates for the soluble lysosomal enzymes, are yet unknown.

For the majority of NCL genes, there is a common disease phenotype that causes a complete absence of function. Nevertheless, for some NCLs, certain phenotypes that result from mutations with a lower impact on gene function manifest at a later age of onset. Additionally, there are instances of different mutations in the same gene that lead to entirely diverse diseases. Studies on patients with mutations in multiple NCL genes have also been conducted. For instance, one patient was found to be heterozygous for mutations in *CLN5* and also to carry a single mutation in *CLN6* (Mole and Cotman, 2015). These examples show the NCL genes' high degree of heterogeneity and variability, which can cause one gene to exacerbate or ameliorate the phenotype of the disease.

Table 1. 1. NCL gene/protein names, functions, and NCL clinical phenotypes.

Gene	Protein	NCL type (Clinical phenotype)	Main storage material
CLN1/PPT1	PPT1, palmitoyl protein thioesterase, lysosomal enzyme	Infantile, late infantile, juvenile, and adult	Saposins A and D
CLN2/TPP1	TPP1, tripeptidyl peptidase 1, lysosomal Enzyme	Late infantile	Subunit c of ATP synthase
CLN3	CLN3, lysosomal transmembrane protein	Juvenile	Subunit c of ATP synthase
CLN4/DNAJC5	DNAJC5, DnaJ Heat Shock Protein Family (Hsp40) Member C5	Adult	Subunit c of ATP synthase
CLN5	CLN5, soluble lysosomal protein	Late infantile	Subunit c of ATP synthase
CLN6	CLN6, transmembrane protein of ER	Late infantile and adult	Subunit c of ATP synthase
CLN7/MFSD8	MFSD8, lysosomal transmembrane protein of MFS facilitator family	Late infantile	Subunit c of ATP synthase
CLN8	CLN8, transmembrane protein of ER	Late infantile	Subunit c of ATP synthase
CLN9	Not known. *CLN9 is used for an NCL disease subtype with onset in the juvenile range.*	Juvenile (Schulz et al., 2004)	Subunit c of ATP synthase
CLN10/CTSD	CTSD, cathepsin D, lysosomal protein with multiple functions	Congenital, late infantile, and juvenile	Saposins A and D
CLN11/GRN	GRN, progranulin	Adult	
CLN12/ATP13A2	ATP13A2, ATPase cation transporting 13A2	Juvenile	
CLN13/CTSF	CTSF. cathepsin F	Adult	
CLN14/KCTD7	KCTD7, potassium channel tetramerization domain containing 7	Infantile	
CLCN6	CLCN6, chloride voltage-gated channel 6	Late-onset (Poët et al., 2006)	
SGSH	SGSH, N-sulfoglucosamine sulfohydrolase	Late-infantile and adult	

1.1.1 NCLs classification

Research has provided evidence indicating that NCL diseases exhibit a greater degree of genetic heterogeneity than initially believed. This is due to the fact that mutations occurring in the same gene can result in varying patterns of disease progression (Kousi et al., 2012; Lebrun et al., 2011). Initially, NCL diseases were classified according to the age of onset (congenital, infantile, late infantile, juvenile, and adult). Alternatively, these diseases were also categorised based on the researchers who made significant contributions in their study, such as Hatia-Santavuori, Jansky-Bielschowsky, Batten, Spielmeyer-Vogt, or Kufs. In certain instances, NCLs were additionally classified as "Finnish" or "Turkish" variants when they were discovered among those particular populations. However, it is important to note that mutations in the genes associated with NCLs can manifest and be observed globally, and are not exclusive to those described populations (Lebrun et al., 2009). Consequently, a novel comprehensive nomenclature for NCL has been developed. The updated terminology recognizes each NCL from a combined genetic and clinical perspective; it provides information on the specific gene mutated as well the age at disease onset (Williams and Mole, 2012).

1.1.1.1 Congenital NCL

Individuals affected with any form of NCL present an initial period of healthy development, with the exception of congenital NCL, which significantly impacts patients from birth and ultimately results in premature mortality in early childhood. The observed symptoms encompass epileptic seizures occurring either during foetal development or immediately after birth, in addition to microcephaly. It is important to note that the only congenital form of NCL is known as CLN10 disease. This disease is associated with the deficit of the lysosomal enzyme known as cathepsin D, and it is caused by a mutation in *CLN10* (Siintola et al., 2006).

1.1.1.2 Infantile NCLs

The aetiology of infantile-onset NCL can be attributed to genetic disruptions involving *CLN1*, *CLN14*, or *CLCN6*.

Symptoms of the infantile CLN1 disease often manifest in affected patients between the ages of 6 to 24 months. In the initial stages, there is a noticeable decrease in tone and social interaction, accompanied by a subsequent and rapid deterioration of psychomotor abilities. This is further characterised by the presence of myoclonus (abrupt, transient, and involuntary contraction or trembling of a muscle or group of muscles), seizures, and visual loss. The disorder is caused by mutations in *CLN1*, resulting in a deficit of the lysosomal enzyme known as palmitoyl protein thioesterase 1 (PPT1) (Autti et al., 2011; Santavuori et al., 1993).

Infantile CLN14 disease is characterised by clinical manifestations such as myoclonus, developmental degeneration, and visual impairment. The aetiology of this condition can be attributed to a genetic mutation in *CLN14/KCTD7*, which encodes for a potassium channel (Staropoli et al., 2012).

Individuals diagnosed with CLCN6 exhibit a gradual deterioration of the cerebral cortex, significant delays in development, reduced muscle tone, sensory peripheral neuropathy, loss of vision due to cortical impairment, and respiratory insufficiency often occurring between 18 and 23 months of age (Polovitskaya et al., 2020).

1.1.1.3 Late-infantile NCLs

Mutations in *CLN2* are responsible for the majority of cases of late-infantile NCL. However, there are other genes, including *CLN1*, *CLN5*, *CLN6*, *CLN7*, *CLN8*, *CLN10*, and *SGSH*, which can also result in the late-infantile onset of this condition.

Individuals diagnosed with the classic late infantile NCL (CLN2) present a gradual deterioration in their developmental and psychomotor abilities, typically observed between the ages of 2 and 3 years. Additionally, the onset of epilepsy is commonly observed within the age range of 2 to 4 years. These symptoms are thereafter accompanied by vision failure, primarily observed in the macula region (Chang et al., 2011). The aetiology of this condition can be attributed to genetic mutations occurring in *CLN2*, leading to a deficient lysosomal enzyme tripeptidyl peptidase 1 (TPP1) (Chang et al., 2011).

The CLN5 disease with late-infantile onset often manifests between the ages of 4 and 17 years. It has been previously referred to as the "Finish variant", but it has been observed to occur worldwide (Lebrun et al., 2009). This disease is clinically characterised by a loss of psychomotor abilities, ataxia, epileptic spasms, and visual impairment (Åberg et al., 2011b).

The onset of CLN6 disease typically occurs between 18 months and 8 years of age, and it is clinically associated with motor regression, dysarthria, ataxia, visual impairment, and seizures (Alroy et al., 2011).

The age of onset for CLN7 disease spans from 2 to 7 years, and it has been previously designated as the "Turkish variant". However, it is important to note that this condition can manifest globally. This disorder is characterised by the occurrence of seizures, followed by a progressive impairment in motor function, myoclonus, cognitive decline, and visual loss (Elleder et al., 2011).

There are two different manifestations of the CLN8 disease: the late-infantile form and the variant commonly referred to as "Northern Epilepsy". The late-infantile variant of CLN8 exhibits

symptoms such as visual impairment, myoclonic seizures, progressive deterioration of motor and cognitive functions, and premature mortality, typically occurring between the ages of 5 and 10. The "Northern Epilepsy" form is characterised by the presence of progressive myoclonus epilepsy; however, it does not exhibit any correlation with visual impairment.

The late-infantile variant of CLN10 has been observed in one patient from Germany, who presented visual impairment and ataxia, followed by continuous psychomotor decline. The presence of two heterozygous missense mutations in *CLN10* resulted in residual CTSD activity at the genetic level (Steinfeld et al., 2006).

The occurrence of mucopolysaccharidosis type IIIA (MPSIIIA), a disease with symptoms typically appearing in late infancy, is mostly attributed to mutations in *SSGH* (Sleat et al., 2009).

1.1.1.4 Juvenile NCLs

The classic juvenile NCL is caused by mutations in *CLN3*, and is the most prevalent NCL. However, it is worth noting that mutations in *CLN1* and *CLN12* can also lead to the juvenile NCL phenotype.

The manifestation of CLN3 disease often occurs in children aged 4 to 7 years, characterised by the development of blindness resulting from retinal regression. This is then accompanied by a gradual deterioration in cognitive function and the emergence of behavioural problems. Patients with CLN3 experience seizures as the disease progresses, typically controlled with the administration of medication. The CLN3 disease has been associated with the presence of parkinsonian traits, a movement disorder. In certain cases, the administration of L-DOPA has shown potential as a treatment for this condition. Individuals with CLN3 disease experience the onset of a characteristic acute dysarthria, typically around the age of 10. Affected individuals living into their twenties, can also develop a cardiac impairment, leading to death within the third decade of life (Åberg et al., 2011a).

The juvenile-onset NCL, which is caused by mutations in *CLN1*, typically manifests between the ages of 5 and 10. This condition is characterised by a high incidence of cognitive decline, seizures, and motor regression. Blindness often occurs during the latter stages of development, generally between the ages of 10 and 14 years.

CLN12 disease is characterised by juvenile-onset and is presented with progressive development of spinocerebellar ataxia, bulbar syndrome (including dysarthria, dysphagia, and dysphonia), myoclonus, rigidity, impairment of speech, and intellectual deterioration, among other symptoms (Mukherjee et al., 2019).

1.1.1.5 Adult NCLs

The aetiology of the classic adult NCL, also referred to as Kufs disease, can be attributed to genetic mutations in *CLN4*. However, alternative NCL genes have also been implicated in the manifestation of this particular form of adult onset NCL. These genes include *CLN1*, *CLN6*, *CLN11*, *CLN13*, and *SGSH*.

CLN4 disease is associated with mutations occurring in the *DNAJC5* gene. Notably, it is the only autosomal dominant form of NCL. Patients present various symptoms, such as ataxia, progressive dementia, seizures, and myoclonus, after 30 years (Nosková et al., 2011a).

The adult onset CLN1 disease is manifested after reaching 18 years of age. This is characterised by the start of cognitive impairment and depression, which is then followed by ataxia, parkinsonism, and vision loss (Ramadan et al., 2007).

The adult-onset CLN6 disease is associated with the Kufs A type variant. This NCL form often begins to emerge around the age of 30, presenting with increasing myoclonic epilepsy. This is then followed by the development of dementia, ataxia, and significant dysarthria (Alroy et al., 2011; Berkovic et al., 1988).

The CLN13 disease, sometimes referred to as the Kufs type B variant, exhibits symptoms similar to dementia shown in type A. Kufs type B differs from type A based on the absence of epilepsy and dysarthria (Arsov et al., 2011; Berkovic et al., 1988). This adult-onset NCL is caused by a deficiency of the lysosomal enzyme known as cathepsin F.

CLN11 disease results from mutations in *GRN*, and is characterised by recurrent seizures (epilepsy), vision loss, cerebellar ataxia, and intellectual deterioration. Individuals affected with this condition present symptoms in adolescence or early adulthood (https://medlineplus.gov/genetics/condition/cln11-disease/).

A mutation in *SGSH* was identified in a single patient diagnosed with adult-onset NCL (Gardner and Mole, 2021).

1.1.2 Variant late-infantile NCL CLN7

In this project, research will be focused on the variant late-infantile-onset NCL (vLINCL) CLN7. According to clinical data, the vLINCL CLN7 often manifests between the ages of 2 to 7 years and is characterised by epileptic seizures, progressive cognitive and motor decline, vision loss, and early mortality (Haltia, 2003). According to magnetic resonance imaging (MRI), patients with the vLINCL CLN7 at different stages of the disease progression, typically exhibit cerebral and

cerebellar atrophy at variable degrees, along with alterations in the cerebral white matter on the periventricular regions. Additionally, electroretinogram analyses are frequently found to be abnormal in these patients (Kousi et al., 2009a).

Although this condition can occur anywhere in the globe, *CLN7*, also known as Major Facilitator Superfamily (MFS) Domain 8 (*MFSD8*), was first identified in Turkish patients, hence the name of the "Turkish variant". However, a fraction of Turkish patients with vLINCL was shown to also have four different mutations in *CLN8* and two different mutations in *CLN6*, indicating genetic heterogeneity in the "Turkish variant" NCL (Ranta et al., 2004; Siintola et al., 2005). A few years later, a novel gene for the Turkish vLINCL CLN7 was identified and characterised. This gene is the *MFSD8*, which was described after homozygosity mapping of 10 families (Siintola et al., 2007). After this finding, *MFSD8* was identified as the gene responsible for the vLINCL CLN7 phenotype.

1.1.2.1 MFSD8 gene and protein

MFSD8 is located on chromosome 4q28.2 and has 13 exons and 12 introns (https://databases.lovd.nl/shared/refseq/MFSD8_NM_152778.2_table.html), with a transcript length of 4,516 bps. It is predicted to encode a 518-aa protein of 57.63 kDa with 12 transmembrane-spanning domains (**Figure 1.1**). *MFSD8* is evolutionarily conserved in different species, having a single orthologue in each vertebrate species. Mouse and zebrafish orthologues are ~82% and ~61% exact to the human *MFSD8*, respectively (Siintola et al., 2007).

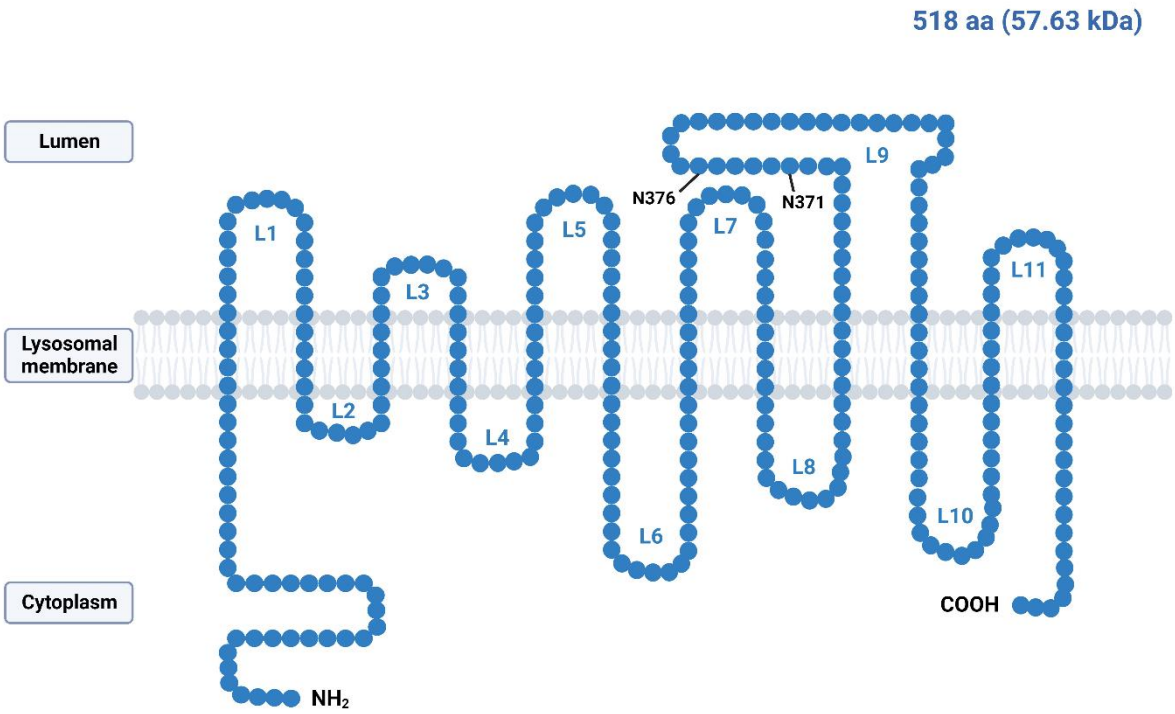

Figure 1. 1. Schematic representation of MFSD8. MFSD8 is described as a lysosomal transmembrane protein of 518 aa (~57.63 kDa) with 12 transmembrane domains and 11 loops (L1-L11) on the luminal and cytoplasmic surfaces. The N-terminus and the C-terminus face the cytoplasm within the cell. MFSD8 presents two predicted N-glycosylation sites at the 371 and 376 aa position which reside in the luminal loop L9 connecting the transmembrane domains 9 and 10. Figure based on Khan et al. (2017) and Sharifi et al. (2010).

A number of lysosomal proteins, including lysosome-associated membrane protein 1 (LAMP1), cathepsin D (CTSD), and lysobisphophatidic acid (LBPA), have been shown to specifically co-localise with MFSD8 in previous studies (Sharifi et al., 2010; Siintola et al., 2007; Steenhuis et al., 2012, 2010). LAMP1 is a lysosomal membrane glycoprotein that plays a crucial role in lysosomal biogenesis and autophagy (Cheng et al., 2018). The lysosomal-dependent protein homeostasis in the brain, particularly in neurons, is maintained by CTSD, a crucial protease involved in the degradation of a variety of substrates in the lysosomes (Hossain et al., 2021). In vertebrates, late endosomes and lysosomes contain LBPA, also known as bis(monoacylglycero)phosphate (BMP), a phospholipid that is essential for the breakdown of sphingolipids and regulation of endosomal cholesterol (Antonny et al., 2018; Gallala and Sandhoff, 2011; Goldstein and Brown, 1977; Schulze and Sandhoff, 2014). This lysosomal co-localisation of MFSD8 with lysosomal proteins indicates that MFSD8 might be an integral lysosomal membrane protein, as it is most frequently described in the literature (Sharifi et al., 2010; Siintola et al., 2007; Steenhuis et al., 2012, 2010). Similarly, the majority of the other identified NCL proteins present lysosomal localisation – CLN1/PPT1,

CLN2/TPP1 and CLN10/CTSD are soluble lysosomal enzymes (Hellsten et al., 1996; Press et al., 1960; Sleat et al., 1997; Verkruyse and Hofmann, 1996; Vesa et al., 1995), whereas *CLN3* and *CLN5* encode for lysosomal proteins, which function remains unknown (Järvelä et al., 1998; Savukoski et al., 1998; Isosomppi et al., 2002). Conversely, CLN6 localises exclusively to the ER, while CLN8 localises to both the ER and the ER-Golgi compartment (Heine et al., 2004; Lonka et al., 2000; Mole et al., 2004).

MFSD8 is conserved in vertebrates and ubiquitously expressed in the organism (Siintola et al., 2007). MFSD8 is a member of the MFS protein family, which is one of the largest families of membrane solute transporters that reside ubiquitously in all types of organisms (Pao et al., 1998). These transporters are single-polypeptide carriers that only enable the transport of small solutes as a response to chemiosmotic ion gradients. Specifically, the solutes transported by the MFS permeases include monosaccharides, oligosaccharides, inositols, drugs, amino acids, nucleosides, organophosphate esters, Krebs cycle metabolites, and various organic and inorganic anions and cations (Pao et al., 1998). The MFS permeases are composed of 17 different phylogenetic subfamilies correlating with their function, each of which transports a specific type of substrate. All the MFS permeases have either 12 or 14 spanning transmembrane domains, similar to MFSD8 (Pao et al., 1998). In humans, the most alike proteins to MFSD8 are the MFS domain containing 9 (MFSD9 or MGC11332), tetracycline transporter-like protein (TETRAN), solute carrier family 18 member 2 (SLC18A2 or VMAT2), and solute carrier family 22 member 18 (SLC22A18 or ORCTL2). The MFSD9 and TETRAN proteins are predicted to present tetracycline-transporter activities. SLC18A2 translocates monoamines from the cytosol to synaptic vesicles, while the SLC22A18 is involved in the transport of organic cations (Liu and Edwards, 1997; Reece et al., 1998).

Invertebrates have also been found to contain MFSD8-like proteins. For instance, the proteins that are most comparable to MFSD8 in *Saccharomyces cerevisiae* are Jen1p, Git1p, Ykr105co, and Ycr023cp, all of which are members of the MFS (Casal et al., 1999; Fisher et al., 2005; Patton-Vogt and Henry, 1998; SOARES-SILVA et al., 2003). In *Drosophila melanogaster*, *DmeI/Cln7* is the orthologue of *MFSD8* (FlyBase) (https://flybase.org/reports/FBhh0000687.html). The proteins CG8596-PA and CG5760-PA, which are both members of the MFS, are also similar to MFSD8 in *D. melanogaster*. In *Caenorhabditis elegans*, there are various proteins like MFSD8, most of which are part of the MFS and also present protein domains involved in transport (Siintola et al., 2007).

1.1.2.2 *MFSD8* mutations

Disease-causing mutations in *MFSD8* are predominantly observed in homozygous forms, with two exceptions of heterozygosity, as described thereafter. The identified mutations are distributed across several regions of *MFSD8*, meaning that there is not a region more affected that could lead to a specific type of protein disruption.

The homozygous missense mutation c.881C>A is the most commonly observed mutation in individuals with CLN7 disease. This particular mutation has been predominantly detected in patients of Roma descent from the Czech Republic (https://www.ucl.ac.uk/ncl-disease). This single nucleotide change results in a substitution of threonine (Thr, T) with lysine (Lys, L) at position 294 (p.Thr294Lys; T294K) situated in the predicted seventh luminal loop of MFSD8 (Kousi et al., 2009a). The missense mutation c.1361T>C (p.Met454Thr; M454T) has been observed as the second most common mutation. It has been found in homozygous form in patients from India, Iran, and Turkey (Khan et al., 2017; Zare-Abdollahi et al., 2019). Additionally, this mutation has been identified in patients of Indian descent in a heterozygous form, along with another missense mutation c.1219T>C (p.Trp407Arg; W407R) (Patiño et al., 2014). The residues at positions 407 and 454, specifically tryptophan (Trp, W) and methionine (Met, M), exhibit strict conservation among vertebrates. This observation is supported by several protein alignment studies, indicating that mutations in these residues may potentially lead to a decrease in the stability of MFSD8 protein structure (Patiño et al., 2014). The W407R mutation is situated within a sequence of amino acids that is highly conserved, specifically between the ninth and tenth transmembrane domains. On the other hand, the p.M454T mutation is found in the eleventh transmembrane domain of MFSD8. The homozygous splice-site mutation c.754+2T>A, which specifically affects the donor-splice site of intron 8 and leads to an altered splicing pattern, is identified as the third most commonly occurring mutation (Siintola et al., 2007). The presence of this mutation has also been observed in a patient diagnosed with CLN7, who exhibited compound heterozygosity together with the c.1102-2delA mutation. This mutation involves the deletion of an adenine at the second-to-last nucleotide of intron 11, resulting in a splicing defect (Kousi et al., 2009). Other homozygous mutations have been identified in CLN7 patients, including the p.Arg233Gly, p.Tyr298*, p.Gly310Asp, p.Asp368His, p.Gly429Asp, p.Arg35*, c.1103-2del, p.Arg139His, p.Ala157Pro, c.863+1G>C, p.Met209Ilefs*3, c.863+3_863+4insT, p.Gly52Arg, p.Glu381*, p.Arg482*, p.Met1Thr, p.Pro447Leu, p.Tyr121Cys, p.Pro412Leu, c.63-4delC, and c.554-1G>C variants. These mutations can be classified as missense, nonsense, or splice-site mutations (**Figure 1.2**, **Table 1.2**).

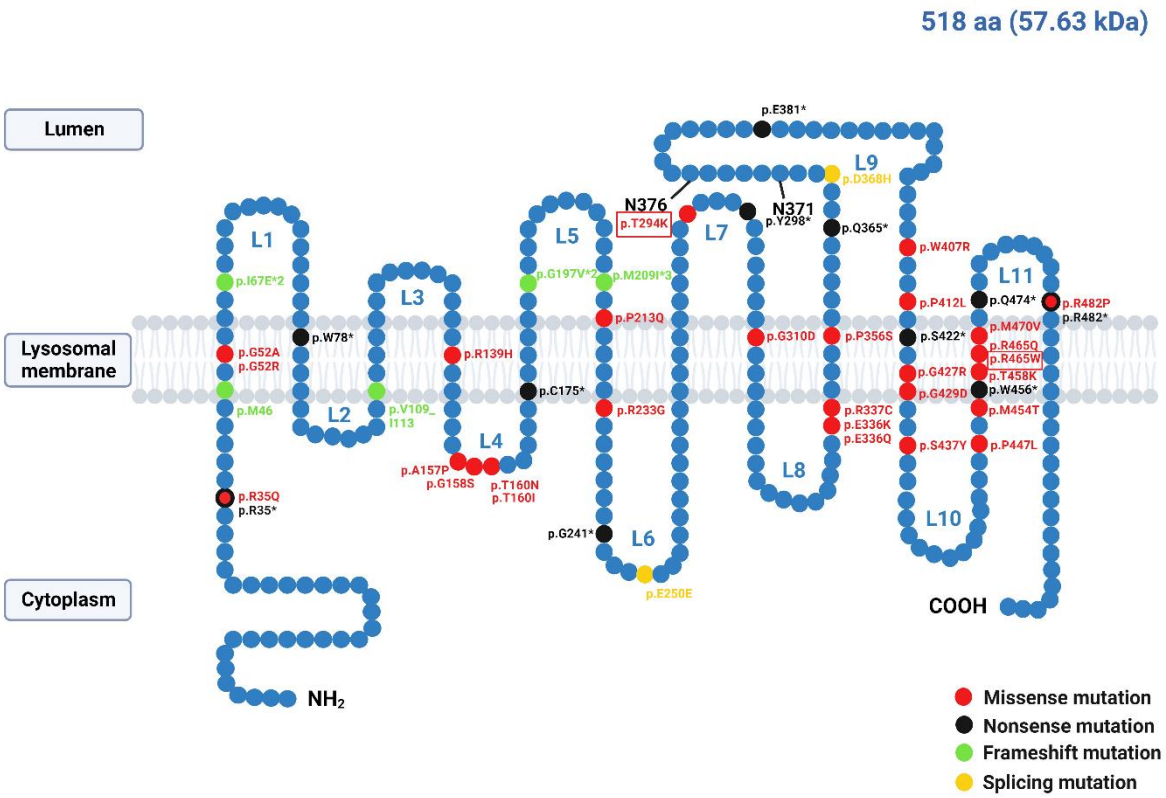

Figure 1. 2. Schematic representation of the CLN7 disease-causing mutations. The MFSD8 protein is described as a lysosomal transmembrane protein of 518 aa (57.63 kDa) with 12 transmembrane domains and 11 loops (L1-L11) on the luminal and cytoplasmic surfaces. The N-terminus and the C-terminus face the cytoplasm within the cell. The MFSD8 protein presents two predicted N-glycosylation sites at the 371 and 376 aa position which reside in the luminal loop L9 connecting the transmembrane domains 9 and 10. The coloured dots represent mutations in *MFSD8* that cause the vLINCL CLN7 with their approximate location within the MFSD8 protein. Each colour describes a different type of mutation: red refers to missense mutations, black represents nonsense mutations, green refers to frameshift mutations, and yellow corresponds to splicing mutations (only splicing mutations affecting exons are represented). Figure based on Khan et al. (2017) and Sharifi et al. (2010).

Table 1. 2. Mutations in CLN7/MFSD8. Adapted from the NCL Mutations Database (UCL) (https://www.ucl.ac.uk/ncl-disease).

Mutation (amino acid change)	Nucleotide change	Location in the MFSD8 gene	Type of mutation	Location in the MFSD8 protein	Reference
p.Arg233Gly	c.697A>G	Exon 7	Substitution (missense; generation of an exonic ESS site)	L6	Siintola et al., 2007
-	c.754+2T>A	Intron 8	Substitution (alteration of the WT donor site)	-	Kousi et al., Brain, 2009
p.Tyr298*	c.894T>G	Exon 10	Substitution (nonsense)	L7	Siintola et al., 2007
p.Gly310Asp	c.929G>A	Exon 10	Substitution (missense)	TM8	Siintola et al., 2007
p.Asp368His	c.1102G>C	Exon 11	Substitution (alteration of the WT donor site; alteration of an exonic ESE site)	L9	Siintola et al., 2007
p.Gly429Asp	c.1286G>A	Exon 12	Substitution (missense)	TM10	Siintola et al., 2007
p.Arg35*	c.103C>T	Exon 3	Substitution (nonsense)	N-terminal	Aiello et al., 2009
p.Thr294Lys	c.881C>A	Exon 10	Substitution (missense)	L7	Aiello et al., 2009
p.Arg465Trp	c.1393C>T	Exon 13	Substitution (missense)	TM11	Kousi et al., Brain, 2009
p.Gly52Arg	c.154G>A	Exon 3	Substitution (missense)	TM1	Aiello et al., 2009
-	c.863+3_863+4insT	Intron 9	Insertion (alteration of the WT donor site)	-	Aiello et al., 2009
p.Glu381*	c.1141G>T	Exon 12	Substitution (nonsense)	L9	Aiello et al., 2009
p.Arg482*	c.1444C>T	Exon 13	Substitution (nonsense)	L11	Aiello et al., 2009
-	c.2T>C	Exon 2	Substitution (missense)	-	Aiello et al., 2009
-	c.863+1G>C	Intron 9	Substitution (alteration of the WT donor site)	-	Aiello et al., 2009
p.Met209Ilefs*3	c.627_643del	Exon 7	Deletion (frameshift)	L5	Aiello et al., 2009
p.Arg139His	c.416G>A	Exon 5	Substitution (missense)	TM4	Kousi et al., Brain, 2009
p.Ala157Pro	c.468_469delinsCC	Exon 6	Deletion insertion (missense)	L4	Kousi et al., Brain, 2009
-	c.1103-2del	Intron 11	Deletion (alteration of the WT acceptor site)	-	Kousi et al., Brain, 2009
p.Gln87*	c.259C>T	Exon 5	Substitution (nonsense)	TM2	Kousi et al., 2012
p.Tyr121Cys	c.362A>G	Exon 5	Substitution (missense)	TM3	Stogmann et al., 2009
p.Pro447Leu	c.1340C>T	Exon 12	Substitution (missense)	L10	Aiello et al., 2009
-	c.63-4del	Intron 2	Deletion (no significant splicing motif alteration detected)	-	Kousi et al., 2009
p.Pro412Leu	c.1235C>T	Exon 12	Substitution (missense)	L9	Aldahmesh et al., 2009

Mutation (amino acid change)	Nucleotide change	Location in *MFSD8* gene	Type of mutation	Location in MFSD8 protein	Reference
p.Thr160Asn	c.479C>A	Exon 6	Substitution (missense)	L4	Kousi et al., 2012
p.Thr160Ile	c.479C>T	Exon 6	Substitution (missense)	L4	Kousi et al., 2012
-	c.554-1G>C	Exon 6	Substitution (alteration of the WT donor site)	-	Kousi et al., 2012
-	c.754+1G>A	Intron 8	Substitution (alteration of the WT donor site)	-	Kousi et al., 2012
p.Thr458Lys	c.1373C>A	Exon 13	Substitution (missense)	TM11	Kousi et al., 2012
p.Met470Val	c.1408A>G	Exon 13	Substitution (missense)	TM11	Kousi et al., 2012
p.Arg465Gln	c.1394G>A	Exon 13	Substitution (missense)	TM11	Kousi et al., 2012
p.Gln474*	c.1420C>T	Exon 13	Substitution (nonsense)	L11	Kousi et al., 2012
p.Glu336Gln	c.1006G>C	Exon 11	Substitution (missense)	L8	Roosing et al., 2014
p.Gly158Ser	c.472G>A	Exon 6	Substitution (missense)	L4	Mandel et al., 2014
-	c.863+2dup	Intron 9	Duplication (alteration of the WT donor site; activation of an intronic cryptic donor site)	-	https://www.ucl.ac.uk/ncl-disease/
p.Trp407Arg	c.1219T>C	Exon 12	Substitution (missense)	L9	Patino et al., 2015
p.Met454Thr	c.1361T>C	Exon 13	Substitution (missense)	TM11	Patino et al., 2015
p.Trp456*	c.1367G>A	Exon 13	Substitution (nonsense)	TM11	https://www.ucl.ac.uk/ncl-disease/
p.Trp78*	c.233G>A	Exon 5	Substitution (nonsense)	TM2	Khan et al., 2017
-	c.63-1G>A	Intron 2	Substitution (alteration of the WT acceptor site)	-	https://www.ucl.ac.uk/ncl-disease/
-	c.554-5A>G	Intron 6	Substitution (activation of intronic cryptic acceptor site)	-	Ren, XT. et al., 2019
p.Cys175*	c.525T > A	Exon 6	Substitution (nonsense)	TM5	Kozina et al., 2018
p.Val109_Ile113del	c.325_339del	Exon 5	Deletion (frameshift)	TM3	Bereshneh and Garshasbi, 2018
p.Gly197Valfs*2	c.590del	Exon 7	Deletion (frameshift)	L5	Bauwens et al., 2019
p.Ile67Glufs*3	c.493+3A>C	Intron 5	Substitution (frameshift)	L1	Bauwens et al., 2019
p.Met46fs	c.136_137del	Exon 3	Deletion (frameshift)	TM1	Qiao et al., 2022
p.Pro213Gln	c.638C>A	Exon 7	Substitution (missense)	TM6	https://www.ucl.ac.uk/ncl-disease/
p.Gly241*	c.721G>T	Exon 8	Substitution (nonsense)	L6	Kose et al., 2021

Mutation (amino acid change)	Nucleotide change	Location in the MFSD8 gene	Type of mutation	Location in the MFSD8 protein	Reference
p.Gln365*	c.1093C>T	Exon 11	Substitution (nonsense)	L9	Kose et al., 2021
p.Arg482Pro	c.1445G>C	Exon 13	Substitution (missense)	L11	Birtel et al., 2018
p.Ser437Tyr	c.1310C>A	Exon 12	Substitution (missense)	L10	https://www.ucl.ac.uk/ncl-disease/
p.Gly427Arg	c.1279G>A	Exon 12	Substitution (missense)	TM10	https://www.ucl.ac.uk/ncl-disease/
p.Glu250Glu	c.750A>G	Exon 8	Substitution (alteration of auxiliary sequences: significant alteration of ESE/ESS motifs ratio, new acceptor splice site: activation of a cryptic acceptor site)	L6	Reith et al., 2022
-	c.755-2726_998+1981delinsGTA	Intron 8 – Intron 10	Deletion insertion	-	Poncet et al., 2022
p.Glu336Lys	c.1006G>A	Exon 11	Substitution (missense)	L8	Poncet et al., 2022
p.Arg337Cys	c.1009C>T	Exon 11	Substitution (missense)	L8	Poncet et al., 2022
p.Arg35Gln	c.104G>A	Exon 3	Substitution (missense)	N-terminal	Poncet et al., 2022
p.Pro356Ser	c.1066C>T	Exon 11	Substitution (missense)	TM9	Xiang et al., 2021
-	c.1102+2T>C	Intron 11	Substitution (broken WT donor site: alteration of the WT donor site)	-	Xiang et al., 2021
p.Ser422*	c.1265C>A	Exon 12	Substitution (nonsense)	TM10	Poncet et al., 2022
p.Gly52Ala	c.155G>C	Exon 4	Substitution (missense)	TM1	Poncet et al., 2022
-	c.998+1669A>G	Intron 10	Substitution (new donor splice site: activation of a cryptic donor site)	-	Poncet et al., 2022

Abbreviations: L, loop; TM, transmembrane domain.

1.1.2.3 MFSD8 mutations in other neurodegenerative disorders

Recent advances in the field of genome sequencing have revealed that *MFSD8*, along with several other genes, plays a role in various neurodegenerative disorders that affect adults, including amyotrophic lateral sclerosis (ALS) and frontotemporal dementia (FTD), macular dystrophies (maculopathies), retinal dystrophies (retinopathies), and retinitis pigmentosa (RP). However, *MFSD8* mutations have also been identified in childhood neurodevelopmental diseases like autism spectrum disorder (ASD). In the context of these diseases, it has been observed that *MFSD8* mutations are often manifested in a heterozygous manner.

1.1.2.3.1 MFSD8-associated retinopathies

Inherited maculopathies and cone diseases, including achromatopsia (ACHM), cone dystrophy (COD), and cone-rod dystrophy (CRD), are estimated to have a global prevalence ranging from 1 in 30,000 to 1 in 40,000 individuals (Hamel, 2007; Michaelides et al., 2004). Isolated maculopathies are characterised by the progressive degeneration of the central inner retina (Bauwens et al., 2020). The symptoms associated with ACHM typically manifest shortly after birth and encompass diminished visual acuity, sensitivity to light, inherited pendular nystagmus, and compromised colour perception. In these instances, the use of full-field electroretinography (ERG) is commonly employed to assess the lack or decline of cone responses (Kohl et al., 2000; Thiadens et al., 2009). Furthermore, the application of optical coherence tomography (OCT) is employed for the evaluation of the degeneration of inner and outer cone segments, which manifests as a disruption of the ciliary layer and a reduction in cell number inside the cone photoreceptor layer. The retinal pigment epithelium (RPE) experiences a decline as age-related macular degeneration (ACHM) advances during the second decade of life. This decline is accompanied by a continuous loss of cones and the subsequent development of central visual impairment (Thiadens et al., 2010). Both COD and CRD are primarily inherited in an autosomal recessive manner, however, they can manifest in other Mendelian inheritance patterns. There are a total of eight different genes that are responsible for autosomal recessive COD, with three of these genes being specifically associated with ACHM, a condition that can progress to COD. In the context of autosomal recessive CRD, a total of 18 genes have been linked to its manifestation. Among those genes, the ATP binding cassette subfamily A member 4 gene (*ABCA4*) is the most prevalent (Bauwens et al., 2020). In recent years, the use of linkage analysis and next-generation sequencing techniques has resulted in the discovery of previously unknown genes responsible for autosomal recessive maculopathies (Audo et al., 2012; Roosing et al., 2013; Zeitz et al., 2013). Roosing et al. (2013) reported the identification of two patients exhibiting compound heterozygosity for mutations in *MFSD8*. One

individual carried the genetic variations p.Glu381* (c.1141G>T) and p.Glu336Gln. The second individual exhibited heterozygosity for the identical missense variant (p.Glu336Gln; c.1006G>C) previously detected, as well as for the variant c.1102G>C, which is predicted to lead to the production of a truncated protein (p.Lys333Lysfs*3) (Roosing et al., 2015) (**Figure 1.3**). The aforementioned mutations resulted in the development of nonsyndromic macular dystrophy characterised by central cone impairment, which can be attributed to the presence of MFSD8 genetic variants.

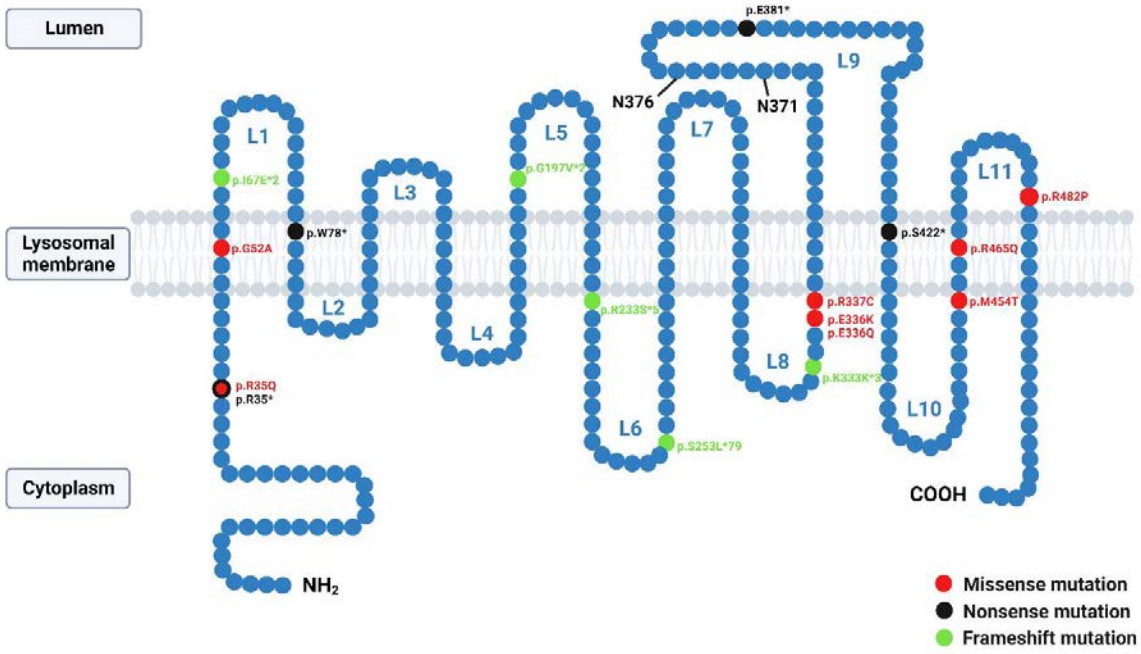

Figure 1. 3. Schematic representation of mutations in the *MFSD8* gene associated with retinopathies. The coloured dots represent mutations in *MFSD8* gene that cause retinopathies with their approximate location within MFSD8. Each colour describes a different type of mutation: red refers to missense mutations, black represents nonsense mutations, and green refers to frameshift mutations. Figure based on Khan et al. (2017) and Sharifi et al. (2010).

Similarly, Khan et al. (2017) identified six cases of isolated macular disease characterised by compound heterozygous alleles of *MFSD8*, consistently noting the prevalence of the c.1006G>C (p.Glu336Gln) variant. Moreover, an additional six cases were identified as having a homozygous mutation at position c.1361T>C (p.Met454Thr), and these individuals presented symptoms of a generalized retinopathy. In this particular instance, the patients were exhibited homozygosity with respect to an *MFSD8* mutation that is generally regarded as mild. The individuals that carried the p.Glu336Gln mutation in a compound heterozygous form were identified to be in *trans* with either a loss-of-function mutation (c.103C>T, p.Arg35* or c.233G>A, p.Trp78*) or a missense mutation

(c.1394G>A, p.Arg465Gln) (**Figure 1.3**). These patients did not exhibit any symptoms indicative of a neurological condition (Khan et al., 2017). The localisation of MFSD8 in the synaptic terminals of photoreceptors in mice retina has been observed. Additionally, it has been found that macular photoreceptors display a heightened sensitivity to variations in *MFSD8* (Khan et al., 2017).

Birtel et al. (2018) identified a homozygous variant (c.1445G>C, p.Arg482Pro) located in exon 13 of *MFSD8* (**Figure 1.3**). This variant was found to cause non-syndromic retinitis pigmentosa without any observable neurological disorders. This study also provided evidence of *MFSD8*'s role as a gene associated with non-syndromic retinopathy, specifically having a less severe mutation (Birtel et al., 2018). RP is a prevalent congenital retinal degeneration, occurring in approximately 1 in every 4,000 individuals (Hamel, 2006). The condition is distinguished by the gradual deterioration of rod and cone photoreceptors, resulting in the manifestation of night blindness and concentric visual field loss throughout adolescence. Subsequently, individuals experience central visual loss later in adulthood (Salmaninejad et al., 2019). Wang et al. (2021) also documented novel mutations in *MFSD8*. The identified variant, c.998C3_998C6del, was observed in a Chinese prenatal instance in a compound heterozygous form. In this case, while one allele of *MFSD8* was completely deleted, while the other allele exhibited exon 10 skipping, resulting in an impact on RNA and protein translation (Yihui Wang et al., 2021).

Bauwens et al. (2020) reported the identification of two additional heterozygous *MFSD8* mutations in a female patient who was diagnosed with atypical Stargardt disease at the age of 5. The patient in question has two *MFSD8* variants: the c.590del (p.Gly197Valfs*2), located in exon 7, and the c.439+3A>C variant (**Figure 1.3**). Additionally, there was one heterozygous *ABCA4* variant, specifically the c.3113C>T (p.Ala1038Val) variant (Bauwens et al., 2020). The c.439+3A>C (p.Ile67Glufs*3) mutation of *MFSD8* leads to the exclusion of exon 5 (241 bp) during ribonucleic acid (RNA) processing, resulting in the production of a truncated protein. This truncated protein ceases expression within the second transmembrane domain (Bauwens et al., 2020).

The aforementioned research has reported that the coexistence of hypomorphic and loss-of-function *MFSD8* alleles, or the presence of homozygous mild *MFSD8* alleles, results in the development of isolated maculopathies or retinopathies with macular involvement or RP (Birtel et al., 2018; Khan et al., 2017; Roosing et al., 2015). However, in a study conducted by Zare-Abdollahi et al. (2019), individuals with an isolated maculopathy were found to carry both heterozygous and homozygous missense *MFSD8* variants. This finding challenges the previous belief that all homozygous missense mutations in *MFSD8* are exclusively linked to vLINCL,

thereby suggesting a broader spectrum of associations for these mutations (Zare-Abdollahi et al., 2019).

In a recent study, Poncet et al. (2022) reported the presence of 12 different biallelic variants in *MFSD8*, which have been associated with the development of inherited retinal degeneration (IRD). This condition encompasses various subtypes such as macular dystrophy (MD), cone dystrophy (COD), and cone-rod dystrophy (CRD) (Poncet et al., 2022). Among those variants, there were a total of seven mutations that had not been previously documented. These mutations consisted of four missense mutations, one nonsense mutation, one deep intronic mutation, and one large deletion that encompassed two exons. A total of six patients presented isolated retinal degeneration, wherein each patient carried at least one missense variant. Furthermore, the remaining allele in these patients displayed either another missense or a predicted loss-of-function mutation. One of the novel missense variants identified in the study was the c.1006G>A (p.Glu336Lys) variant. This residue is located within the extracellular loop denoted as L9. The remaining three missense variants that were found are the c.104G>A (p.Arg35Gln), c.155G>C (p.Gly52Ala), and c.1009C>T (p.Arg337Cys) (**Figure 1.3**). The novel deep intronic variant c.998+1669A>G was identified by intron analysis. This particular variant is predicted to generate a splice donor site, leading to the insertion of a pseudoexon spanning 140 bp between exons 10 and 11. Another mutation (c.750A>G; p.Arg233Serfs*5,=) was identified five nucleotides upstream of the 3' end of exon 8. This mutation causes the production of two transcripts: one that is normal and another that lacks exon 8. Consequently, this results in the formation of a null allele. The nonsense mutation identified as c.1265C>A (p.Ser422*) was shown to be associated with COD, while the large deletion spanning exons 9 and 10, referred to as variant c.755-2726_998+1981 delinsGTA (p.Ser253Leufs*79), was observed to cause early-onset severe retinal dystrophy (EOSRD) (Poncet et al., 2022) (**Figure 1.3**).

Kolesnikova et al. (2023) documented the discovery of five previously unreported biallelic mutations in *MFSD8*, which were found to be associated with isolated retinal disease. One of the individuals, who was diagnosed with RP at the age of 19, was compound heterozygous for the prevalent c.1361T>C (p.Met454Thr) variant alongside with a novel mutation c.863+2 that affects gene splicing. The mutation c.1361T>C (p.Met454Thr) is located in the 11th transmembrane domain and induces alterations in protein folding. A novel instance of isolated retinal disease, previously linked to the syndromic vLINCL, was identified. This case involved the presence of the c.754+2T>A variant in combination with the c.1361T>C (p.Met454Thr) missense mutation. The mutation c.754+2T>A is present within intron 8 of *MFSD8* and results in altered splicing (Kolesnikova et al., 2023). This exemplified the combination of several variants, resulting in a less

severe protein defect and manifesting as isolated retinal disease phenotype. In contrast, each variant on its own can cause a more severe pathology, which could be vLINCL disease (Khan et al., 2017).

1.1.2.3.2 *MFSD8* variants associated with ALS and FTD

Amyotrophic Lateral Sclerosis (ALS; also known as Motor Neuron Disease) is an infrequent neurodegenerative disease that affects the lower and upper motor neurons (LMN and UMN, respectively). The age of onset often occurs between the ages of 50 and 60, and those affected by the condition typically experience pronounced respiratory failure within a span of 2 to 4 years after the onset of the disease (Hobson and McDermott, 2016). The initial identification of the gene associated with ALS occurred in 1993, with the discovery of superoxide dismutase (*SOD1*) (Rosen et al., 1993a). Nevertheless, over 130 genes have been identified with genetic variants as underlying contributory factors contributing to disease. For instance, Nagy et al. (2022) conducted a study wherein they employed whole exome sequencing (WES) to examine previously unexplored genes related to ALS in a cohort of 21 Hungarian patients (Nagy et al., 2022). One of the genes identified in the study was *MFSD8*, along with several others. The study reported the presence of a nonsense mutation (p.Q304*) in the eighth transmembrane domain of MFSD8 (or end of the L7, according to UniProt) (**Figure 1.4**). This MFSD8 variant involves the substitution of glutamine with an early stop codon, leading to a truncated form of the protein. This alteration has the potential to induce lysosomal dysfunction and affect the development of ALS (Nagy et al., 2022).

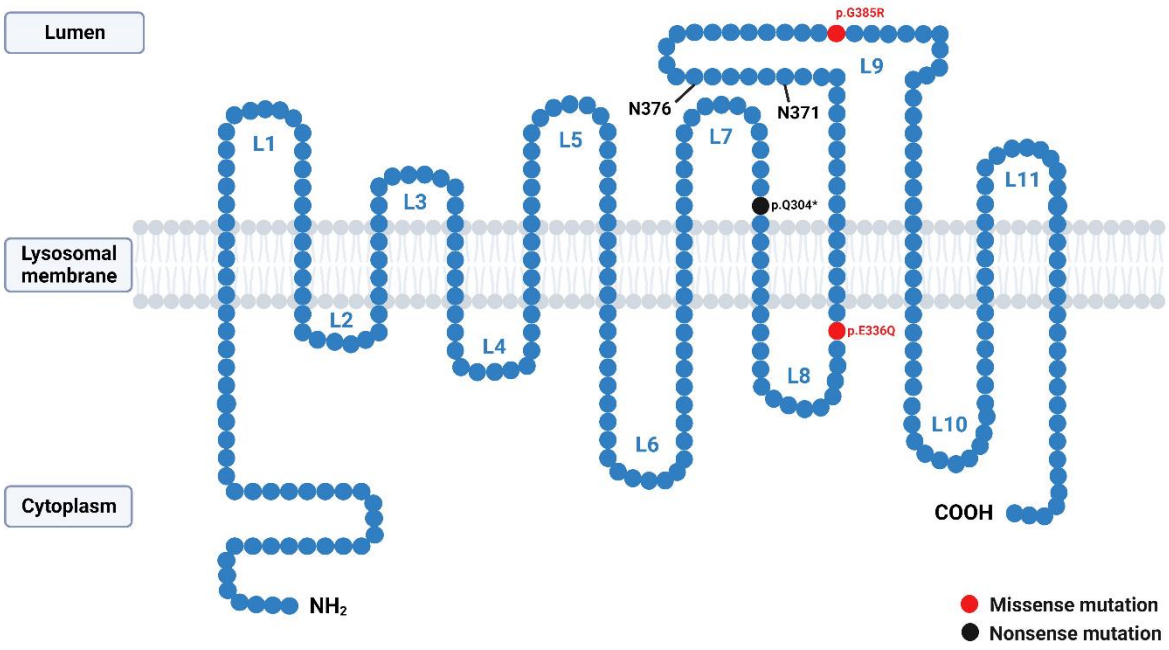

Figure 1. 4. **Schematic representation of mutations in *MFSD8* associated with ALS and FTLD.** The coloured dots represent mutations in the *MFSD8* gene that cause ALS or FTLD with their approximate location within MFSD8. Each colour describes a different type of mutation: red refers to missense mutations, and black represents nonsense mutations. Figure based on Khan et al. (2017) and Sharifi et al. (2010).

Frontotemporal lobar degeneration (FTLD) is a neurodegenerative disorder characterised by the degeneration of the frontal and temporal lobes. This degeneration leads to a diverse range of clinical symptoms, which are classified as FTD (Olszewska et al., 2016). FTLD constitutes around 5-10% of all instances of dementia and exhibits a gradual deterioration of behaviour and language skills (Gorno-Tempini et al., 2011; Mercy et al., 2008; Onyike and Diehl-Schmid, 2013; Rascovsky et al., 2007). The predominant aetiology of genetic FTLD cases can be attributed to alterations in three specific genes: *MAPT*, granulin (*GRN*), and chromosome 9 open reading frame 72 (*C9orf72*). The application of next-generation sequencing (NGS) has enabled the discovery of novel genetic risk factors for FTLD. For instance, Geier et al. (2019) identified some uncommon mutations (E336Q and G385R) in MFSD8 among individuals diagnosed with FTLD. These mutations were associated with atypical protein levels of MFSD8 and notable deviations in lysosomal and autophagy-related markers when compared to individuals without FTLD. These findings indicate that *MFSD8* variants may serve as new risk factors for FTLD (Geier et al., 2019). Similarly, Ogonowski et al. (2023) have identified a rare coding variant in *MFSD8*, specifically the missense mutation c.1153G>C (p.Gly385Arg) (**Figure 1.4**), which has been found to potentially contribute to the pathobiology of FTLD (Ogonowski et al., 2023).

1.1.2.3.3 *MFSD8* mutations in autism spectrum disorder (ASD)

ASD is an inherited heterogeneous developmental disorder characterised by a range of symptoms and aetiological factors that are not yet fully understood. It is typically initially observed in infancy or early childhood and is defined by impaired communication skills and behavioural abnormalities (Al Backer, 2015). However, ASD has been implicated in certain neurological disorders with known aetiologies, such as Rett syndrome, Landau-Kleffner syndrome, and Christianson syndrome (Al Backer, 2015; Pescosolido et al., 2014). Certain causes of regressive autism have been documented to involve different genetic variants that are unrelated to the aforementioned disorders. For instance, a female patient displaying symptoms of NCL with a Rett-like onset was found to have compound heterozygous variants of *MFSD8* and *CLN5* (Craiu et al., 2015). Additionally, Jin et al. (2020) reported the case of a 7-year-old male patient who carried heterozygous missense mutations in *EHMT1* (c.1513G>A, p.Gly505Ser) and *MFSD8* (c.353A>G,

p.Asn118Ser) (**Figure 1.5**). This patient exhibited a decline in physical, cognitive, and verbal abilities, leading to a diagnosis of ASD.

In their study, Rahman et al. (2021) described a 4-year-old male patient from Bangladesh who presented progressive myoclonic epilepsy (PME) and was found to carry a homozygous *MFSD8* mutation. This missense mutation was the c.850G>C (p.Ala284Pro) variant, situated within exon 9 of *MFSD8* (Rahman and Fatema, 2021).

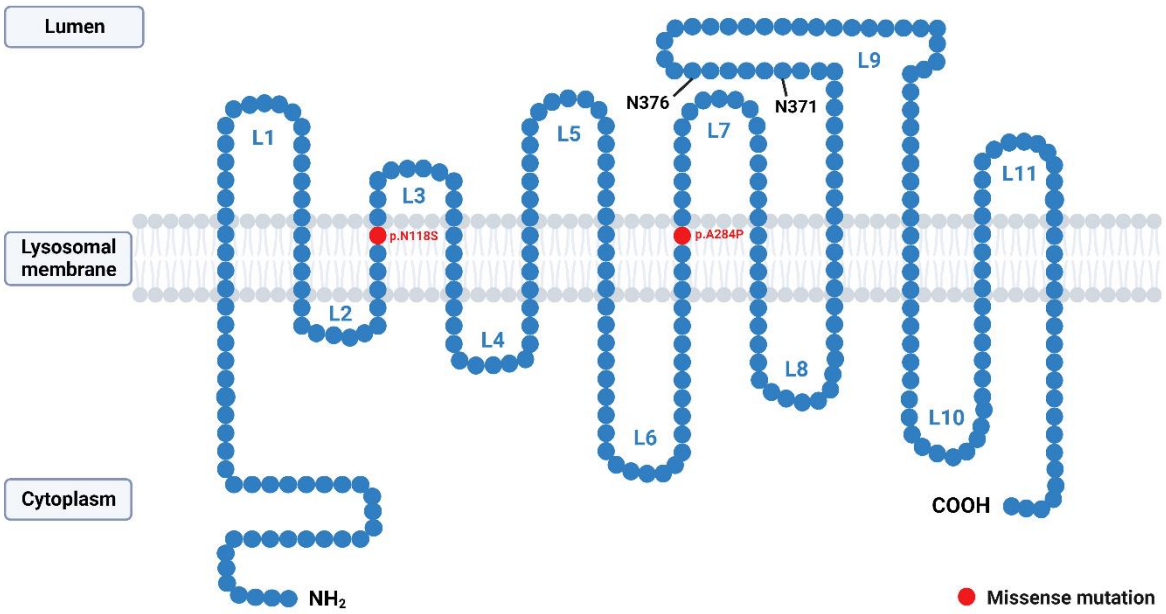

Figure 1. 5. Schematic representation of mutations in *MFSD8* associated with ASD. The coloured dots represent mutations in *MFSD8* that cause ASD with their approximate location within the MFSD8 protein. The red colour refers to missense mutations. Figure based on Khan et al. (2017) and Sharifi et al. (2010).

Collectively, the aforementioned cases and novel variants in *MFSD8* exemplify the remarkable range of phenotypic variability associated with this gene, rendering it a captivating and crucial subject of investigation. The range of pathological conditions resulting from *MFSD8* encompasses ALS and FTD, isolated macular involvement, generalized rod-cone dystrophy, and systemic vLINCL. Therefore, it is essential to conduct a more extensive investigation into the molecular biology and genetics of *MFSD8* to elucidate the intricate interplay of different alleles and their respective and collective effects on the folding and functionality of the protein. This would improve understanding of the phenotypic variability, given the absence of a known genotype-phenotype correlation or unifying mechanism.

1.2 Autophagy in neurodegenerative diseases

Autophagy is an intracellular degradation mechanism that regulates the digestion and recycling of impaired cellular components, damaged organelles, and protein aggregates through autophagosomes. Autophagosomes refer to double-membrane structures located within the cells that actively sequester and encapsulate cytoplasmic components that have experienced damage. These autophagosomes then transport the encapsulated material to lysosomes, where it undergoes degradation through enzymatic digestion (Mizushima et al., 2008; Tsukada and Ohsumi, 1993). This mechanism facilitates the generation of cellular energy, a vital process for the survival of cells under conditions of nutrient deprivation and serves as a fundamental component in the maintenance of cellular homeostasis.

The occurrence of various human neurodegenerative disorders, including AD, ALS, Parkinson's disease (PD), and Huntington's disease (HD), can be attributed to genetic mutations resulting in defective or altered protein function and/or the accumulation of potentially harmful proteins, which disrupt the normal functioning of autophagy. Consequently, certain areas of research are currently focusing on the development of pharmaceuticals to facilitate the elimination of harmful debris or damaged organelles accumulating due to defective autophagy (Boland et al., 2018; Menzies et al., 2017). Furthermore, other studies have shown that autophagy has the potential to induce neuronal death, suggesting that targeted suppression of autophagy may also serve as a viable therapeutic strategy in some circumstances (Liu and Levine, 2015).

1.2.1 Initiation of autophagy

Autophagy involves the formation of autophagosomes through the fusion of vesicles generated from different membrane origins, including the plasma membrane, ER, Golgi apparatus, and mitochondria (Hailey et al., 2010; Hayashi-Nishino et al., 2009; Ravikumar et al., 2010; Yen et al., 2010; Ylä-Anttila et al., 2009). The formation of these vesicles gives rise to the phagophore, a membranous sac that undergoes a transformation into a cup-shaped double membrane. This double membrane then proceeds to engulf portions of the cytoplasm as its two edges close. The production of autophagosomes is reliant upon the participation of several autophagy (ATG) proteins. Phagophore formation is a process that encompasses the involvement of the ATG5-ATG12-ATG16L1 complex and catalytic activities, facilitated by ATG7 and ATG10 (Menzies et al., 2015). The phagophore membrane encloses ATG9 and the microtubule-associated protein 1A/1B-light chain 3 (LC3), playing a crucial role in the process of autophagosome biogenesis. The process of LC3 cleavage involves the action of ATG4B, which results in the formation of LC3-I. Subsequently, LC3-I associates with phosphatidylethanolamine through the involvement of ATG7

and ATG3, leading to the formation of LC3-II (Kabeya et al., 2000). Upon the expansion of the phagophore and the subsequent convergence of its two edges for fusion, the ATG5-ATG12-ATG16L1 complex detaches from the outer membrane. In contrast, LC3-II remains associated with the autophagosome that has been formed. Following the process of autophagosome closure, the autophagosomes are transported to the perinuclear area within the cell. Subsequently, fusion occurs between the autophagosomes and the lysosomes, leading to the degradation of their contents (**Figure 1.6**). Moreover, the involvement of soluble N-ethylmaleimide-sensitive factor activating protein receptors (SNAREs) in the process of autophagosome production and degradation is of utmost importance, as they facilitate the fusion of vesicles (Fader et al., 2009; Furuta and Amano, 2010).

The initiation of autophagy is controlled by the ULK1/ULK2-ATG3-FIP200 complex. In addition, this complex participates as a sensor for upstream signalling through three crucial pathways: the mTOR complex 1 (mTORC1), adenosine monophosphate (AMP)-activated protein kinase (AMPK), and p53 pathways (Alers et al., 2012; Füllgrabe et al., 2014). Specifically, mTORC1 inactivates the ULK1/ULK2-ATG3-FIP200 complex by phosphorylation of ULK1 or ULK2 (**Figure 1.6**). On the other hand, autophagy is activated by AMPK through the phosphorylation of ULK1 at different sites that differ from those targeted by mTORC1. The modulation of autophagy by p53 occurs through transcriptional regulation, whereby p53 upregulates the expression of pro-autophagic proteins such as ELK1, ELK2, AMPK, and tuberous sclerosis 2 protein (TSC2) (Füllgrabe et al., 2014). In contrast, p53 that is not actively involved in transcriptional processes and is located in the cytoplasm interacts with FIP200 to exert a negative regulatory effect on autophagy. This leads to the inhibition of the development of the ULK complex (Morselli et al., 2011).

The ULK1/ULK2-ATG3-FIP200 complex modulates the initiation of autophagy through the PI3K complex, which contains the vacuolar protein sorting 34 (VPS34 or PIK3C3), VPS15 (or PIK3R4), Beclin 1 and ATG14L (or barkor). The formation of PtdIns3P on new autophagosomes necessitates the presence of the VPS34 complex, which in turn enables the recruitment of PtdIns3P-binding proteins like WD repeat domain phosphoinositide-interacting protein 1 (WIPI1) and WIPI2 to the membranes of autophagosomes (Dooley et al., 2014; Menzies et al., 2015; Russell et al., 2013).

Several receptor proteins, also known as adaptor proteins, have been discovered that play a crucial role determining substrate specificity in autophagy (Stolz et al., 2014). For instance, p62 (also known as sequestosome 1, SQSTM1), next to *BRCA1* gene 1 protein (NBR1), nuclear domain 10

protein 52 (NDP52 or CALCOCO2), and optineurin have the ability to selectively bind their cargo for degradation (Bjørkøy et al., 2005; Kirkin et al., 2009). These proteins can recognize ubiquitylated proteins, which would be the cargoes, through ubiquitin-binding domains and afterwards attach to LC3 on autophagosomes (Pankiv et al., 2007; Rogov et al., 2014).

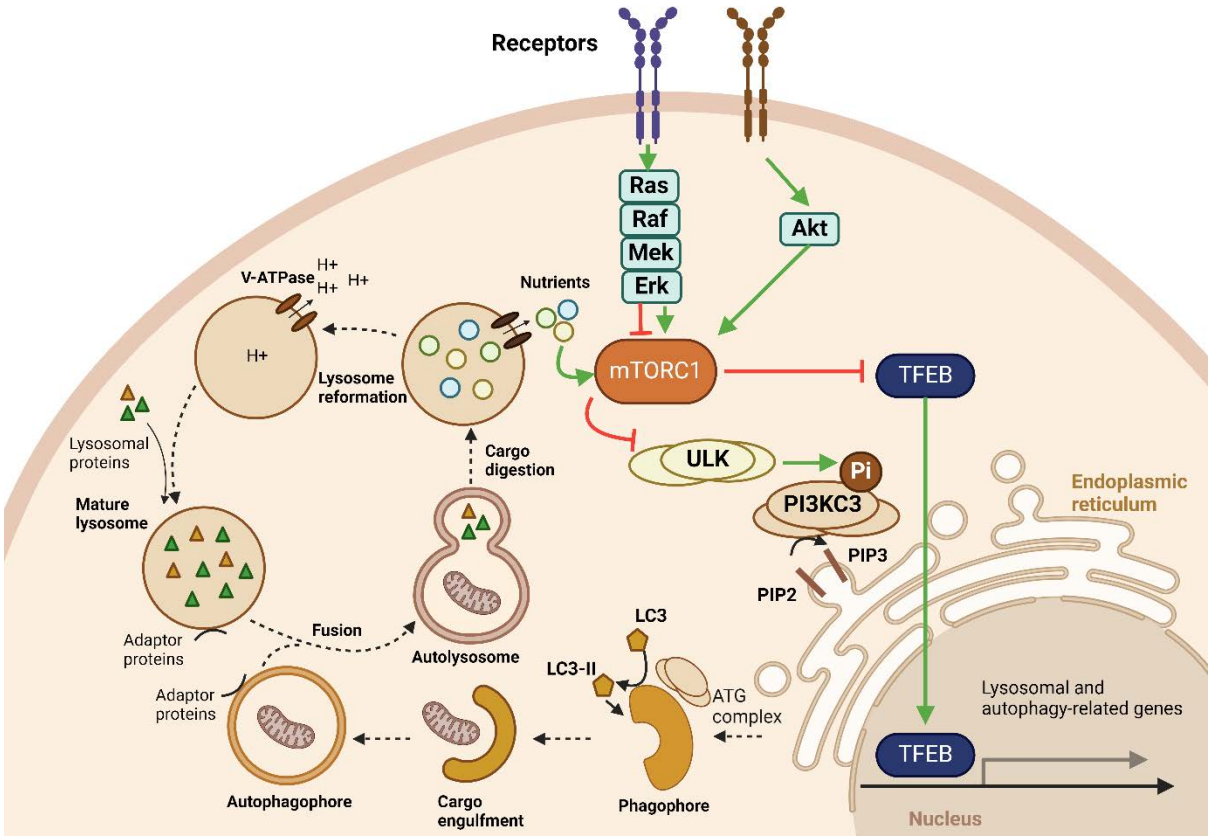

Figure 1. 6. Autophagosome formation and autophagy regulation. Autophagosome formation occurs in multiple stages: initiation, nucleation, membrane expansion, closure, and fusion with lysosomes. During initiation, the ULK1/2 complex initiates the nucleation of the phagophore under nutrient-deprived conditions. Subsequently, the class III phosphatidylinositol 3-kinase (PtdIns3K, PI3KC3) complex generates phosphatidylinositol 3-phosphate (PIP3) to recruit autophagy-related (ATG) proteins at the phagophore during the nucleation stage. The ATG12-ATG5-ATG16L1 complex and LC3-II facilitate the expansion of the phagophore, with contributions from ATG9A vesicles and lipid transfer. During the closure stage, the phagophore edges close to form the autophagosome and then the autophagosome fuses with the lysosome, forming an autolysosome where degradation occurs. Autophagy regulation include the mTOR, AMPK, and PI3K-Akt pathways. The mTOR pathway inhibits autophagy by phosphorylating and inactivating the ULK1/2 complex under nutrient-rich conditions; suppressed during nutrient starvation, leading to autophagy activation. The AMPK pathway activates autophagy by phosphorylating and activating the ULK1/2 complex under low energy conditions. The PI3K-Akt pathway negatively regulates autophagy by activating mTOR; inhibition of PI3K or Akt promotes autophagy by reducing mTOR activity. Figure based on Gąsiorkiewicz et al. (2021).

1.2.2 Mitophagy in neurological disorders

Mitochondria are organelles enclosed by a double membrane that play a crucial role in various essential cellular processes, including the production of adenosine-5'-triphosphate (ATP), the synthesis and transport of phospholipids, calcium signalling, and the maintenance or iron balance (Raffaello et al., 2016; Spinelli and Haigis, 2018; Tamura and Endo, 2017). These organelles serve as sites for several processes, such as apoptosis, innate immune response, and differentiation of cells (Lisowski et al., 2018; Mehta et al., 2017). Due to the production of reactive oxygen species (ROS) on the electron transport chain, mitochondria face ongoing oxidative stress which can ultimately result in structural and functional deterioration (Wong et al., 2017).

There are two forms of mitochondria in the brain: non-synaptic and synaptic. Non-synaptic mitochondria come from glial cells or neuronal cells, whereas synaptic mitochondria come from the synaptic region (Völgyi et al., 2015). Neurons rely on a significant amount of ATP to facilitate the synthesis of synaptic vesicle, transport substances along the axon, control ion gradients, and sustain the mitochondrial membrane potential (Iwata and Vanderhaeghen, 2021). Several studies have demonstrated that mitochondrial health has a substantial influence on the functioning of neurons and might potentially effect brain development and neuroplasticity through metabolic changes, regulation of calcium levels, programmed cell death (apoptosis), autophagy, and mitochondrial dynamics (Büeler, 2021; Khacho et al., 2017). Furthermore, mitochondria also have a significant impact on the growth of neurites, the restructuring of dendrites, and the secretion of neurotransmitters during the differentiation of neurons (Ozgen et al., 2022).

The key indicators of mitochondrial dysfunction in the ageing process encompass inadequate ATP production, mutations in mitochondrial deoxyribonucleic acid (mtDNA), increased generation of mitochondrial ROS, reduced levels of antioxidant enzymes, increased release of pro-apoptotic factors, and oxidative damage to lipids, nucleic acids, and proteins (Mishra and Thakur, 2022; Navarro et al., 2008). The cellular antioxidants and enzymes that capture free radicals, such as catalase (CAT), glutathione peroxidase (GPx), and superoxide dismutase (SOD), eliminate most of the produced ROS. Nevertheless, a minor fraction of ROS manages to evade this elimination and can potentially cause damage to mitochondrial DNA, proteins, and lipids (Cui et al., 2011). Over time, the accumulation of mutations produces targeted harm to the respiratory chain complexes and excessive formation of ROS, finally resulting in impaired mitochondrial function.

Additionally, dysfunction of mitochondria has been associated with several aged-related clinical disorders, such as AD and PD. Strong evidence indicates that the process of ageing results in notable changes in the structure and function of mitochondria, which ultimately leads to the death

of neurons (Campo et al., 2016; Mishra and Thakur, 2022). It has been hypothesised that a disruption in the control of normal mitochondria during ageing might be a shared pathway in age-related neurodegenerative disorders. Consequently, to preserve mitochondrial homeostasis and optimal ageing, neuronal cells might have developed intricate and interrelated regulatory systems to control the generation of mitochondria and eliminate defective ones. Accordingly, the autophagic system selectively recognises and transports malfunctioning mitochondria to the lysosome to degrade them. The process of mitochondria degradation is a catabolic process known as mitophagy, which helps maintain the integrity and number of mitochondria in different cell types (Pickles et al., 2018). The mitochondria in tissues that require ATP, including the brain, skeletal muscle, heart, liver, and kidney, are highly developed to ensure an adequate balance between energy demand and supply. During the process of mitophagy, the fusion of autophagosomes and lysosomes leads to the formation of autophagolysosomes (in the general process of macroautophagy or autophagy), which in this case results in the degradation of dysfunctional mitochondria (Kubli and Gustafsson, 2012).

1.2.3 Autophagosomes in neurons

Autophagosome formation in neurons differs from that in other cell types due to its distinct spatiotemporal characteristics. While the same set of autophagy proteins is involved, the process occurs specifically at the distal tip of the axon and undergoes retrograde trafficking towards the soma (Maday et al., 2012). The proteins implicated in the process of autophagosome maturation in neurons include the STX17-containing SNARE complex, Rab7, EPG5, and the homotypic fusion and protein sorting (HOPS) complex (Bains et al., 2011; Cheng et al., 2017; Peng et al., 2012; Takáts et al., 2013; Zhao et al., 2013).

Several neurodegenerative diseases, including HD, PD, and ALS, present the accumulation of autophagic vacuoles (AVs) in affected neurons. This accumulation of AVs ultimately results in neuronal cell death (Nixon et al., 2008). The increase in the number of AVs can be attributed to the disruption of autolysosome formation and function. This disruption hinders the process of autophagy and disrupts the trafficking of endocytic materials, ultimately resulting in the impairment of a certain subset of neurons (Zhao and Zhang, 2018).

1.2.4 Lysosomes

Lysosomes are cellular organelles enclosed by a membrane that contain enzymes responsible for the degradation of many intracellular biological polymers, including proteins, nucleic acids, carbohydrates, and lipids. They function as the cell's recycling centre to maintain cellular homeostasis. Lysosomes are involved in the degradation and breakdown of both extracellular

materials that have been internalised by the cell, as well as intracellular components that are deemed unnecessary or harmful. Lysosomes are commonly depicted as spherical vacuoles in their most basic form; however, their size and shape can exhibit variability depending on the nature of the components they contain for the purpose of digestion (Cooper, 2000).

Over 30 different human genetic diseases, collectively referred to as LSDs, are caused by mutations in the genes that encode the degradative enzymes within the lysosomes (Platt et al., 2012). In addition, lysosome dysfunction has been implicated in a diverse range of human pathologies, encompassing neurodegenerative diseases (Appelqvist et al., 2013; Bajaj et al., 2019; Cox and Cachón-González, 2012). There are additional exceptions of mutations that result in lysosomal storage disorders. One such example is the deficiency in the enzyme that catalyses the attachment of mannose-6-phosphate to lysosomal enzymes within the Golgi apparatus. This disease leads to a broad defect in the integration of lysosomal enzymes into lysosomes, thereby hindering their ability to conduct their degradative function (Cooper, 2000).

The enzymes found in lysosomes are classified as acidic hydrolases (e.g. cathepsins). These enzymes show optimal functionality within the acidic pH range 4.5-5.5, which is in contrast to the neutral pH of 7.2 commonly observed in the cytoplasm. Consequently, to maintain the acidic internal pH of the lysosomes, a proton pump in the lysosomal membrane – the vacuolar ATPase (V-ATPase) – actively transports H^+ ions (protons) from the cytosol into the lysosome. This pumping activity is achieved through the consumption of energy in the form of ATP hydrolysis (Cooper, 2000). Lysosomes are responsible for the uptake and degradation of materials resulting from processes such as endocytosis, phagocytosis, and autophagy. These materials include cytoplasmic contents such as damaged ER, mitochondria, and other lysosomes (Bright et al., 2016; Chen et al., 2010; Cinque et al., 2020; Khaminets et al., 2015; Maejima et al., 2013; Pickles et al., 2018). The number of lysosomes can fluctuate in response to cellular requirements, such as autophagy triggered by starvation and the distribution of lysosomes during cell division. Additionally, lysosomes have the ability to adjust in response to both extra- and intracellular signals to maintain cell homeostasis (Yang and Wang, 2021).

1.2.4.1 Lysosome biogenesis

The formation of the lysosomes requires the simultaneous production of lysosomal proteins and the transport from endosomes to lysosomes. This process starts in the ER, where lysosomal hydrolases are synthesised and modified through the addition of oligosaccharides. Subsequently, the hydrolases are transported to the Golgi apparatus, where the process of phosphorylation occurs on the mannose residues of the majority of lysosomal hydrolases (**Figure 1.7**). The

mannose 6-phosphate receptor (MPR) recognizes these phosphorylated hydrolases and the hydrolase-MPR complex is encompassed by clathrin-coated vesicles at the trans-Golgi network (TGN), which are then delivered to early-endosomes. Some hydrolases do not require the MPR for transportation to endosomes (Braulke and Bonifacino, 2009; Luzio et al., 2014). Lysosomal membrane proteins are delivered to the lysosomes through two different pathways: the direct and the indirect pathway. In the direct pathway, lysosomal membrane proteins are initially synthesized at the TGN and subsequently transported directly to endosomes. Conversely, in the indirect pathway, these proteins are first delivered to the plasma membrane before undergoing endocytosis to reach the early endosomes (Braulke and Bonifacino, 2009; Luzio et al., 2014; Saftig and Klumperman, 2009; Yang and Wang, 2021). The trafficking of endosomal proteins to lysosomes relies on the transformation of early endosomes into late endosomes. In this process, the early endosome-specific Rab5 and phosphatidylinositol 3-phosphate (PtdIns3P, PI3P) are replaced by Rab7 protein specific to late endosomes and phosphatidylinositol 3,5-bisphosphate (PtdIns(3,5)P_2, PI(3,5)P_2) (Gillooly et al., 2000; Huotari and Helenius, 2011; Schink et al., 2016). The endosomal proteins that are not intended for transport to the lysosomes undergo recycling by either the retromer-dependent and retromer-independent pathways (McNally and Cullen, 2018). The process of late endosome-lysosome fusion involves the participation of several key proteins, including the Rab7 small GTPase, the HOPS multi-subunit tethering complex, and SNARE proteins (Lürick et al., 2018; Luzio et al., 2010).

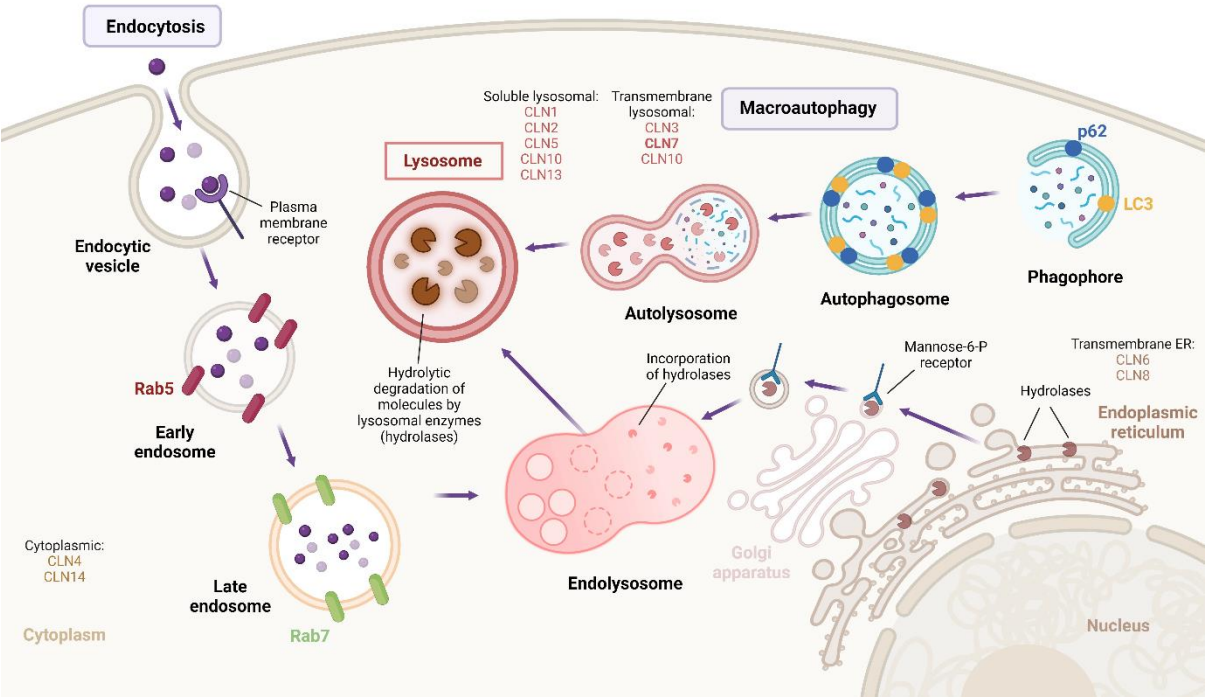

Figure 1. 7. Lysosome biogenesis and cellular localisation of the NCL proteins. Lysosome take proteins and cargos from many pathways. During endocytosis, endocytic vesicles are formed in the plasma membrane. Receptors that are not intended for lysosomes undergo recycling and are returned to either the plasma membrane or the Golgi apparatus. Early endosomes, which contain the protein Rab5, are transformed into late endosomes, characterised by the protein Rab7, which subsequently merge with lysosomes. Lysosomal hydrolases are produced and altered through the attachment of oligosaccharides in the ER and then transferred to the Golgi apparatus. Once the mannose residues in the oligosaccharide chain are identified by the mannose-6-phosphate receptor (MPR), the complexes formed by the hydrolase and MPR are transported to endolysosomes. In the case of macroautophagy (also referred to as autophagy), autophagic cargoes are transported to lysosomes through the fusion of autophagosomes and lysosomes. Lysosomes are generated from digestive lysosomes (endo-, phago-, and autolysoosmes) through the process of tubulation and scission, resulting in the formation of protolysosomes, which then develop into functional lysosomes (Yang and Wang, 2021). The majority of the NCL proteins are comprised in some of the cellular compartments that participate in this process. Specifically, CLN1, CLN2, CLN5, CLN10, and CLN13 are soluble lysosomal proteins, whereas CLN3, CLN7, and CLN10 are lysosomal transmembrane proteins. Additionally, CLN6 and CLN8 are described as transmembrane ER proteins, while CLN4 and CLN14 are cytoplasmic.

Rab proteins are members of the Ras-like GTPases superfamily and are crucial for various processes related to membrane trafficking. These processes include the production of vesicles and the transportation of vesicles in endocytosis, exocytosis, and autophagy (Agola et al., 2011; Chua et al., 2011; Tanida, 2011). GTPases shuttle between two distinct states: the GDP-bound state, which is characterised by inactivation, and the GTP-bound state, which is associated with

activation. This transition depends on the binding and subsequent hydrolysis of GTP (Cherfils and Zeghouf, 2013). There are different Rab proteins, each of which is localised to certain intracellular compartments and interacts with different proteins to regulate specific steps of vesicular trafficking (Zerial and McBride, 2001). In the case of Rab5 protein, it is found in early endosomes and recruits effector proteins to regulate the formation of endocytic vesicles, the generation of PI3P, the homotypic fusion of early endosomes, their motility on actin and microtubules, and the activation of downstream signalling pathways specifically within early endosomes (Bucci et al., n.d.; Gorvel et al., 1991; Miaczynska et al., 2004; Nielsen et al., 1999). Rab4 is also present in early endosomes, where modulates the exit of recycling cargoes back to the plasma membrane or to recycling endosomes (Sheff et al., 1999). Rab11 controls recycling to the plasma membrane in early endosomes (Jovic et al., 2010). Rab7a and Rab7b are two distinct Rab7 proteins present in mammals, which are localised in different cellular compartments and control different steps. Rab7a, usually referred to as Rab7, primarily localises to late endosomes and modulates the transport of molecules to late endocytic compartments. Specifically, it facilitates the movement of molecules from early endosomes to late endosomes and from late endosomes to lysosomes (Bucci et al., 2000). This cellular process is responsible for regulating the progression of early endosomes into late endosomes, facilitating the transportation of substances from late endosomes to lysosomes, promoting lysosome biogenesis and facilitating the fusion of late endosomes and lysosomes in the perinuclear region of the cytoplasm (Girard et al., 2014; Jovic et al., 2010). Furthermore, Rab7a is involved in multiple physiological processes, such as apoptosis (Edinger et al., 2003), neurotrophin trafficking and signalling, neurite outgrowth (Deinhardt et al., 2006; Saxena et al., 2005), phagocytosis (Harrison et al., 2003), as well as autophagy and mitophagy (Hyttinen et al., 2013; Yamano et al., 2014). In contrast, Rab7b is located within the TGN and late endosomes, and its primary function involves the regulation of transport from endosomes to the Golgi apparatus (Progida et al., 2012, 2010).

The HOPS multi-subunit complex, responsible for vacuolar/lysosomal homotypic fusion and protein sorting, exhibits a flexible structure like that of a seahorse, measuring between 28 to 35 nm in length. Notably, this complex possesses two Rab-binding sites located at opposite ends (Bröcker et al., 2012). The interaction between the HOPS and Rab7 GTPase Ypt7 via the subunits Vps41 and Vsp39 of HOPS (Ostrowicz et al., 2010) enables the fusion of late endosomes, AP-3 vesicles and autophagosomes with vacuoles, and homotypic fusion (Bröcker et al., 2010; Nickerson et al., 2009). In addition, inside the HOPS structure, the larger side is comprised of Vps33, which is responsible for interacting with SNARE proteins.

SNARE proteins are a type of membrane-associated proteins that contain specific domains of ~60 amino acids. These domains are predicted to create coiled-coil structures (Duman and Forte, 2003). SNAREs play a pivotal role in the fusion process of membranes in eukaryotic cells, including the fusion of synaptic vesicles with the plasma membrane (Han et al., 2017).

Lysosomes can also be generated through the process of phagocytosis, wherein phagosomes containing apoptotic cell remains or other molecules follow a maturation process characterised by the recycling of phagocytic receptors and alterations in phagosomal lipids and proteins. This process enables the fusion of phagosomes with lysosomes for the degradation of phagosomal contents (Wang and Yang, 2016). Similarly, lysosomes can also arise from autophagosomes that undergo a process of maturation to fuse with late endosomes/lysosomes This fusion process involves the action of proteins such as Rab7, HOPS, and SNARE, as it happens in the abovementioned endosome-lysosomes fusion (Yang and Wang, 2021). In this case, incipient autophagosomes and vesicles originating from the endosomal compartments fuse to generate degradative autolysosomes. These autolysosomes serve as the structures that contain both autophagic and lysosome components, including hydrolases responsible for content degradation (Eskelinen, 2005).

1.2.5 MFSD8 as a lysosomal transmembrane protein

The NCLs have been classified as LSDs, and *CLN7/MFSD8* is associated with the vLINCL subtype. Some studies have shown that MFSD8, when overexpressed, co-localises with lysosomal markers, suggesting its potential role in facilitating transport across the lysosomal membrane (Siintola et al., 2007) (**Figure 1.1**). Additionally, native untagged MFSD8 has been found to localise to the lysosomes and late endosomes. This localisation was determined by studying its co-localisation with the late endosomal/lysosomal marker LAMP1 (Sharifi et al., 2010). These findings indicate the existence of lysosomal targeting motifs within the MFSD8 sequence. These motifs, such as dileucine- or tyrosine-based motifs, are typically found in the cytosolic tails of lysosomal membrane proteins (Bonifacino and Traub, 2003). The N-terminal region of the human MFSD8 protein encompasses a [DE]XXXL[IL]-type dileucine motif (9-EQEPLL-14). This motif is conserved in vertebrates and is considered as a crucial factor in determining the localisation of the protein to lysosomes. The 22-EWDIL-26 motif can be also considered another dileucine-type motif, even though it is neither canonical nor conserved among vertebrates. The C-terminal region encloses two tyrosine-based motifs (503-YKRL-506 and 513-YGRI-516) that are conserved to varying degrees among vertebrates. The fifth cytosolic loop of MFSD8 contains an additional tyrosine-based, specifically at residues 441 to 445, denoted as 441-YSKIL-445 (Sharifi et al., 2010).

MFSD8 has been recently described to encode for a **transmembrane lysosomal protein** potentially functioning as a **chloride channel**, which regulates the transport of chloride ions from the lysosome to the cytosol (Yayu Wang et al., 2021). However, there is a limited understanding of its molecular biology. The mechanistic explanation for the loss of MFSD8 protein function at the lysosomes, and its subsequent impact on disease, has not been elucidated, hence hindering our comprehension of the underlying link between cause and effect. Therefore, the lack of insights and knowledge regarding the underlying mechanism of vLINCL caused by mutations in *MFSD8* requires further study based on the molecular biology of MFSD8. For that reason, this study aims to assess and characterise MFSD8 at both cellular and molecular levels to enhance comprehension of the underlying molecular mechanisms contributing to the development of the disease, as the vast majority of the work on CLN7 disease has been conducted in cells that are not directly related to neurological diseases.

1.3 Studies on the variant late-infantile NCL CLN7

Several studies have been conducted in naturally occurring or genetically modified animal models of CLN7 disease, including *Drosophila melanogaster*, mice, Chihuahua dogs, and macaques (Brudvig and Weimer, 2022; Chen et al., 2020; Connolly et al., 2019; Faller et al., 2016; McBride et al., 2018a; Rowe et al., 2022). Some of these studies employing different animal models were established to improve the understanding of the molecular pathogenicity; the gene expression and protein function, or investigation of a potential gene therapy for CLN7 (Brudvig and Weimer, 2022; Chen et al., 2022, 2020). Although CLN7 disease has been identified as a promising candidate for gene therapies that target the brain, it is important to note that there is currently no cure or treatment available for this disease.

Kim et al. (2019) developed the first "N-of-1" therapeutic drug for a patient diagnosed with a rare disease – the vLINCLN CLN7. This drug was tailored specifically to target the patient's particular pathogenic mutation, serving as an example of personalised genomic medicine. They identified a new type of splicing mutation and, within a year, they created a customised drug using antisense oligonucleotides to modify the splicing and treat the patient. This treatment successfully reduced seizures and did not cause any major side effects. The 22-nucleotide antisense oligonucleotide was called Milasen and has a similar backbone and sugar chemistry modifications (phosphorothioate and 2'-O-methoxyethyl) as nusinersen, an FDA-approved drug for treating infantile-onset muscular dystrophy (Finkel et al., 2016). This therapy for CLN7 disease corroborates the need of the intact endogenous gene and a proper splicing process to develop an effective approach to restore *MFSD8* in CLN7 patients.

Additionally, Chen et al. (2022) reported an *in vivo* preclinical model, in which adeno-associated virus serotype 9 (AAV9) with the full-length *MFSD8* were administered intrathecally to *Mfsd8*$^{-/-}$ mice, using either a high or low dose, resulting in noticeable effects that varied depending on the age and dosage. Administering a high dose of AAV9/*MFSD8* between postnatal days 7 and 10 led to prominent expression of MFSD8 mRNA, a decrease in the accumulation of SCMAS and glial fibrillary acidic protein immunoreactivity, improvement in impaired behaviours, a doubling of the lifespan, and higher body weight. This intrathecal delivery of AAV9/*MFSD8* seemed to be harmless and effective (Chen et al., 2022). However, it should be acknowledged that animal models may not fully replicate the pathophysiology of human disease, which can limit their effectiveness in assessing drug efficacy during clinical trials (Grskovic *et al.*, 2011). The constraints associated with the use of animal models to investigate pathology and disease in neurological disorders mostly stem from differences in brain cell types and neuronal networks. Furthermore, in the context of neurological diseases (Okano and Yamanaka, 2014), as well as cardiac diseases (Parrotta et al., 2019), there are significant challenges associated with accessing the site of injury and obtaining tissue samples.

1.4 Models of study for neurodegenerative diseases

1.4.1 Animal models: *in vivo* disease models

Animal models have been employed in the investigation of neurodegenerative diseases, as they provide insights into the aetiology and pathobiology of these disorders (Jankowsky et al., 2002; McGowan et al., 2006). However, these models have limitations since they typically involve the overexpression of mutant proteins, which might interfere with the pathology in the animal and hinder the comprehension of the initiation and development of neurodegenerative disorders (Hartung, 2008; Kokjohn and Roher, 2009). Moreover, the utilisation of animal models give rise to ethical concerns about their application in research. In 1959, Russel and Burch introduced the principle of the 3Rs, which addresses ethical concerns by reducing the quantity of animals used in experiments, refining methods to enhance animal welfare, and replacing animal use with alternative methods (Russell and Burch, 1959). Therefore, in order to adhere to the 3Rs principle, it is necessary to create and use innovative models to better understand the underlying mechanisms of neurodegenerative diseases. This will ultimately pave the way for these models to be employed in the development of therapeutic strategies. Furthermore, other constraints of animal models also arise from the dissimilarities and variations among those species (Barroca et al., 2022; Cendelin et al., 2022). Specifically, mouse models have been generated and extensively used to investigate the influence of environmental and genetic factors on neurodegenerative disorders (Bloom et al., 2005;

Trancikova et al., 2011; Wong et al., 2002). Nevertheless, these genetic models are unable to accurately replicate all the clinical characteristics of human neurodegenerative disorders. For instance, mouse models of AD, PD, and HD rarely exhibit significant neuronal cell death or the gradual deterioration of the nervous system that defines these human disorders (Blesa and Przedborski, 2014; Jankowsky and Zheng, 2017). Moreover, there is also emerging data that highlight inherent functional differences between human and mouse cells. These distinctions encompass various aspects such as developmental stages, the speed of protein degradation, RNA processing, cell biology of glia cells, and global transcriptomes (Dawson et al., 2018; Han et al., 2013; Oberheim et al., 2009; Rayon et al., 2020; Zhang et al., 2016). The variations inherent to each species are probably responsible for some of the difficulties encountered when using mouse-based models to simulate human diseases.

1.4.2 Human cell/tissue models: *in vitro* disease model

The use of human tissue for the investigation of neurodegenerative diseases is limited due to the challenge of acquiring brain or spinal cord tissue from patients at different stages of the disease. Therefore, it is crucial to generate models that replicate the progression of neurodegenerative diseases to gain a deeper understanding of the pathogenesis and pathobiology of such conditions. Utilising induced pluripotent stem cells (iPSCs) is a highly promising method for modelling and studying neurodegenerative diseases *in vitro*. iPSCs can be produced through the process of reprogramming somatic cells, including fibroblasts and peripheral blood cells, collected from both healthy individuals and patients, as it is described below.

1.4.2.1 Stem cells and iPSCs

Ever since their first identification in the 1960s, stem cells have played a crucial role in the field of biology. Stem cells are characterised by their capacity to undergo differentiation into many cell lineages – also known as pluripotency – and sustain self-renewal indefinitely without undergoing senescence. Senescence is a cellular reaction marked by a permanent halt in growth and other observable changes, such as the release of proinflammatory substances (McHugh and Gil, 2017). It contributes to regular development and the maintenance of tissue homeostasis and is a typical feature of ageing, defined by the irreversible exit from the cell cycle in response to cellular damage and stress (Zhang et al., 2022). Pluripotent stem cells are especially valuable since they have the ability to transform into any type of cell found in the adult body. This makes them extremely effective for producing cells that are difficult to obtain from original tissue, such as neurons. Pluripotent stem cells are exclusively present in the developing embryo during its pre-implantation phase, subsequent to which their capacity and ability of pluripotency and self-renewing diminish.

Although embryonic stem cells (ESCs) can be useful in research, their isolation presents both technical and ethical issues. In 2006, Takahashi and Yamanaka published a significant report that presented a technique for producing induced pluripotent stem cells (iPSCs), thereby resolving these issues (Singh et al., 2015; Takahashi and Yamanaka, 2006). Through the exposure of fully matured cells to a combination of reprogramming factors, Takahashi and Yamanaka successfully produced iPSCs that closely resemble ESCs in terms of their characteristics. Subsequently, several other reprogramming factors, along with alternative techniques such as viral vectors, have been produced for this objective. Furthermore, the emergence of clustered regularly interspaced palindromic repeats (CRISPR-Cas9) technology has facilitated the production of iPSCs containing any identified mutation.

iPSCs are highly useful for disease modelling, and they can even be used to generate patient-derived models, which greatly contributes to research in the field of personalised medicine, making them a useful model to study CLN7 disease.

1.4.2.2 iPSC technology: cell reprogramming

Both somatic cell nuclear transfer (SCNT) and ESC fusion can transform a specialised cell into a state with increased potential for differentiation (Bradley et al., 1984; Doetschman et al., 1987; Gurdon, 1962; Gurdon et al., 1958). These findings indicated the presence of unidentified reprogramming factors than can remove somatic cell memories through an epigenetic mechanism. To identify these reprogramming factors, Takahashi and Yamanaka proposed the hypothesis that genes which are especially active in ESCs have a role in determining the unique properties, such as their ability to differentiate and proliferate (Karagiannis et al., 2019). Additionally, they postulated that these factors have the potential to convert specialised somatic cells into cells that resemble embryonic stem cells. By employing subtraction, they detected expressed-sequence tags (ESTs) that were more abundant in mouse ES complementary DNA (cDNA) pools. By utilising this sequencing data, they acquired complete sequences of cDNAs that encode previously undiscovered genes responsible for pluripotency in both ESCs and the inner cell mass. They assigned the name ESC-associated transcripts (ECATs) to these cDNAs (Mitsui et al., 2003).

Through the examination of each ECAT gene, Takahashi and Yamanaka identified 24 genes that qualified as potential reprogramming factors. In light of the improbability that all 24 factors were necessary for the production of ESC-like cells, their next objective was to narrow down the potential reprogramming factors to a minimal set. Through the elimination of one element from the collection of 24 genes, a total of 24 combinations were examined for reprogramming, After the initial set of trials, the number of potential genes was reduced to 10. A further set of studies

demonstrated that the omission of any gene of four specific genes consistently impaired the development of colonies. Conducting experiments on various combinations of these four genes verified that when the transcription factors OCT3/4, SOX2, KLF4, and c-MYC (referred to as OSKM) were overexpressed in mouse fibroblasts, it was possible to produce ESC-like cells, also known as induced pluripotent stem cells (iPSCs) (Takahashi and Yamanaka, 2006).

Following their successful generation of mouse iPSCs, Takahashi and Yamanaka subsequently proved that the identical set of four factors was adequate for generating human iPSCs (Takahashi et al., 2007). Concurrently, James Thomson and his team reported the generation of human iPSCs employing a distinct combination of four factors (Yu et al., 2007). Among the factors examined, OCT3/4 and SOX2 were found to be shared, whereas NANOG and LIN28 were shown to be different compared to Takahashi and Yamanaka's study. Following this advancement, researchers have employed this method to convert a specific somatic cell type into an iPSC state. This process has shown that it provides the cell the ability to differentiate into practically any cell type found in the body.

Throughout the years, several models have been suggested to elucidate the mechanism that induce cellular reprogramming into the pluripotent state. The variabilities and inefficiencies in iPSC generation have resulted in a wide range of methods for iPSC development, including the use of viruses, DNA, RNA, or recombinant proteins.

1.4.2.3 Human iPSCs generation and characterisation

The utilisation of iPSCs has emerged as a significant breakthrough in neuroscience research, addressing ethical concerns and resolving source restrictions associated with the use of ESCs (derived directly from the disrupted embryo) or primary cell cultures in the production of disease models for neurodegenerative disorders.

Human iPSCs (hiPSCs) are mostly cultured and maintained in the form of colonies due to their limited viability as individual cells, in contrast to mice iPSCS. The process of passaging new colonies of hiPSCs needs mechanical manipulation, and it typically requires approximately five to ten passages for the cells to achieve stability and adapt to enzymatic separation (Lerou et al., 2008). Various characteristics and criteria have been established to describe and identify reprogrammed cells that have achieved effective reprogramming. These encompass the evaluation of pluripotency, morphology, as well as molecular and functional properties. When examining morphology, hiPSCs exhibit specific characteristics, which include possessing a large nucleus and a reduced amount of cytoplasm (Krasnova et al., 2022) (**Figure 1.8**).

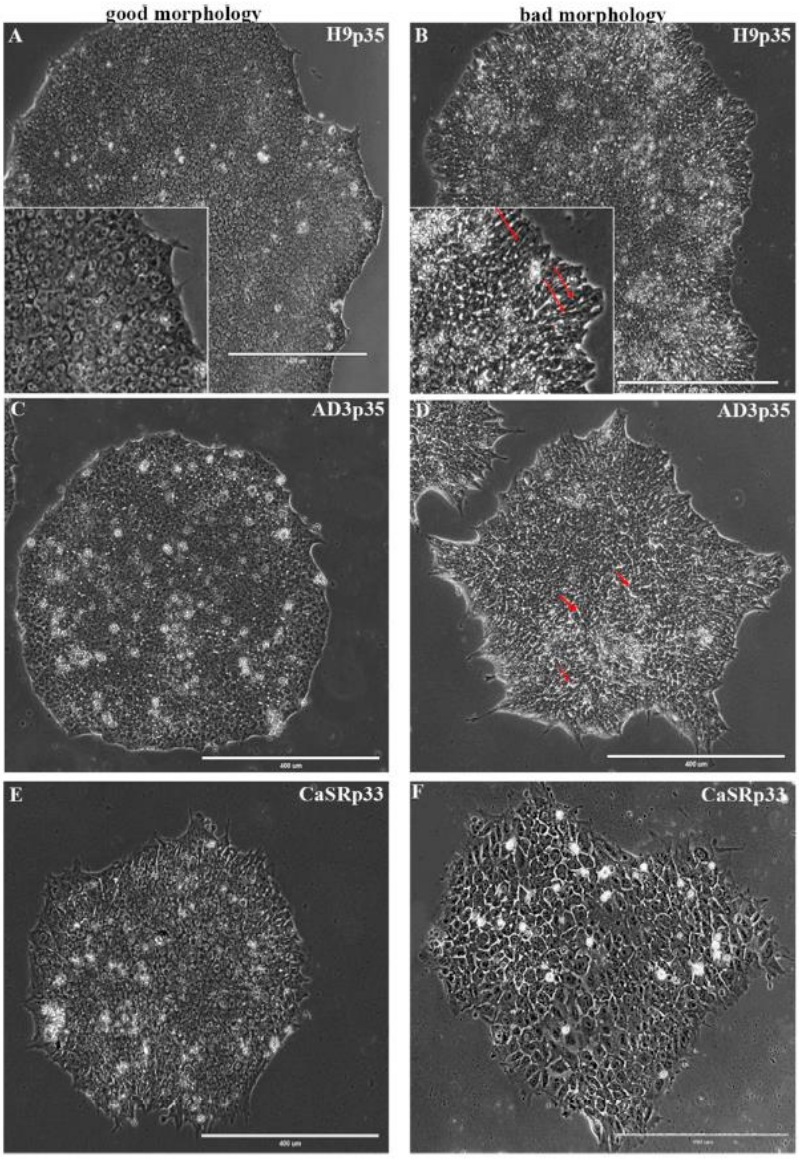

Figure 1. 8. Morphological characteristics of hiPSC colonies exhibiting different phenotypes. (**A**, **C**, **E**) Representative images of high-quality hiPSC colonies, characterised by a flat structure, well-defined edges, and a high ratio of nucleus to cytoplasm. The cells within these colonies are closely packed, with square-shaped nucleoli. (**B**, **D**, **F**) Characteristic morphology of more differentiated hiPSC colonies, exhibiting a modified cell structure (elongated cells indicated by long arrows) and cells that are loosely arranged with evident phase-bright gaps between them (small arrows). During the initial 3-4 days after plating, colonies may display a less compact arrangement as they expand. (Scale bar = 400 μm). Images adapted from Krasnova et al. (2022).

Additionally, hiPSCs must show the ability for indefinite self-renewal (Robinton and Daley, 2012a; Wakao et al., 2012). In order to be considered iPSCs at the molecular level, several criteria must be met. First, iPSCs must exhibit the presence of stem cells markers, including pluripotency factors such as OCT3/4, SOX2, and NANOG, as well as cell surface antigens like SSEA-3/-4 and TRA-1-60/-80 (Castro-Viñuelas et al., 2020) (**Figure 1.9**). Second, functional telomerase expression is necessary. Third, retroviral silencing gene expression, specifically the activation of de novo methyltransferases and Trim28, must occur (Lei et al., 1996; Wolf and Goff, 2007). Finally, iPSCs should demonstrate epigenetic similarities to ESCs, such as DNA methylation at the promoters of pluripotency genes, X chromosome reactivation in female cells, and the presence of bivalent domains at developmental genes (Bernstein et al., 2006; Maherali et al., 2007; Rideout et al., 2001; Wernig et al., 2007).

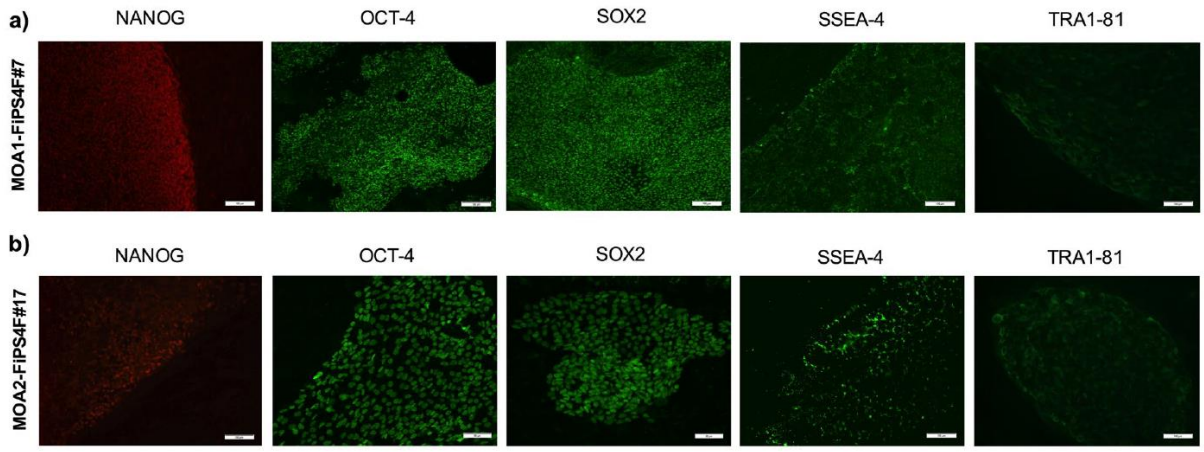

Figure 1. 9. Expression of pluripotency-associated proteins in hiPSCs using immunofluorescence. (**a**) Immunofluorescences staining showing the presence of pluripotency markers, such as NANOG, OCT-4, SSEA-4, and TRA-1-81 in the iPSC-line MOA1-FiPS4F#7 (iPSC-line from patient with rhizarthrosis and non-erosive hand OA in the right hand) (Scale bar = 100 μm). (**b**) Immunofluorescence staining showing the presence of pluripotency markers, including NANOG, OCT-4, SSEA-4, and TRA-1-81 in the iPSC-line MOA2-FiPS4F#17 (iPSC-line from patient with rhizarthrosis and non-erosive hand OA in both hands) (Scale bar = 100 μm, except for the images of OCT-4 and SOX2, where the scale bar is 50 μm). Images adapted from Castro-Viñuelas et al. (2020).

In order to fulfil their intended purpose, iPSCs must have the ability to differentiate into the three embryonic germ layers (ectoderm, endoderm, and mesoderm) (Jaenisch and Young, 2008). The endoderm is the first set of cells of the three germ layers and is the embryonic precursor of several organs such as the thyroid, lungs, pancreas, liver, and intestines. These cells undergo four developmental steps, including proliferation and induction of pluripotent stem cells (PSCs), the dissociation of stem cell-derived endoderm and mesoderm germ layers formed from stem cells,

anterior-posterior patterning, and bifurcation of the liver and pancreas (Muhr et al., 2023). In vertebrates, the mesodermal cells grow surrounding the notochord, ultimately give rise to the vertebral column that extends towards the midbrain. The mesoderm is divided into three different embryonic precursors, which are the paraxial (also known as axial), intermediate, and lateral (or lateral plate) regions. These mesodermal embryonic precursors play a crucial role in the development of diverse cell types and tissues, including smooth, cardiac, and skeletal muscle, kidney, reproductive system, tongue and pharyngeal arches, connective tissue, bone, cartilage, dermis and subcutaneous layers, dura mater, vascular endothelium, blood cells, microglia, and adrenal cortex (Muhr et al., 2023). Additionally, it is worth noting that throughout embryonic development, the ectoderm undergoes a transformation and gives rise to the neuroectoderm, a crucial component responsible for the formation of the brain and spinal cord (Muhr et al., 2023) (**Figure 1.10**).

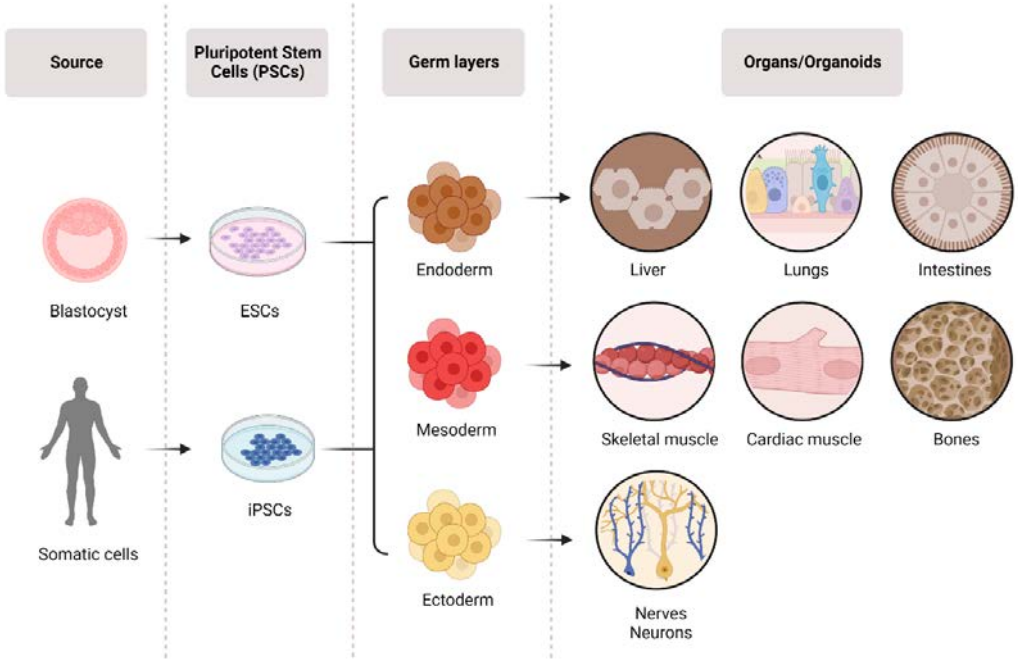

Figure 1. 10. Origin and development of pluripotent stem cells (PSCs). Blastocysts, which represent an early stage of embryonic development, contain a population of pluripotent cells known as embryonic stem cells (ESCs). These ESCs are characterised by their capacity for self-renewal and their ability to differentiate into all three primary germ layers: ectoderm, mesoderm, and endoderm. In contrast, somatic cells, which are fully differentiated cells obtained from adult tissues, can be reprogrammed through the introduction of specific transcription factors to generate induced pluripotent stem cells (iPSCs). These iPSCs exhibit properties similar to ESCs, including pluripotency and the potential to differentiate into derivatives of all three embryonic germ layers. The three primary germ layers – endoderm, mesoderm, and ectoderm – give rise to distinct organ systems during embryonic development. The endoderm is responsible for the development of the gastrointestinal tract, respiratory system, and liver. The mesoderm generates the kidneys, bones, and blood circulatory system, whereas the ectoderm undergoes differentiation to form the brain. ESCs and iPSCs can also be used *in vivo* for the purpose of generating organoids to study human developmental biology.

1.4.2.4 Factors influencing cell differentiation from iPSCs

Cell differentiation from iPSCs can be influenced by various factors that either hamper or stimulate the process. The efficacy of differentiation can be hampered by several challenges, including the lack of uniformity in embryoid body (EB) size, which can lead to nonhomogeneous and asynchronous differentiation, impacting the overall quality and consistency of the differentiated cells (Di Baldassarre et al., 2018). This can be overcome in some cases by the use of a determined number of iPSCs when generation the EBs in cell culture. Additionally, the epigenetic memory of reprogrammed cells can influence differentiation efficiency. This epigenetic memory refers to residual epigenetic markers from the original somatic cells, which can affect the differentiation potential and behaviour of iPSCs (Di Baldassarre et al, 2018). Variability in the quality of iPSCs generated due to technical challenges in the reprogramming process can also result in poor differentiation outcomes during differentiation (Di Baldassarre et al., 2018). Moreover, the use of conventional methods using murine feeder cells or other reagents generated from different species can present significant challenges when aiming to obtain differentiated cells for clinical applications. In these cases, the differentiation methods need to be adapted to exclude xenogeneic antigens (Netsrithong et al., 2024).

Conversely, numerous strategies have emerged that stimulate and optimise cell differentiation. These include the identification and application of optimal conditions specific for different cell lineages (Yasui et al., 2021). In addition, there is evidence demonstrating that electrical stimulation and other biophysical stimuli can promote differentiation. For instance, electrical stimulation has been shown to enhance cardiac differentiation of iPSCs (Iberite et al., 2022). Similarly, mechanical stimuli can help recreate a biomimetic environment, aiding in the differentiation and maturation of specific cell types like skeletal muscle cells (Iberite et al., 2022). Additionally, co-culturing iPSCs with muscle cell populations or using human origin feeder cells can enhance differentiation by also providing a more supportive and biomimetic environment (Iberite et al., 2022). Furthermore, feeder-free and serum-free monolayer methods for deriving hematopoietic cells from iPSCs can provide high-purity cells, making them suitable for both research and clinical applications (Netsrithong et al., 2024). Developing and optimising differentiation protocols that are reproducible across different iPSC lines can significantly enhance the efficiency and consistency of the differentiation process (Iberite et al., 2022).

1.4.2.5 Neural differentiation of iPSCs

The utilisation of patient-derived iPSCs holds promise for investigating specific neurological disorders, overcoming the constraints associated with animal models, ethical concerns, and the

scarcity of human samples (Saha and Jaenisch, 2009). For certain cell types, such as human brain cells, it is not possible to obtain them from living individuals. While post-mortem tissues can be used for research purposes, they often do not provide a reliable model for studying disease mechanism due to the effect of secondary and tertiary consequences of the disease that the tissues have suffered. iPSCs have the capacity to undergo differentiation into neural stem cells (NSCs) in a 3-dimensional (3D) environment (known as neurospheres), 2-dimensional (2D) NSCs (referred to as neural rosettes), and primitive NSCs (Elkabetz et al., 2008; Shin et al., 2019). NSCs are tripotent cells that have the ability to differentiate into three distinct neural lineage cells: neurons, astrocytes, and oligodendrocytes (Glaser et al., 2007).

In the context of this study, enzymatic dissociation can be employed to differentiate rosette-forming NSCs into Neural Progenitor Cells (NPCs), which represent an intermediate stage of individual cells capable of generating both neurons and glial cells. This technique has contributed to significant advancements in neural differentiation models, facilitating the study neurological disorders (Malatesta et al., 2000; Merkle et al., 2004; Noctor et al., 2001; Tamamaki et al., 2001).

1.5 Use of iPSC-derived neural cells to model neurodegenerative diseases

The cellular models of neurodegenerative diseases vary in complexity, ranging from basic two-dimensional monolayers obtained from immortalised cell lines to elaborate three-dimensional multicellular organoids that closely resemble actual tissue. These are capable of reproducing numerous disease characteristics and *in vivo* physiological environments. Several studies have used two-dimensional cell cultures obtained from iPSCs for modelling these diseases.

1.5.1 iPSC-derived cell cultures to model Alzheimer's disease

AD is the most common neurodegenerative disorder, characterised by the build-up of beta-amyloid (Aβ) plaques and neurofibrillary tangles (Tanzi and Bertram, 2005). These tangles are formed by the presence of microtubule tau inside neurons. Patients with AD experience cognitive impairments and memory decline due to neuronal degeneration, mostly affecting the medial temporal lobe and neocortical regions (Davis et al., 1995). Exposure to environmental variables and possessing the E4 allele of the apolipoprotein E (*APOE ε4*) gene are associates with a higher likelihood of developing sporadic AD. APOE ε4 proteins had significantly lower efficacy in the degradation of Aβ plaques compared to the APOE ε2 and APOE ε3 alleles. Early-onset familial AD is characterised by the occurrence of mutations in the amyloid precursor protein (APP), presenilin 1 (*PSEN 1*), and presenilin 2 (*PSEN 2*) genes (Dorszewska et al., 2016).

Wang *et al.* (2018) observed and elevation in the generation of Aβ and p-tau levels in hiPSC-derived APOE ε4 neurons. The study, which focused on two-dimensional analysis, also observed

degeneration of GABAergic neurons caused by the APOE ε4 variation. Nevertheless, the pathogenic behaviour was eradicated through the post-conversion of APOE ε4 to isogenic APOE ε3 utilising the APOE structural corrector PH002. This not only validates the disease-causing activity of APOE ε4 associated with AD, but also emphasised a novel strategy for targeting AD related to APOE ε4 (Wang et al., 2018). This study exemplifies the integration of two-dimensional modelling with iPSCs to overcome challenges like specie variability, as iPSCs are ethically derived from humans. The methodology also reduces the need of animals, such as mice models, as they do not possess APOE ε4.

1.5.2 iPSC-derived cell cultures to model Parkinson's disease

PD is another severe neurodegenerative disorder characterised by impaired motor function and it is the second most common neurological condition, following AD. The dopaminergic neurons located in the substantia nigra are affected and harmed by several mechanisms, such as the aggregation and misfolding of α-synuclein, mitochondrial apoptosis, and excitotoxicity (Beal, 1998; Exner et al., 2012; Yasuda and Mochizuki, 2010). The disease manifests later in life and can be classified into two forms: the idiopathic type, which occurs without a known cause, and the rare familial variation. Both types exhibit the characteristic symptoms of bradykinesia (slowness of movement), tremor, and muscle rigidity. Gene-linked PD is characterised by several mutations in the α-synuclein gene, leucine-rich repeat kinase 2 (*LRRK2*), and PTEN-induced kinase 1 (*PINK1*) genes. LRRK2 is an essential protein that plays a crucial role in autophagy and the preservation of cellular functioning (Skibinski et al., 2014).

A study conducted by di Domenico *et al.* (2019) developed a co-culture of neurons and astrocytes to investigate the communication between midbrain dopaminergic (mDA) neurons and astrocytes obtained from mutant LRRK2-iPSCs. In comparison to the healthy controls, the mutant G2019SLRRK2 mDA-astrocyte model accurately reproduced the characteristic phenotype of PD (Domenico et al., 2019). This encompasses the accumulation of α-synuclein, premature cell death, and structural changes such as membrane loss in the mDA neurons. Astrocytes provide a neuroprotective effect in cells by clearing debris, promoting inflammation, and reducing the harmful effects of excessive glutamate activity (Sidoryk-Wegrzynowicz et al., 2011). Nevertheless, di Domenico's research showed that when PD-derived astrocytes were cultured together with healthy control neurons, the astrocytes actively participated in the degeneration of the healthy dopaminergic neurons.

1.5.3 iPSC-derived cell cultures to model amyotrophic lateral sclerosis

ALS is a neurodegenerative disease characterised by the gradual impairments of motor function. This occurs due to the degeneration of the upper motor neurons in the brainstem and the lower motor neurons in the spinal cord (Chou and Norris, 1993; Rothstein, 2009). The adult-onset typically affects individuals who are 55 years of age or older. ALS is classified by two forms: sporadic ALS (SALS) and familial ALS (FALS). The primary mutant genes linked to FALS are TAR DNA-binding protein 43 (*TDP-43*), *SOD1*, and *C9orf72* (Cudkowicz et al., 1997; DeJesus-Hernandez et al., 2011; Renton et al., 2011; Rosen et al., 1993b; Sreedharan et al., 2008; Yokoseki et al., 2008).

Egawa *et al.* (2012) differentiated iPSCs obtained from familial ALS patients, who possess mutations in the TDP-43 protein, into motor neurons as a model to study the ALS aetiology and drug screening. These motor neurons produced from iPSCs of ALS patients displayed cytosolic aggregates resembling those observed in post-mortem tissue from ALS patients. Additionally, these motor neurons had elevated levels of mutant TDP-43, which was present in an insoluble state and bound to a spliceosomal factor called SNRPB2. Their investigation involved the analysis of four compounds, and they discovered that anacardic acid, a histone acetyltransferase inhibitor, successfully restored the aberrant ALS motor neuron phenotype (Egawa et al., 2012). These results indicated that motor neurons produced from iPSCs taken from ALS patients could be a valuable resource for studying the causes of ALS and for evaluating potential drugs.

1.5.4 iPSC-derived cell cultures to model Huntington's disease

Huntington's disease (HD) is an inherited neurological condition characterised by the amplification of CAG repeats in the huntingtin (*Htt*) gene (MacDonald et al., 1993). The expansion of the CAG repeat sequence leads to the deterioration of the GABAergic projection neurons in the striatum areas, resulting in the appearance of involuntary movement and mental disorders (Glass et al., 2000; Snowden et al., 1998). There is currently no effective treatment for HD and, despite being identified over twenty years ago, the precise mechanism behind the neurodegeneration of HD is still not completely understood. However, Zhang *et al.* (2010) were considered the first researchers to create a HD model using iPSCs. They generated neural precursor cells and human striatal neurons from fibroblasts of patients suffering from HD using the protocol of embryoid body formation. To accomplish this, the HD-NSCs were exposed to a differentiation condition that involved the combination of morphogens and neutrophins to promote the differentiation of the cells to the striatal lineage. The striatal neurons and neuronal precursors produced from HD-iPSCs possessed the identical CAG expansion found in the HD

patient, as well as the expression of markers such as the dopamine- and cyclic AMP-regulated phosphoprotein (DARPP-32) for neurons in the striatum. Furthermore, the HD-NSCs exhibited increased caspase activity when deprived of growth factors, in contrast to NSCs derived from normal iPSCs (N. Zhang et al., 2010). Therefore, these specialised cells have the potential to generate a human HD cell model that can be effective for investigating HD mechanisms and drug screening.

1.5.5 iPSC-derived cell cultures to model CLN7 disease

To date, iPSCs have been employed to investigate the release and uptake of disease-related proteins in neurodegenerative diseases, including tau in AD, α-syn in PD, SOD in ALS, and mHTT in Huntington's disease, among others. However, no CLN7 patient-derived iPSC-based model have been employed so far to study the vLINCL CLN7.

Utilising iPSC-derived cells to study neurodegenerative disorders can be a potent method to provide a human-based system to understand the mechanisms behind the onset and development of these diseases. For those reasons, this project will use CLN7-patient derived iPSCs that will be differentiated into NPCs to study the molecular mechanism of the vLINCL CLN7 by reproducing the characteristic phenotype of this disease. Specifically, two NPC types carrying the disease-causing mutations p.T294K and p.R465W will be compared to wild-type (WT, control) NPCs in order to elucidate in more depth the cellular and molecular biology of MFSD8 by conducting protein expression and protein-protein interactions assays.

Thesis aims and rationale

A better understanding of the mechanisms underlying the vLINCL CLN7 is imperative to the development of potential therapeutic strategies to treat this disease and improve or increase patients' lifespan. CLN7 disease is a complex condition, and due to the severity and early onset of this disorder, the patients suffering from it require a lot of help and care, given the fact that there are currently no strategies to target the CLN7 disease and prevent the progression of the disease. Consequently, understanding the cellular and molecular biology of MFSD8 and uncovering novel insights into the pathogenesis of CLN7 disease can revolutionise the research field of NCLs and other adult neurodegenerative disorders that have been identified with the same disease-causing mutations and significantly impact patient survival and patients' quality of life.

As previously introduced, despite significant advances in targeted and personalised therapies, such as the example of N-of-1 therapies using antisense oligonucleotides, no established treatment is currently available, and CLN7 patients' lifespan continues to be overly short. Although some studies have shown the use of adeno-associated viral (AAV) gene therapy as a potential therapeutic

strategy to ameliorate the disease in preclinical models (Chen et al., 2022), no current evidence demonstrates an effective impact of this gene therapy in advanced clinical studies. Therefore, understanding the underlying mechanisms of some *CLN7* mutations and CLN7 protein interactions is imperative for the identification of novel targets and the generation of more effective therapeutic modalities that prevent the failure of the development of CLN7 disease treatment.

Strong evidence suggests that MFSD8 plays a central role in the lysosome, a key player in cellular recycling and homeostasis, where MFSD8 may function as a chloride channel (Yayu Wang et al., 2021). However, other studies have shown the presence of MFSD8 in the nucleus (Geier et al., 2019), which remains to be demonstrated. Consistent with this, previous proteomics data from McKay's group have shown downregulation of nuclear genes in CLN7 patient-derived NPCs compared to age-matched controls. Therefore, it is important to address the potential impact of different possible MFSD8 localisations within the cell and the corresponding function in each cellular compartment using relevant models. This is not only crucial to advance our understanding of the MFSD8 cellular mechanism in the vLINCL CLN7 but can also provide novel insights into its treatment and improvement of other adult neurodegenerative diseases caused by heterozygous mutations in the same gene, including ALS, FTLD, maculopathies, and retinopathies. In this context, the development of novel cellular processes targeting approaches that effectively prevent the deleterious effects of CLN7 disease can be particularly attractive. However, only targeting a particular cellular process can hamper other aspects of cell functioning or be detrimental to the rest of the cells. For that reason, it is also important to investigate the potential MFSD8 interactors to address future clinical research in more specific targets as an alternative to treatments based on gene editing.

Considering the above observations, the main objective of this PhD study is to test the central hypothesis that **MFSD8 also localises to the nucleus and plays a crucial role in neuron survival and homeostasis in CLN7 disease**. To obtain evidence that demonstrates this, as well as provide novel insights into the cellular and molecular pathogenesis of CLN7 disease, the four specific aims of this work are the following:

Aim 1) To generate NPCs from CLN7 patient-derived iPSCs and age-matched controls as a relevant model to study the vLINCL CLN7.

For this aim, previously generated iPSCs from two CLN7 patients carrying different mutations and a control donor will be differentiated into NPCs using an established method by Dr Lorna FitzPatrick (a former member of McKay's group). The pluripotency state of the iPSCs will be

analysed before employing these cells for further differentiation and the neuronal expression markers of the generated NPCs will be also evaluated to characterise both cell types. After NPC generation, cells will be stored, expanded, and utilised from passages 6 to 12 to study CLN7 disease pathogenesis and the MFSD8 protein.

Aim 2) To study the effects of CLN7 disease underlying pathogenic characteristics in different cell compartments *in vitro* and how they could be ameliorated. The cell compartments studied will include the lysosomes, autophagosomes, and mitochondria. Considering that autophagy is impaired in many neurodegenerative diseases, the expression of different autophagy proteins will be observed in control and CLN7-derived NPCs, as well as the co-localisation of MFSD8 in various vesicular compartments.

As part of this aim, we have established a collaboration with the group of Prof Diego Medina from TIGEM in Naples to determine whether tamoxifen, as an FDA-approved drug, could contribute to the clearance of lysosomal Gb3 in control and CLN7 patient-derived NPCs. We hypothesise that tamoxifen can be repurposed and used in CLN7 patients to ameliorate the lysosomal phenotype observed in CLN7 disease. Another collaboration was established with the group of Prof Juan P Bolaños from the University of Salamanca for the accomplishment of this aim. Our hypothesis is that the compound AZ67, which is an inhibitor of the glycolytic enzyme PFKFB3 in mitochondria, can restore mitochondrial condensation in the perinuclear region of cells. These compounds will be tested *in vitro*, using CLN7 patient-derived and control NPCs, followed by fluorescence staining of the lysosomes to assess the effect of tamoxifen. Moreover, mitochondria of NPCs will be stained to elucidate whether AZ67 can re-establish them in the treated cells. Finally, we will observe whether MFSD8 co-localises to any vesicular cell compartment, and we will study how autophagy is affected in CLN7 patient-derived NPCs compared to control NPCs by immunocytochemistry.

Aim 3) To characterise MFSD8 to gain a deeper understanding of its function within the cell.

To achieve this aim, the expression of MFSD8 will be first evaluated in different cell types, such as HEK293T cells, SH-SY5Y cells, as well as CLN7 patient-derived and control NPCs using immunocytochemistry. This aim will also include the observation of MFSD8 in the cytoplasmic and nuclear fraction of NPCs by immunoblotting. In addition, the previously predicted and studied post-translational modifications of MFSD8 will be assessed using the treatments with the corresponding enzymes. This work will help us establish a better understanding of MFSD8 molecular biology so that more precise knowledge is available for potential future MFSD8-targeting approaches.

Aim 4) To explore the potential protein binding partners of MFSD8 to provide new insights into the precise MFSD8 function and identify alternative signalling pathways as therapeutic targets to ameliorate CLN7 disease and other adult dementias associated with this gene.

This aim will be achieved by first visualising the predicted protein-protein interactions of MFSD8 that have previously been reported using the STRING database to gain an initial understanding and use for further comparisons with experimental data. We will pull down the endogenous MFSD8 from SH-SY5Y cells, given that they are neuroblastoma cells that are easy to maintain and will provide enough material for the co-immunoprecipitation experiment. This co-immunoprecipitation experiment will help us isolate MFSD8 along with its potential interactors, subsequently aiming to identify them using mass spectrometry-based proteomics to understand whether MFSD8 could be involved in other specific signalling pathways that could serve as novel targets for the design of alternative treatments for CLN7 disease. The mass spectrometry experiments will be conducted by the Bio-MS facilities from The University of Manchester and the proteomics analysis from the mass spectrometry data obtained will be assessed by Dr Jon Humphries from Manchester Metropolitan University.

Chapter 2

Materials and Methods

2.1 Cell Culture

2.1.1 Cell sources

Most experiments described in this work were performed on derivatives of a human WT iPSC line (control) and two different CLN7 patient-derived iPSC lines, which were previously obtained and dedifferentiated from skin fibroblasts by former members of the McKay's group. These iPSC lines were derived by episomal reprogramming of children skin fibroblasts from two CLN7 patients and an age-matched healthy donor as a control. Additional information on these cell lines and their derivation is provided in **section 2.1.6**.

Some experiments also included the use of HEK293T cells and SH-SY5Y as an alternative to study the molecular biology of the MFSD8 protein for comparison and as additional cell lines easier to culture and maintain when experiments required large amounts of cells or input material. The HEK293T cells were kindly provided by Glenn Ferris (Manchester Metropolitan University), and the SH-SY5Y cells were provided by Prof Mark Slevin (Manchester Metropolitan University).

2.1.2 Materials and reagents used in cell culture

Components	Supplier	Catalogue No.
DMEM (1X)	Corning®	15-013-CV
DMEM/F-12 (1:1) + GlutaMAX™	Gibco™	10565-018
Essential 8™ Medium (E8)	Gibco™	A1517001
Matrigel® hESC-Qualified Matrix, LDEV-free	Corning®	354277
Fetal Bovine Serum (FBS)	Gibco™	11570506
L-Glutamine (200 mM)	Corning®	25-005-CI

Penicillin-Streptomycin Solution (50X)	Corning®	30-001-CI
MycoZap™ Prophylactic	Lonza™	VZA-2031
Opti-MEM™ Reduced Serum Medium	Gibco™	31985070
Dimethyl Sulfoxide (DMSO)	Thermo Scientific™	D1391
Dulbecco's Phosphate Buffered Saline (DPBS)	Lonza™	BE17-512F
KnockOut™ Serum Replacement (KSR)	Gibco™	10828028
MEM Non-Essential Amino Acids Solution (100X) (NEAA)	Gibco™	11140050
N-2 Supplement (100X)	Gibco™	17502048
B-27™ Supplement (50X), serum free	Gibco™	17504044
β-mercaptoethanol (50 mM)	Gibco™	31350010
Recombinant Human FGF-basic (154 a.a.)	PreproTech®	100-18B
Heparin sodium salt (2 mg/mL)	Sigma-Aldrich®	H3149
Y-27632 dihydrochloride (ROCK inhibitor)	Bio-Techne®	1254
Bafilomycin A1 from *Streptomyces griseus*	Sigma-Aldrich®	B1793
Thapsigargin	Sigma-Aldrich®	T9033
AZ PFKFB3 67	Bio-Techne®	5742
Cycloheximide solution	Sigma-Aldrich®	C4859
TrypLE™ Express Enzyme (1X), no phenol red	Gibco™	12604013
Mytomycin C	Calbiochem®	475820
Lipofectamine™ LTX Reagent with PLUS™ Reagent	Invitrogen™	A12621
Mr. Frosty™ Freezing Container	Thermo Scientific™	5100-0001

2.1.3 Medium preparation and storage

Human embryonic stem cell (hESC) medium was prepared for hiPSCs culture on inactivated mouse embryonic fibroblasts (iMEFs) as a feeder layer for hiPSCs. MEF cells secrete necessary growth factors into the medium for pluripotency maintenance and they supply a cellular matrix for embryonic stem (ES) cells to grow. Essential 8™ Medium (Gibco™) was prepared for feeder-free iPSCs culture on Matrigel® Matrix by the addition of the Essential 8™ Supplement (50X) to the 500 mL Essential 8™ Basal Medium. Neural induction medium (NIM) was prepared and used

for culturing neurospheres and NSCs. Additionally, neural expansion medium (NEM) was employed for culturing NPCs. Working aliquots of 50 ml were prepared for all media to minimise the risk of contamination.

Plates and flasks for feeder-free iPSCs, NSCs and NPCs culture were previously coated with Matrigel® Matrix (Corning ®) (1 ml of Matrigel® Matrix in 30 ml of DMEM/F-12) for 30 min-2 h at 37ºC or at 4ºC overnight. For iPSCs culture on feeders, 2×10^5 iMEFs were plated on previously coated wells with autoclaved 0.1% gelatin (at 37ºC for 30 min-2 h or at 4ºC overnight).

Media	Components
Medium for HEK293T cells	DMEM (1X) supplemented with: 10% FBS 2% L-Glutamine 1% Pen/Strep
Medium for SH-SY5Y cells	DMEM/F-12 (1:1) supplemented with: 10% FBS 2% L-Glutamine 1% Pen/Strep
Human Embryonic Stem Cells (hESC) medium (for hiPSCs on MEFs)	DMEM/F-12 (1:1) + GlutaMAX™ supplemented with: 2% L-Glutamine 20% KSR 1X NEAA (100X) 1X N-2 Supplement (100X) 0.1 mM β-mercaptoethanol (50 mM) 10 ng/ml Recombinant Human FGF-basic 1% Pen/Strep 0.2% MycoZap™ Prophylactic
Essential 8™ Medium (for feeder-free hiPSCs)	Essential 8™ Basal Medium supplemented with: Essential 8™ Supplement (50X) 1% Pen/Strep 0.2% MycoZap™ Prophylactic
Neural Induction Medium (NIM) (for NSCs)	DMEM/F-12 (1:1) + GlutaMAX™ supplemented with: 1X NEAA (100X) 1X N-2 Supplement (100X) 20 ng/ml Recombinant Human FGF-basic 0.1% Heparin 1% Pen/Strep 0.2% MycoZap™ Prophylactic
Neural Expansion Medium (NEM) (for NPCs)	DMEM/F-12 (1:1) + GlutaMAX™ supplemented with: 1X NEAA (100X) 1X N-2 Supplement (100X)

	1X B-27™ Supplement (50X) 20 ng/ml Recombinant Human FGF-basic 0.1% Heparin 1% Pen/Strep 0.2% MycoZap™ Prophylactic

2.1.4 Routine cell culture and maintenance of HEK293T cells

HEK293T cells are a human embryonic kidney 293 cell line that expresses a mutant version of the SV40 large T antigen. These cells were cultured on complete Dulbecco's Modified Eagle Medium (DMEM) (Gibco™) (supplemented with 10% Fetal Bovine Serum, 2% L-Glutamine, and 1% Penicillin/Streptomycin) and they were passaged every two or three days at a split ratio of 1:3-1:4 when they reached 80-90% confluency. TrypLE™ Express Enzyme was used as a dissociation agent and the medium was replaced every two days. For freezing, HEK293T cells were harvested and resuspended in freezing medium (90% FBS and 10% DMSO) in cryotubes and stored overnight in a Mr. Frosty™ Freezing Container at -80°C before transfer into liquid nitrogen for long-term storage.

2.1.5 Routine cell culture and maintenance of SH-SY5Y cells

SH-SY5Y cells are a human neuroblastoma cell line, they were cultured on complete DMEM/F-12 (Gibco™) (10% Fetal Bovine Serum, 2% L-Glutamine, and 1% Penicillin/Streptomycin) and were passaged every three days at a split ratio of 1:6-1:10 when they were at 80-90% confluency. The experiments were performed at passages 8-20. TrypLE™ Express Enzyme was utilised as a dissociation agent and the medium was replaced every two days. For freezing, SH-SY5Y cells were harvested and resuspended in freezing medium (90% FBS and 10% DMSO) in cryotubes and stored overnight in a Mr. Frosty™ Freezing Container at -80°C before transfer into liquid nitrogen for long-term storage.

2.1.6 Culture of human induced Pluripotent Stem Cells (hiPSCs) and derivatives

Most experiments described in this project were performed using CLN7 patient-derived iPSCs. Two cell lines – $CLN7^{T294K/T294K}$ (from 380Pa) and $CLN7^{R465W/R465W}$ (from 474Pa) – of hiPSCs with two different missense mutations in the *CLN7/MFSD8* gene (p.Thr294Lys and p.Arg465Trp), respectively, were derived by episomal reprogramming of child skin fibroblasts isolated from two patients with classic late infantile CLN7 disease by previous members of the McKay's group as well as a control cell line (from age-matched Normal Human Dermal Fibroblasts, NHDF). The CLN7 patient 380Pa is a female diagnosed at 2.5 years old who was homozygous for the most common mutation c.881C>A causing a missense mutation (p.Thr294Lys) (Kousi et al., 2009b). The patient 474Pa is a male diagnosed at 4.5 years old who was homozygous for a more severe

mutation c.1393C>T causing also a missense mutation (p.Arg465Trp). iPSC lines were generated from dermal fibroblasts obtained from the BD repository held at University College London (UCL) (https://www.ucl.ac.uk/ncl-disease/) and control iPSCs were generated from dermal fibroblasts from a 6-year-old donor.

From now on in this report, the cells derived from the healthy donor will be referred to as wild-type (WT) iPSCs/NPCs, whereas the cells carrying the p.Thr294Lys mutation from the 380Pa patient will be named $CLN7^{T294K/T294K}$ iPSCs/NPCs and the cells mutated at p.Arg465Trp, generated from the patient 474Pa will be called $CLN7^{R465W/R465W}$ iPSCs/NPCs.

hiPSCs were cultured on iMEFs as a feeder layer in hESC medium. MEF cells secrete necessary growth factors into the medium for pluripotency maintenance and they supply a cellular matrix for embryonic stem (ES) cells to grow. For passaging, hiPSC colonies were picked with a 200 μL pipette tip in fresh hESC (or E8) medium and plated in new 6-well plates previously seeded with iMEFs. Once hiPSC colonies were stable on iMEFs, they were transferred to feeder-free plates. For that, the hiPSC colonies were also picked with a 200 μL pipette tip in new E8 supplemented medium and plated in Matrigel® Matrix coated 6-well plates.

Plates and flasks for feeder-free iPSCs, NSCs, and NPCs culture were previously coated with Matrigel® Matrix (Corning ®) (1 ml of Matrigel® Matrix in 30 ml of DMEM/F-12) for 30 min-2 h at 37ºC or at 4ºC overnight. For iPSCs culture on feeders, 2×10^5 iMEFs were plated on previously coated wells with autoclaved 0.1% gelatin (at 37ºC for 30 min-2 h or at 4ºC overnight).

2.1.6.1 Mitotic inactivation of MEFs for iPSC culture

Inactivated mouse embryonic fibroblasts (iMEFs) were used as a feeder layer to maintain stem cell pluripotency and to promote colony expansion. For this, MEFs were inactivated using Mitomycin C. Tissue culture flasks (T75 flasks) were coated with autoclaved 0.1% gelatin (in ddH_2O) for a minimum of 20 min at room temperature in the cell culture cabinet. Then, the gelatin was removed and MEFs were plated in those coated T75 flasks and cultured in complete DMEM (4.5 g/L glucose) supplemented with 10% FBS (v/v), 2% (v/v) L-Glutamine, 1% (v/v) non-essential amino acids (NEAA), and 1% Penicillin/Streptomycin. The cells were maintained at 37ºC and 5% CO_2 in humidified conditions and the medium was replaced every other day. When MEFs reached 80-90% confluency, 5 mL of TrypLE™ Express Enzyme was used to enzymatically detach the cells from the flasks and they were centrifuged at 234 ×*g* for 5 min. The supernatant was discarded, and the cells were resuspended in the volume of complete DMEM required to passage them at a split ratio of 1:4 into new T75 flasks coated with gelatin. When MEFs reached 80-90% confluency at passage 4, they were mitotically inactivated with Mitomycin C to generate iMEFs. The mitotic

inactivation of MEFs was conducted by incubating these cells with complete DMEM and 0.1 μg/μL of Mitomycin C for 3 h at 37°C and 5% CO_2. After mitotic inactivation, the inactivated MEFs were washed three times with Dulbecco's Phosphate Buffered Saline (DPBS) and enzymatically detached from the flasks using TrypLE™ Express Enzyme. The iMEFs were then centrifuged at 234 ×*g* for 5 min. After centrifugation, the supernatant was discarded and the iMEFs were resuspended in freezing medium (10% DMSO in FBS) with approximately 5×10^6 cells/mL (in each cryotube). These cryotubes containing the iMEFs were stored at -80 °C and defrosted when required for use in iPSCs culture. For use as a feeder layer in the culture of iPSCs, the iMEFs were plated at a density of 5×10^4 cells/well in 6-well plates previously coated with 0.1% autoclaved gelatin.

2.1.7 Neural differentiation

iPSCs colonies (control, $CLN7^{T294K/T294K}$, and $CLN7^{R465W/R465W}$) were cultured on Matrigel® Matrix in 6-well plates up to 80% confluency. Cells were washed with PBS and dissociated with TrypLE™ Express Enzyme. They were centrifuged at 84 ×*g* for 8 min and resuspended in Essential 8™ supplemented Medium. Cells were counted using a Neubauer chamber and 7,500 cells per well were plated on V-Shaped Bottom plates (low-attachment 96-well plate) in 100 μl of Neural Induction Medium (NIM) and ROCK inhibitor (1:1000). Half of the medium (50 μl) was changed every day during 5 days after cell plating to allow cells to form spheroids (also known as embryoid bodies). After 5 days of medium change, 10-15 spheroids per well were plated in 6-well plates previously coated with Matrigel ® Matrix. If cells were forming neural rosettes and neural tubes at this point, they were considered NSCs. Cell medium (NIM) was changed every other day for 4-5 days before cells detached and neural rosettes were picked with a 200 μl pipette tip and replated to new 6-well plates (coated with Matrigel® Matrix). That was considered another cell passage. After 1-2 passages, cells were differentiated into NPCs. For that, NSCs (neural rosettes and neural tubes) were dissociated with TrypLE™ Express and centrifuged at 84 ×*g* for 8 min. The cell pellet was resuspended in NEM, and cells were plated on new 6-well plates coated with Matrigel® Matrix to generate NPCs which grow as single cells.

2.1.8 Culture of Neural Progenitor Cells (NPCs)

NPCs (WT, $CLN7^{T294K/T294K}$, and $CLN7^{R465W/R465W}$) were cultured on NEM and they were passaged every week at a split ratio of 1:2 when they reached a 90% confluency. These cells were maintained in 6-well plates, T25, and T75 flasks for further experiments when they were at passage 6-12, representing the lifespan of the vLINCL CLN7.

2.2 Cellular biology

2.2.1 Nuclear fractionation

Cells (HEK293T and SH-SY5Y) were harvested and centrifuged at 104 ×*g* for 5 min. The cell pellet was washed with phosphate-buffered saline (PBS) and span down at 104 ×*g* for 2 min. A cytoplasmic homogenisation buffer [10 mM HEPES pH 7.9, 60 mM KCl, 1 mM ethylenediaminetetraacetic acid (EDTA), 1 mM PMSF, 0.075% v/v NP-40 and PIC] was added to the pellet, vigorously vortexed, incubated on ice for 4 min, and vortexed again. This mix was centrifuged at 1500 ×*g* and 4ºC for 10 min – being the supernatant the cytoplasmic fraction. The pellet was resuspended in the nuclear extraction buffer (20 mM Tris-HCl, 420 mM NaCl, 1.5 mM $MgCl_2$, 0.2 mM EDTA pH 8, 1 mM PMSF, 25 % v/v glycerol and PIC) and incubated on ice for 30 min homogenising it with a syringe (25 G) 10 times. The mix was centrifuged at 5625 ×*g* and 4ºC for 40 min – being the supernatant the nuclear fraction. The cytoplasmic fraction was detected by western blotting using anti-ERK1/2 as a marker for the cytoplasmic fraction and anti-Lamin B1 as a marker of the nuclear fraction.

Reagents	Supplier	Catalogue No.
HEPES > 99.5%	Sigma-Aldrich®	H4034
	Acros Organics	172572500
EDTA	Fisher Scientific™	S311-500
Phenylmethylsulphonyl fluoride (PMSF) (Protease inhibitor)	Sigma-Aldrich®	P7626
Potassium chloride (KCl)	Sigma-Aldrich®	P9541
NP-40 Surfact-Amps™ Detergent Solution	Thermo Scientific™	85124
Protease Inhibitor Cocktail (PIC)	Sigma-Aldrich®	P8340
Tris-HCl (Trizma hydrochloride, Tris hydrochloride)	Sigma-Aldrich®	T5941
Sodium chloride (NaCl)	Sigma-Aldrich®	S7653-5Kg
Magnesium chloride ($MgCl_2$)	Sigma-Aldrich®	M8266
Glycerol	Honeywell	G7893
Dulbecco's Phosphate Buffered Saline (DPBS)	Lonza™	BE17-512F

Buffers	Components
Buffer A: cytoplasmic homogenisation buffer (1 mL)	10 mM HEPES (pH 7.9) 60 mM KCl 1 mM EDTA 1 mM PMSF 0.075% v/v NP-40 PIC (1:1000)
Buffer B: nuclear extraction buffer	20 mM Tris-HCl 420 mM NaCl 1.5 mM $MgCl_2$ 0.2 mM EDTA pH 8 1 mM PMSF 25 % v/v glycerol PIC (1:1000)

Note: PMSF and PIC were added before use.

2.2.2 Immunofluorescence staining

Cells cultured in 12-well plates or Nunc® Lab-Tek® Chamber Slide™ system (8 wells) were washed twice with PBS and permeabilised and fixed with 100% ice-cold methanol for 5 min (on ice or at -20ºC). Permeabilisation was not carried out when staining for cell surface proteins; therefore, 4% paraformaldehyde (PFA) was used for 10 min at room temperature in those cases for cell fixation. Cells were washed again with PBS three times. Cells were blocked with blocking solution (2% BSA, 1% goat serum, 0.1% TWEEN® 20) for 30 min on the rocker. The primary antibodies anti-TRA-1-60, anti-OCT3/4, and anti-SOX2 were prepared in the blocking solution at 1:200; and anti-Nanog and anti-MFSD8 were prepared in the blocking solution at a 1:100 dilution. Cells were incubated with primary antibodies for 2 h at room temperature and washed three times with PBS. PBS was removed by decantation of the plates. Secondary antibodies (Alexa Fluor ™ 488 and Alexa Fluor ™ 568) were prepared at a 1:500 dilution in blocking solution and cells were incubated with them for 1 h at room temperature (in the dark). Cells were washed three times with PBS. To stain cell nuclei, a 1 mg/ml 4',6-Diamidino-2-phenylindole (DAPI) solution (D9542, Sigma-Aldrich) used at 1:1000 in PBS was added to the cells for 15-30 min or a drop of the DAPI Mounting (Vectashield®) solution was added to each well. In the first case, cells were washed three times with PBS and they were ready to image after the addition of PBS to each well. In the second case, cells were incubated at 4ºC overnight before imaging them. All the immunocytochemistry experiments were conducted using negative controls, which consisted of omitting the primary antibody and only using the secondary antibodies. In any of those negative controls without primary antibodies, fluorescence signal was detected. Cells were imaged using the Leica 6000CTR

Live cell imaging fluorescent microscope (for plates), the Zeiss Imager M2 microscope (for slides), the THUNDER fluorescence microscope and the STELLARIS Confocal Microscope (both for slides). Quantification of the fluorescence intensity of the images was conducted using ImageJ software.

Materials and Reagents	Supplier	Catalogue No.
Bovine serum albumin (BSA)	Sigma-Aldrich®	A2153
Normal goat serum	Vector Laboratories	S-1000-20
Triton X-100	Sigma-Aldrich®	T9284
VECTASHIELD® Antifade Mounting Medium with DAPI	Vector Laboratories	H-1200-10
Nunc® Lab-Tek® Chamber Slide™ system (8 wells)	Thermo Scientific™	154453

Antibody	Supplier	Catalogue No.	Dilution
Anti-TRA-1-60 antibody (mouse)	Sigma-Aldrich®	MAB4360	1:200
Anti-Oct3/4 Rabbit Polyclonal	Abcam	ab19857	1:200
Anti-SOX2 Polyclonal Goat	R&D Systems	AF2018	1:200
Anti-Nanog Rabbit Polyclonal	Abcam	ab80892	1:100
Anti-MFSD8 Rabbit Polyclonal	Invitrogen™	PA5-60832	1:100
DAPI	Sigma-Aldrich®	D9542	1:1000
Anti-SQSTM1/p62 Mouse	Abcam	Ab56416	1:100
Anti-ATG161L Rabbit	Abcam	ab187671	1:100
Anti-ATG4B Rabbit	Abcam	ab154843	1:100
Anti-ATG9A Rabbit	Abcam	ab108338	1:100
Anti-ATG5 Rabbit	Abcam	ab108327	1:100
Anti-LC3B Rabbit	Abcam	ab192890	1:100
Anti-Beclin1	Abcam	ab207612	1:100
Alexa Fluor™ 488 GAR ReadyProbes™ reagent with NZ derived BSA	Invitrogen™	R37116	2 drops/mL
Alexa Fluor™ 568 goat anti-mouse IgG (H+L)	Invitrogen™	A11004	1:500

Alexa Fluor ™ 488 goat anti-rabbit IgG (H+L)	Invitrogen™	A11008	1:500
Alexa Fluor™ 568 donkey anti-goat IgG (H+L)	Invitrogen™	A11057	1:500
Alexa Fluor™ 568 goat anti-rabbit IgG (H+L)	Invitrogen™	A11011	1:500
Alexa Fluore™ 488 donkey anti-goat IgG (H+L)	Invitrogen™	A11055	1:500

2.3 Molecular biology

2.3.1 Post-translational modifications (PTMs)

2.3.1.1 PNGase F treatment (deglycosylation)

Peptide N-glycanase F (PNGase F) (9109-GH, R&D Systems) was used to remove any possible N-linked glycans from SH-SY5Y cell lysates. Before PNGase F treatment, sample denaturation was conducted in a 30 μl reaction volume using 1X Denaturing buffer [10X Denaturing buffer composition: 5% sodium dodecyl sulfate (SDS) and 50 mM DTT] and incubated at 100ºC for 10 min. The reaction mixture was cooled to room temperature and centrifuged. Then 3 μl of 10% Triton® X-100 were added to a final concentration of 1.67%. PNGase F was diluted to 0.167 ng/μl. The reaction mixture was divided in two and 15 μl were combined with 15 μl 0.167 ng/μl and the other 15 μl of reaction were mixed with 15 μl of Assay Buffer (0.1 M Tris, pH 7.5) as a control. The PNGase reaction mixtures were incubated at 37ºC for 30 min followed by immunoblotting.

2.3.1.2 SUMO Protease treatment (deSUMOylation)

Small ubiquitin-like modifier (SUMO) Protease (12588-018, Invitrogen™) was used to cleave any potential ubiquitin-like (UBL) protein SUMO attached to the MFSD8 protein to examine whether the heavy bands observed in immunoblots, was due to SUMO addition during post-translational modifications. For this, the manufacturer's protocol was followed. Specifically, SH-SY5Y were cultured and harvested at 80-90% confluency. Then, cell lysates were obtained and after the measurement of protein concentration using the bicinchoninic acid (BCA) assay, 20 μg of protein were added to a 1.5 mL microcentrifuge tube. Additionally, 20 μL of 10X SUMO protease buffer +/- Salt, ddH2O (to a final volume of 190 μL), and 10 μL of SUMO Protease (10 units) were added to the tube. The total volume of 200 μL was mixed and incubated at 30ºC in a heat block. Subsequently, 20 μL aliquots were removed at 2, 2, 4, and 6 h and kept at -20ºC in different 1.5 mL microcentrifuge tubes until the experiment was complete. Following this, the samples were

mixed with 5x protein loading buffer and incubated at 95.5°C for 5-10 min to proceed to Western blotting.

2.3.1.3 Phosphatase treatment (dephosphorylation)

A total of 10 μg protein obtained from SH-SY5Y cell lysates were combined with ddH_2O to a total volume of 40 μL. Then, 5 μL of 10× NEBuffer for protein metallophosphatases (PMP) was added and 5 μL of 10 mM $MnCl_2$ (both provided by the kit) was added to make a total reaction volume of 50 μL. The Lambda Protein Phosphatase (1 μL) was added to the samples (n = 3) and only the reaction buffer was added to the negative control samples (n = 3). All the samples were incubated at 30°C for 30 min in a heat block and then, they were transferred to 60°C for 1 h. After that, 10 μL of 5× protein loading buffer was added to each sample and they were incubated at 95.5°C for western blotting.

2.3.2 Cycloheximide treatment

SH-SY5Y cells, WT, $CLN7^{T294K/T294K}$, and $CLN7^{R465W/R465W}$ NPCs were treated with Cycloheximide (CHX) (ab120093, Abcam) at a concentration of 100 μg/mL for 0 h and 18 h to inhibit protein synthesis. After 18 h of incubation with CHX, cells were washed with PBS and scraped with ice-cold PBS. Cells harvested were collected in a 15 mL Falcon tube and centrifuged at 300 ×*g* for 5 min. The supernatant was discarded, and the cell pellets were placed on ice for the obtention of cell lysates for further use in Western blot experiments.

2.3.3 Bafilomycin A1 and Thapsigargin treatment

Control, $CLN7^{T294K/T294K}$ and $CLN7^{R465W/R465W}$ NPCs were treated with a concentration of 100 nM of Bafilomycin A1 (Baf A1) for 6-8 h depending on the experiment and following previous studies to exacerbate lysosomal dysfunction and observe its effects in different cellular organelles and vesicles, and proteins linked to autophagy.

Thapsigargin was also used to assess its link with Bafilomycin A1 and the sarcoplasmic/endoplasmic reticulum Ca^{2+}-ATPase (SERCA) pathway in a concentration of 100 nM following the same procedure as described for Baf A1.

2.3.4 Limited proteolysis

The resistance and protein stability of the different MFSD8 mutations was assessed by limited proteolysis. WT, $CLN7^{T294K/T294K}$ and $CLN7^{R465W/R465W}$ NPCs were cultured in T25 flasks and harvested by cell scraping in ice-cold PBS after a wash with PBS. Cells were centrifuged at 150 ×*g* for 5 min and cell pellets were incubated on ice for 30 min with 200 μL RIPA buffer (with protease inhibitors at a concentration of 1:1000 and phosphatase inhibitors at 10 μL/mL). A BCA Assay

was carried out to measure the protein concentration of each sample. Equal amounts of WT, $CLN7^{T294K/T294K}$, and $CLN7^{R465W/R465W}$ NPC lysates (8 μg in a total volume of 16 μL with ddH_2O) were incubated with trypsin (TPCK treated, dissolved in 1 mM HCl to 10 mg/mL stock) (Sigma-Aldrich®) in concentrations ranging from 125 μg/mL to 0 μg/mL. Proteolysis was stopped by adding 4 μL of 5× protein loading buffer (Laemmli buffer) and incubating them at 95.5°C for 5-10 min. Samples were immediately loaded onto a sodium dodecyl-sulfate polyacrylamide gel electrophoresis (SDS-PAGE) and a Western blot was conducted.

2.3.4 Western blotting

After cell harvesting and obtaining the cell lysates, using radioimmunoprecipitation assay (RIPA) buffer with protease inhibitors at 1:1000 and phosphatase inhibitors at 10 μL/mL), equal amounts of protein (measured by BCA assay) were mixed with 5× SDS-loading buffer, incubated for 10 min at 95.5ºC, separated by SDS-PAGE (10% polyacrylamide gel) and blotted onto a polyvinylidene difluoride (PVDF) membrane (Millipore) for 2 h at 100 V using a tank transfer. After membrane blocking with 5% BSA in 1× Tris-buffered saline with 0.1% Tween® 20 (TBST) buffer, western blots were probed with the primary antibodies anti-MFSD8 (PA5-60832, ThermoFisher), anti-β-actin (A2228, Sigma-Aldrich) and anti-H3 (05-928, Sigma-Aldrich) at 4ºC overnight, followed by detection with horseradish peroxidase (HRP) secondary antibodies (α-mouse and α-rabbit) and visualized using Immobilon Western Chemiluminescent HRP Substrate and LI-COR Odyssey Fc. MFSD8 protein band intensities were measured and compared to the total MFSD8 protein on each cellular fraction using ImageJ. To probe blotting membranes with different antibodies of similar molecular weight, blotting membranes were stripped using a 0.5 M sodium hydroxide (NaOH) solution for 20 min at room temperature on the rocker. They were washed with 1× TBST buffer 3 times for 6 min at room temperature on the rocker and the same steps previously described were followed to incubate the membranes with primary and secondary antibodies, as well as the developing solution.

Materials and Reagents	Supplier	Catalogue No.
Fisherbrand™ Cell Scrapers	ThermoFisher™	08-100-242
DPBS (1X) without Calcium and Magnesium	Lonza™ BioWhittaker™	04-479Q
Radioimmunoprecipitation assay buffer (RIPA buffer)	Sigma-Aldrich®	R0278
Protease Inhibitor Cocktail 2 (1:1000) (PIC)	Sigma-Aldrich®	P5726-1ML
Phosphatase Inhibitor Cocktail 2 (10 µL/mL)	Sigma-Aldrich®	P5726
TWEEN® 20	Sigma-Aldrich®	P1379-100ML
Tris Base	Fisher Scientific™	BP1652-1
Tris-HCl (Trizma hydrochloride, Tris hydrochloride)	Sigma-Aldrich®	T5941
Glycine (White Crystals or Crystalline Powder)	Fisher Scientific™	BP3811
Sodium chloride (NaCl)	Sigma-Aldrich®	S7653-5Kg
Sodium dodecyl sulfate (SDS)	Fisher Scientific™	S/5200/53
30% Acrylamide/Bis Solution, 29:1	Bio-Rad	1610156
N,N,N',N'-tetramethylethylenediamine (TEMED)	Sigma-Aldrich®	T9281-25ML
Ammonium persulfate (APS)	Sigma-Aldrich®	A3678
Bovine serum albumin (BSA)	Sigma-Aldrich®	A2153
PageRuler™ Prestained Protein Ladder	ThermoFisher™	26616

Buffers and solutions	Components
5× Protein loading buffer (Laemmli buffer)	3 mL 20% SDS 3.75 mL 1 M Tris buffer (pH 6.8) 9 mg bromphenol blue 1.16 mg DTT 4.5 mL glycerol Up to 15 mL with dH_2O (final volume)
10× Tris-buffered saline (TBS) (pH 7.6)	200 mM Tris Base 1.5 M NaCl dH_2O
1× Tris-buffered saline with 0.1% Tween® 10 (TBST)	10% TBS (pH 7.6) 0.1% Tween® 20
Running buffer	Tris Base Glycine 0.1% SDS dH_2O
Blotting buffer	Tris Base Glycine 20% methanol (100% stock) dH_2O
Separating gel solution (10%)	4.1 mL ddH_2O 3.3 mL Acrylamide bis (30%) (Bio-Rad) 2.5 mL Tris-HCl (1.5 M, pH 8.8) 100 µL 10% SDS 10 µL N,N,N',N'-tetramethylethylene-diamine (TEMED) 32 µL 10% Ammonium persulfate (APS)
Stacking gel solution (4%)	6.1 mL ddH_2O 1.3 mL Acrylamide bis (30%) (Bio-Rad) 2.5 mL Tris-HCl (0.5 M, pH 6.8) 100 µL 10% SDS 10 µL N,N,N',N'-tetramethylethylene-diamine (TEMED) 100 µL Ammonium persulfate (APS)

Antibody	Supplier	Catalogue No.	Dilution
ERK1/ERK2 Monoclonal	Invitrogen™	13-6200	1:500
Anti-Lamin B1 Mouse McAb	Proteintech	66095	1:1000
Monoclonal Anti-β-actin (mouse)	Sigma-Aldrich®	A2228	1:40000
Anti-MFSD8 Rabbit Polyclonal	Invitrogen™	PA5-60832	1:500
Anti-MFSD8 Rabbit Polyclonal	Proteintech	24298-1-AP	1:1000
Polyclonal Goat Anti-Mouse Immunoglobulins (HRP)	Dako	P0447	1:2000
Stabilized Peroxidase Conjugated Goat Anti-Rabbit (H+L)	Invitrogen™	32460	1:500
Mouse Anti-Rabbit Ig Light-Chain Specific (HRP) (Co-IP)	Cell Signaling	D4W3E	1:1000

2.3.5 Co-immunoprecipitation (co-IP)

The co-immunoprecipitation of endogenous MFSD8 in SH-SY5Y cells was conducted following the protocol published by Lagundžin D *et al.* (Lagundžin et al., 2022). For that, SH-SY5Y cells were cultured in 100 mm plates and they were harvested by scraping with PBS when they were at 80-90% confluency. To obtain a total of 2.5 mg/mL protein per sample, two 100 mm plates were harvested and merged, representing one sample. A total of four sample replicates were obtained and, after the corroboration of the presence of the MFSD8 protein by Western blotting (using 5 μL of each sample), the samples were sent for mass spectrometry analysis.

Buffers and solutions	Components
Lysis buffer (1mL/sample)	10 mM HEPES (pH 7.4) 10 mM KCl 0.05% (v/v) Nonidet P-40 Protease inhibitors (10 μL/1 mL) (added at the time of use) Phosphatase inhibitors (10 μL/1 mL) (added at the time of use) ddH_2O
0.1% BSA solution (filtered) (20 mL)	0.02 g BSA 20 ml PBS
Bead washing buffer A (BW-A) (10 mL)	10 mM HEPES (pH 7.4) 10 mM KCl 50 mM NaCl 1 mM $MgCl_2$ 0.05% (v/v) Nonidet P-40 ddH_2O
Bead washing buffer B (BW-B) (10 mL)	10 mM HEPES (pH 7.4) 10 mM KCl 0.07% (v/v) Nonidet P-40 ddH_2O
Sample elution buffer (SE)	0.5 M NH4OH (pH 11.0) 0.5 mM EDTA ddH_2O

2.3.6 Mass spectrometry and data processing of MS-based proteomics

Samples were prepared for in-gel digestion following the gel-top analysis methodology. The day before sending the samples to the Bio-MS facilities (University of Manchester) for mass spectrometry (MS), an SDS-PAGE electrophoresis gel was run. For this, 40 μL of the immunoprecipitated protein was mixed with a 5× loading buffer and incubated at 95.5°C for 5-10 min. A 10% separating gel (no stacking gel was added) was prepared and the 45-50 μL of each sample was loaded onto the gel leaving one lane empty between each sample to avoid cross-contamination from the different samples. The SDS-PAGE gel was run at 120 V for 10 min to allow the samples to enter the separating gel (2-5 mm target). The gel was immediately stained with InstantBlue™ Coomassie Stain in a new and clean square Petri dish at room temperature overnight (on the rocker). The day after, the IntantBlue™ Coomassie Stain was removed and the gel was washed and kept in high-quality water (ddH_2O) to be sent for mass spectrometry analysis (conducted by the Bio-MS facilities at the University of Manchester).

For mass spectrometry, samples were subjected to in-gel trypsin digestion, in which protein samples were reduced and alkylated (blocking cysteine residues to obtain linear peptides to search

against the database later on). The peptides were then eluted and recovered from the gel and they were separated by reverse phase liquid chromatography (LC), where hydrophilic peptides elute first. In contrast, hydrophobic peptides elute later as the gradient of acetonitrile is increased in the LC. As peptides eluted from the LC, they were ionised by electrospray ionisation (ESI) and drawn into the vacuum of the mass spectrometer. Masses (mass over charge, m/z) of the peptides were measured, selected for fragmentation and then, the fragments' m/z were measured again. These data constituted the raw data from mass spectrometry, which particularly contained information about peptide m/z, intensities, and fragment m/z ions. These raw files were used to search against a database of proteins (Swissprot and TrEMBL = UniProt). A human database was selected, and search parameters/tolerances were selected to fit with the sample preparation (cysteines plus additional mass of the alkylating reagent used) and the mass spectrometry used (types of ions and fragments). The software was used to create a likely set of proteins in the sample for statistical matching, and every peptide and protein identification had a *p*-value. The cut-offs that suited the false discovery rate (FDR) of choice were selected and a variety of metrics were also used for protein abundance measurements. In this case, spectral counts were used, which are the number of times a protein has a peptide identified. Mascot (https://www.matrixscience.com/) was first used to conduct the database searches, and then the data were loaded into Scaffold (https://www.proteomesoftware.com/products/scaffold-5). In Scaffold, the filters 95% protein and 90% peptide confidence were used, with a minimum of two peptides per protein to export a loss of protein identifications with the spectral counts (total spectrum count) or unique peptides (provides a level of identification confidence). The data was then normalised by dividing the spectrum count for each protein by the summed spectral counts for each sample and the ratios from these normalised spectral counts were calculated. This raw data analysis was conducted in collaboration with Dr Jon Humphries (Manchester Metropolitan University).

For further functional annotation analysis of Gene ontology (GO) and pathway enrichment, the protein identifications (using the official gene names) were submitted to ShiniGO 0.77 (http://bioinformatics.sdstate.edu/go/) software and DAVID web server (https://david.ncifcrf.gov/tools.jsp).

2.3.7 Data analysis

Except for the MS-based proteomics data, the statistical significance of all experimental data of this work was determined using GraphPad Prism 9.4 Software (GraphPad, USA). The normality of all data was first determined by a Quantile-Quantile (Q-Q) plot, to confirm the normal distribution of the data. Additionally, a Saphiro-Wilk test was conducted on GraphPad to further confirm the normality of the data. If data was normally distributed and unpaired, one-way analysis

of variance (ANOVA) was used to compare the variance of group means within a normally distributed dataset containing three or more groups with only one independent variable, or within a normally distributed dataset with more than two independent variables. A two-way ANOVA was used to determine the variance of normally distributed datasets containing three or more groups with two independently defined groups, or for normally distributed datasets containing three or more independent variables. Post-hoc analysis was conducted on all ANOVA tests using Tukey analysis. For datasets without normal distribution and unpaired, a non-parametric Mann-Whitney test was used to confirm significance, followed by a post-hoc analysis using Dunn's test as a more representative method for comparison of small samples of biological replicates. Data were considered statistically significant when $*p < 0.05$, $**p < 0.01$, $***p < 0.001$, $****p < 0.0001$. Notice that most of the *p*-values are expressed in the graphs representing the analysed data. Schematic representation images were created with BioRender. The data obtained from MS, which were used for GO enrichment analysis using ShinyGO 0.77 and DAVID, are mostly represented by Fold Enrichment (FE) followed by the *p*-value and the corrected *p*-value using FDR. Fold enrichment represents the percentage of genes in the list belonging to an enriched pathway or GO term, divided by the corresponding percentage in the background. FDR is the estimated probability that a gene set with a given enrichment score (normalised for gene set size) represents a false positive. It is calculated based on the nominal *p*-value from the hypergeometric test.

Chapter 3

Generation of human NPCs as a model to study the vLINCL CLN7

Summary

This chapter covers the development of the first human stem cell-based model for the variant late infantile NCL CLN7 through direct differentiation of patient-derived iPSCs to Neural Progenitor Cells (NPCs). An established protocol for the generation of Neural Stem Cells (NSCs) and NPCs is presented, demonstrating improved efficiency in generating neuron-like cells from somatic cells. Using different cell culture media composed of distinct supplements, two patient (T294K and R465W) and one control (WT) iPSC types were differentiated into NPCs to investigate the molecular biology of MFSD8 in the following chapters. The patient-derived iPSCs, as well as the differentiated NPCs, were subjected to characterisation through immunocytochemistry to assess pluripotent and neural phenotypes, respectively. A successful neural differentiation was obtained, despite having to address several attempts, particularly for one of the mutated iPSC types, which suggested that the state and stability of iPSCs may be key factors for achieving efficient and effective differentiation.

Introduction

3.1 Rationale of the generation of NPCs to study CLN7 disease

This work was primarily based on the generation of NPCs from CLN7 patient-derived iPSCs and an age-matched healthy donor (control, WT) for their further use in downstream experiments. The reason it was decided to generate NPCs is that they are cells with the most committed neural phenotype that remain proliferative for extended passages. Additionally, NPCs represent an earlier

stage of neural development compare to mature neurons. This makes them particularly useful for studying neurodegenerative disorders that manifest in childhood like the vLINCL CLN7.

The study conducted by FitzPatrick *et al.* (2018) demonstrated that homogeneous cultures of NPCs derived from iPSCs can be established, and these cells remain phenotypically stable for over 15 passages. Additionally, this gave us a stable platform to study and compare disease and control in analogous cells.

3.2 Characteristics of human induced Pluripotent Stem Cells (hiPSCs)

Despite the advancement in somatic cell reprogramming methods, the great heterogeneity and low efficiency of some somatic cell reprogramming methodologies require the characterisation of hiPSCs before their application in downstream technologies. hiPSCs can be generated from individual patients and can be used for disease modelling, drug screening, and regenerative medicine (Robinton and Daley, 2012b; Takahashi et al., 2007). Although iPSCs exhibit an ESC-like morphology, sorting iPSCs based on those characteristics is not sufficient to isolate fully reprogrammed iPSCs, as partially reprogrammed mouse and human iPSCs do not differ significantly in morphology from fully reprogrammed clones (Okita et al., 2007). For instance, when using nucleofection of three or four plasmids for cell reprogramming, it is highly probable that many cells only receive some of those plasmids and not all of them, causing partial reprogramming. Therefore, it is crucial to examine the expression of all those factors in the reprogrammed cells before using them in further experiments.

Combining positive and negative surface and intracellular markers allows the selection and expansion of *bona fide* iPSCs and NPCs, in this instance. In this study, we specifically looked at the expression of OCT-3/4, SOX2, NANOG, and TRA-1-60 for pluripotency, as well as Nestin, BLBP, and Pax 6 for neural expression.

3.2.1 Octamer-binding transcription factor 3/4 (OCT-3/4)

The octamer-binding transcription factor 3/4 (OCT-3/4) is a crucial regulatory gene that controls the pluripotency and self-renewal abilities of ESCs (Boyer et al., 2005). Specifically, OCT-3/4 is a transcription factor essential for the differentiation of the embryo into the three germ layers. When OCT-3/4 is overexpressed, stem cells differentiate into the endoderm and mesoderm, while its downregulation results in the differentiation of stem cells into the trophectoderm, which forms the placenta in humans (Choi and Baek, 2018).

3.2.2 SRY box-containing gene 2 (SOX2)

SRY box-containing gene 2 (SOX2) is an essential transcription factor, which regulates different phases of embryonic development and ESC differentiation. SOX2 plays a key role in cell cycle exit and the differentiation of NSCs, as well as re-establishing pluripotency in somatic cells by reprogramming them into iPSCs (Ring et al., 2012). When SOX2 is overexpressed, it induces differentiation of iPSCs into the neural lineage, having the ability to reprogram fibroblasts into NSCs (Ring et al., 2012). In the initial state of stem cell reprogramming, the transcription factor SOX2 plays a crucial role in directing cellular differentiation towards neural ectoderm (Zhang and Cui, 2014), mesoderm, and trophectoderm. Additionally, SOX2 downregulates the expression of genes associated with the mesendodermal lineage, a rare cell population that emerges transiently during gastrulation in embryonic development. Over 1200 genes control SOX2-induced differentiation, and one of them is OCT-3/4. Overexpression of OCT-3/4 is regulated by the upregulation of SOX2 and conversely, indicates that SOX2 is crucial in the pluripotency of ESCs and activation of OCT-3/4 (Masui et al., 2007).

3.2.3 NANOG

NANOG is a homebox transcription factor and it plays a crucial role in the regulation of self-renewal and pluripotency of ESCs. Its stabilisation is important for maintaining the stemness of ESCs (Jin et al., 2016). NANOG is rapidly degraded by the ubiquitination-proteasome system (UPS) as it has a relatively short half-life (Choi and Baek, 2018). It has been reported that this transcription factor facilitates the recruitment of OCT4, SOX2, and oestrogen-related receptor beta (Esrrb), another transcription factor involved in ES self-renewal, at several regulatory sites in mice, primarily targeting the initiation of transcription. Additionally, NANOG recruits Brg1 and enhances chromatin accessibility at these sites. NANOG is also necessary to preserve H3K27me3, a repressive histone mark, at genes related with differentiation. Therefore, NANOG utilises specific molecular mechanisms to promote self-renewal and prevent differentiation. When LIF is present, NANOG enhances the ability of cells to renew by modifying the network responsible for maintaining pluripotency and by increasing the accessibility of chromatin and facilitating the binding of other pluripotency factors to several enhancers. When LIF is not present, NANOG prevents differentiation by maintaining H3K27me3 at genes involved in development (Heurtier et al., 2019).

3.2.4 TRA-1-60 and TRA-1-81

Human pluripotent stem cells are characterised by the expression of TRA-1-60 and TRA-1-81 plasma membrane surface antigens, which are carbohydrate epitopes (Wright and Andrews, 2009).

These antigens, whose specific molecular identities remain unidentified are widely utilised as indicators of undifferentiated pluripotent human stem cells (Pera et al., 2000).

3.2.5 Stage-specific embryonic antigens-3 and-4 (SSEA-3 and SSEA-4)

SSEA-3 and SSEA-4 are cell surface antigens expressed in hESCs and their expression decreases as the cells undergo differentiation (Reubinoff et al., 2000; Thomson et al., 1998). Specifically, SSEA-3 and SSEA-4 are epitopes on glycosphingolipids called GL-5 and GL-7 and they are initially detected on the pluripotent cells of the inner cell mass during early stages of human preimplantation (Henderson et al., 2002; Kannagi et al., 1983). Cell sorting and gene expression analyses have indicated that the presence of SSEA-3 diminished quickly during the process of cell differentiation (Enver et al., 2005; Henderson et al., 2002). Two types of hESCs have been suggested: SSEA-3+ cells, which have the ability of self-renewal and can transition to SSEA3- cells, which can also undergo self-renewal, but they have a tendency to differentiate. Both cell types in hESCs with karyotic defects are expected to exhibit a preference for self-renewal (Enver et al., 2005). These studies depend on the association between SSEA-3 expression and the undifferentiated sate of the cells, but little is known about the role of this antigens (Brimble et al., 2007).

3.3 Specific proteins for neural stem cells (NSCs) characterisation

3.3.1 Nestin

Nestin is an intermediate filament protein that is observed in dividing cells during the initial stages of nervous system development and in the adult brain (Gilyarov, 2008; Lendahl et al., 1990). It serves as a marker for neural stem cells. The activity of this protein is crucial for the survival and self-renewal of NSCs both *in vivo* and *in vitro*. Hence, it is additionally proposed that nestin could potentially play a role in the viability and regenerative capabilities of several other highly replicating stem cell populations, apart from embryonic NSCs (Park et al., 2010).

3.3.2 Pax6

Paired box 6 (Pax6) is a transcription factor significantly involved in the process of determining neuronal fate and promoting the proliferation of NSCs. It plays a role in the placement of the neocortex and the formation of upper-layer neurons by recognising progenitor cells in the subventricular zone (SVZ) (Land and Monaghan, 2003; Tarabykin et al., 2001). Pax6 expression can transition hESCs from a state of proliferation to a state of differentiation into neuroectoderm (NE). The ability described is a direct conversion of cell fate, as opposed to an indirect mechanism involving the promotion of cell proliferation or the survival of existing neural epithelial cells in hESCs (Schroeder, 2008). Initially, it should be noted that hESCs, when subjected to conventional

growth conditions, do not exhibit the expression of Pax6. Furthermore, the overexpression or knockdown of Pax6 does not result in any significant changes in cell proliferation or survival. Additionally, by time-lapse monitoring, it has been observed that the activation of Pax6 prompts the transformation of cells into columnar neuroectodermal cells, which then undergo migration and aggregation, ultimately leading to the formation of rosettes. Moreover, on a molecular scale, Pax6 exhibits direct binding to pluripotent genes and NE genes (X. Zhang et al., 2010).

Either Pax6a and Pax6b exhibit binding affinity to the promoters of pluripotent genes, such as OCT-3/4 and NANOG, resulting in the repression of their expression. However, it is noteworthy that only Pax6a has binding capacity to the promoters of NE genes, hence facilitating the activation of NE genes. Therefore, the involvement of Pax6 in defining the fate of NE is accomplished by the coordinated action of Pax6a and Pax6b, which effectively inhibit the self-renewal of hESCs. Consequently, this inhibition initiates the process of cellular differentiation and directs the cells towards the NE fate, mostly through the influence of Pax6a. Merely suppressing pluripotent factors is insufficient for inducing the differentiation of ESCs or epiblast cells (which give rise to the three primary germ layers: ectoderm, endoderm, and mesoderm) into NE. This phenomenon is evidenced by the observation that the overexpression of Pax6b, a transcription factor lacking neural-inducing properties, induces the differentiation of hESCs away from their pluripotent state, resulting in their transformation into trophoblast cells (which develop into a large part of the placenta). The observed phenomena bear resemblance to the extraembryonic result of ESC when OCT-3/4, NANOG, or SOX2 are suppressed (Chew et al., 2005; Fong et al., 2008; Hay et al., 2004; Hyslop et al., 2005). Therefore, the initiation of the differentiation process is triggered by the repression of pluripotent genes, although this factor alone does not fully account for the differentiation of embryonic germ layers. Pax6a is widely regarded as the principal inductive signal responsible for determining the NE fate. Pax6a has been observed to form associations with a specific group of neural genes, corresponding to the neural phenotypes. Pax6b, while not possessing direct neural induction capabilities on its own, enhances the neural inductive abilities of Pax6a through their interaction. This interaction between Pax6b and Pax6 a is crucial for effectively suppressing pluripotent genes, which is required for initiating the expression of neural genes (X. Zhang et al., 2010).

3.3.3 BLBP

Brain lipid binding protein (BLBP), is a member of the fatty acid-binding proteins (FABPs) family. FABPs are cytoplasmic proteins that play a role in the uptake and targeting of fatty acids. Even though the BLBP protein is widely utilised as a marker for radial-glia cells during the development of both the embryonic and adult brain, it has been reported that NSCs express many features of

radial glia, including molecular markers such as BLBP (Pollard et al., 2006). Radial glia is a specific type of cell commonly linked to the development of the nervous system during the formation of cortical layers in the brain. However, certain cells known as radial glia-like cells can be detected in the adult central nervous system, serving as neurogenic progenitors and contributing to homeostasis after injury (Miranda-Negrón and García-Arrarás, 2022). As a result, BLBP has been commonly used as an NSC marker gene during neurogenesis (Kumar et al., 2020).

Results

3.4 Generation of an *in vitro* model to study CLN7 disease

The first aim of this study was to generate a 2D neural cell model to investigate the vLINCL CLN7 at a cellular and molecular level. To generate these 2D models of neuron-like cells, two CLN7 and control (WT) iPSC clones were differentiated into NSCs and NPCs.

3.4.1 iPSCs genotype and cell culture

In this project, we established a potential clinically significant model through the generation of neural progenitor cells (NPCs) from induced pluripotent stem cells (iPSCs) generated from patients. The generation of hiPSCs was accomplished by the reprogramming of dermal fibroblasts by previous members of our research group. The skin fibroblasts were obtained from two patients presenting the classical vLINCL CLN7 disease, as well as one control donor. Patient 380Pa, a female diagnosed at the age of 2.5 years, exhibited homozygosity for the common missense mutation c.881C>A (p.Thr294Lys, T294K), which is known to be a prevalent mutation in the Roma community (Kousi et al., 2009a). Patient 474Pa was, a male diagnosed at the age of 4.5 years, and was also homozygous for a more severe missense mutation, the c.1393C>T (p.Arg465Trp, R465W). This study presents a novel model in CLN7 disease using iPSCs obtained from patients with the variant late-infantile NCL (vLINCL) CLN7. We specifically used three different human-derived iPSC types – one obtained from an aged-matched healthy control (WT) and the other two cell types obtained from different patients suffering from CLN7 disease. These cells are referred to as WT iPSCs, $CLN7^{T294K/T294K}$ iPSCs, and $CLN7^{R465W/R465W}$ iPSCs throughout this thesis according to the homozygous mutations that the patients presented. This cell model was employed to analyse the underlying pathobiology of CLN7, being one of the first studies using this approach for investigating CLN7 disease.

To start the cell culture of iPSCs and ensure their stability *in vitro*, the cells were initially plated on a layer of iMEFs until the formation of different colonies was observed. After obtaining stable colonies, iPSCs were then grown under feeder-free conditions (on plates coated with Matrigel®

Matrix), to prevent any potential contamination by iMEFs in further experiments (**Figure 3.1**). Subsequently, these cells underwent expansion and were stored for utilisation in downstream applications. The primary aim of culturing iPSCs was to obtain NPCs through the process of neural differentiation These NPCs were later used in numerous experiments conducted in this study.

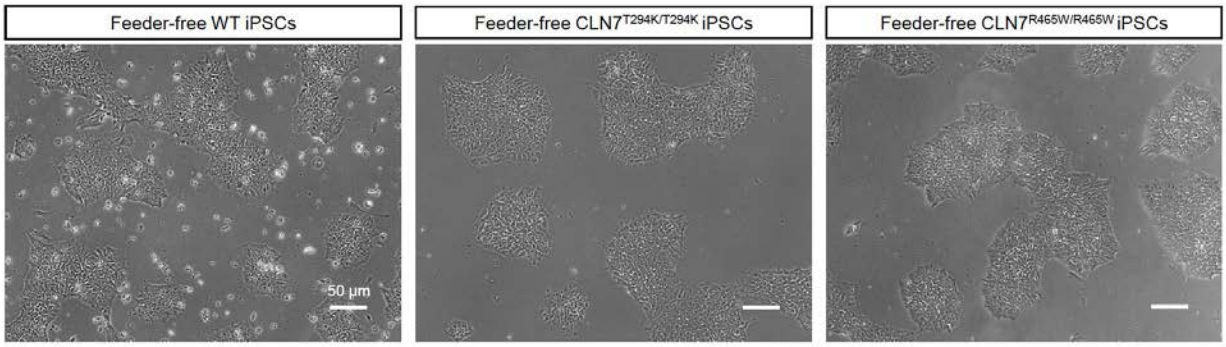

Figure 3.1. Morphological appearance of WT, CLN7$^{T294K/T294K}$, and CLN7$^{R465W/R465W}$ iPSCs. Representative light microscopy images of individual stem cell colonies from cultures with the indicated genotypes. Scale bar = 50 µm. The feeder-free iPSCs were cultured on 6-well plates (coated with Matrix® Matrigel). iPSCs grow in colonies showing a large nucleus and a lower area of cytoplasm. Images were obtained using an EVOS® Imaging System microscope (Total magnification = 100×).

3.4.2 iPSCs express the pluripotency markers OCT-3/4, SOX2, NANOG, and TRA-1-60

Before initiating the differentiation process of iPSCs into neuronal cells, WT and CLN7 iPSCs underwent characterisation using immunofluorescence staining. Pluripotency markers, including OCT-3/4, SOX2, NANOG, and TRA-1-60, were utilised for this purpose. The characterisation of iPSCs was achieved by conducting immunocytochemistry analysis along with the observation of the morphology of the colonies in culture using a light microscope. These methods were employed to confirm the identity of the cells as iPSCs.

As shown in **Figure 3.2**, the pluripotency markers OCT-3/4, SOX2, NANOG, and TRA-1-60 were present in the three different iPSC types, including the WT, CLN7$^{T294K/T294K}$ iPSCs, and CLN7$^{R465W/R465W}$ iPSCs. Specifically, it can be observed that either OCT-3/4, SOX2, and NANOG are expressed in the nucleus of the cells, whereas TRA-1-60 is a marker present on the surface of the cells, as previously described in **section 3.2.4**. These results indicate that the three different types of iPSCs used were expressing pluripotency, and therefore can be considered PSCs. When considering the colony shape, the presence of a large nucleus relative to the cytoplasmic area of

the cells, and the round morphology and brightness of the cells as observed under a light microscope (**Figure 3.2**), it provides further evidence supporting the notion that these cells possess pluripotency and stemness characteristics. The expression of pluripotency markers in WT iPSCs was found to be similar to that of CLN7$^{T294K/T294K}$ and CLN7$^{R465W/R465W}$ iPSCs. This suggested that both control (WT) and CLN7-derived iPSCs were appropriate for differentiation into NPCs and could be utilised for further research on the CLN7/MFSD8 protein.

However, there are some details on the expression of the pluripotency markers that should be acknowledged. Immunofluorescence staining using anti-TRA-1-60 and anti-OCT3/4 was only conducted in CLN7-mutated iPSCs. Regarding the staining with anti-NANOG, there is some bright staining, shown in **Figure 3.2c**, which might be artefactual or corresponding to iMEFs from the periphery of the iPSCs colonies, as it is a pluripotency transcription factor in embryonic stem cells. Additionally, in the SOX2 panel (**Figure 3.2d**) there are some large cells (more visible in the CLN7$^{T294K/T294K}$ iPSC colony) with cytosolic staining. These can be differentiated cells at the periphery of the iPSC colonies, likely undergoing a neural differentiation.

a

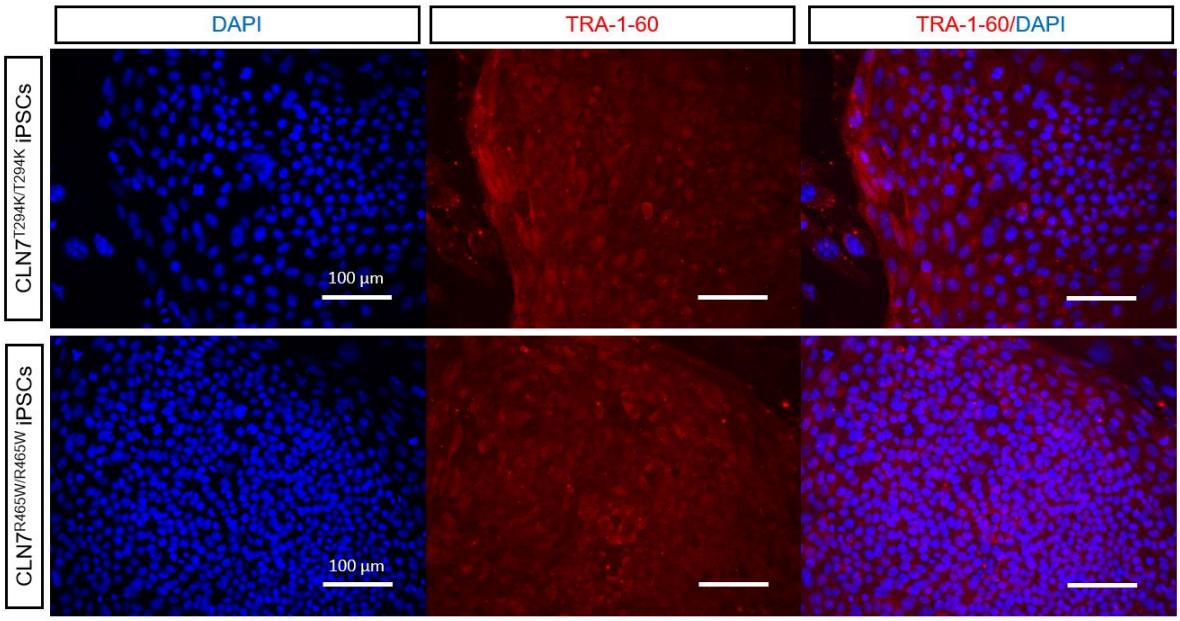
DAPI
TRA-1-60
TRA-1-60/DAPI
CLN7T294K/T294K iPSCs
CLN7R465W/R465W iPSCs
100 µm
100 µm

b

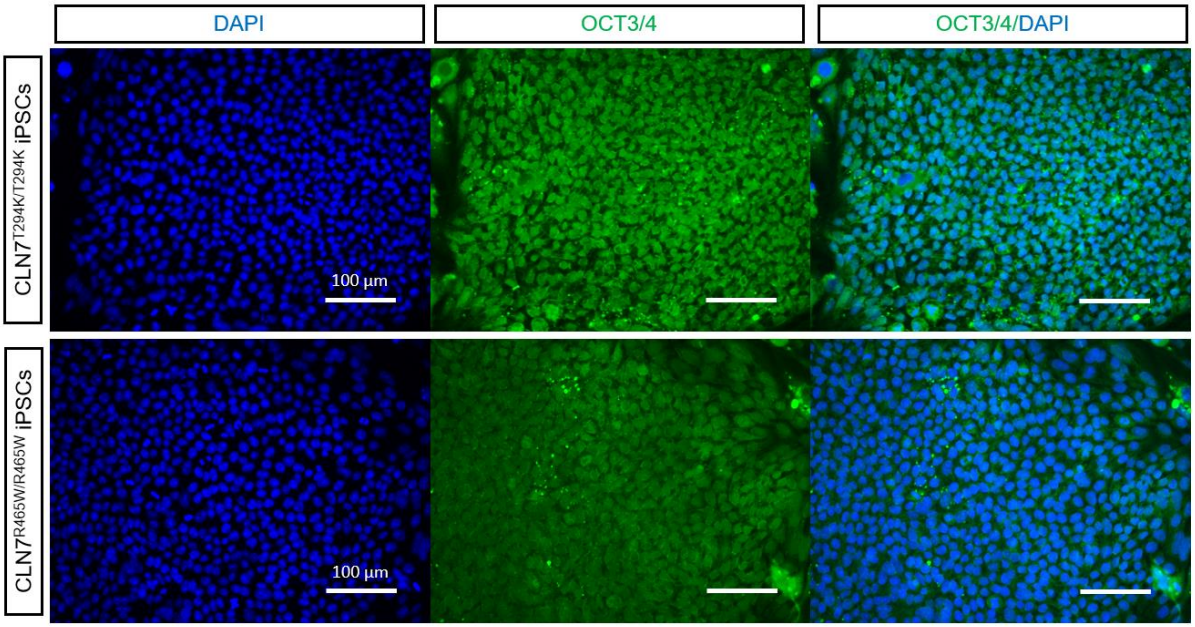
DAPI
OCT3/4
OCT3/4/DAPI
CLN7T294K/T294K iPSCs
CLN7R465W/R465W iPSCs
100 µm
100 µm

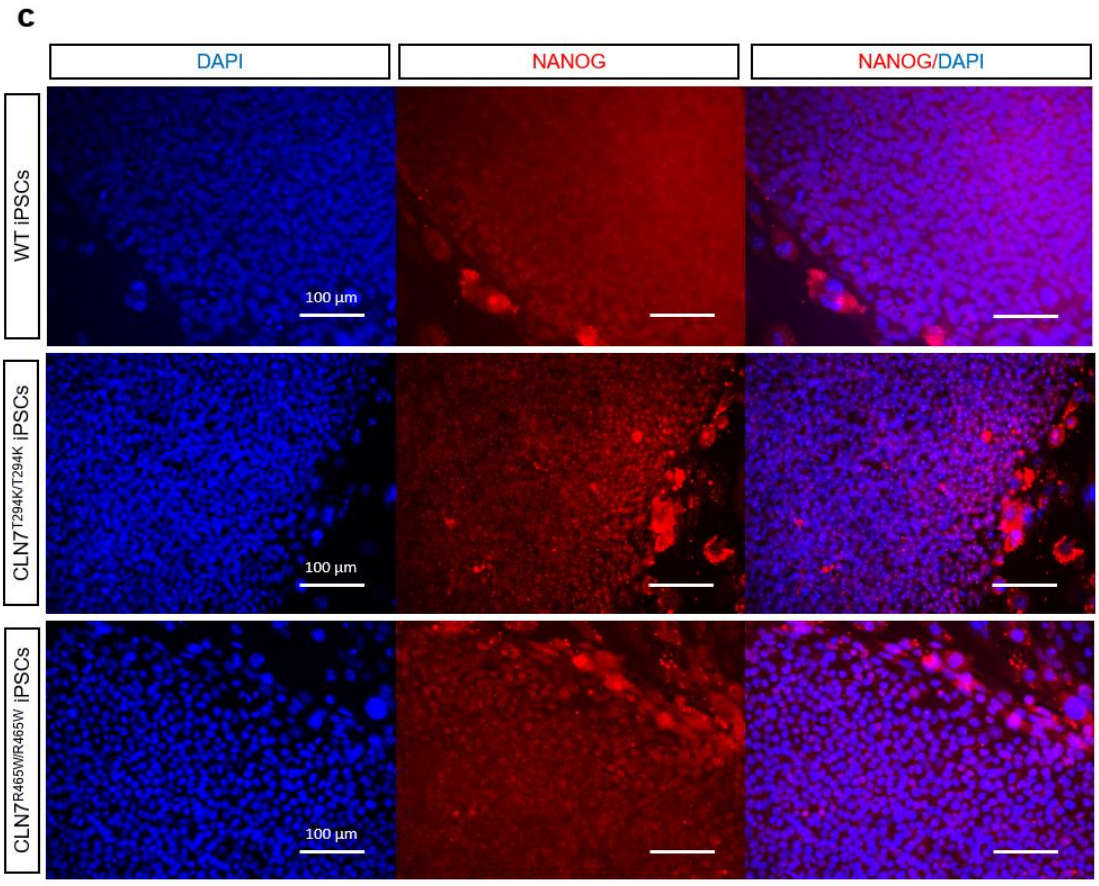
c
DAPI
NANOG
NANOG/DAPI
WT iPSCs
CLN7T294K/T294K iPSCs
CLN7R465W/R465W iPSCs
100 µm

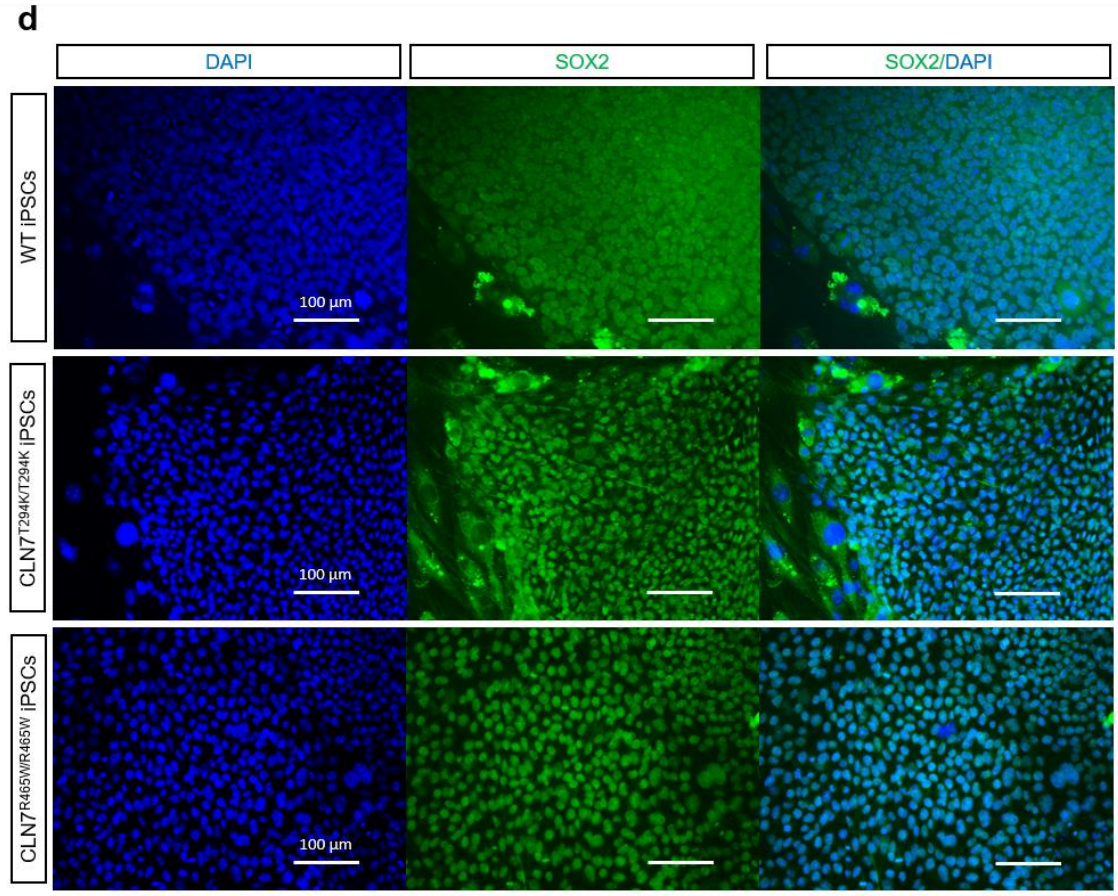
d
DAPI
SOX2
SOX2/DAPI
WT iPSCs
CLN7T294K/T294K iPSCs
CLN7R465W/R465W iPSCs
100 µm

Figure 3.2. Expression of PSC markers in WT, CLN7$^{T294K/T294K}$, and CLN7$^{R465W/R465W}$ iPSCs on iMEFs. Representative fluorescence images of WT, CLN7$^{T294K/T294K}$, and CLN7$^{R465W/R465W}$ iPSC colonies cultured in 12-well plates (onto iMEFs) stained with the pluripotency antibodies (**a**) anti-TRA-1-60, (**b**) anti-OCT-3/4, (**c**) anti-NANOG, and (**d**) anti-SOX2. TRA-1-60 is presented as a surface marker, whereas OCT-3/4, NANOG and SOX2 are nuclear proteins. Images were obtained using a Leica 6000CTR fluorescent microscope (Scale bar = 100 μm).

3.4.3 Validation of the neural differentiation protocol using SHEF ESCs

In this project, the neural differentiation protocol established and validated by FitzPatrick *et al.* (2018) was used to generate NSCs and NPCs (see **Materials and Methods section 2.1.7**). These cells were then used to study CLN7 disease. The Shef3 ESC cell line was utilised in the study conducted by FitzPatrick *et al.* (2018) to investigate the process of neural differentiation from ESCs to NPCs. The neural specification model proposed by FitzPatrick *et al.* (2018) thoroughly described each stage, using microarray data. Consequently, they used Shef3 ESCs for method optimisation of neural differentiation to NSCs and NPCs, given that their neural differentiation had already been extensively characterised.

3.4.4 Neural differentiation of iPSCs to NSCs

Following the protocol developed and validated by FitzPatrick *et al.* (2018), iPSCs were cultured in low attachment V-bottom 96-well plates. The cell culture medium used was NIM supplemented with PVA, which served to promote the formation of neurospheres (**Figure 3.4**). The NIM consisted of DMEM/F-12 with GlutaMAX™, supplemented with other factors, including NEAA, N-2 supplement, bFGF, and heparin to initiate neural induction in iPSCs.

The three different types of iPSCs used in this study were counted and plated simultaneously, enabling their differentiation to be assessed at the same time under identical experimental conditions. Following this protocol, it required several attempts for the iPSCs to successfully generate neurospheres. As depicted in **Figure 3.3**, following a series of media replacements and cell culture conditions, it was observed that the CLN7$^{T294K/T294K}$ and CLN7$^{R465W/R465W}$ iPSCs did not exhibit neurosphere formation. Instead, the cells formed aggregates, but in a dispersed manner. The WT iPSCs were observed to initiate the formation of small neurospheres, which became more apparent on the fifth day following cell plating (**Figure 3.3**). The WT exhibited small neurosphere formation, however, upon their transfer to 6-well plates for NSC generation, they did not show the formation of neural tubes and rosettes, which are often observed as indicators of NSCs. As a result, these cells were unable to produce NSCs, and the small neurospheres were unsuitable for further experiments.

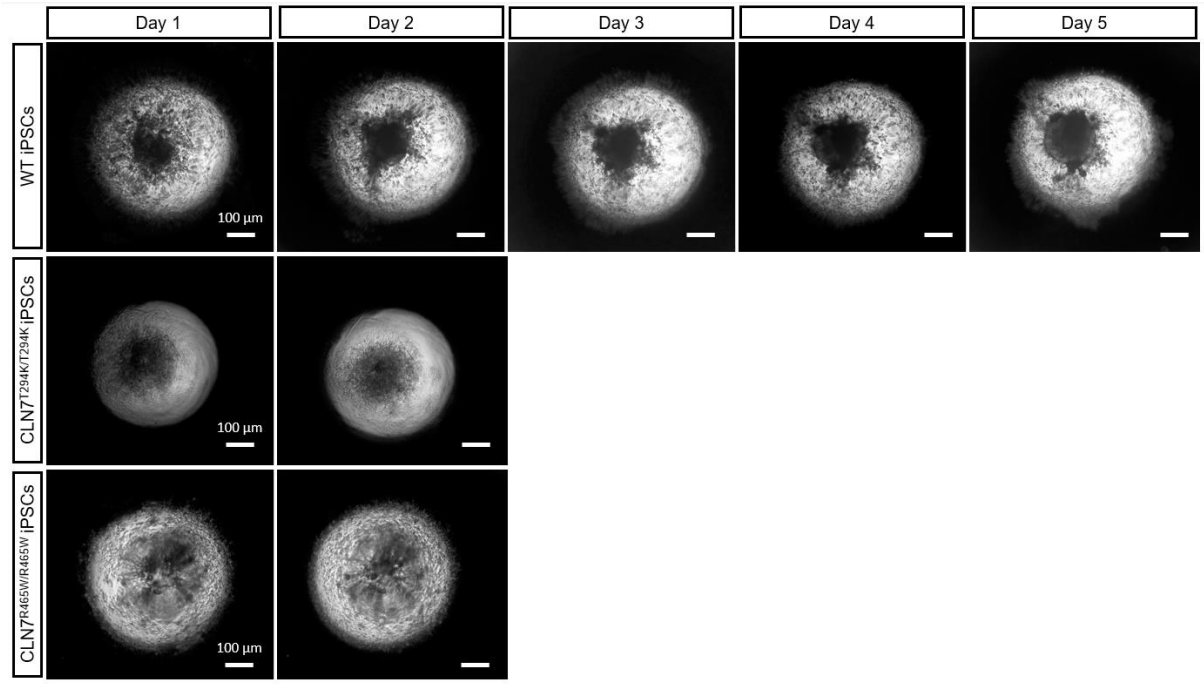

Figure 3.3. Unsuccessful neural differentiation of iPSCs. Representative images of the unsuccessful neural differentiation using WT, CLN7$^{T294K/T294K}$, and CLN7$^{R465W/R465W}$ iPSCs (at passage 22). Although the established protocol was followed, iPSCs failed to form neurospheres during the first attempts. On day 5 after cell plating, WT iPSCs seemed to form small neurospheres, which could not form NSCs. Images were obtained using an EVOS® Imaging System microscope (Scale bar = 100 µm) (Total magnification = 40×).

Despite making several attempts to strictly adhere to the established protocol for neural differentiation and engaging in conversation with the protocol's author to modify different steps and settings, distinct batches of iPSCs were decided to be used instead. Surprisingly, the subsequent neural differentiation attempts were successful as evidenced by the well-defined neurospheres that were observed as early as day 1 following the initial plating of iPSCs (**Figure 3.4**). It was observed that all three types of iPSCs could produce neurospheres. Notably, the CLN7$^{R465W/R465W}$ iPSCs displayed well-defined neurospheres, which were consistently observed across all iPSCs (**Figure 3.4**). Collectively, the several attempts undertaken and the generation of neurospheres using different cell types following the established protocol without any modifications, suggest that the process of neural differentiation could potentially be influenced by the state, quality, or stability of iPSCs.

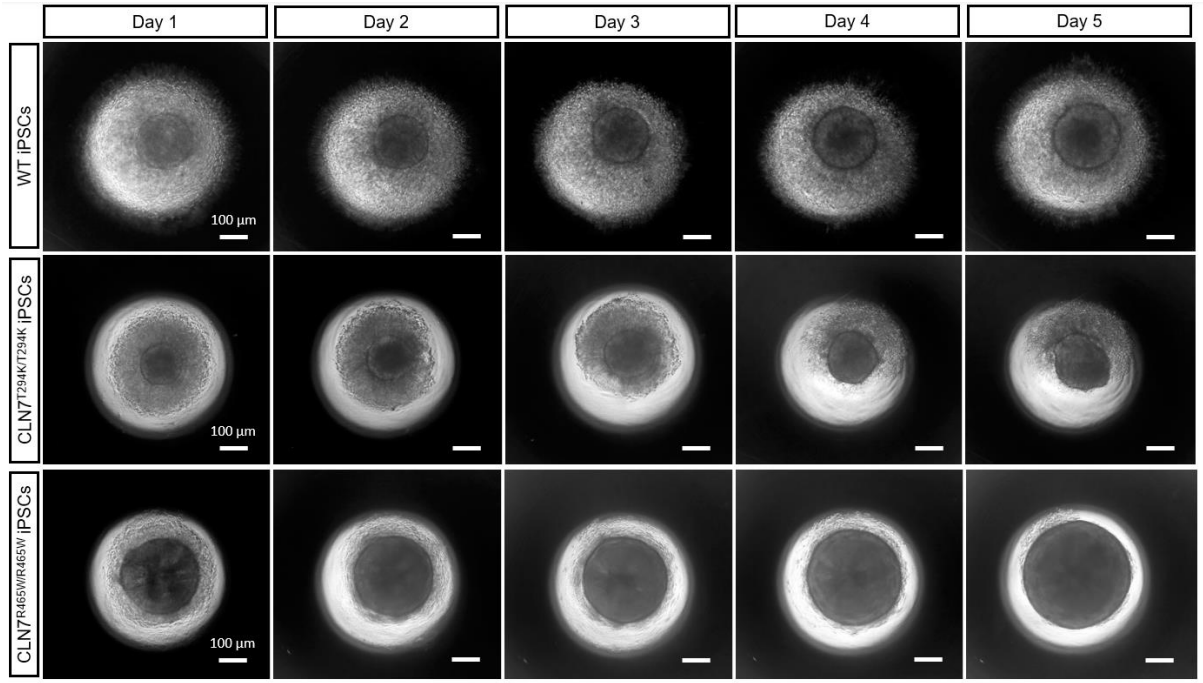

Figure 3.4. Morphological appearance of neurospheres on neural differentiation using iPSCs. Representative images of neural differentiation using a new batch of WT, CLN7$^{T294K/T294K}$, and CLN7$^{R465W/R465W}$ iPSCs (passage 23). The formation of neurospheres could be observed from day 1 after iPSCs plating in V-bottom 96-well plates. Images were obtained using an EVOS® Imaging System microscope (Scale bar = 100 µm) (Total magnification = 40×).

To generate NSCs, around 10-15 neurospheres per well were plated in 6-well plates and cultured with NIM. The presence of NSCs could be inferred from the observation of neural tubes and neural rosettes, as shown in the magnified images presented in **Figure 3.5**. Following the formation of NSCs, the areas containing neural tubes and rosettes were picked after 4-5 days. These picked cells were then passaged to expand the NSC population.

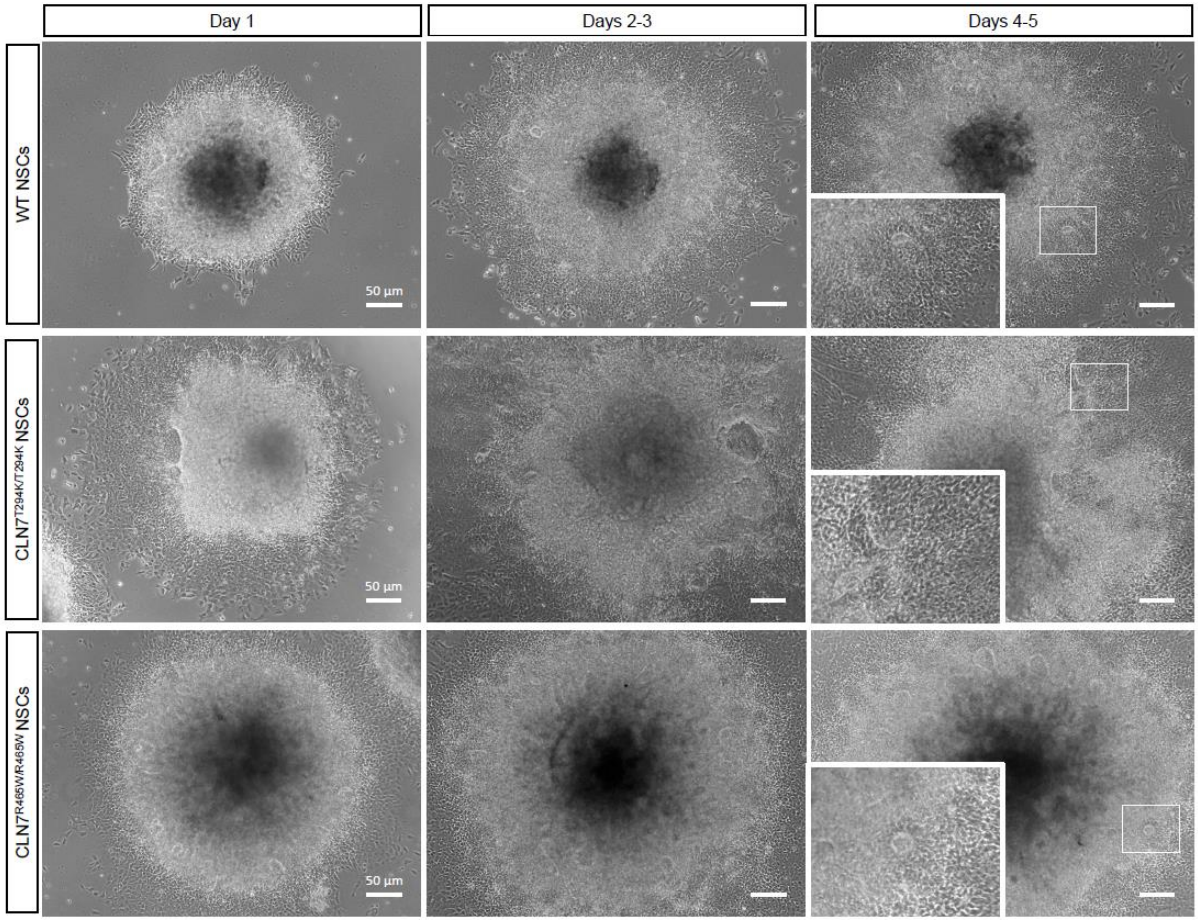

Figure 3.5. Morphological appearance of WT, CLN7$^{T294K/T294K}$, and CLN7$^{R465W/R465W}$ NSCs. The plated neurospheres started to generate neural tubes and rosettes on days 2-3 after plating. The neural tubes and rosettes became more visible on days 4-5 of cell culture. Images were obtained using an EVOS® Imaging System microscope (Scale bar = 50 µm) (Total magnification = 100×).

3.4.5 Neural differentiation of NSCs to NPCs

WT, CLN7$^{T294K/T294K}$, and CLN7$^{R465W/R465W}$ NSCs were further differentiated to generate NPCs (**Figure 3.7**). These NPCs were the intended cell population for the development of this project based on the vLINCL CLN7 model. To do this, the previously acquired NSCs in the form of neural tubes and neural rosettes were gently dissociated and plated onto 6-well plates that were coated with Matrigel® Matrix. The cells were then grown in NEM. Following the plating, the cells exhibited a growth pattern characterised by individual cell formation rather than the formation of colonies (**Figure 3.7**). This observation led to the classification of these cells as NPCs. This classification was further supported by the results obtained from immunostaining these cells with neural expression markers. Following the generation of NPCs, these cells were employed at passages 6 to 12 to simulate the acquisition of CLN7 disease phenotypes. Furthermore, the NPCs exhibited a decrease of growth at a uniform pace upon reaching passage 17, with a subset of them

displaying signs of senescence (a state of permanent growth arrest without the death of cells). One notable finding in the context of culturing and maintaining NPCs is the requirement for a specific confluency level, around 40%, for them to proliferate optimally. Failure to achieve this confluency at seeding density results in reduced cell division rates and potential senescence of the NPCs.

3.4.6 NPCs express the neural markers Nestin, Pax6, and BLBP

The three different cell types of NPCs (WT, CLN7$^{T294K/T294K}$,and CLN7$^{R465W/R465W}$) generated following the neural differentiation protocol outlined in **section 3.5.1** and **Materials and Methods section 2.1.7**, were subsequently subjected to immunostaining with SOX2, Nestin, Pax6, and BLBP to validate their neural phenotype. Nestin, Pax6, and BLBP are considered early neural markers, indicating their role in the early stages of brain development. Conversely, SOX2 serves as a marker for pluripotency, signifying its association with the ability of cells to differentiate into several cell types. All WT, CLN7$^{T294K/T294K}$, and CLN7$^{R465W/R465W}$ NPCs stained positive for these four antibodies, indicating their neural cell identity (**Figure 3.6**). However, despite its primary role in regulating various stages of embryonic development and the differentiation of ESCs, it is expected that SOX2 would be present in stem cells, including early neural stem cells. Nevertheless, it is worth noting that the expression of this protein tends to be rather low. This could be attributed to its capacity to induce cellular differentiation towards neural ectoderm (Zhang and Cui, 2014).

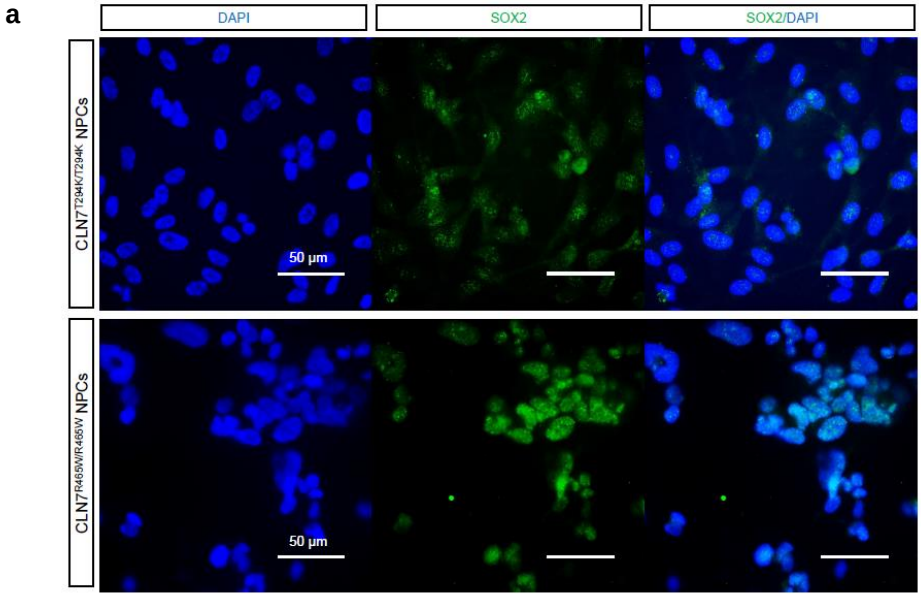
a
DAPI
SOX2
SOX2/DAPI
CLN7T294K/T294K NPCs
CLN7R465W/R465W NPCs
50 µm
50 µm

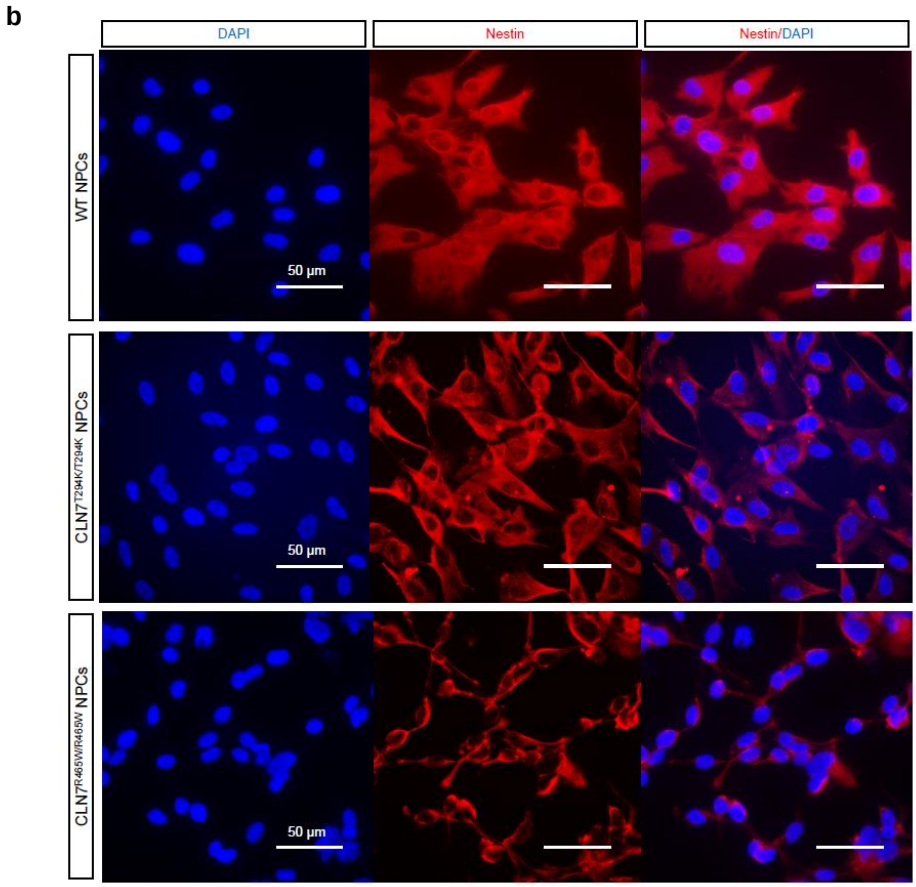
b
DAPI
Nestin
Nestin/DAPI
WT NPCs
CLN7T294K/T294K NPCs
CLN7R465W/R465W NPCs
50 µm
50 µm
50 µm

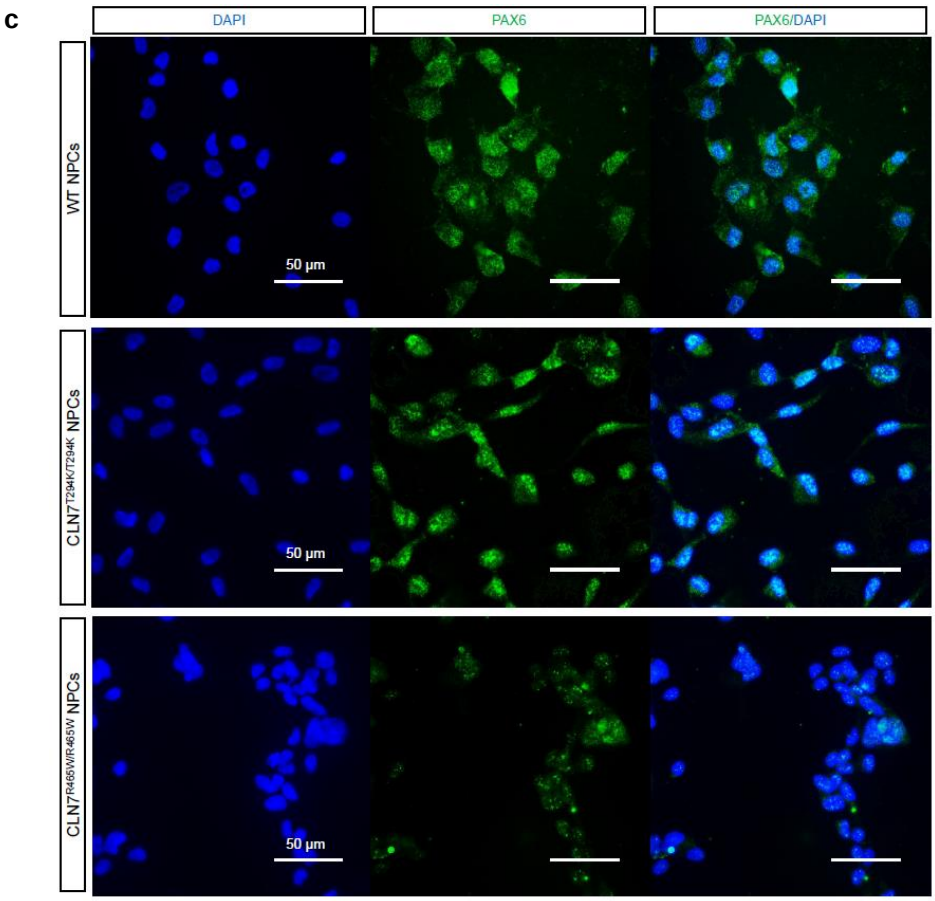
c
DAPI
PAX6
PAX6/DAPI
WT NPCs
CLN7T294K/T294K NPCs
CLN7R466W/R466W NPCs
50 µm

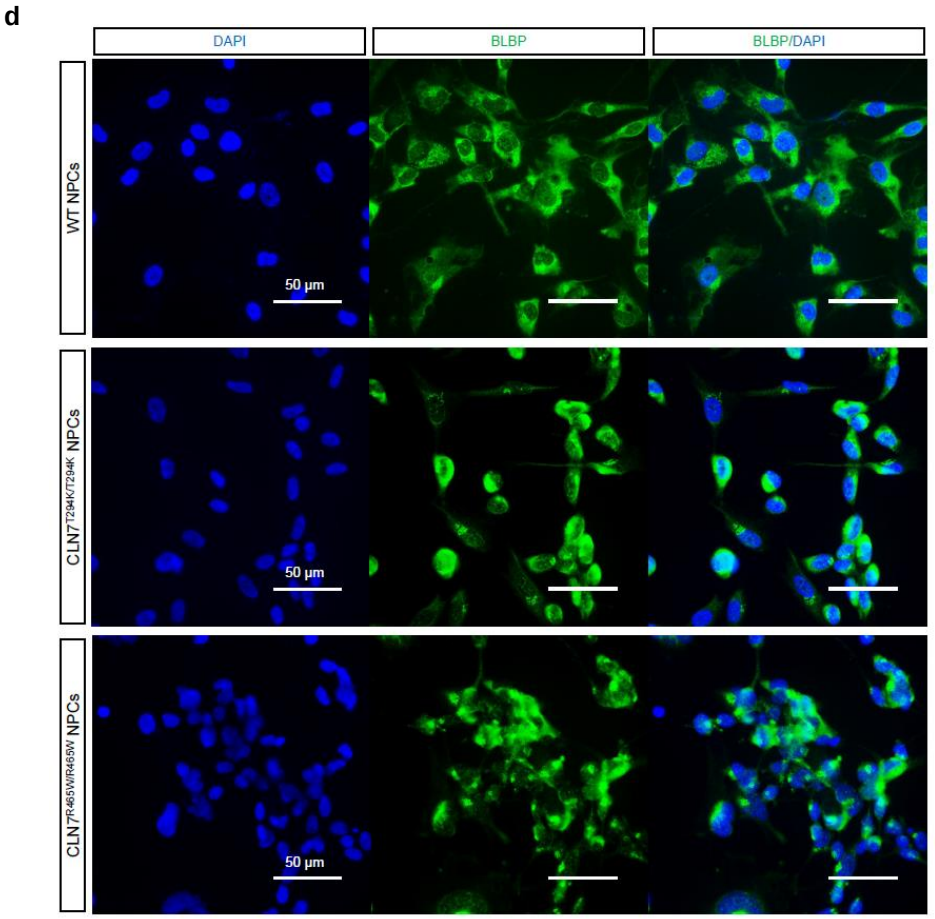
d
DAPI
BLBP
BLBP/DAPI
WT NPCs
CLN7T294K/T294K NPCs
CLN7R466W/R466W NPCs
50 µm

Figure 3.6. Expression of neural markers in WT, CLN7$^{T294K/T294K}$, and CLN7$^{R465W/R465W}$ NPCs. Representative fluorescence images of WT, CLN7$^{T294K/T294K}$, and CLN7$^{R465W/R465W}$ NPCs cultured in 8-well chamber slides (on Matrigel® Matrix) stained with the antibodies (**a**) anti-SOX2, (**b**) anti-Nestin, (**c**) anti-Pax6, and (**d**) anti-BLBP. Images were obtained using a THUNDER fluorescence microscope (Scale bar = 100 μm).

Even though the three distinct cell types of NPCs stained positive for the neural markers of Nestin, Pax6, and BLBP, there are some notable differences. Regarding SOX2 staining, it was only conducted in WT NPCs, and CLN7$^{R465W/R465W}$ NPCs and there were some differences in SOX2 expression. Although both cell types present nuclear SOX2, the WT NPCs seemed to display more cytosolic SOX2, indicating their neural differentiated state (**Figure 3.6a**).

In the panel of Nestin, WT NPCs exhibited a more intense and broader cytoplasmic staining, compared to the CLN7$^{T294K/T294K}$ NPCs, which presented slightly fainter staining. In contrast, in CLN7$^{R465W/R465W}$ NPCs, the cytoplasmic area stained with Nestin seemed smaller, compared to WT and CLN7$^{T294K/T294K}$ NPCs (**Figure 3.6b**). Considering that Nestin is a cytoplasmic marker, these differences could be due to the cell morphology, as CLN7$^{R465W/R465W}$ NPCs tend to present a more differentiated morphology with thinner protrusions than WT and CLN7$^{T294K/T294K}$ NPCs (described below in **section 3.4.7**).

In the panel of Pax6, this marker is mostly expressed in the nucleus of WT and CLN7 NPCs, with an additional expression of Pax6 in the cytoplasm of WT and CLN7$^{T294K/T294K}$ NPCs (**Figure 3.6c**); a difference that could also be attributed to cell morphology, as CLN7$^{R465W/R465W}$ always exhibited thinner cytoplasm and protrusions than WT or CLN7$^{T294K/T294K}$ NPCs. These variations could be due to distinct differentiation states or a more severe disease phenotype caused by the p.R465W mutation.

In the case of BLBP staining, the three types of NPCs exhibited similar expression and localisation of this marker, being mostly present in the cytoplasm of the cells (**Figure 3.6d**). However, slight differences in intensities can be observed when comparing WT and CLN7 NPCs, which can also be attributed to differences in cell morphology.

3.4.7 Potential differences in cell morphology in CLN7$^{R465W/R465W}$ NPCs

During the expansion of CLN7$^{R465W/R465W}$ NPCs, it was noted that these cells seemed to exhibit a more differentiated cell morphology compared to the WT and CLN7$^{T294K/T294K}$ NPCs, especially after passages 6-8. The CLN7$^{R465W/R465W}$ NPCs exhibited a greater number of thin protuberances resembling neural projections compared to WT and CLN7$^{T294K/T294K}$ NPCs (**Figure 3.7**). This

morphological characteristic could be indicative of a more advanced differentiated phenotype, as NPCs exhibit a more rounded morphology and are characterised by the absence of extensive neurite processes (Kang et al., 2017). Additionally, the potentially higher differentiated phenotype of the CLN7$^{R465W/R465W}$ NPCs could be associated with a decreased cell adhesion on glass (even on coated surfaces with Matrigel Matrix®). Consequently, a higher concentration of the coating matrix (1:15) was required, as opposed to the standard 1:30 ratio we typically employed, particularly when conducting immunocytochemistry assays. Despite the similar expression of neural markers observed in the three types of NPCs used in this study, the distinctive morphological characteristics displayed by the CLN7$^{R465W/R465W}$ NPCs may suggest a higher degree of differentiation or aberrant functioning of other proteins within these cells. This finding correlated with the increased severity observed in patients carrying the homozygous R465W mutation in CLN7 disease. It would require further investigation as to whether this morphology relates to the R465W mutation or is an artefact of differences during targeted differentiation.

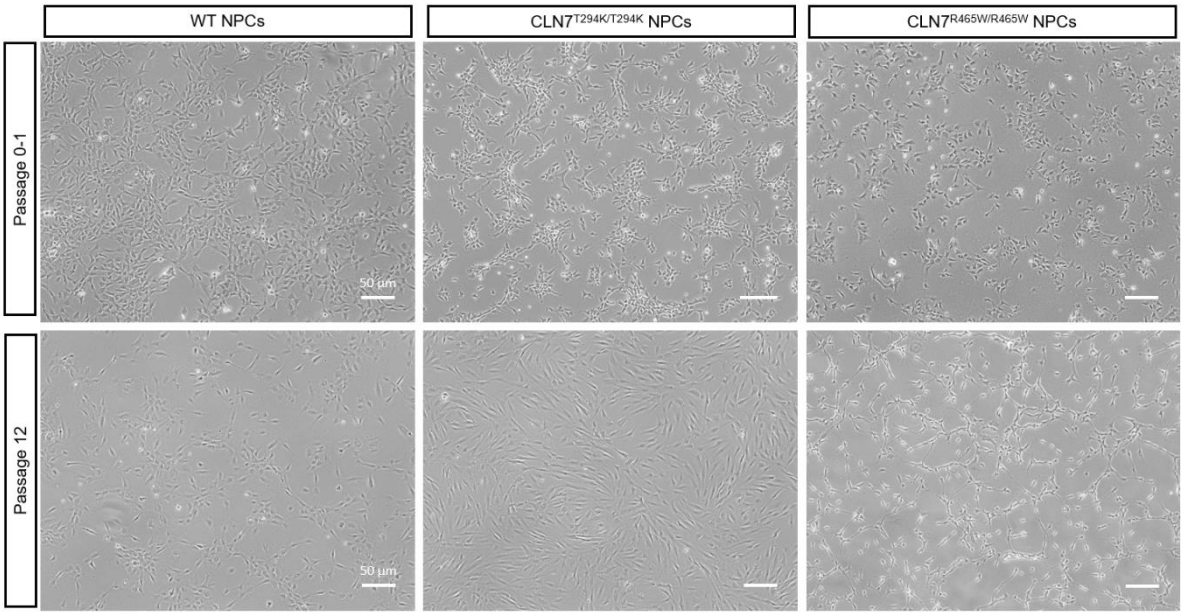

Figure 3.7. Morphological appearance of WT, CLN7$^{T294K/T294K}$, and CLN7$^{R465W/R465W}$ NPCs. The NSCs forming neural tubes and rosettes were picked and plated in 6-well plates coated with Matrigel Matrix®. These cells were culture in NEM and, from passage 0, they started growing as single cells (NPCs). Images were obtained using an EVOS® Imaging System microscope (Scale bar = 50 µm) (Total magnification = 100×).

Limitations

Although this study demonstrates the use of iPSCs and their subsequent differentiation into NPCs that exhibit the expression of markers associated with pluripotency and neural development, respectively, it is important to note the presence of some limitations. One potential limitation of the study is the exclusive reliance on morphology and immunocytochemistry for the characterisation of iPSCs and NPCs. While numerous studies have primarily characterised stem cells using this methodology, it is important to use additional approaches to validate their genotype. In this study, it would have been advantageous to employ the reverse transcription-quantitative polymerase chain reaction (RT-qPCR) techniques, along with trilineage differentiation and flow cytometry, to identify pluripotency and stem cell markers. The decision to disregard the implementation of other characterisation approaches was influenced by the time constraints, challenges encountered, and the multiple attempts required to generate the NPCs. Furthermore, alternative, or additional antibodies may have been employed for the characterisation of iPSCs and NPCs. For instance, other cell surface markers such as SSEA-3/4 and TRA-1-81 could have been used for the evaluation of pluripotency in iPSCs. Moreover, the characterisation of NPCs could have involved the utilisation of antibodies against doublecortin, beta III tubulin, NeuroD1, TBR1, and stathmin 1, for example, which are markers for immature neurons. Nevertheless, Nestin, Pax6, and BLBP have been used in numerous published research as common markers for NPCs (Cheng et al., 2014; Mohamad et al., 2013). Additionally, the stage of NSCs could have been identified by immunostaining employing specific markers such as Nestin and SOX2. However, considering the limited time available and the primary objective of obtaining NPCs from iPSCs, my focus was mainly directed towards characterising the initial cells (iPSCs) and the cells generated through the neural differentiation protocol – the NPCs.

Conclusions

This chapter describes the effective differentiation of iPSCs into NPCs, despite the considerable time needed and several attempts required to accomplish it. The challenges associated with the production of NPCs may be attributed to the quality and stability of iPSCs, as exemplified in this study through the utilisation of identical clones in many attempts to generate NPCs. Using different iPSC clones, a successful generation of NPCs was achieved. This facilitated conducting further experiments, which aimed to explore the potential cellular and molecular mechanisms underlying the pathogenesis of CLN7 disease, using stem cells derived from CLN7 patients, with a focus on the MFSD8 protein.

Chapter 4

CLN7 patient iPSC-derived NPCs present an autophagic-lysosomal phenotype that is ameliorated with Tamoxifen and AZ67

Summary

The previous chapter presented the process of generating NPCs from patient-derived iPSCs. Given the observed localisation of MFSD8 in the lysosomes in previously reported studies, this chapter aims to elucidate and corroborate the potential co-localisation MFSD8 within the lysosomes and other cellular compartments using NPCs specified from vLINCL patients and control iPSCs. This will be achieved through immunocytochemistry techniques, including co-staining with lysosomes, autophagosomes, endosomes, and mitochondria. The findings presented in this chapter indicate that MFSD8 may localise within lysosomes and autophagosomes. Consequently, further investigation was conducted to evaluate autophagy dysfunction in CLN7 disease by examining the expression of different autophagy proteins. Due to the observed autophagic-lysosomal dysfunction in the vLINCL CLN7, this chapter also examines various therapeutic strategies that may improve the observed pathological features in lysosomes and mitochondria, such as the accumulation of the glycosphingolipid globotriaosylceramide (Gb3) in the lysosomes and the condensation of mitochondria in the perinuclear region of the CLN7 patient-derived NPCs.

Introduction

4.1 Impairment of autophagy in neurons

Neurons regulate the process of autophagy in response to alterations in energy homeostasis and nutrient intake (Kaushik et al., 2011). Autophagy is observed to be increased in cortical, Purkinje, and hypothalamic neurons following nutrient restriction, as well as in motor neurons during

starvation (Alirezaei et al., 2010; Kaushik et al., 2011). The kinase complex known as the mechanistic target of rapamycin (mTOR) plays a pivotal role in mediating the link between cellular metabolism and autophagy (Shimobayashi and Hall, 2014). In physiologically normal conditions, mTOR hinders autophagy by phosphorylating the protein ULK1/ATG1. Nevertheless, starvation induces the activation of AMPK and the inhibition of mTOR, both of which subsequently activate ULK1, initiating the process of autophagy. Autophagy is crucial in the survival and plasticity of neurons. When autophagy is impaired, it can result in cellular malfunction. Conversely, an excessive level of autophagy can induce cell death, most likely through the mechanism of apoptosis (Nikoletopoulou et al., 2015; Tan et al., 2014). Malfunctions in autophagy have been identified as potential factors in the development of progressive neurodegeneration within neuronal cells (Hara et al., 2006; Komatsu et al., 2006). Furthermore, defects in autophagy have been associated with several neurodegenerative disorders (Tan et al., 2014).

4.1.2 Proteins involved in autophagy and neurological disorders

4.1.2.1 Autophagy-related (ATG) proteins

Autophagy is a cellular mechanism in which cytosolic components are encapsulated in a double-membrane structure known as an autophagosome (Mizushima et al., 2011). This autophagosome then merges with a lysosome or vacuole, promoting the degradation of its enclosed contents through the action of lysosomal hydrolases (see **sections 1.2.2 and 1.2.3**). The regulation of autophagy is controlled by a group of proteins known as autophagy-related (ATG) proteins, which can be categorised into six different functional units: ATG1-kinase complex, phosphatidylinositol (PI) 3-kinase complex, membrane protein ATG9, ATG2-ATG18 complex, ATG12 conjugation system, and ATG8 conjugation system (Mizushima et al., 2011; Noda and Inagaki, 2015). The first phase of autophagy involves the development of the pre-autophagosomal structure (PAS), where most ATG proteins are assembled. Subsequently, the combined functions of these ATG proteins lead to the generation of autophagosomes from the PAS (Suzuki et al., 2007, 2001). ATG4 is the only protease out of several ATG proteins and plays a crucial role as a necessary component in the ATG8 conjugation system, which is a unique mechanism within the process of autophagy (Ichimura et al., 2000, 2000). The initial step in the ATG8 conjugation mechanism involves the enzymatic processing of nascent ATG8 by ATG4, resulting in the exposure of a glycine residue located at the C-terminus. The E1 enzyme, ATG7, adenylates the C-terminus of processed ATG8 in an ATP-dependent manner, resulting in the formation of an ATG8-ATG7 thioester intermediate. This intermediate facilitates the formation of another thioester intermediate between the ATG8 and the E2 enzyme, ATG3. Ultimately, ATG8 is selectively translocated to the amino group of phosphatidylethanolamine (PE), leading to the formation of the ATG8-PE conjugate.

This conjugate is characterised by the covalent attachments of the C-terminal carboxyl moiety of ATG8 to the amine group of PE by an amide bond. The completion of the conjugation reaction needs the presence of the E3-like ATG12-ATG5-ATG16 complex, which is produced by ubiquitin-like conjugation reactions (Hanada et al., 2007; Noda et al., 2013).

Certain neurological disorders have been correlated with mutations or functional impairment in ATG proteins. Specifically, the p.V471A single nucleotide polymorphism in the *ATG7* gene has been associated with earlier onset Huntington's disease (Meng et al., 2019). Moreover, homozygous loss-of-function mutations in ATG5 and ATG7 have been found to cause neurological diseases characterised by cerebellar ataxia and neurodevelopmental delay (Yamamoto et al., 2023).

4.1.2.2 Beclin 1

Beclin 1 plays a crucial role in the localisation of autophagic proteins to the PAS. It interacts with multiple cofactors, including Atg14L, UVRAG, Bif-1, Rubicon, Ambra1, HMGB1, nPIST, VMP1, SLAM, IP3R, PINK, and surviving, to regulate the lipid kinase Vps-34 protein. This regulation leads to the formation of Beclin 1-Vps34-Vps15 core complexes, which in turn promote autophagy (He and Levine, 2010, p. 1). Several studies have indicated that Beclin 1 is involved in the regulation of autophagy and membrane trafficking, which participate in various physiological and pathological processes. Additionally, impairment of Beclin 1 has been associated with numerous diseases, including neurodegeneration (Kang et al., 2011). For instance, Beclin 1 levels are reduced in the brains of patients with AD. This reduction is linked to impaired autophagy, which may contribute to the accumulation of amyloid-β (Aβ) plaques and hyperphosphorylated tau protein (Jaeger and Wyss-Coray, 2010). Brain samples from patients with HD also show altered Beclin 1 levels, suggesting a potential role in the pathogenesis of this neurodegenerative disorder (Zhu et al., 2018). Moreover, Beclin 1 has been shown to play a role in the clearance of α-synuclein, a protein that accumulates in Parkinson's disease and Lewy body disease. Overexpression of Beclin 1 can activate autophagy, reduce α-synuclein accumulation, and ameliorate associated neuritic alterations in experimental models (Spencer et al., 2009).

4.1.2.3 LC3

The microtubule-associated protein 1A/1B-light chain 3 (LC3) is a soluble protein that is present in several mammalian tissues. During the process of autophagy, a cytosolic variant of LC3 (LC3-I) undergoes conjugation with phosphatidylethanolamine, resulting in the formation of LC3-phosphatidylethanolamine conjugate (LC3-II), which is captured by autophagosomal membranes. The fusion of autophagosomes with lysosomes results in the formation of autolysosomes, where

the intracellular components enclosed within the autophagosomes undergo degradation through the action of lysosomal hydrolases. Simultaneously, the LC3-II protein within the lumen of autolysosomes is degraded. Therefore, the lysosomal degradation of the autophagosomal marker LC3/II serves as an indicator of autophagic activity triggered by starvation. Consequently, the detection of LC3 by Western blotting or immunofluorescence has emerged as a viable approach for monitoring autophagy and its associated mechanisms, such as autophagic cell death (Tanida et al., 2008).

LC3 has also been implicated in some neurological disorders. For instance, in CLN3 disease, an increased expression of LC3-II has been observed in post-mortem brain samples from patients with this NCL variant (Pezzini et al., 2023).

4.1.2.4 p62/SQSTM1

Under normal circumstances, around 30% of proteins that are newly produced within the cell undergo misfolding (Schubert et al., 2000). Cellular proteostasis is regulated by two distinct mechanisms: the ubiquitin-proteasome system (UPS) and autophagy. These autonomous systems are involved in the degradation of diverse substrates and exhibit cooperative function. Certain ubiquitinated proteins, such as the ubiquitin-binding protein p62 (or sequestosome-1, SQSTM1), are commonly found in both systems. p62 serves as an autophagy substrate and is utilised as an indicator of autophagy activity. In a study, it was demonstrated that p62 functions as a mediator for the transportation of ubiquitinated proteins to the proteasome, facilitating their subsequent degradation (Korolchuk et al., 2009). Additionally, it possesses the ability to translocate between the nucleus and cytoplasm to form associations with ubiquitinated cargoes, enabling the maintenance of protein quality control in both the nuclear and cytosolic compartments. Modulating the expression of p62 can induce alterations in the abundance and spatial distribution of ubiquitinated proteins, hence exerting a significant impact on cellular viability. Therefore, an aberrant amount of p62 has been found to potentially contribute to the development of certain disorders (Liu et al., 2016). For example, in ALS, mutations in p62/SQSTM1 can lead to impaired protein degradation and increased cellular stress (Ma et al., 2019). In AD, increasing p62/SQSTM1 levels has been suggested as a potential therapeutic strategy to enhance Aβ clearance through autophagy activation (Cecarini et al., 2020).

4.1.3 Proteins present in vesicular compartments and their association with neurological disorders

4.1.3.1 Endosomal RAB5 and RAB7

The endocytic system in eukaryotic cells constitutes a very intricate network of membrane compartments, each having distinct functions in the cargo sorting, distribution, and degradation of cellular cargo (Conner and Schmid, 2003; Gruenberg and Maxfield, 1995; Mellman, 1996; Pelkmans and Helenius, 2003). Following internalisation in early endosomes, cargo intended for recycling is transported back to the cell surface by recycling endosomes, while cargo designated for degradation is carried to late endosomes and subsequently to lysosomes. While there exists a general agreement regarding the arrangements of the endocytic pathway in relation to organelles and trafficking pathways, the specific processes behind the transportation between different endosomal compartments remain unresolved. The endocytic system has several crucial components, including vesicle coats and adaptors, which play a significant role in intracellular transport. Additionally, important regulators of intracellular transport have been identified such as SNAREs and Rab GTPases. Both SNAREs and Rab GTPases are present as extensive families across eukaryotic genomes, exhibiting a notable abundance in distinct membrane compartments, and actively participating in nearly all membrane trafficking processes (Bock et al., 2001; Söllner et al., 1993; Zerial and McBride, 2001). Rab GTPases play a crucial role in facilitating membrane anchoring before SNARE-mediated fusion (Rothman and Söllner, 1997; Zerial and McBride, 2001). Furthermore, they serve as membrane organisers by modulating a diverse array of soluble effector molecules. Distinct membrane domains are occupied by RAB5, RAB4, and RAB11 sequentially throughout the path of recycling cargo (Sönnichsen et al., 2000). On the other hand, late endosomes are comprised of different domains of RAB7 and RAB9 (Barbero et al., 2002). The cargo intended for degradation is initially internalised into RAB5 domains located on early endosomes and then becomes present in RAB7 domains situated on late endosomes. Therefore, transport between endosomes can be characterised as the movement of cargo between membranes that contain distinct Rab machinery.

The dysfunction of RAB5 and RAB7 has been associated with several neurological disorders. RAB5 plays a critical role in mediating endocytic processes, and its dysregulation has been implicated in AD. Abnormal overactivation of RAB5 has been observed in post-mortem brain samples of AD patients, leading to increased endocytosis and enlarged early endosomes. This overactivation is associated with the accumulation of β-amyloid peptides, a hallmark of AD, which contributes to neuronal dysfunction and disease progression (Guadagno and Progida, 2019; Xu et al., 2019). RAB5 is also implicated in HD. The Huntingtin-HAP40 complex, which regulates early

endosome motility, is a novel RAB5 effector and is upregulated in HD. This suggests that RAB5 dysregulation may contribute to the pathogenesis of HD by affecting endosomal trafficking and cellular homeostasis (Jordan et al., 2022).

4.1.3.2 Lysosomal LAMP1 and LAMP2

Lysosomes are encompassed by a restricting membrane that exhibits several functions. These functions include acidification, sequestration, and transport. Acidification refers to the role of the membrane in maintaining an acidic environment within the lysosome. Sequestration involves the retention of active lysosomal enzymes within the lysosome through the limiting membrane (Kornfeld and Mellman, 1989). Lastly, the membrane facilitates the transport of degradation products from the lysosomal lumen to the cytoplasm (Fukuda, 1991; Lloyd and Forster, 1986; Peters and von Figura, 1994). The membranes of lysosomes encompass a variety of proteins that are extensively glycosylated with N-linked glycans. Among these proteins are lysosome-associated membrane proteins 1 and 2 (LAMP1 and LAMP2), which exhibit structural similarities (Granger et al., 1990). While LAMP2 shows ubiquitous expression, its primary localisation is within the late endosomes and lysosomes (Lippincott-Schwartz and Fambrough, 1987). LAMP2 has been identified as a receptor involved in the specific import and degradation of cytosolic proteins within the lysosome, a process known as chaperone-mediated autophagy (Cuervo and Dice, 1998, 1996). Additionally, it has been reported that the deficiency of Lamp2 results in the premature death of around 50% of Lamp2-deficient mice (Tanaka et al., 2000). Additionally, the presence of autophagic vacuoles has been detected in many tissues affected by LAMP2 deficiency, such as muscle, heart, pancreas, and liver. This glycoprotein LAMP2 is of significant importance in the process of lysosome formation and autophagy (Eskelinen, 2006). LAMP2 deficiency has been associated with lysosomal storage diseases, particularly affecting the midbrain. Studies on Lamp-2-deficient mice have also revealed neuropathological changes, suggesting its importance in central nervous system function (Furuta et al., 2015)

4.1.3.3 Mitochondrial protein ATP5A

The mitochondrial adenosine 5'-triphosphate (ATP) synthase is a complex consisting of many proteins, responsible for the synthesis of ATP from adenosine diphosphate (ADP) and inorganic phosphate (Pi). ATP5A, also known as the mitochondrial α-F1 subunit of ATP synthase, is one of the catalytic subunits of the ATP synthase complex. Within the cell, the tricarboxylic acid (TCA) cycle serves as the primary catabolic pathway for utilising glucose metabolism by-products within the mitochondria. This cycle generates NADH and succinate, which are then supplied to the electron transport chain (ETC) located in the mitochondrial inner membrane (Chan, 2006;

Koopman et al., 2010). The ETC promotes the development of a proton gradient across the inner membrane of the mitochondria by utilising NADH and succinate as redox carriers derived from the TCA cycle. The cell's energy carrier, ATP, is produced by the last component of the ETC, known as complex V or mitochondrial FoF1-ATP synthase, utilising the proton gradient as a driving factor (Habersetzer et al., 2013; Martínez-Reyes and Cuezva, 2014; Yoshida et al., 2001). Some studies suggest that mitochondrial dysfunction is an important feature of neurodegenerative diseases, such as AD, and appears in the initial phases of disease progression (Baloyannis, 2006; Dumont et al., 2011; Gibson et al., 1998; Tillement et al., 2011). Furthermore, another study has indicated a decrease in ATP synthase activity and ATP levels within the brains of individuals diagnosed with AD. In general, neurons exhibit a greater susceptibility to mitochondrial dysfunction as a result of their elevated energy requirements and reliance on respiration for ATP production. This, in turn, leads to the occurrence of oxidative stress and neuroinflammation (Joshi et al., 2019). Additionally, it has been observed that SCMAS and other mitochondrial protein components are enriched in lysosomal lipofuscin in BD neurons. Consequently, neuronal damage might follow as a result of these pathological processes (Misrani et al., 2021; Wang et al., 2020).

4.1.4 Mechanism of action of Bafilomycin A1

The fusion of autophagosomes with lysosomes and the subsequent acidification of autolysosomes are crucial late stages in the autophagic process that are essential for maintaining functional autophagic flux and cellular homeostasis (Beau et al., 2011). Bafilomycin A1 is an inhibitor of the V-ATPase that disrupts both of these processes. The V-ATPase is an enzyme consisting of two distinct complexes, V_1 and V_0. V_1 is located in the cytosol, while V_0 is embedded in the lysosome membrane. Together, these complexes comprise a hetero-multimeric structure. The V-ATPase is composed of a total of 15 different subunits, each of which plays a unique role in the assembly and docking process or on the lysosome membrane (Marshansky and Futai, 2008). Bafilomycin A1 is classified as a macrolide (a class of antibiotic) compound that specifically interacts with the V-ATPase ATP6V0C/V0 subunit c. As a consequence, it inhibits the process of lysosomal acidification by blocking the movement of protons (H^+) into the lysosomal lumen (Yoshimori et al., 1991; Zhang et al., 1994). When considering all those characteristics of bafilomycin A1 it is widely accepted that its inhibitory effect on autphagosome-lysosome fusion is attributed to the obstruction of V-ATPase pump activity. However, the study conducted by Mauvezin et al. (2015) revealed that the absence of V-ATPase subunits, while significantly impacting lysosomal pH, did not block the fusion between autophagosomes and lysosomes (Mauvezin et al., 2015). This finding suggests that the acidification process mediated by V-ATPase is not a fundamental requirement for the fusing of vesicles. Therefore, bafilomycin A1 could potentially impact fusion via an

alternative target. A study by Ganley et al. (2011) indicated that the compound thapsigargin, which acts as an inhibitor of the ATP2A/SERCA Ca^{2+}-transporting ATPase, effectively inhibits the fusion process between autophagosomes and late endosomes (Ganley et al., 2011). It is worth noting that, apart from its effect on V-ATPases, the administration of bafilomycin A1 also eliminates the elongation of autophagosomes generated by Seipin, an integral membrane protein found in the endoplasmic reticulum. This observation is in line with the concept that bafilomycin A1 functions as an inhibitor of the SERCA-dependent Ca^{2+} gradient, which is necessary for the localised release of Ca^{2+} during fusion. To provide more evidence for this concept, it is noteworthy that cells treated with bafilomycin A1 exhibit a substantial rise in cytosolic calcium (Ca^{2+}), similar to the impact reported with thapsigargin (Ganley et al., 2011; Mauvezin et al., 2015). Overall, the data presented in Mauvezin's study (2011) provide evidence that bafilomycin A1 specifically acts on the V-ATPase located in the lysosome to inhibit the acidification of its lumen (Mauvezin et al., 2015). Additionally, it separately inhibits Ca-P60A/SERCA, leading to the disruption of the fusion between autophagosomes and lysosomes. Therefore, these combined effects result in a significant blockage of the autophagic flux (Mauvezin et al., 2015).

4.2 Glycosphingolipid globotriaosylceramide (Gb3) in the lysosomes

The glycosphingolipid globotriaosylceramide (Gb3) is classified within the glycosphingolipids (GSLs) group, which is a diverse set of membrane lipids consisting of a ceramide backbone that is covalently bonded to a glycan moiety (D'Angelo et al., 2013). GSLs play a role in the regulation of membrane-protein function and are involved in facilitating cell-cell interactions. These entities possess the capacity to control cellular differentiation, proliferation, and programmed cell death. Mutations in the GLA gene encoding the lysosomal enzyme α-galactosidase A (α-GalA), cause Fabry disease, which is a congenital X-linked glycosphingolipid storage condition. This disease is classified as one of around 50 monogenic LSDs (Boustany, 2013; Germain, 2010).

4.3 Pro-glycolytic enzyme PFKFB3 in neurons

Glycolysis is commonly recognised as a metabolic mechanism that promotes cell survival by fulfilling the energy requirements of cells during periods of mitochondrial bioenergetic stress or in the absence of oxygen (Bolaños et al., 2010). Nevertheless, it has been observed that various cell types in brain tissue exhibit noticeable variations in their metabolic requirements (Almeida et al., 2004, 2001; Bolaños et al., 1994). The metabolic utilisation of glucose via glycolysis in neurons is often minimal, as it is mostly metabolised by mitochondrial oxidative phosphorylation or the pentose-phosphate pathway (PPP). The PPP plays a crucial role in maintaining the redox status of neurons (Delgado-Esteban et al., 2000; García-Nogales et al., 2003; Herrero-Mendez et al., 2009;

Rodriguez-Rodriguez et al., 2013). In contrast, astrocytes mostly acquire their cellular energy requirements through glycolysis, thereby supplying neurons with lactate as a metabolically oxidizable fuel (Almeida et al., 2004).

One crucial determinant of these metabolic characteristics is the enzyme 6-phosphofructo-2-kinase/fructose-2,6-bisphosphatase-3 (PFKFB3), which promotes glycolysis and is typically not present in neurons but is highly abundant in astrocytes (Herrero-Mendez et al., 2009). The activity of PFKFB3 results in the production of fructose-2,6-bisphosphate (F2,6BP), which acts as a strong positive correlator of the rate-limiting enzyme in glycolysis, known as 6-phosphofructo-1-kinase (PFK1) (El-Maghrabi et al., 2001; RIDER et al., 2004). The continual degradation of the PFKFB3 protein in neurons is a result of its ubiquitylation by the E3 ubiquitin ligase known as anaphase-promoting complex/cyclosome-Cdh1 (APC/C-Cdh1). It has been observed that the activity of APC/C-Cdh1 is comparatively higher in neurons than in astrocytes (Herrero-Mendez et al., 2009). It is worth mentioning that under specific neuropathological circumstances, such as excitotoxicity, the functioning of APC/C-Cdh1 in neurons is suppressed, hence enabling the stabilisation of PFKFB3 protein within the cell. The activation of neuronal PFKFB3 leads to an increase in glucose consumption via glycolysis, resulting in a simultaneous reduction in the PPP (Maestre et al., 2008; Rodriguez-Rodriguez et al., 2012). This decrease in the PPP activity induces redox stress, ultimately leading to apoptotic cell death (Rodriguez-Rodriguez et al., 2012).

4.3.1 Inhibition of PFKFB3 with AZ67

AZ67 is a small molecule that effectively inhibits the activity of the isoform 3 of the PFKFB family – the PFKFB3 (Emini Veseli et al., 2021). Additionally, it prevents the oxidation of NADPH, redox stress, and apoptotic cell death induced by the stimulation of glycolysis in mouse primary neurons under excitotoxic and oxygen-glucose deprivation/reoxygenation conditions. Moreover, *in vivo* injection of AZ67 in mice significantly reduced motor discoordination and brain injury in the middle carotid artery blockage in an ischemia/reperfusion model. These findings demonstrated that the pharmacological inhibition of PFKFB3 is a potential therapeutic approach for the protection of neurons (Burmistrova et al., 2019).

Aims and objectives

The aim of this chapter was to investigate the impact of CLN7 disease on specific cellular characteristics shared across different intracellular compartments *in vitro*, including the lysosomes, autophagosomes, and mitochondria, which are key organelles implicated in the pathogenesis of this neurodegenerative disorder. In the context of impaired autophagy in many different neurodegenerative diseases, this work also aimed to study autophagy-associated proteins in WT

and CLN7-derived NPCs. Additionally, the co-localisation of MFSD8 with different vesicular compartments was examined. These research goals were achieved through the following objectives:

i) To evaluate the potential co-localisation of MFSD8 with distinct vesicular compartments within the cells using immunofluorescence staining.

ii) To assess autophagy in both WT and CLN7 NPCs through immunocytochemical analysis of established autophagy markers.

iii) To determine the efficacy of tamoxifen, an FDA-approved drug, in facilitating the clearance of lysosomal globotriaosylceramide (Gb3) accumulation in both WT and CLN7 patient-derived NPCs.

iv) To study whether inhibiting the glycolytic enzyme PFKFB3 can restore mitochondrial condensation in both WT and CLN7 patient-derived NPCs.

Results

4.4 MFSD8 localisation within the cell

Given that MFSD8 seems to be localised in the lysosomes (Sharifi et al., 2010; Steenhuis et al., 2012, 2010), the next objective was to corroborate this localisation of MFSD8 using NPCs. Consequently, immunocytochemistry was conducted on wild-type (WT), $CLN7^{T294K/T294K}$, and $CLN7^{R465W/R465W}$ NPCs to evaluate the co-localisation of MFSD8 using lysosomal and other vesicular markers. To accomplish this, the antibodies employed in the study included anti-RAB5, a marker for early endosomes, anti-RAB7, to target late-endosomes, anti-LC3 and anti-p62/SQSTM1, which are proteins involved in autophagosomes, anti-LAMP2, which serves as a target to identify lysosomes, and anti-ATP5A, a marker for mitochondria.

Regarding the co-localisation of MFSD8 with endosomes, it could be observed that MFSD8 might co-localise with early endosomes in WT NPCs, as demonstrated through co-staining with anti-RAB5 (**Figure 4.1**). In contrast, MFSD8 did not demonstrate co-localisation with RAB7 protein, indicating a lack of localisation of MFSD8 in late endosomes (**Figure 4.2**).

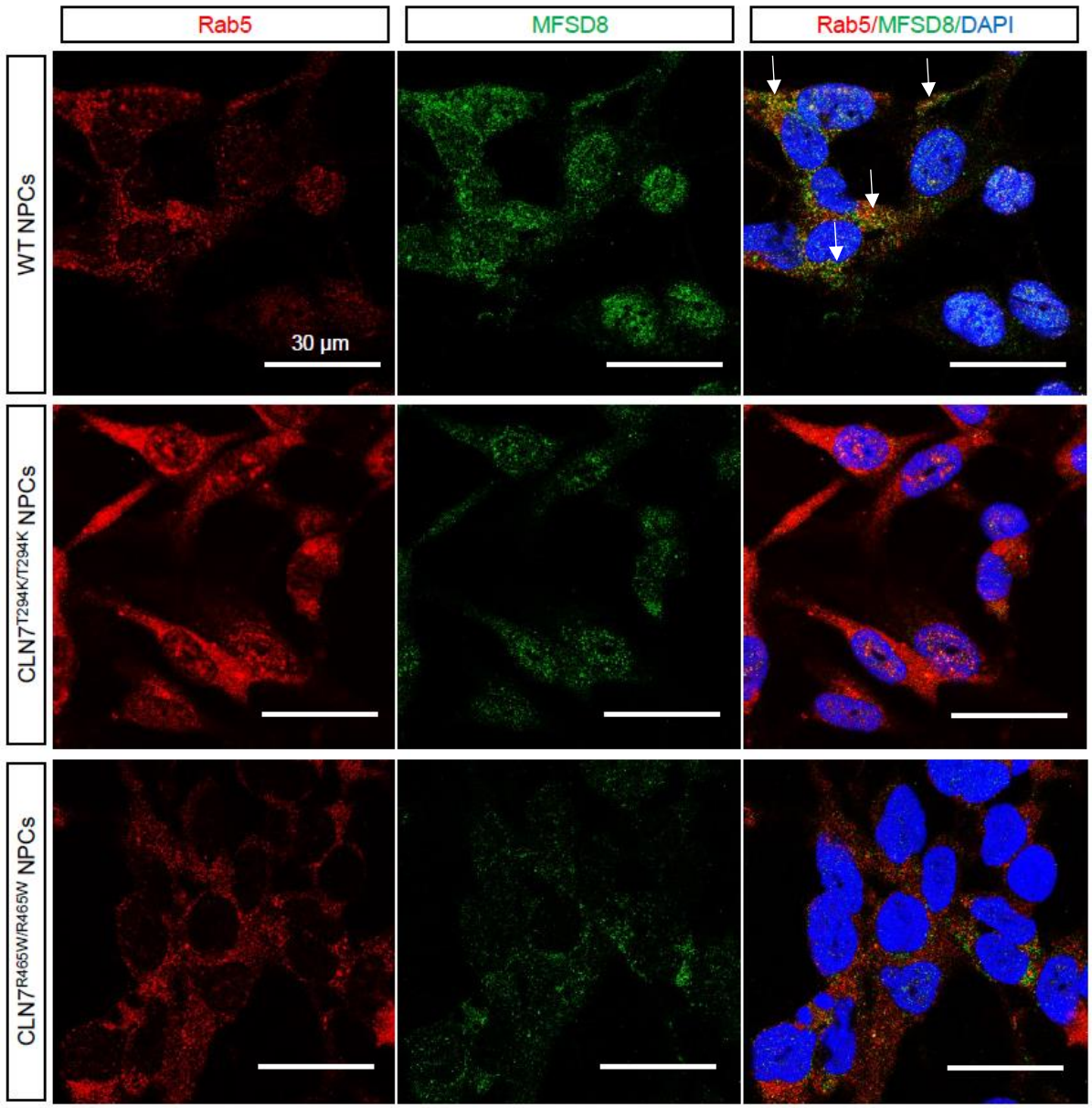

Figure 4. 1. Immunocytochemistry of MFSD8 co-localisation with early endosomes in WT, CLN7$^{T294K/T294K}$, and CLN7$^{R465W/R465W}$ NPCs. MFSD8 co-staining with endosomes was determined by immunofluorescence staining with Rab5 used as a marker for early endosomes. Control (WT) and CLN7 patient-derived (CLN7$^{T294K/T294K}$ and CLN7$^{R465W/R465W}$) NPCs were stained with Rab5 (red), MFSD8 (green), and DAPI (blue; cell nuclei). The white arrows indicate co-localisation between MFSD8 and RAB5. Images were taken using a Leica STELLARIS 5 confocal microscope. Scale bar = 30 µm. (n = 2, biological replicates).

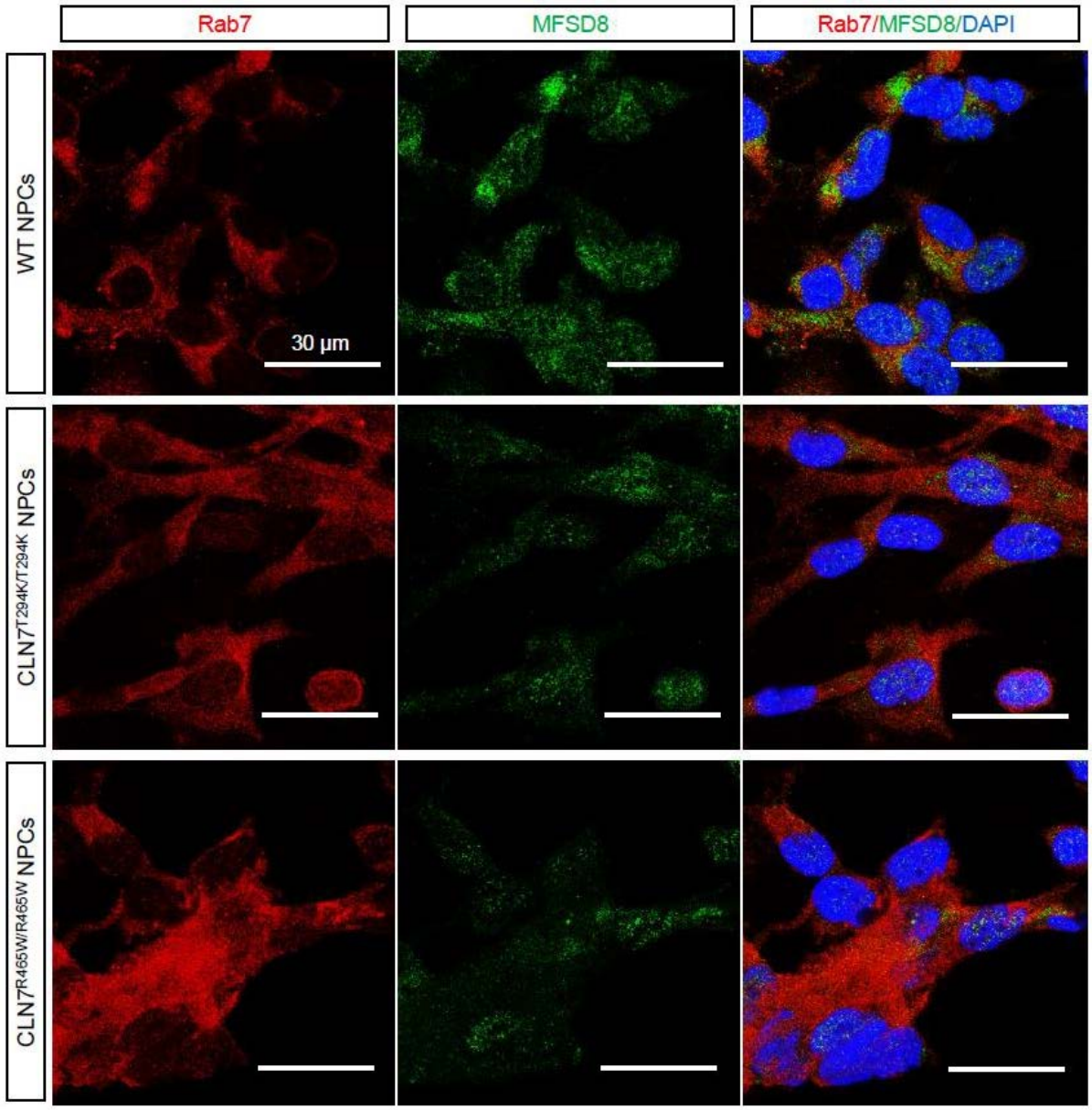

Figure 4. 2. Immunocytochemistry of MFSD8 co-localisation with late endosomes in WT, CLN7$^{T294K/T294K}$, and CLN7$^{R465W/R465W}$ NPCs. MFSD8 co-staining with endosomes was determined by immunofluorescence staining with Rab7 used as a marker for late endosomes. Control (WT) and CLN7 patient-derived (CLN7$^{T294K/T294K}$ and CLN7$^{R465W/R465W}$) NPCs were stained with Rab7 (red), MFSD8 (green), and DAPI (blue; cell nuclei). Images were taken using a Leica STELLARIS 5 confocal microscope. Scale bar = 30 µm. (n = 2, biological replicates).

The immunocytochemistry results additionally demonstrated that the co-localisation of MFSD8 with LC3 was observed in certain regions, with a more pronounced presence in the NPCs derived from healthy individuals (WT NPCs) compared to those derived from patients with CLN7 (**Figure 4.3**). Similarly, the co-localization of MFSD8 and p62/SQSTM1 was seen, particularly in the WT NPCs. However, it is worth noting that p62/SQSTM1 exhibited lower expression levels and appeared as larger dots, whereas LC3 presented a more scattered distribution throughout the cytoplasm (**Figures 4.3-4.4**).

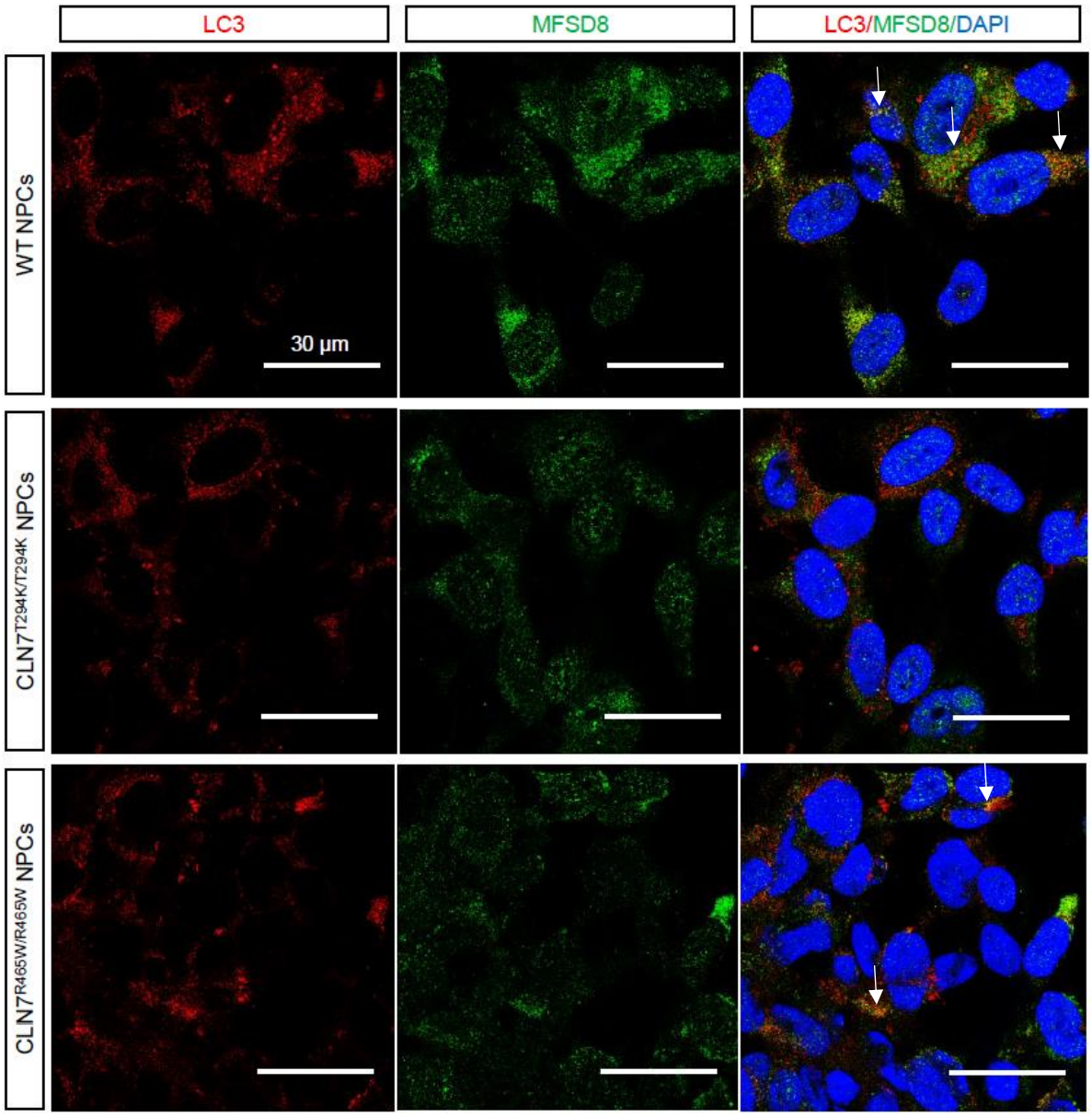

Figure 4. 3. Immunocytochemistry of MFSD8 co-localisation with autophagosomes in WT, CLN7$^{T294K/T294K}$, and CLN7$^{R465W/R465W}$ NPCs. MFSD8 co-staining with autophagosomes was determined by immunofluorescence staining with LC3 used as a target for autophagosomes. Control (WT) and CLN7 patient-derived (CLN7$^{T294K/T294K}$ and CLN7$^{R465W/R465W}$) NPCs were stained with LC3 (red), MFSD8 (green), and DAPI (blue; cell nuclei). The white arrows indicate co-localisation between MFSD8 and LC3. Images were taken using a Leica STELLARIS 5 confocal microscope. Scale bar = 30 µm. (n = 2, biological replicates).

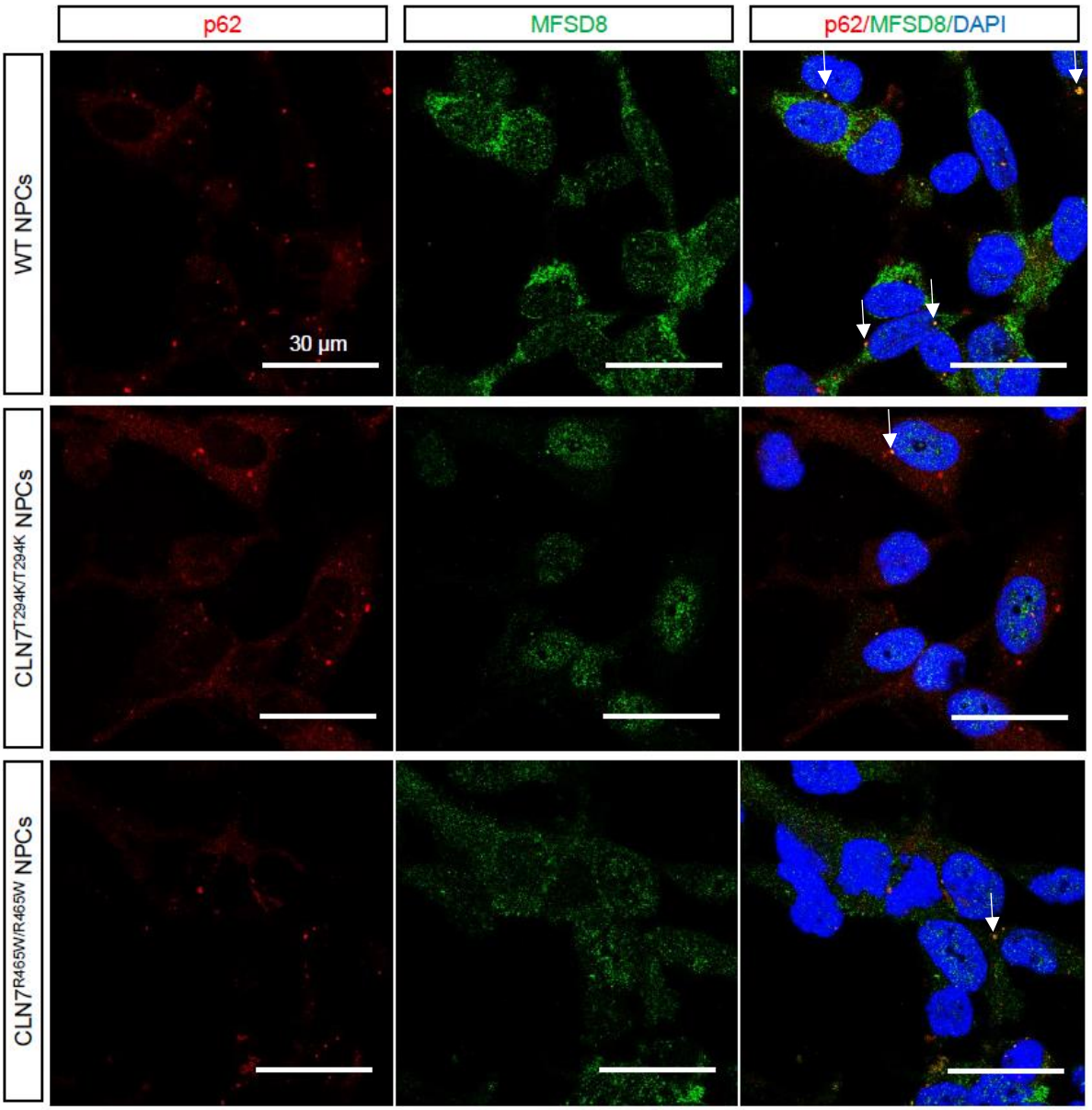

Figure 4. 4. Immunocytochemistry of MFSD8 co-localisation with autophagosomes in WT, CLN7$^{T294K/T294K}$, and CLN7$^{R465W/R465W}$ NPCs. MFSD8 co-staining with autophagosomes was determined by immunofluorescence staining with p62/SQSTM1 used as a marker for autophagosomes. Control (WT) and CLN7 patient-derived (CLN7$^{T294K/T294K}$ and CLN7$^{R465W/R465W}$) NPCs were stained with p62/SQSTM1 (red), MFSD8 (green), and DAPI (blue; cell nuclei). The white arrows indicate co-localisation between MFSD8 and p62. Images were taken using a Leica STELLARIS 5 confocal microscope. Scale bar = 30 µm. (n = 2, biological replicates).

The results of this study suggested that there might be certain co-localisation between the MFSD8 protein and LAMP2 in WT NPCs, providing support for the notion that part of the MFSD8 protein may be present in lysosomes (Wang et al., 2021) (**Figure 4.5**). In contrast, it was observed that the MFSD8 protein did not exhibit localisation within the lysosomes in the NPCs generated from patients with CLN7. Furthermore, it was observed that lysosomes might exhibit a greater degree of enlargement and display distinct patterns of distribution in the cells carrying mutations on the *CLN7* gene (**Figure 4.5**).

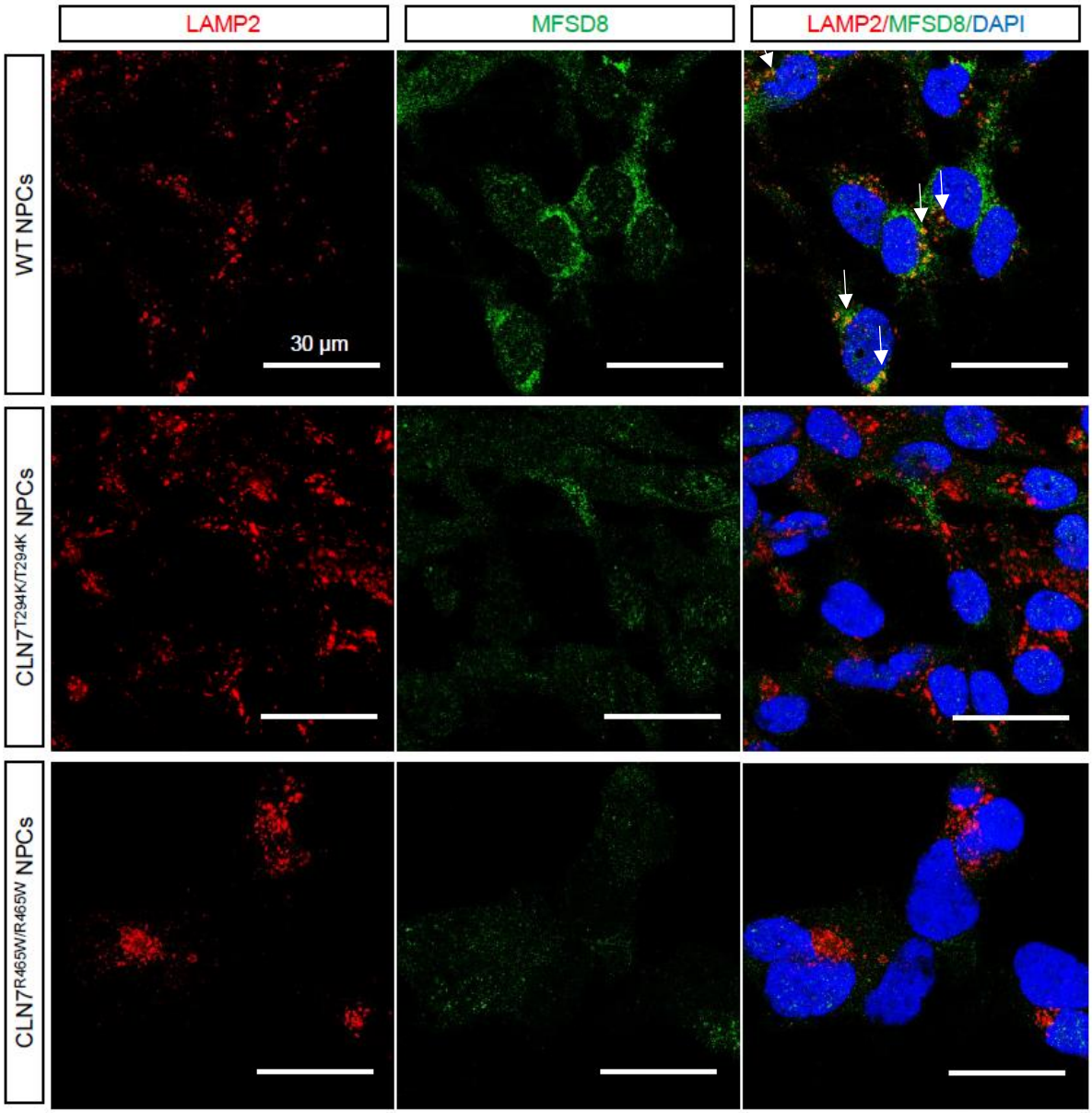

Figure 4. 5. Immunocytochemistry of MFSD8 co-localisation with lysosomes in WT, CLN7$^{T294K/T294K}$, and CLN7$^{R465W/R465W}$ NPCs. MFSD8 co-staining with lysosomes was assessed by immunofluorescence staining with LAMP2 used as a lysosomal marker. Control (WT) and CLN7 patient-derived (CLN7$^{T294K/T294K}$ and CLN7$^{R465W/R465W}$) NPCs were stained with LAMP2 (red), MFSD8 (green), and DAPI (blue; cell nuclei). The white arrows indicate co-localisation between MFSD8 and LAMP2. Images were taken using a Leica STELLARIS 5 confocal microscope. Scale bar = 30 µm. (n = 2, biological replicates).

When assessing the potential co-localisation of MFSD8 with mitochondria in both WT and CLN7-mutated NPCs, the results showed that MFSD8 may not localise within mitochondria (**Figure 4.6**). Interestingly, and consistent with our previous findings on the condensation of mitochondria in CLN7 disease (see **section 4.8**), it could be observed that mitochondria exhibited thinner structures and were distributed throughout the cytoplasm in WT NPCs. Conversely, in $CLN7^{T294K/T294K}$ and $CLN7^{R465W/R465W}$ NPCs, mitochondria displayed a more compacted arrangement in the perinuclear region (**Figure 4.6**).

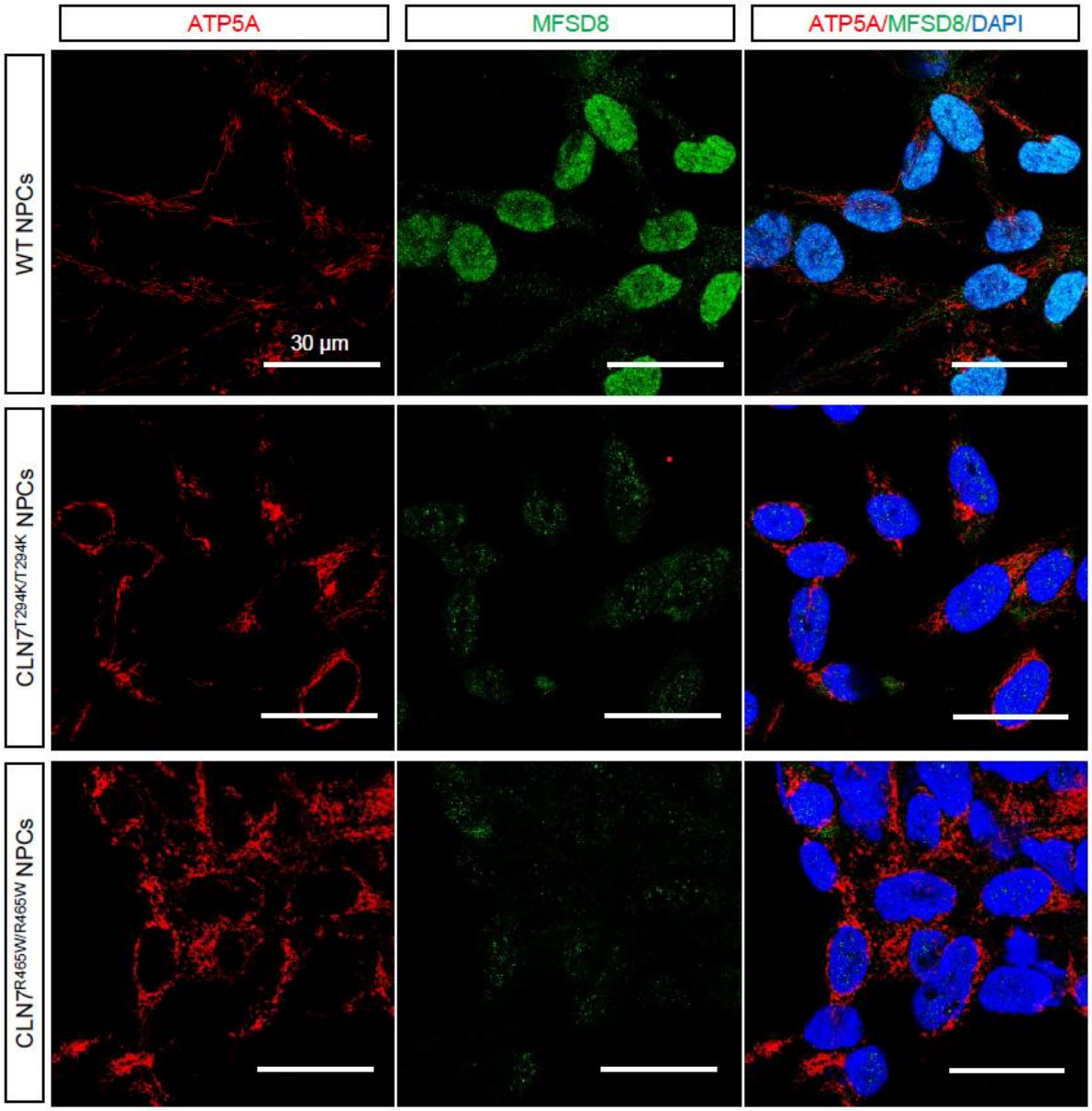

Figure 4. 6. Immunocytochemistry of MFSD8 co-localisation with mitochondria in WT, CLN7$^{T294K/T294K}$, and CLN7$^{R465W/R465W}$ NPCs. MFSD8 co-staining with mitochondria was determined by immunofluorescence staining with ATP5A used as a marker for mitochondria. Control (WT) and CLN7 patient-derived (CLN7$^{T294K/T294K}$ and CLN7$^{R465W/R465W}$) NPCs were stained with ATP5A (red), CLN7/MFSD8 (green), and DAPI (blue; cell nuclei). Images were taken using a Leica STELLARIS 5 confocal microscope. Scale bar = 30 µm. (n = 2, biological replicates).

The primary objective of this work was to investigate the potential co-localisation of the MFSD8 protein with various vesicular compartments located inside the cytoplasm of the cell. However, it is worth noting that the expression of MFSD8 was also observed in the nucleus of the cells (**Figures 4.1-4.6**). Consistently with the differences observed between control (WT) cells and cells with CLN7 mutations, there seem to be discernible variations in the expression of MFSD8 across these cell types. Therefore, the analysis of this discovery will be addressed in this chapter (see **section 4.5**) and the subsequent chapters of this thesis.

Given the possible co-localisation of p62 and LC3 with MFSD8, as observed in this work, the next aim was to examine the potential impact of CLN7 disease on autophagy. These proteins are associated with autophagic flux, which is known to be compromised in various neurodegenerative diseases. Therefore, some autophagy markers were employed to investigate autophagy in the vLINCL CNL7 in the following section.

4.5 MFSD8 localises to the cytoplasm and nucleus and its expression is higher in WT NPCs than in CLN7 NPCs

As observed in **Figures 4.1-4.6**, immunocytochemistry assays revealed that MFSD8 not only localises to the cytoplasm but also localises to the nucleus. Comparing MFSD8 expression on the images obtained from immunofluorescence staining, it can be observed that MFSD8 seems to be expressed slightly differently in the control (WT) NPCs, compared to the CLN7/MFSD8-mutated NPCs ($CLN7^{T294K/T294K}$ and $CLN7^{R465W/R465W}$). Therefore, to evaluate the potential existence of significant differences in the expression of MFSD8 among the three cell types used in this study, a quantification of the fluorescence intensity of cytoplasmic and nuclear MFSD8 was conducted (**Figure 4.7**).

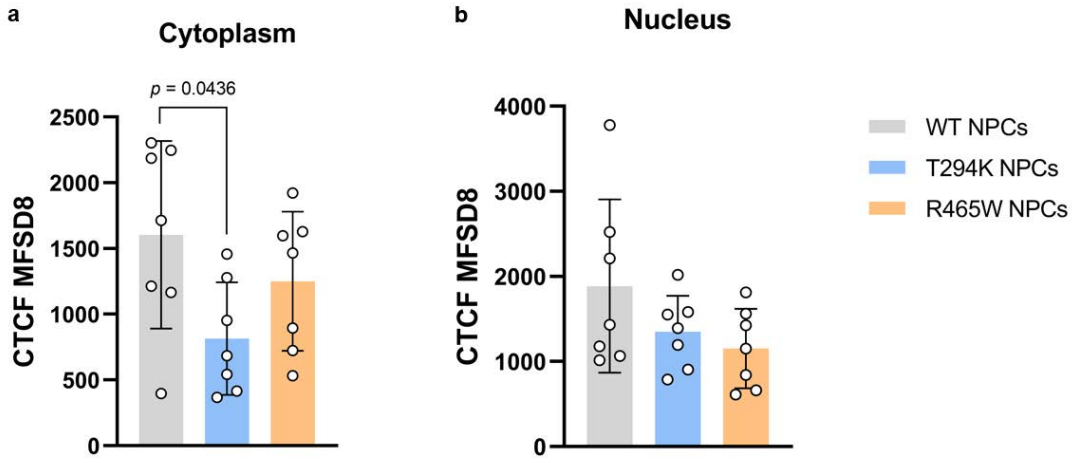

Figure 4.7. MFSD8 protein expression in the cytoplasm and nucleus of control and CLN7 patient-derived NPCs. The protein expression of MFSD8 in the cytoplasm and nucleus of WT, CLN7$^{T294K/T294K}$, and CLN7$^{R465W/R465W}$ NPCs was assessed by quantification of the corrected total cell fluorescence (CTFC) from the immunocytochemistry assay of the vesicular markers using ImageJ software. (**a**) Quantification of the expression of cytoplasmic MFSD8 protein in control (WT) and CLN7 patient-derived NPCs. (**b**) Quantification of the expression of nuclear MFSD8 protein in control (WT) and CLN7 patient-derived NPCs. (n = 7, biological replicates) (One-way ANOVA, Tukey's post hoc test). Mean ± SD.

The analysis of the immunocytochemistry assay showed that the expression of MFSD8 was significantly higher in the cytoplasm of WT NPCs in comparison to the cytoplasmic expression of MFSD8 in the CLN7$^{T294K/T294K}$ NPCs ($p = 0.0436$). The analysis revealed no statistically significant variation in the nuclear expression of MFSD8 among the three cell types (**Figure 4.7**). Although WT NPCs co-stained for MFSD8 and ATP5A seemed to visually exhibit a higher nuclear expression of MFSD8 than CLN7 NPCs (**Figure 4.6**), MFSD8 did not exhibit that higher expression in the other co-localisation images of WT NPCs. This different staining in nuclear MFSD8 of WT NPCs could be attributed to nuclear background in that specific staining with ATP5A.

4.6 Autophagy is impaired in the vLINCL CLN7

Considering that autophagy is impaired in many neurodegenerative diseases (Corti et al., 2020; Fujikake et al., 2018; Menzies et al., 2017a; Park et al., 2020), the next experiment aimed to demonstrate whether autophagy was also affected in the vLINCL CLN7. To achieve that, different autophagy antibodies were used for immunostaining of WT and CLN7-derived NPCs after treatment with 100 nM bafilomycin A1 (Baf A1) for 6 h and without bafilomycin A1 as control. The purpose of employing bafilomycin A1 was to exacerbate the phenotype of the cells regarding

its role in autophagy dysfunction by preventing autophagasome-lysosome fusion and inducing autophagic shunting. The autophagy targets assessed in this study were ATG4B, ATG5, ATG9A, ATG16L1, Beclin-1, LC3B, and p62/SQSTM1. The expression of these autophagy-related proteins was observed by immunocytochemistry using confocal microscopy, followed by the quantification and analysis of the corrected total cell fluorescence (CTCF) in the cytoplasm of the cells. The main interest was to compare the WT NPCs (control, without bafilomycin A1) with the WT NPCs after the treatment with Bafilomycin A1, as well as the WT with the CLN7-derived NPCs ($CLN7^{T294K/T294K}$ and $CLN7^{R465W/R465W}$) all without bafilomycin A1. This would allow a better understanding of the CLN7 phenotype in autophagy. A co-localisation experiment with MFSD8 would have been of great interest, but its was not possible due to the origin of the primary antibodies for MFSD8 and autophagy proteins, as they were all obtained from the same species (rabbit).

First, this study showed that the expression levels of ATG4B were significantly higher in $CLN7^{T294K/T294K}$ and $CLN7^{R465W/R465W}$ NPCs compared to WT NPCs, all without Baf A1 ($p = 0.0053$, $p = 0.0002$, respectively) (**Figures 4.8 and 4.9a**). Similarly, the levels of ATG5 were found to be elevated in the $CLN7^{T294K/T294K}$ and $CLN7^{R465W/R465W}$ NPCs compared to WT NPCs treated with vehicle (**Figures 4.8 and 4.9b**). Regarding ATG9A, its expression augmented in WT NPCs following Baf A1 treatment ($p = 0.0086$) (**Figure 4.9c**), as well as in the $CLN7^{T294K/T294K}$ and $CLN7^{R465W/R465W}$ NPCs with the vehicle, compared to WT NPCs ($p = 0.0012$ and $p = 0.0436$, respectively) (**Figure 4.9c**). In contrast, ATG16L1 levels showed no significant increase in CLN7 NPCs compared to WT NPCs treated either with vehicle or Baf A1 (**Figures 4.8 and 4.9d**), being the highest levels of ATG16L1 present in WT NPCs (**Figure 4.9d**). This observation suggested that ATG16L1 was not affected by the CLN7 phenotype or lysosomal dysfunction exacerbated with Baf A1. The expression of Beclin 1 was found to be significantly higher in WT NPCs treated with Baf A1 compared to WT NPCs treated with vehicle ($p = 0.0001$) (**Figures 4.8 and 4.9e**). Similarly, Beclin 1 expression levels were also significantly higher in $CLN7^{T294K/T294K}$ NPCs treated with Baf A1 compared to $CLN7^{T294K/T294K}$ NPCs treated with vehicle ($p = 0.0042$) (**Figures 4.8 and 4.9e**). The expression of LC3B exhibited a notable increase in WT NPCs treated with Baf A1 compared to WT NPCs treated with vehicle ($p = 0.0172$). Similarly, there was an increase in LC3B levels in NPCs with the T294K mutation when treated with the vehicle, as compared to WT NPCs (**Figures 4.8 and 4.9f**). Finally, p62 displayed greater expression in WT NPCs treated with Baf A1 ($p < 0.0001$), as well as in $CLN7^{T294K/T294K}$ and $CLN7^{R465W/R465W}$ NPCs treated with vehicle ($p = 0.0004$, $p < 0.0001$, respectively), compared to WT NPCs (**Figure 4.9g**). Moreover, it was observed that the levels of p62 in $CLN7^{T294K/T294K}$ NPCs were elevated following the exacerbation

of their autophagy-deficient phenotype with Baf A1, in comparison to CLN7$^{T294K/T294K}$ NPCs treated with vehicle ($p = 0.0009$) (**Figure 4.9g**).

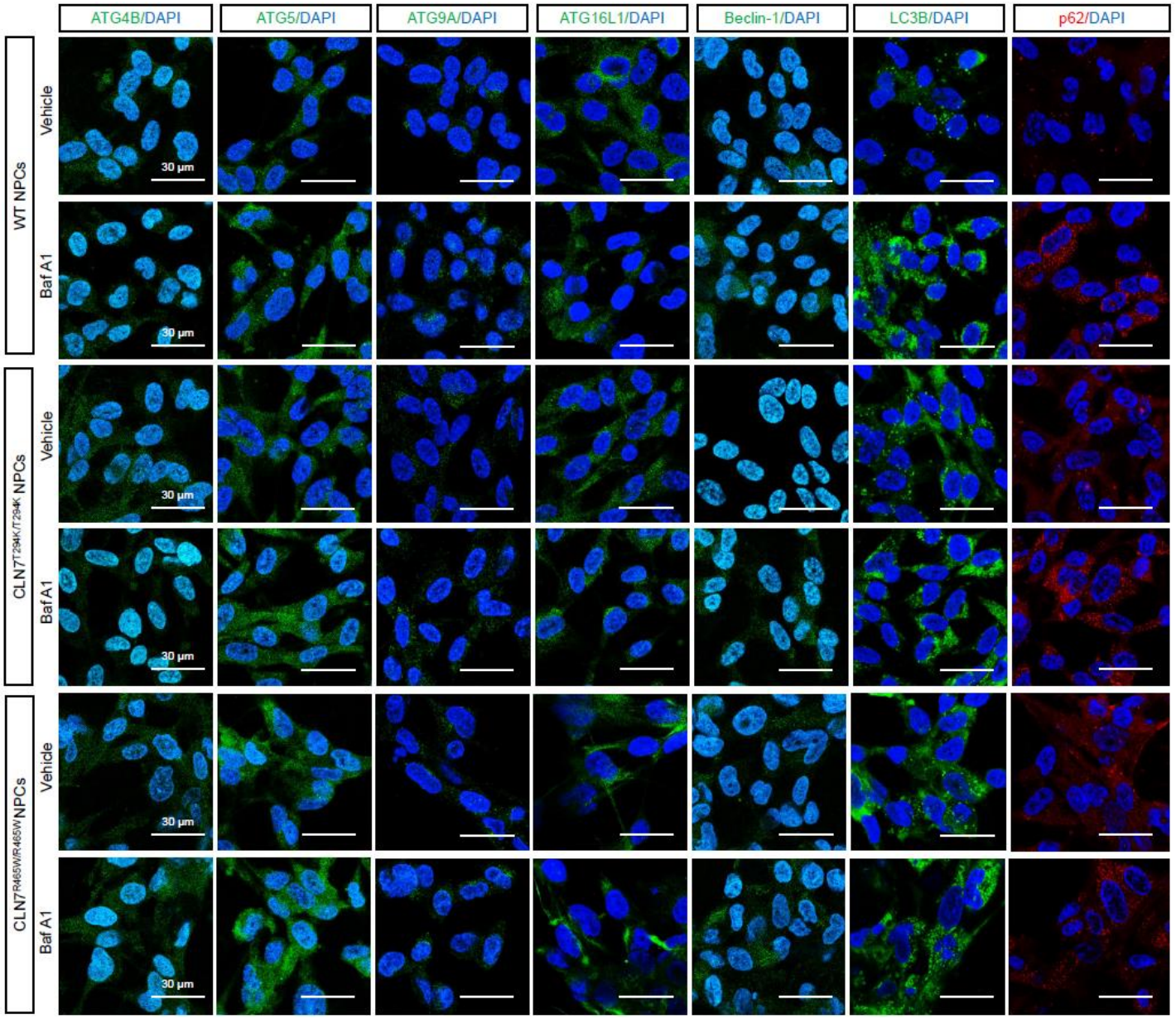

Figure 4. 8. Immunocytochemistry of autophagy markers in WT, $CLN7^{T294K/T294K}$, and $CLN7^{R465W/R465W}$ NPCs. The effect of Bafilomycin A1 (Baf A1) on autophagy in control (WT) and CLN7 patient-derived NPCs ($CLN7^{T294K/T294K}$, $CLN7^{R465W/R465W}$) was assessed by immunofluorescence staining. Cells were treated with vehicle (DMSO) or Baf A1 (100 nM) for 6 h. Following that, cells were stained for the autophagy markers ATG4B (green), ATG5 (green), ATG9A (green), ATG16L1 (green), Beclin-1 (green), LC3B (green), and p62/SQSTM1 (red). DAPI (blue) was used to stain the nuclei of the cells (n = 7, technical replicates). Images were taken using a Leica STELLARIS 5 confocal microscope (Scale bar = 30 µm).

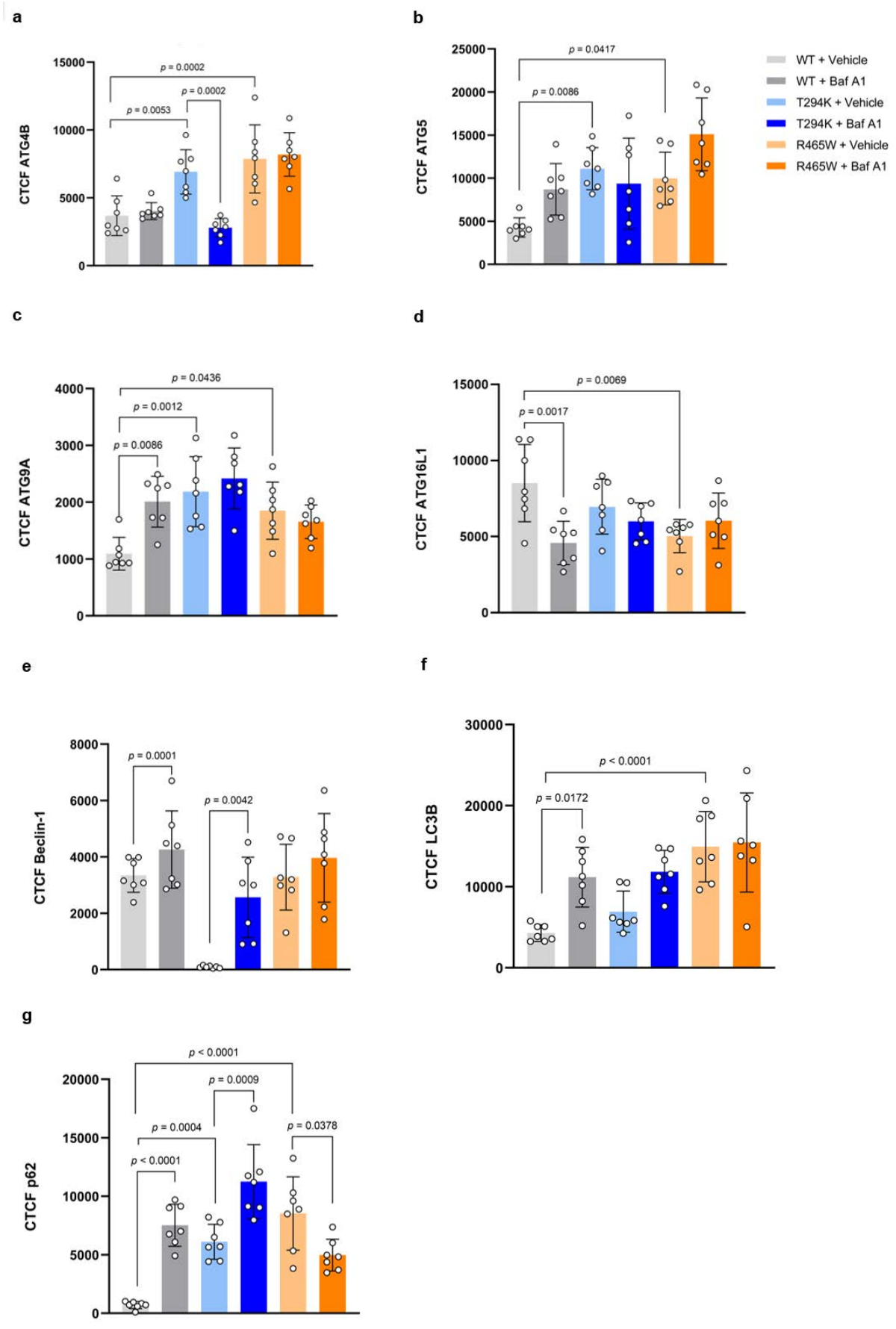
a
CTCF ATG4B
15000
10000
5000
0
p = 0.0002
p = 0.0002
p = 0.0053
b
CTCF ATG5
25000
20000
15000
10000
5000
0
p = 0.0417
p = 0.0086
WT + Vehicle
WT + Baf A1
T294K + Vehicle
T294K + Baf A1
R465W + Vehicle
R465W + Baf A1
c
CTCF ATG9A
4000
3000
2000
1000
0
p = 0.0436
p = 0.0012
p = 0.0086
d
CTCF ATG16L1
15000
10000
5000
0
p = 0.0069
p = 0.0017
e
CTCF Beclin-1
8000
6000
4000
2000
0
p = 0.0001
p = 0.0042
f
CTCF LC3B
30000
20000
10000
0
p < 0.0001
p = 0.0172
g
CTCF p62
20000
15000
10000
5000
0
p < 0.0001
p = 0.0009
p = 0.0004
p = 0.0378
p < 0.0001

Figure 4. 9. Autophagy is impaired in the vLINCL CLN7. The expression of different autophagy markers in the cytoplasm of WT, CLN7$^{T294K/T294K}$, and CLN7$^{R465W/R465W}$ NPCs was assessed by quantification of the corrected total cell fluorescence (CTFC) from the immunocytochemistry assay using Image J software. Cells were treated with vehicle (DMSO) or Baf A1 (100 nM) for 6 h. Following that, cells were stained for the autophagy markers ATG4B, ATG5, ATG9A, ATG16L1, Beclin-1, LC3B, and p62, and images were taken using a Leica STELLARIS 5 confocal microscope. (**a**) Expression of ATG4B in control (WT) and CLN7 patient-derived NPCs. (**b**) Expression of ATG5 in control (WT) and CLN7 patient-derived NPCs. (**c**) Expression of ATG9A in control (WT) and CLN7 patient-derived NPCs. (**d**) Expression of ATG16L1 in control (WT) and CLN7 patient-derived NPCs. (**e**) Expression of Beclin-1 in control (WT) and CLN7 patient-derived NPCs. (**f**) Expression of LC3B in control (WT) and CLN7 patient-derived NPCs. (**g**) Expression of p62/SQSTM1 in control (WT) and CLN7 patient-derived NPCs. (n = 7, technical replicates) (One-way ANOVA, Tukey's post hoc test). Mean ± SD.

These results showed that most ATG proteins, including ATG4B, ATG5, and ATG9A were significantly highly expressed in the NPCs with CLN7 phenotype compared to WT NPCs, except for the ATG16L1, whose expression remained unaffected by the CLN7 phenotype or the lysosomal impairment by Baf A1, or it was even reduced in the CLN7 NPCs with the mutation p.R465W compared to control NPCs (**Figure 4.9d**). Similarly, Beclin-1 expression did not exhibit significant differences between WT NPCs and CLN7 NPCs. However, the levels of LC3 and p62 seemed to be also affected by the CLN7 phenotype, compared to healthy (WT) NPCs.

4.7 Tamoxifen promotes the clearance of lysosomal Gb3 in CLN7 patient-derived NPCs

Prof Diego Medina's research group (from the Telethon Institute of Genetics and Medicine, TIGEM, in Naples, Italy) found that the pathological manifestation of CLN3 and CLN7 diseases can be attributed to the aberrant accumulation of Gb3 in the lysosomes. This finding has been observed in both *in vitro* and *in vivo* models. Consequently, Medina's group decided to use the Shiga Toxin subunit B (STX) assay to identify Food and Drug Administration (FDA)-approved compounds that possess the capability to diminish the accumulation of Gb3 in lysosomes. This was achieved by assessing the co-localisation of Gb3 with the lysosomal membrane protein LAMP1 in arising retinal pigment epithelia (ARPE)-CLN3 KO cells (Soldati et al., 2021). A total of 1280 drugs approved by the FDA were subjected to screening, leading to the discovery of nine compounds with potential activity. The compounds mentioned consist of two drugs from the stilbenoid class (tamoxifen and toremifene), which are selective oestrogen receptor modulators. Additionally, there is one alkaloid (apomorphine), three phenylpiperazines (itraconazole, ketoconazole, and aripiprazole), a derivative of cholesterol (pregnenolone), a diphenylmethane compound (benztropine), and an acetylcholinesterase inhibitor (donepezil dihydrochloride). All

nine compounds underwent additional confirmation and testing using the same STX assay, employing a dose-response format to ascertain the effective concentration (EC50) and assess cell viability (Soldati et al., 2021). The administration of tamoxifen led to a significant decrease in the accumulation of lysosomal STX, exhibiting the highest potency with an EC50 value of 0.75 μM, while maintaining cellular viability intact (data not shown). A slight decrease in the number of nuclei was found just at the most concentrated tamoxifen dosage, indicating a potential sign of cytotoxicity at levels exceeding 30 μM (Soldati et al., 2021).

Tamoxifen is a pharmaceutical drug that has been authorised by both the European Medicines Agency (EMA) and the FDA. It has been utilised for numerous years in the treatment of breast cancer and various other conditions associated with hormonal imbalances. Significantly, it is noteworthy that this intervention has been deemed safe for use in paediatric individuals (Gayi et al., 2018). Due to the drug's extensive and well-established prescription, Medina's group decided to focus on tamoxifen for subsequent investigations. Therefore, in collaboration with Diego Medina's group, we studied the effect of tamoxifen in a cell model of Batten disease, specifically in the vLINCL CLN7. In this study, we utilised NPCs obtained from patient-derived iPSCs. Through immunofluorescence staining, we successfully verified that the application of tamoxifen at a concentration of 10 μM facilitates the elimination of lysosomal Gb3, which was identified with STX, within nestin-positive CLN7 NPCs (**Figure 4.10**). Particularly, CLN7 NPCS that were generated from fibroblasts from the CLN7 patient Pa474, carrying the homozygous mutation R465W, were employed. This suggests the application of tamoxifen as a potential therapeutic strategy for CLN7 disease.

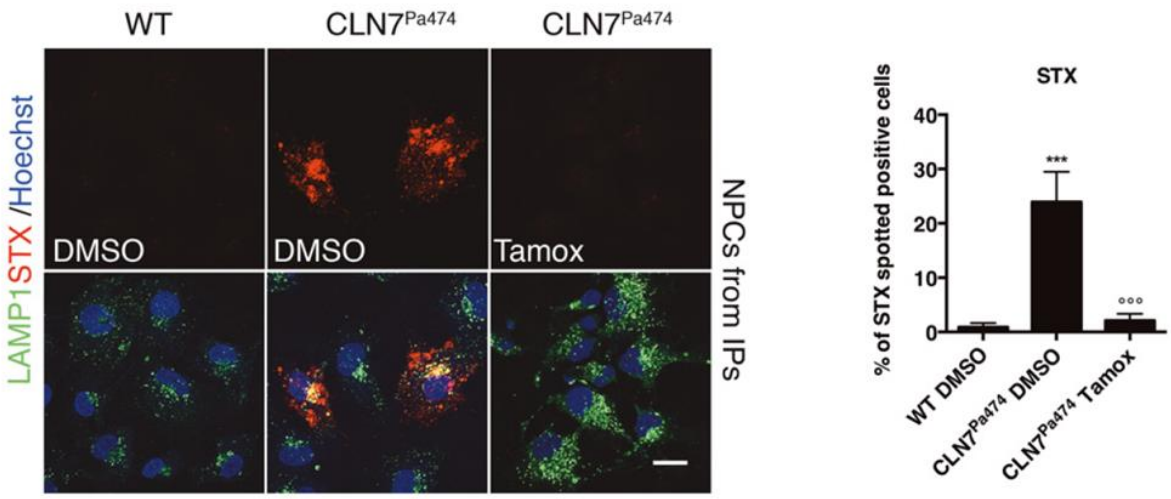

Figure 4. 10. Tamoxifen contributes to the reduction of lysosomal Gb3 in Pa474 CLN7 NPCs. Representative confocal images and quantification of STX staining within the lysosome of WT NPCs and NPCs obtained from Pa474 CLN7 ($CLN7^{R465W/R465W}$) patient-induced iPSCs. The NPCs were subjected to two different conditions: treatment with DMSO or tamoxifen (10 μM) for 48 h. (*** compared to WT, °°° compared to $CLN7^{Pa474}$ DMSO). Data are presented as mean ± SD, ***/°°°$P \leq 0.0001$, as determined by ANOVA (n = 3 biological replicates in duplicate) (Scale bar = 20 μm). Data analysed by Diego Medina's group.

4.8 Inhibition of PFKFB3 restores mitochondrial condensation in CLN7 patient-derived NPCs

Prof. Juan P. Bolaños' research group from the Institute of Functional Biology and Genomics (IBFG) (Universidad de Salamanca, CSIC, Salamanca, Spain) found that the application of pharmacological inhibition targeting PFKFB3 effectively reverses mitochondrial abnormalities and characteristic features associated with *Cln7*$^{\Delta ex2}$ disease in an *in vivo* model. The destabilisation of PFKFB3 in neurons enhances glucose consumption via the pentose phosphate pathway (PPP) and mitigates oxidative stress associated with damage (García-Nogales et al., 2003; Herrero-Mendez et al., 2009; Vaughn and Deshmukh, 2008). This is due to its involvement in providing $NADPH(H^+)$, a crucial cofactor for the regeneration of glutathione (Ben-Yoseph et al., 1996; Hothersall et al., 1979). Consequently, Bolaños' group aimed to evaluate the potential correlation between the activity of PFKFB3 and the occurrence of CLN7 disease. They accomplished this by suppressing the activity of PFKFB3 by using a specifically targeted compound called AZ67 (Boyd et al., 2015). *In vivo*, AZ67 showed the ability to hinder the accumulation of SCMAS, lipofuscin, and reactive astroglia in the cortex (data not shown). Additionally, AZ67 was observed to inhibit the accumulation of SCMAS and lipofuscin in the hippocampus and cerebellum of the *Cln7*$^{\Delta ex2}$ mice.

To evaluate the potential practical applications of these findings, an analysis was conducted on NPCs that were produced from iPSCs obtained from both control subjects and two individuals suffering from CLN7 disease who carried homozygous missense mutations. In collaboration with Bolaños' group, previous members from our lab found that CLN7 patient-derived NPCs exhibited elevated staining of SCMAS (Lopez-Fabuel et al., 2022). Additionally, an increase in mitochondrial ROS (mROS) was observed (Lopez-Fabuel et al., 2022).

During my involvement in this study, I performed immunocytochemistry on NPCs derived from CLN7 patients and healthy controls. These cells were treated with either vehicle (DMSO) or AZ67. Our observations revealed that the CLN7 cells treated with the vehicle displayed mitochondrial condensation in the perinuclear region (**Figure 4.11**). However, this effect was reversed when cells were treated with AZ67 (**Figure 4.11**).

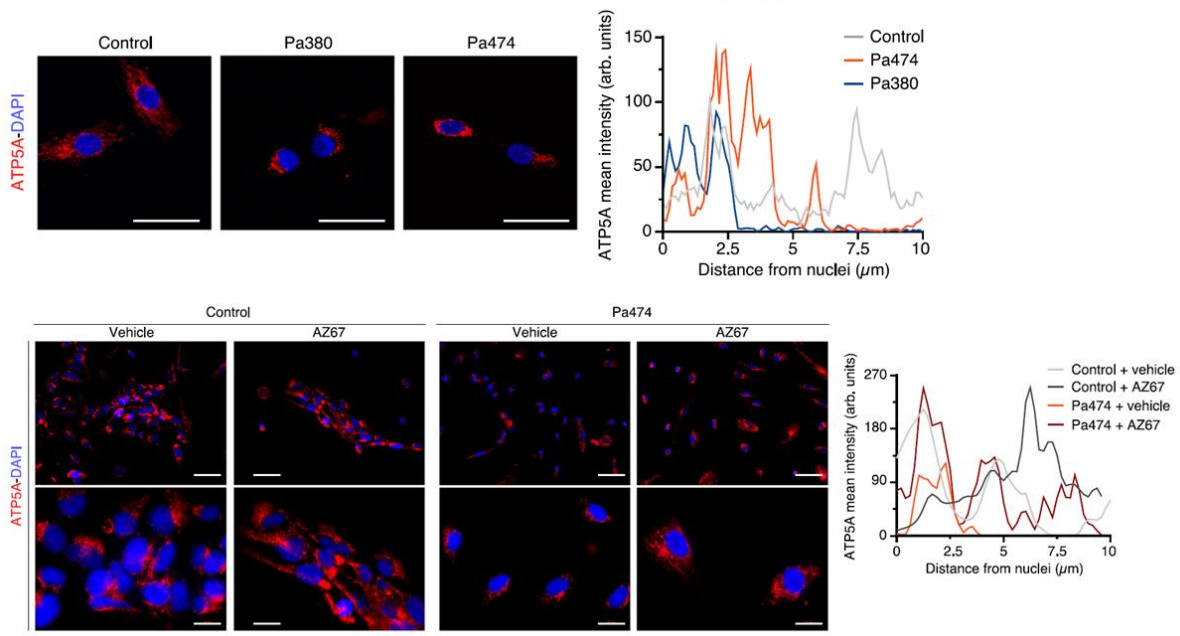

Figure 4. 11. PFKFB3 inhibition in CLN7 patient-derived neural precursor cells restores mitochondrial condensation. (**a**) Representative confocal images and immunocytochemical analysis of the mitochondria marker ATP5A in NPCs derived from the patients Pa380 ($CLN7^{T294K/T294K}$) and, Pa474 ($CLN7^{R465W/R465W}$), and healthy-matched control patients (WT). Scale bar = 50 μm. The graph on the right represents a pixel intensity profile of ATP5A across the maximal axis of the cells starting from the nucleus. (**b**) Representative confocal image of NPCs derived from Pa474 iPSC incubated with AZ67 for 24 h, fixed and subjected to immunocytochemical analysis for ATP5A. Scale bars = 60 μm (upper images of each condition) and 20 μm (lower images of each condition). The graph on the right represents a pixel intensity profile of ATP5A across the maximal axis of the cell that starts from the nucleus. Data analysed by Juan P. Bolaños' group.

Limitations

Although this chapter presents evidence of the possible co-localisation of MFSD8 within lysosomes, autophagosomes, and early endosomes, it is important to understand its inherent limitations. The potential localisation of MFSD8 in these cellular compartments does not necessarily indicate that the protein plays a functional role in these compartments, as they are primarily involved in the recycling and degradation of cellular components. Therefore, to corroborate the localisation of MFSD8 within the lysosomes of the NPCs, it would have been appropriate to perform a lysosomal isolation followed by further investigation using techniques such as Western blotting using lysosomal antibodies. Furthermore, to improve the robustness of our findings, it would have been advantageous to employ a greater number of biological replicates in the immunocytochemistry experiments. Additionally, the incorporation of 3D confocal microscopy imaging would provide a more comprehensive spatial analysis of the potential co-localisation between MFSD8 and the endosomal/lysosomal markers RAB5, p62, and LAMP2. Additionally, a quantitative assessment of co-localisation should be performed using ImageJ software. To enhance the reliability of the findings related to autophagy impairment, it is also necessary to increase the number of biological replicates in the immunocytochemistry experiments. This will contribute to a more robust and conclusive analysis of the autophagy results. In addition, alternative experiments on autophagy, such as the ATG8-turnover assay, could have been employed. This particular assay assesses autophagic flux by quantifying the degradation of ATG8-II in the lysosomes, comparing the levels of ATG8-II in cells treated with a without lysosomal inhibitors. Finally, additional studies should be carried out to elucidate the therapeutic potential of the compounds examined in this study (tamoxifen and AZ67), including pharmacological and toxicity studies to corroborate whether they could be used as an effective CLN7 treatment on their own or in combination with additional treatments to ameliorate the CLN7 disease following clinical studies.

Conclusions

The data presented in this chapter provide evidence about the impact of CLN7 disease on the accumulation of Gb3 within the lysosomes, as well as its potential amelioration using tamoxifen, a repurposed FDA-approved drug. Additionally, the results of this study revealed that the condensation of mitochondria in the perinuclear region of CLN7 NPCs can be reversed through the specific targeting and inhibition of the PFKFB3 enzyme, which is localised within the mitochondria. These findings strengthen the current understanding regarding the localisation of MFSD8 in lysosomes and indicate clear evidence that CLN7 NPCs present a phenotype very similar to that induced by bafilomycin A1 in WT NPCs. In addition, this study has expanded the

potential range of MFSD8 localisations within cells, which will be of fundamental interest for future research to examine the role of MFSD8 in different cellular compartments. Such studies could be crucial in identifying therapeutic drugs that specifically target and ameliorate CLN7 disease.

Chapter 5

Molecular characterisation of MFSD8

Summary

This chapter examines the expression of MFSD8 and its molecular biology in several cell types, such as the human embryonic kidney HEK293T cells, neuroblastoma SH-SY5Y cells, and iPSC-derived NPCs. This was accomplished through immunoblotting of whole cell lysates, as well as nuclear and cytoplasmic fractions obtained using a nuclear isolation protocol. To corroborate the accuracy of the data, some experiments were conducted to validate the specificity of the commercially available primary anti-MFSD8 antibodies used in this project. After analysing the results and observing several protein bands in the expression of MFSD8, some potential post-translational modifications (PTM) in MFSD8 were assessed. The PTMs examined in this study were glycosylation, phosphorylation, and SUMOylation. Some of these PTMs were anticipated, based on the information obtained from PTM databases, and they were studied to further clarify the results of the various blots presented in this chapter and to verify if the bands observed corresponded to different protein isoforms of MFSD8.

Introduction

5.1 Key pathway alterations between CLN7 and WT NPCs

To investigate the involvement of CLN7/MFSD8 in the phenotype of BD, a study was conducted by Dr Aseel Sharaireh, a former member of McKay's group, using unbiased proteomics to perform a comparative analysis between CLN7 NPCs ($iNPC^{BD}$) and WT NPCs ($iNPC^{WT}$) under two conditions: before and after Bafilomycin A1 (here referred to as Baf A) treatment. This experiment applied a quantitative isobaric tag for absolute quantitation (iTRAQ) mass spectrometry. To improve the efficacy and significance of these tests, they incorporated two different CLN7 NPC

types, specifically those with the biallelic mutations p.R465W and p.T294K. These variants were denoted as C1 iNPC^{BD} (or iNPC^{BD1}) and C2 iNPC^{BD} (or iNPC^{BD2}) in **Figure 5.1**, respectively. Additionally, age-matched NPCs obtained from an unaffected male and female donor were added for comparison. These control NPCs were referred to as C1 iNPC^{WT} (or iNPC^{WT1}) and C2 iNPC^{WT} or (iNPC^{WT2}). A Bayesian analysis (it uses probability statements to address research inquiries related to unknown factors) matrix comparison was conducted to analyse three biological replicates of four experimental groups with either vehicle (Veh) or Baf A1 treatment (**Figure 5.1A**). In this study, a comprehensive analysis was carried out on a total of 5619 proteins, where only those proteins exhibiting a fold change > 2 and a *p*-value < 0.05, when compared to the control groups, were considered for further investigation. The results of the study indicated that there were no proteins that exhibited significant differences between iNPC^{WT1} and iNPC^{WT2}. However, a total of 45 proteins showed significant differences between iNPC^{BD1} and iNPC^{BD2}. This observation provided strong evidence of similarities between the WT samples and BD samples, while also accounting for any variations due to sex differences. The comparison between iNPC^{BD1+2} and iNPC^{WT1+2} under basal conditions resulted in the identification of 762 upregulated and 599 downregulated proteins. Additionally, Baf A treatment led to the observation of 147 upregulated and 238 downregulated proteins.

The levels of Golgi-associated vesicular transport and apoptosis were shown to be higher in iNPC^{BD} compared to iNPC^{WT}. In contrast, other cellular metabolic processes, such as the metabolism of amino acids, lipids, and the Pentose Phosphate Pathway (PPP), exhibited differences in the Baf A iNPC^{BD} versus iNPC^{WT} comparison (**Figures 5.1Bi-Bii**). One notable finding is that a significant proportion of proteins, specifically 74% (442 out of 599) that displayed a decrease in expression levels in the iNPC^{BD} group compared to the iNPC^{WT} group were found to be closely linked to the nuclear compartment. The treatment with Veh and Baf A exhibited common GO/Reactome terms, which included *mRNA transcription*, *mRNA splicing*, and *mRNA nuclear export* (**Figure 5.1Ci-Cii**). The observations of increased vesicular transport, lipid metabolism, amino acid metabolism, and glucose metabolism (tricarboxylic acid cycle, TCA; and PPP) correlated with findings reported in prior studies on BD (Danyukova et al., 2018; Lopez-Fabuel et al., 2022). In addition, the increase in apoptosis (programmed cell death) in iNPCs correlates with the pathophysiology of neurodegenerative disorders. The results indicated a separation of cellular activity based on the upregulation of proteins involved with vesicular transport and metabolism (**Figure 5.1D**), and the downregulation of proteins primarily related to nuclear function (**Figure 5.1E**). This observation was consistent with the belief that MFSD8 might have several functional roles when a mutation leads to a loss-of-function (LOF) that impacts

vesicular transport and metabolism, or even a gain-of-function (GOF) that disrupts normal nuclear function.

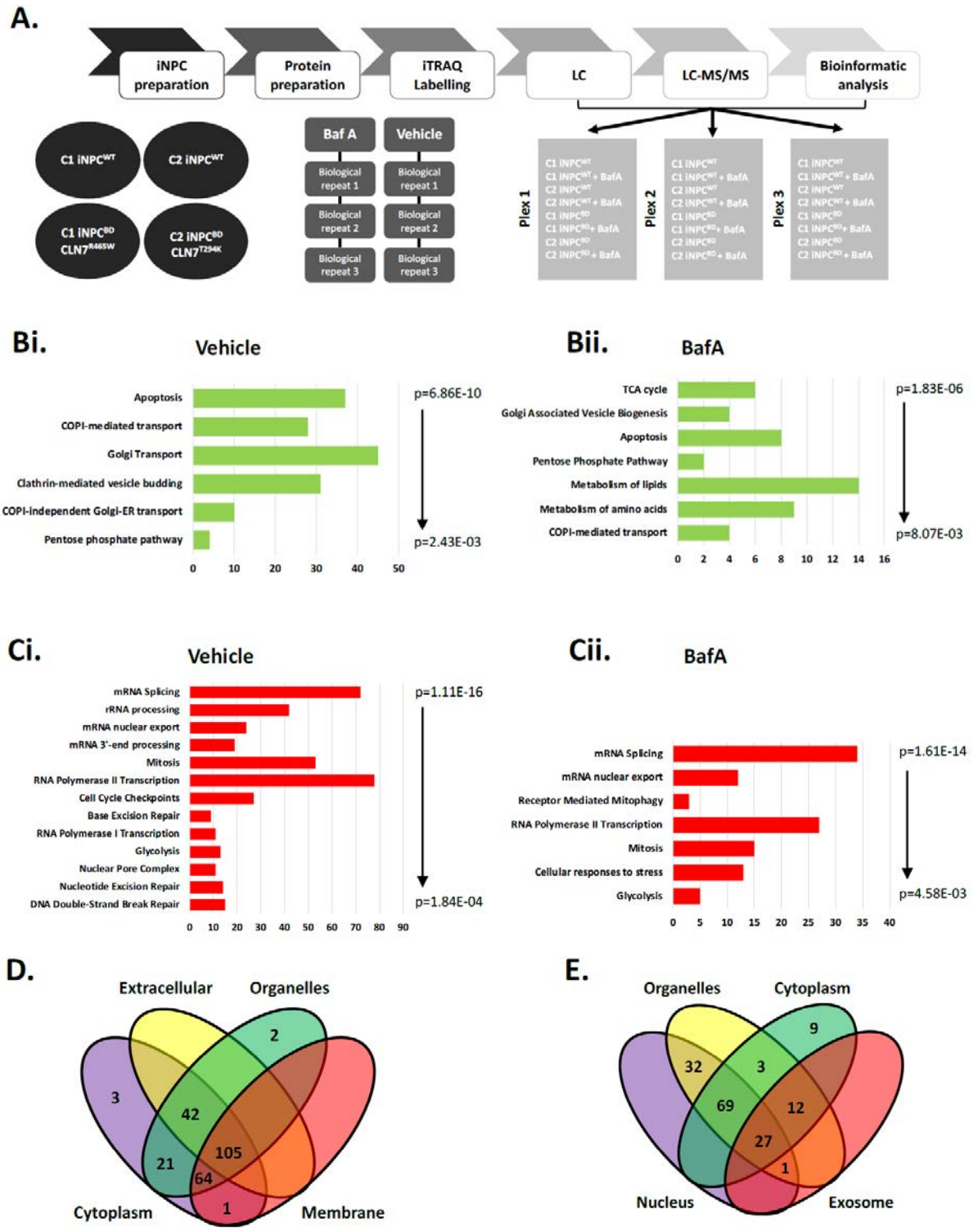

Figure 5. 1. Proteomics comparison of WT and CLN7 NPCs with Bafilomycin A1 treatment. (**A**) Representation of the schematic workflow of iTRAQ mass spectrometry, proteomic quantification, and bioinformatic analysis. The CLN7$^{R465W/R465W}$ NPCs were compared to the WT NPCs using hierarchical Bayesian modelling. (**B-C**) Pathway alterations were discovered using Cytoscape gProfiler with Reactome Pathway. The Reactome protein clusters that showed an increase or decrease in (B) CLN7 (carrying the mutations p.T294K and p.R465W) compared to two (C) WT NPCs, under two different conditions: (i) treatment with vehicle or (ii) treatment with Bafilomycin A1 (BafA), are displayed on the y-axes. The x-axes represent the number of proteins within each cluster that were deregulated. The four samples were analysed together in the three mass-spectrometry runs. Peptides were combined to obtain protein-level quantification, and statistical testing for differential expression was conducted using version 1.0.0 of the developed software 'BayesProt'. (**D-E**) Venn diagram of cellular components for (D) increased or (E) decreased proteins in CLN7 (p.T294K and p.R465W mutations) compared to the two control (WT) NPCs clones without BafA treatment. The data was obtained and analysed by Dr Aseel Sharaireh.

5.2 Post-translational modifications (PTMs) of proteins

Post-translational modifications (PTMs) are the alterations of amino acid side chains of some proteins subsequent to their biogenesis, including selective protease cleavage. Specifically, PTMs are enzymatic processes that induce modifications in protein characteristics through proteolytic cleavage and the addition of modifying groups, including acetyl, phosphoryl, glycosyl, and methyl, to one or more amino acids (Ramazi et al., 2020). There exists an extensive range of over 400 distinct forms of PTMs that exert an impact on several aspects of protein functionality. PTMs can occur in either a specific type of amino acid or many amino acids, resulting in alterations to the chemical characteristics of the changed sites (Huang et al., 2019). PTMs are commonly observed in proteins that have crucial structural and functional roles, including secretory proteins, membrane proteins, and histones. These alterations have a significant effect on various aspects of protein behaviour and properties. These include enzyme functionality and assembly (Ryšlavá et al., 2013), the lifespan of proteins, interactions between proteins (Marshall, 1993), interactions between cells and the extracellular matrix, intracellular transportation of molecules, activation of receptors, solubility of proteins (Caragea et al., 2007; Cundy et al., 2002; Goulabchand et al., 2014; Haltiwanger and Lowe, 2004; Karve and Cheema, 2011; Ohtsubo and Marth, 2006), the folding process of proteins (del Monte and Agnetti, 2014), and their localisation (Audagnotto and Peraro, 2017). Therefore, these alterations are implicated in different biological mechanisms including signal transduction, regulation of gene expression, activation of genes, DNA repair, and control of the cell cycle (Strumillo and Beltrao, 2015; Wang et al., 2015; Wei et al., 2019). PTMs are observed in numerous cellular compartments, such as the nucleus, cytoplasm, endoplasmic reticulum, and Golgi apparatus (Blom et al., 2004).

5.2.1 Glycosylation

Glycosylation is one of the PTMs that consists of an enzyme-directed (biocatalytic) process that can be reversed and takes place in different subcellular compartments, including the ER, Golgi apparatus, cytoplasm, and sarcolemma membrane (Karve and Cheema, 2011; Wang et al., 2019). It occurs in both eukaryotic and prokaryotic membranes, as well as in secreted proteins. It is worth noting that around 50% of the proteins found in the plasma undergo glycosylation (Goulabchand et al., 2014). In this PTM, the attachment of oligosaccharide chains to specific residues occurs through the formation of covalent bonds (when pairs of electrons are shared by atoms). In general, when proteins are formed, they tend towards the aggregation of self-association, and the introduction of a sugar results in an increased volumetric expansion or swelling of the polypeptide structure. Protein aggregation plays a significant role in the folding of molecules and cells, as it fills the intermolecular and intracellular gaps. This, in turn, affects the contacts between adjacent cells, particularly in relation to cell adhesion (Wilk-Blaszczak, n.d.). Glycosylation is typically facilitated by a glycosyltransferase enzyme and commonly occurs in the side chain of various residues including tryptophan (Trp), alanine (Ala), arginine (Arg), asparagine (Asn), aspartic acid (Asp), isoleucine (Ile), lysine (Lys), serine (Ser), threonine (Thr), valine (Val), glutamic acid (Glu), proline (Pro), tyrosine (Tyr), cysteine (Cys), and glycine (Gly) (Huang et al., 2019). However, it is observed to occur with higher frequency on Ser, Thr, Asn, and Trp residues within proteins and lipoproteins (Ohtsubo and Marth, 2006). Based on the specific residues being targeted, glycosylation can be categorised into six different classes: N-glycosylation, O-glycosylation, C-glycosylation, S-glycosylation, phosphoglycosylation, and glypiation (GPI-anchored) (Blom et al., 2004; Karve and Cheema, 2011). N-glycosylation and O-glycosylation are the two main forms of glycosylation that play significant roles in preserving protein structure and functionality (Varki, 1993). Glycosylation contributes significantly to various crucial biological processes, including cell adhesion, cell-cell and cell-matrix interactions, molecular trafficking, activation of receptors, effects on protein solubility, protein folding and signal transduction, protein degradation, as well as intracellular trafficking and secretion of proteins (Caragea et al., 2007; Cundy et al., 2002; Goulabchand et al., 2014; Haltiwanger and Lowe, 2004; Karve and Cheema, 2011; Ohtsubo and Marth, 2006). Glycosylated proteins play a significant role as receptors for viruses and toxins to gain entry into cells via receptor-mediated endocytosis, hence holding therapeutic relevance.

The glycosylation process, which involves the attachment of mannose-6-phosphate, serves a dual purpose in relation to lysosomal proteins. It functions as a targeting signal for lysosomal enzymes and facilitates their protection from digestion. Glycosylation takes place within the ER or Golgi apparatus. A protein that undergoes N-linked glycosylation obtains its carbohydrate chain as a pre-

existing oligosaccharide in the ER. On the other hand, an O-linked glycosylated protein acquires its carbohydrate chain in the Golgi, where oligosaccharides are added individually. The process of N-linked glycosylation begins on the arrival of glycosylated residues, specifically Asn and Arg, within the ER lumen as part of an unfolded nascent peptide. Subsequently, a preformed monosaccharide is transported from a lipid carrier called dolichol, which is attached to the ER membrane, to the polypeptide chain. The process of O-linked glycosylation, which occurs in the Golgi during the latter phases of protein maturation, is facilitated by glycosyl transferases that exhibit specificity towards particular monosaccharides.

5.2.2 Phosphorylation

Phosphorylation is a reversible PTM that exerts a crucial impact on the functionality of numerous enzymes, membrane channels, and other proteins in both prokaryotic and eukaryotic organisms (Edwards and Scott, 2000). The residues that are targeted for phosphorylation include serine (Ser), threonine (Thr), tyrosine (Tyr), histidine (His), proline (Pro), arginine (Arg), aspartic acid (Asp), and cysteine (Cys) (Huang et al., 2019). However, phosphorylation predominantly occurs on Ser, Thr, Tys, and His residues (Panni, 2019). This PTM involves the transfer of a phosphate group from adenosine triphosphate (ATP) to specific residues on the receptor, facilitated by kinase enzymes (enzymes that add phosphate groups, $PO4^{3-}$, to other molecules). In contrast, the enzymatic step of dephosphorylation, which involves the removal of a phosphate group, is facilitated by several phosphatases (Skamnaki et al., 1999). Phosphorylation is an extensively studied PTM and is considered one of the fundamental types of PTMs. It commonly occurs in the cytosol or nucleus, specifically on the target proteins (Duan and Walther, 2015). This PTM has the potential to rapidly modify the functionality of proteins through one of two primary mechanisms: allosteric regulation or binding to interaction domains (Jin and Pawson, 2012). Allosteric regulation is a mechanism by which the activity of a protein is modulated through the binding of a ligand, known as an effector, to a site that is spatially separated from the protein's active site. The active site is responsible for carrying out the protein's characteristic activity, whether it is catalytic (in the case of enzymes) or binding (in the case of receptors). Phosphorylation plays a crucial function in various cellular activities, including replication, transcription, response to environmental stress, cell motility, cellular metabolism, apoptosis, and immunological response (Forrest et al., 2006; Gong et al., 2008; Karve and Cheema, 2011).

5.2.3 SUMOylation

The process of SUMOylation occurs through the involvement of a Small Ubiquitin-Related Modifier (SUMO) protein, which exhibits a three-dimensional conformation resembling that of

ubiquitin protein (Feligioni and Nisticò, 2013; Jentsch and Psakhye, 2013). SUMO has been identified in various eukaryotic organisms. This PTM can occur in both the cytoplasm and nucleus, specifically targeting lysine (Lys) residues (Sedek and Strous, 2013). SUMOylation involves the modification of Lys residues in target proteins through a multi-enzymatic cascade, targeting the ε-amino group of Lys (a primary amine) (Mustfa et al., 2017). In this reaction, the SUMO protein forms a covalent bond with a specific Lys residue located inside the substrate protein. This bonding process is facilitated by three enzymes, known as activating enzyme (E1), conjugating enzyme (E2), and ligase enzyme (E3). Furthermore, the target protein is enzymatically cleaved from its conjugated form by the SUMO protease (Eifler and Vertegaal, 2015). Frequently, SUMOylation modifications take place at a consensus motif WKxE, where W denotes Lys, Ile, Val, or Phe, and X represents any amino acid (Zahiri, 2016). The process of SUMOylation is of significant importance in various fundamental cellular mechanisms, including transcriptional regulation, chromatin structure organisation, cellular macromolecule accumulation, gene expression modulation, signal transduction, and the conservation of genomic integrity (Beauclair et al., 2015; Flotho and Melchior, 2013; Kumar and Zhang, 2015).

5.2.4 Proteolytic cleavage

Proteolytic cleavage is a ubiquitous and irreversible biochemical process characterised by the enzymatic degradation of peptide bonds inside proteins, resulting in the generation of smaller polypeptides or individual amino acids. This degradation process is facilitated by the action of proteases, which catalyse the hydrolysis of these peptide bonds (James, 1999). This PTM can lead to different results such as activation, inactivation, significant changes in protein function, and even the generation of new proteins that exhibit growth factor activity. These cleavage events play a crucial role in the regulation of several biological processes (James, 1999). These processes include DNA replication, cell cycle progression, proliferation of cells, and cell death, alongside pathogenic mechanisms such as inflammation, arthritis, and cardiovascular disease. In the context of protein synthesis and maturation, the specific elimination of the N-terminal methionine and the signal peptide plays a crucial role in ensuring proper protein maturation and subsequent secretion. Certain proteins undergo cleavage of their polypeptide chains, resulting in the formation of a molecule that has four distinct termini, which are connected through disulphide bridges. Proteases play an essential role in regulating protein localisation by eliminating signal, nuclear, and mitochondrial localisation sequences. In the context of viral infection, proteases are involved in the cleavage of pre- and pro-domains and the processing of polyproteins. These proteolytic activities result in the conversion of inactive proteins into their active form(s), inactivation of proteins, or alteration of receptor-binding affinity. Therefore, proteolysis is important in a wide

range of functions beyond the simple cleavage and turnover of proteins, which are crucial processes for maintaining cell homeostasis (Rogers and Overall, 2013).

Aims and objectives

The goal of this chapter was to conduct a molecular analysis of MFSD8 to gain a deeper understanding of its function and its several possible isoforms. Additionally, this study aimed to investigate the potential PTMs of MFSD8 as well as protein stability in mutated MFSD8. This was accomplished by the pursuit of the following objectives:

i) To investigate the expression of MFSD8 in various cell types, such as HEK293T, SH-SY5Y cells, and NPCs, as well as in distinct cellular compartments (nucleus and cytoplasm) in NPCs by Western blotting.

ii) To validate the previously predicted and studied post-translational modifications of MFSD8 in SH-SY5Y cells to better understand the molecular biology of MFSD8.

iii) To study the protein stability of mutated-MFSD8 compared to WT MFSD8 b protein synthesis inhibition and limited proteolysis.

Results

5.3 Validation of the anti-MFSD8 antibodies used in this study and potential MFSD8 isoforms

Considering that the expected molecular weight of the full-length MFSD8 protein is 57-58 kDa, the next objective of this chapter was to verify the specificity of the primary anti-MFSD8 antibodies employed in most of this project's experiments. Two distinct immunoblotting experiments were conducted for this purpose. First, the cell lysates obtained from HEK293T cells were subjected to Western blot analysis. This analysis involved the use of two antibodies: a first primary anti-MFSD8 pAb antibody (#PA5-60832, ThermoFisher), which specifically targets the first 37 amino acids (aa) from the N-terminal region of the protein (referred to as $pAb^{1\text{-}37aa}$), and a second primary antibody, which was found and commercially accessible at the time of the experiments and targets 72 aa from the C-terminal region of MFSD8 (351-421 aa) (#24298-1-AP, Proteintech) (referred to as $pAb^{351\text{-}421aa}$).

Despite variations in band intensity, likely attributed to the particular epitope targeted by each antibody, both antibodies successfully identified multiple predicted MFSD8 bands, providing strong evidence of their specificity (**Figure 5.2a**). The approximate bands identified were of the

following molecular weights: 180 kDa, 120 kDa, 70 kDa, 60 kDa, 58 kDa, 50 kDa, 44 kDa, 40 kDa, 37 kDa, and 33 kDa, among others.

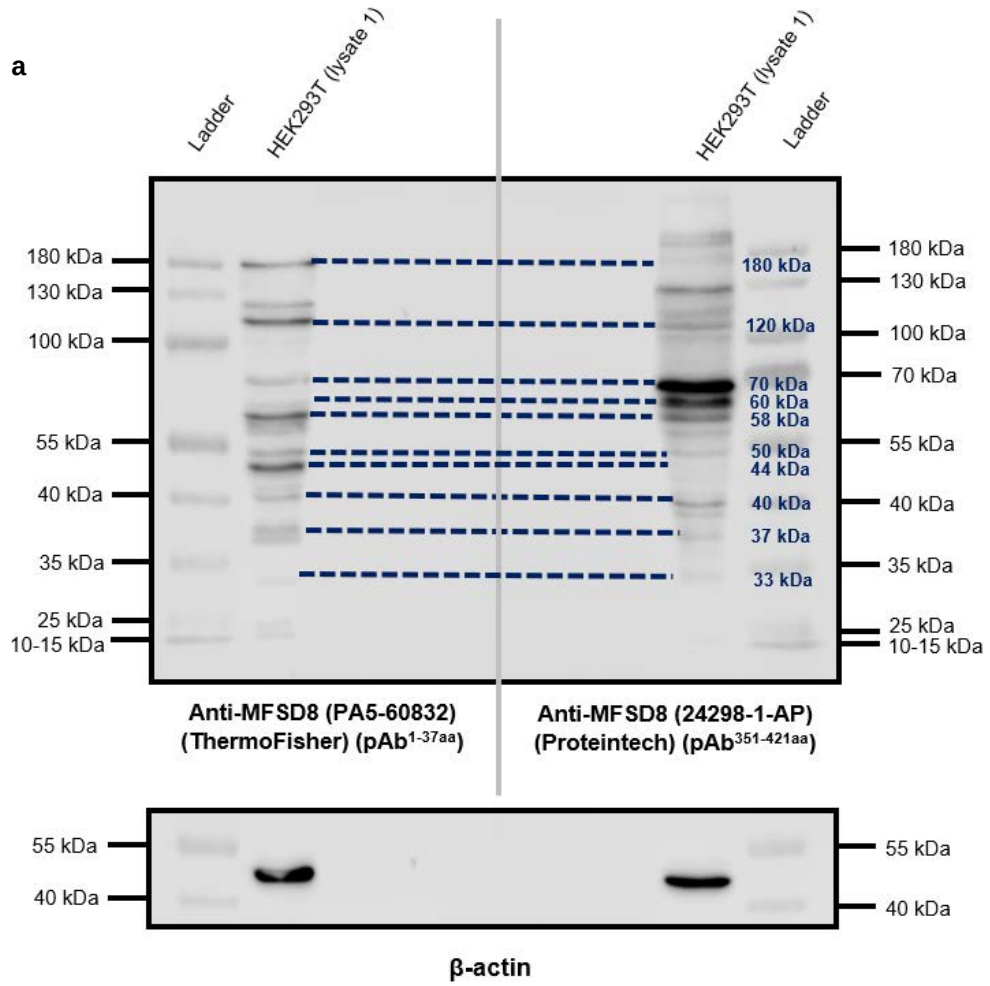
a
Ladder
HEK293T (lysate 1)
HEK293T (lysate 1)
Ladder
180 kDa
130 kDa
100 kDa
55 kDa
40 kDa
35 kDa
25 kDa
10-15 kDa
180 kDa
120 kDa
70 kDa
60 kDa
58 kDa
50 kDa
44 kDa
40 kDa
37 kDa
33 kDa
180 kDa
130 kDa
100 kDa
70 kDa
55 kDa
40 kDa
35 kDa
25 kDa
10-15 kDa
Anti-MFSD8 (PA5-60832) (ThermoFisher) (pAb1-37aa)
Anti-MFSD8 (24298-1-AP) (Proteintech) (pAb351-421aa)
55 kDa
40 kDa
55 kDa
40 kDa
β-actin

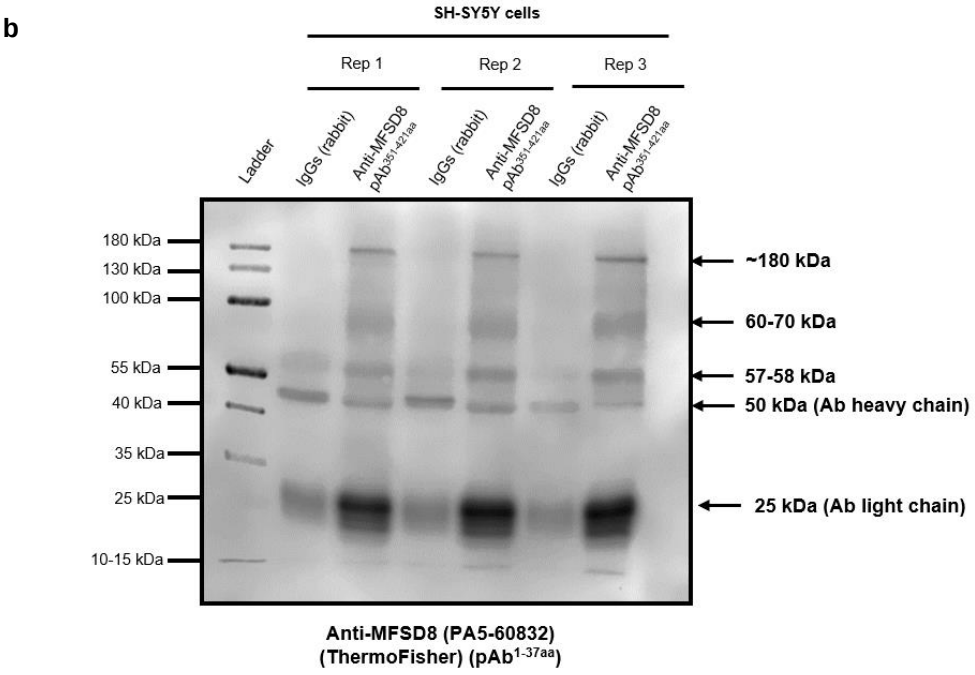
b
SH-SY5Y cells
Rep 1
Rep 2
Rep 3
Ladder
IgGs (rabbit)
Anti-MFSD8 pAb351-421aa
IgGs (rabbit)
Anti-MFSD8 pAb351-421aa
IgGs (rabbit)
Anti-MFSD8 pAb351-421aa
180 kDa
130 kDa
100 kDa
55 kDa
40 kDa
35 kDa
25 kDa
10-15 kDa
~180 kDa
60-70 kDa
57-58 kDa
50 kDa (Ab heavy chain)
25 kDa (Ab light chain)
Anti-MFSD8 (PA5-60832) (ThermoFisher) (pAb1-37aa)

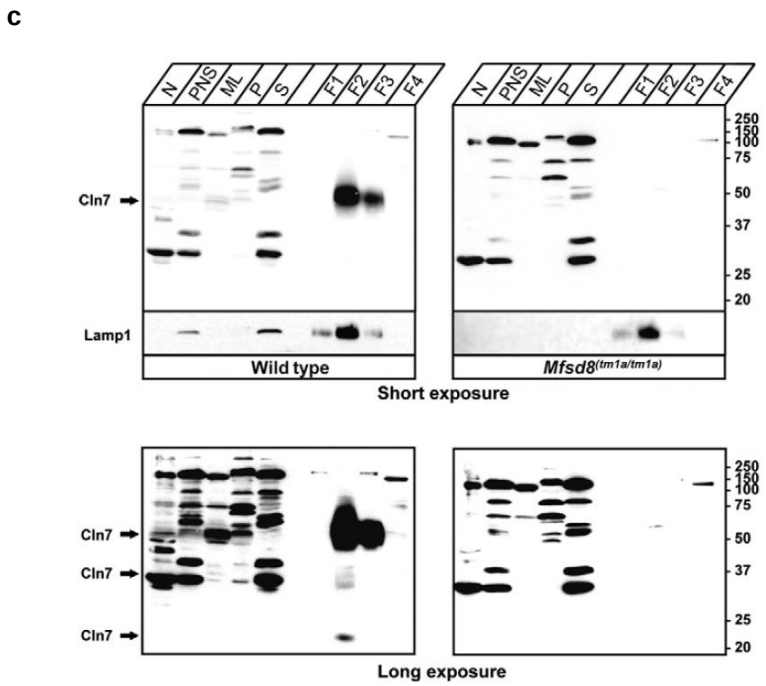

Figure 5. 2. Validation of the specificity of the primary antibodies used to assess MFSD8 protein expression. Immunoblotting of MFSD8 in different cells and experiments, using three available antibodies to validate their specificity and corroborate its expression. (**a**) Immunoblot of MFSD8 in HEK293T cell lysates using the same sample in the same gel, which was probed using two different anti-MFSD8 rabbit polyclonal antibodies ($pAb^{1\text{-}37aa}$ and $pAb^{351\text{-}421aa}$), by cutting the same membrane. (**b**) Immunoblot of a co-immunoprecipitation (co-IP) performed in SH-SY5Y cell lysates, where the antibody used in the co-IP was the $pAb^{351\text{-}421aa}$ and the MFSD8 was probed with the $pAb^{1\text{-}37aa}$. (**c**) Immunoblot obtained from Damme et al. (2014), where they used a mouse-specific antibody generated to detect the Mfsd8 protein expression in mice samples.

Structurally, MFSD7 is a protein with a molecular weight of 57-58 kDa and has 12 transmembrane domains. It has been shown to be associated with endo-lysosomal vesicles (EVL) and functions as a chloride channel (Danyukova et al., 2018; von Kleist et al., 2019; Yayu Wang et al., 2021). To elucidate whether MFSD8 could be expressed in multiple forms, as observed in the blot probed with $pAb^{1\text{-}37aa}$ and $pAb^{351\text{-}421aa}$ (**Figure 5.2a**), the Ensembl database (https://www.ensembl.org/index.html) was consulted to determine the annotation of potential MFSD8 transcript variants. *MFSD8* has 62 potential transcript variants across the 13 exons, with 24 predicted to be protein-coding. Some of these annotated transcripts have been previously reported and could be of interest to understanding their underlying mechanism within the cell. For instance, the *MFSD8* transcript ENST00000641690 is predicted to describe a splice variant that lacks exons 7 and 8 ($CLN7^{\Delta ex7/8}$) (50 kDa), which has been identified in human blood leukocytes

(Siintola et al., 2007). Additionally, the luminal loop 9 (L9) has been demonstrated to be susceptible to proteolytic cleavage, possibly by cysteine proteases (Steenhuis et al., 2012). However, the precise mechanism and site of cleavage are yet unknown. Therefore, additional transcript variants of *MFSD8* are predicted to be produced by cysteine protease cleavage of the full-length MFSD8 (57-58 kDa), resulting in a ~400 aa truncated protein (44 kDa), whilst cysteine cleavage of the CLN7$^{\Delta ex7/8}$ could produce a 336 aa protein variant (37 kDa). Collectively, there is strong evidence supporting the occurrence of both post-transcriptional and post-translational modifications of MFSD8, leading to the formation of multiple potential isoforms (Steenhuis et al., 2012, 2010). These potential MFSD8 isoforms that we propose according to the literature and Ensembl database are shown in **Figure 5.3**.

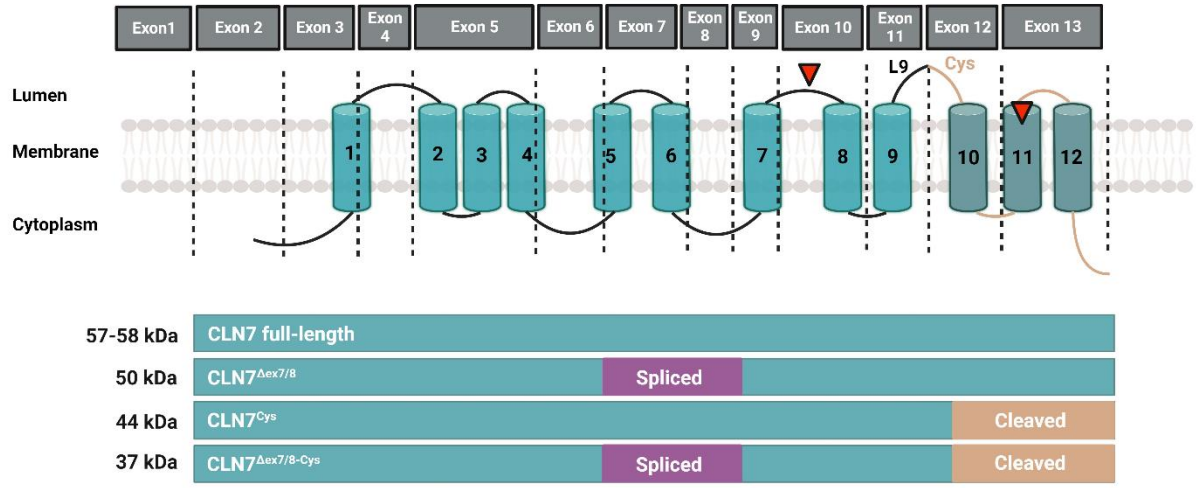

Size	MFSD8 predicted protein isoforms
57-58 kDa	Full-length
50 kDa	Transcript variant Δex7/8 (Siintola et al., 2007)
44 kDa	Transcript variant Cys potease digested (Steenhuis et al., 2012)
37 kDa	Transcript variant Δex7/8 Cys protease digested

Figure 5. 3. Schematic representation of MFSD8 and its different potential isoforms. *MFSD8* contains 13 exons which encode for the MFSD8 protein that encompasses 12 transmembrane domains. MFSD8 is described as presenting different loops that face either the lysosomal lumen or the cytoplasm. Specifically, in the loop L9, there is a proposed Cys cleavage site, where some MFSD8 variants can be cleaved, resulting in a different MFSD8 isoform, such as the CLN7^{Cys}, which could be presenting a molecular weight of 44 kDa. Additionally, some MFSD8 isoforms could be generated as a result of the splicing produced by the deletion of exons 7 and 8, like the CLN7$^{\Delta ex7/8}$, potentially generating a truncated protein of 50 kDa. When the cysteine cleavage occurs along with the splicing due to the deletion of exons 7 and 8, a resulting MFSD8 of 37 kDa is presumably generated, represented as CLN7$^{\Delta ex7/8\text{-}Cys}$ in this study.

As further evidence, both blots (one probed with $pAb^{1\text{-}37aa}$ and the other with $pAb^{351\text{-}421aa}$) showed common bands. However, some bands were present in the blots detected with the $pAb^{1\text{-}37aa}$, whereas they were absent in the blot probed with the $pAb^{351\text{-}421aa}$ antibody. For instance, the $pAb^{351\text{-}421aa}$ should no detect the 44 kDa band because the loop 9 (L9) epitope structure is removed by protease cleavage. The 44 kDa is not present in the blot probed with $pAb^{351\text{-}421aa}$ and the 37 kDa band is most likely not either, even though it cannot be completely demonstrated by the western blot shown (**Figure 5.2**).

An additional experiment to confirm that the two antibodies are specific for MFSD8 was to conduct co-immunoprecipitation (co-IP) with the $pAb^{351\text{-}421aa}$ followed by western blot with the $pAb^{1\text{-}37aa}$ (**Figure 5.2b**). This blot displayed some of the different bands of MFSD8, similar to previous findings in this study, providing more evidence of the specificity of both antibodies used. Specifically, there were three relevant bands detected in this blot with co-IP samples: a large band ~180 kDa, the 70 kDa band, and the 57-58 kDa band (potentially representing the full-length MFSD8). The other two bands will be further investigated in this chapter. However, the protein quantity utilised in this experiment was significantly smaller in comparison to the prior blots depicted in **Figure 5.2a**. This disparity in protein quantity may explain the reduced quality and quantity of the bands observed in this particular set of blots resulting from the co-IP. Additionally, Damme et al. (2014) conducted several blots on the Mfsd8 protein in mice, which also revealed the existence of multiple bands (**Figure 5.2c**). Interestingly, our findings employing human cell lines align with these results.

To examine whether the MFSD8 forms proposed here could result in truncated proteins, as observed in the previous blots, and corroborate that the bands identified in this work correspond to MFSD8 and are not a result of nonspecific binding of the antibodies used, the AlphaFold software was utilised to generate the molecular predicted structure of these putative isoforms. The acquisition of the predicted MFSD8 protein structures was conducted by Prof Sam Hay (Manchester Institute of Biotechnology, The University of Manchester). This study examined four different isoforms of MFSD8: i) the full-length isoform (57-58 kDa), ii) the variant with exons 7 and 8 deleted (50 kDa, $CLN7^{\Delta ex7/8}$), iii) the isoform cleaved at a potential cysteine residue (~44 kDa, $CLN7^{Cys}$), and iv) the isoform with both exons 7 and 8 deleted and cysteine cleaved (~37 kDa, $CLN7^{\Delta ex7/8\text{-}Cys}$) (**Figure 5.4**).

57 kDa (full-length, WT CLN7) model

MAGLRNESEQ EPLLGDTPGS REWDILETEE HYKSRWRSIR ILYLTMFLSS VGFSVVMMSIWPYLQKIDPT ADTSFLGWVI ASYSLGQMVA SPIFGLWSNY RPRKEPLIVS ILISVAANCLYAYLHIPASH NKYYMLVARG LLGIGAGNVA VVRSYTAGAT SLQERTSSMA NISMCQALGFILGPVFQTCF TFLGEKGVTW DVIKLQINMY TTPVLLSAFL GILNIILILA ILREHRVDDS GRQCKSINFE EASTDEAQVP QGNIDQVAVV AINVLFFVTL FIFALFETII TPLTMDMYAWTQEQAVLYNG IILAALGVEA VVIFLGVKLL SKKIGERAIL LGGLIVVWVG FFILLPWGNQFPKIQWEDLH NNSIPNTTFG EIIIGLWKSP MEDDNERPTG CSIEQAWCLY TPVIHLAQFLTSAVLIGLGY PVCNLMSYTL YSKILGPKPQ GVYMGWLTAS GSGARILGPM FISQVYAHWG PRWAFSLVCG IIVLTITLLG VVYKRLIALS VRYGRIQE*

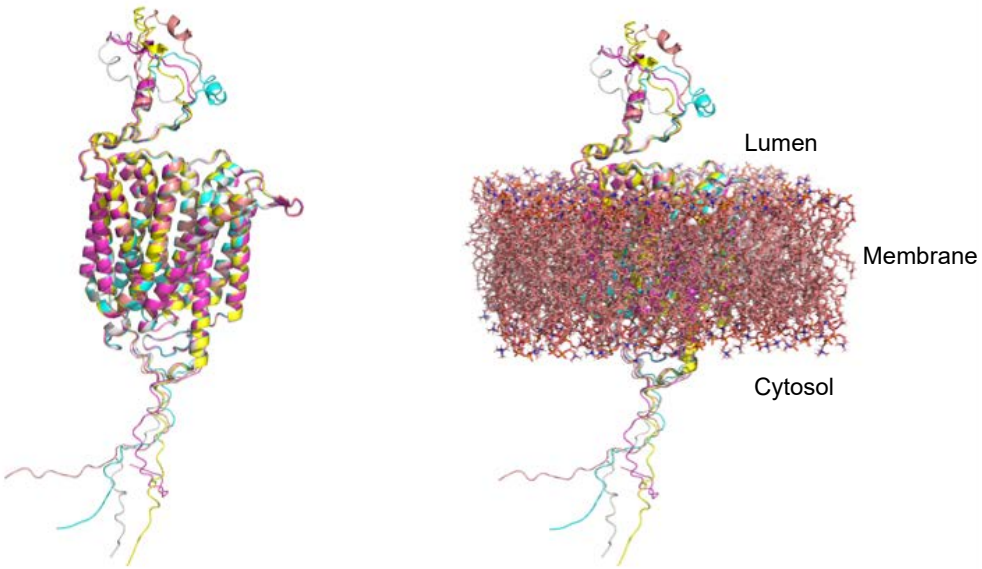

50 kDa (CLN7$^{\Delta ex7/8}$) model

MAGLRNESEQ EPLLGDTPGS REWDILETEE HYKSRWRSIR ILYLTMFLSS VGFSVVMMSI WPYLQKIDPT ADTSFLGWVI ASYSLGQMVA SPIFGLWSNY RPRKEPLIVS ILISVAANCL YAYLHIPASH NKYYMLVARG LLGIGAGNVA VVRSYTAGAT SLQERTSSMA NISMCQALGF ILGPASTDEA QVPQGNIDQV AVVAINVLFF VTLFIFALFE TIITPLTMDM YAWTQEQAVL YNGIILAALG VEAVVIFLGV KLLSKKIGER AILLGGLIVV WVGFFILLPW GNQFPKIQWE DLHNNSIPNT TFGEIIIGLW KSPMEDDNER PTGCSIEQAW CLYTPVIHLA QFLTSAVLIG LGYPVCNLMS YTLYSKILGP KPQGVYMGWL TASGSGARIL GPMFISQVYA HWGPRWAFSL VCGIIVLTIT LLGVVYKRLI ALSVRYGRIQ E*

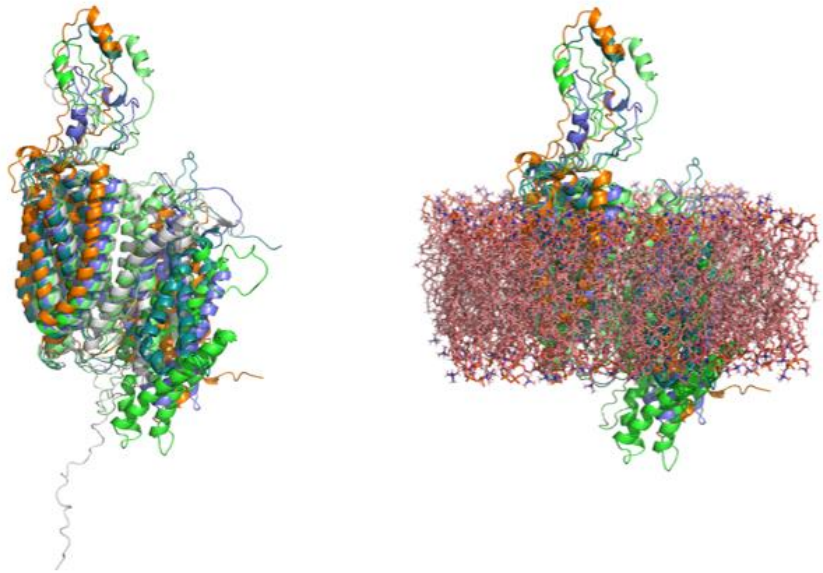

44 kDa (CLN7^{Cys401}) model

MAGLRNESEQ EPLLGDTPGS REWDILETEE HYKSRWRSIR ILYLTMFLSS VGFSVVMMSIWPYLQKIDPT ADTSFLGWVI ASYSLGQMVA SPIFGLWSNY RPRKEPLIVS ILISVAANCLYAYLHIPASH NKYYMLVARG LLGIGAGNVA VVRSYTAGAT SLQERTSSMA NISMCQALGFILGPVFQTCF TFLGEKGVTW DVIKLQINMY TTPVLLSAFL GILNIILILA ILREHRVDDSGRQCKSINFE EASTDEAQVP QGNIDQVAVV AINVLFFVTL FIFALFETII TPLTMDMYAWTQEQAVLYNG IILAALGVEA VVIFLGVKLL SKKIGERAIL LGGLIVVWVG FFILLPWGNQFPKIQWEDLH NNSIPNTTFG EIIIGLWKSP MEDDNERPTG*

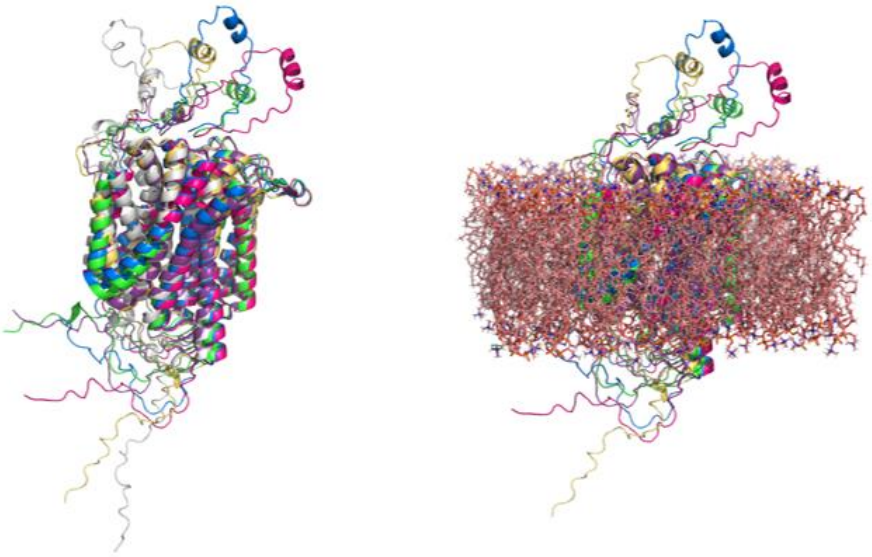

37 kDa (CLN7$^{\Delta ex7/8Cys401}$) model

MAGLRNESEQ EPLLGDTPGS REWDILETEE HYKSRWRSIR ILYLTMFLSS VGFSVVMMSIWPYLQKIDPT ADTSFLGWVI ASYSLGQMVA SPIFGLWSNY RPRKEPLIVS ILISVAANCLYAYLHIPASH NKYYMLVARG LLGIGAGNVA VVRSYTAGAT SLQERTSSMA NISMCQALGFILGPVFQTCF TFLGEKGVTW DVIKLQINMY TTPVLLSAFL GILNIILILA ILREHRVDDSGRQCKSINFE EASTDEAQVP QGNIDQVAVV AINVLFFVTL FIFALFETII TPLTMDMYAWTQEQAVLYNG IILAALGVEA VVIFLGVKLL SKKIGERAIL LGGLIVVWVG FFILLPWGNQFPKIQWEDLH NNSIPNTTFG EIIIGLWKSP MEDDNERPTG*

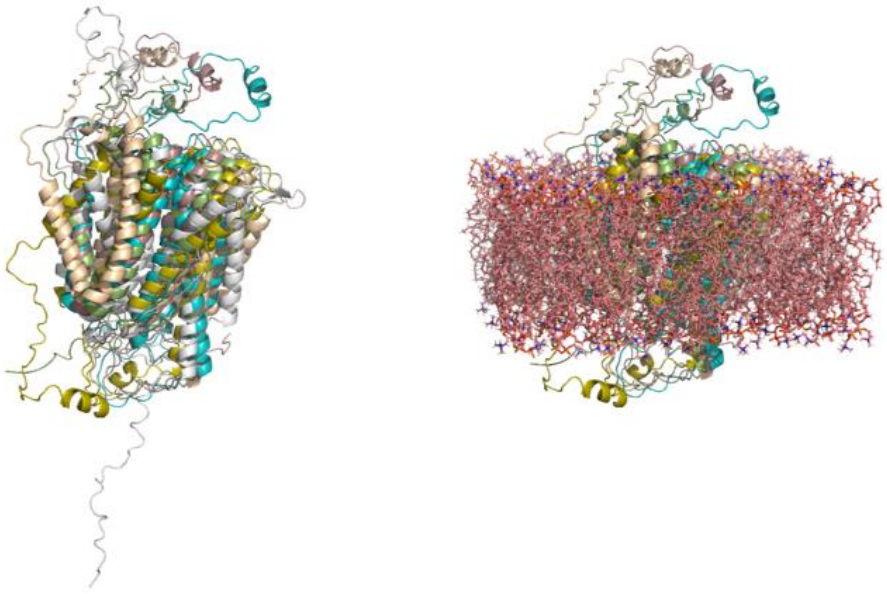

Figure 5. 4. Predicted MFSD8 protein structures using AlphaFold. Structural representation of the full-length and three proposed MFSD8 isoforms using AlphaFold software, with their corresponding protein sequences. The structural images on the left represent the protein itself, whereas the images on the right display the distribution of those MFSD8 forms in the membranes, showing that these isoforms can be present in the membranes as transmembrane proteins either exerting a different function or being dysfunctional. The upper residues of the structural images show the MFSD8 loops facing the lumen of the lysosomes, while the lower residues represent the MFSD8 side that faces the cytoplasm. The structural representations of the MFSD8 protein were obtained and provided by Prof Sam Hay (The University of Manchester).

The findings from the AlphaFold MFSD8 structures (conducted and provided by Prof Sam Hay) demonstrate that all four possible variations of the MFSD8 could integrate into the membrane, irrespective of whether they are truncated proteins (**Figure 5.4**). Nevertheless, the specific regions of the $CLN7^{\Delta ex7/8}$, $CLN7^{Cys401/8}$, and $CLN7^{\Delta ex7/8\text{-}Cys401/8}$ domains are not clearly defined in both the lumen and the cytosol (**Figure 5.4**). These results suggest that the MFSD8 truncated proteins are produced and transported to the cell membranes, where they may play a different role that might either be advantageous or harmful to cellular function.

5.4 MFSD8 localises to the nucleus and is ubiquitously expressed in different cell types

The previous chapter (Chapter 4) demonstrated that MFSD8 is observed in both the nucleus and the cytoplasm. Although previous studies have observed nuclear MFSD8 localisation in neurons and fibroblasts of controls and FTD patients with MFSD8 mutations (Geier et al., 2019), it has not been explicitly documented until now. However, these observations have been regarded as a "cross-reaction artefact" in the study by Sharifi et al. (2010). To provide additional evidence for the nuclear localization of the protein of interest in NPCs, a nuclear fractionation was performed.

First, immunoblotting was performed using various cell types, such as HEK293T cells, SH-SY5Y cells, and NPCs (**Figure 5.5**). These blots revealed many bands indicating different molecular weights of MFSD8, ranging from 180 to 20 kDa (**Figure 5.5, Table 5.1**), which may provide new insights into the possible presence of distinct MFSD8 isoforms expressed across different cells and compartments. The full-length MFSD8 (57-58 kDa) was found to be present in all the cell lines examined in this study, primarily somewhere in the cytoplasm (**Figure 5.5, Table 5.1**). Assuming the specificity of the antibody demonstrated in the previous section, if all the bands seen corresponded to MFSD8, the heaviest bands (ranging from 120 kDa to 180 kDa) could be either oligomers or MFSD8 subjected to PTMs. Following this, the bands expressed below the higher

bands may be cleavage products or splice variants of *MFSD8*. Interestingly, some of the bands obtained in the blots using SH-SY5Y cells and NPCs (WT and CLN7) (**Figures 5.5, Table 5.1**), are consistent with the 57 kDa (full-length MFSD), as well as the proposed 50 kDa band (potentially corresponding to the deletion of exons 7 and 8, as described by Siintola et al. (2007)), the 44 kDa band (cysteine cleaved product), and the 37 kDa band (potentially referring to a product that lacks exons 7 and 8 and is protease cleaved), described in the previous section. However, there are additional bands such as the 39 kDa and 33 kDa and others that have not been characterised yet. For instance, the 33 kDa band seems to be present in SH-SY5Y cells but absent in HEK293T cells (**Figure 5.5a**). Additionally, this band was found to be prominent in WT and CLN7 NPCs (**Figures 5.5b-d**).

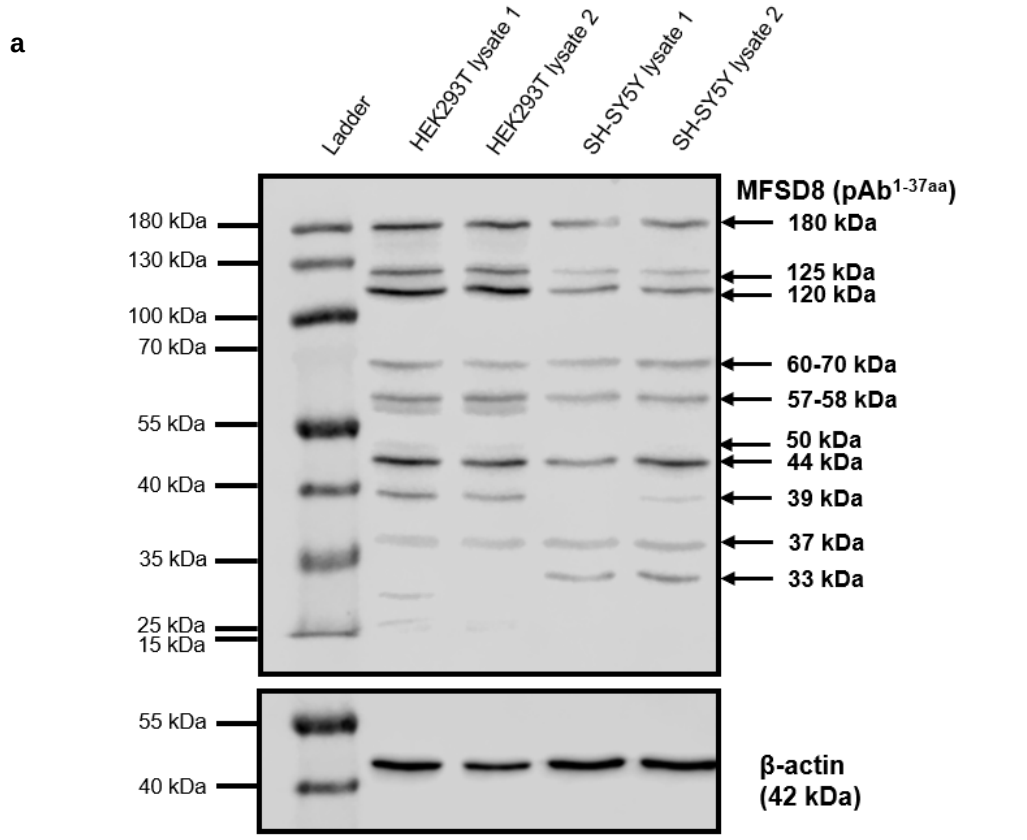
a
Ladder
HEK293T lysate 1
HEK293T lysate 2
SH-SY5Y lysate 1
SH-SY5Y lysate 2
MFSD8 (pAb1-37aa)
180 kDa
130 kDa
100 kDa
70 kDa
55 kDa
40 kDa
35 kDa
25 kDa
15 kDa
180 kDa
125 kDa
120 kDa
60-70 kDa
57-58 kDa
50 kDa
44 kDa
39 kDa
37 kDa
33 kDa
55 kDa
40 kDa
β-actin
(42 kDa)

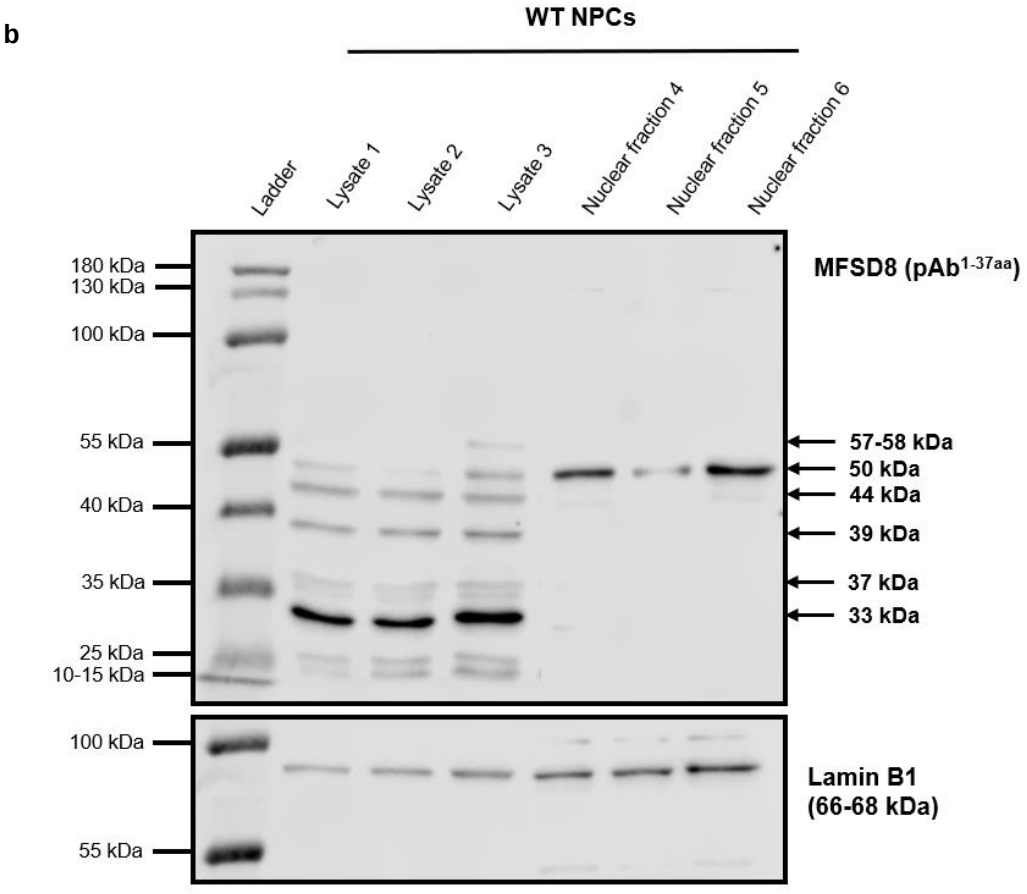
b
WT NPCs
Ladder
Lysate 1
Lysate 2
Lysate 3
Nuclear fraction 4
Nuclear fraction 5
Nuclear fraction 6
MFSD8 (pAb1-37aa)
180 kDa
130 kDa
100 kDa
55 kDa
40 kDa
35 kDa
25 kDa
10-15 kDa
57-58 kDa
50 kDa
44 kDa
39 kDa
37 kDa
33 kDa
100 kDa
55 kDa
Lamin B1
(66-68 kDa)

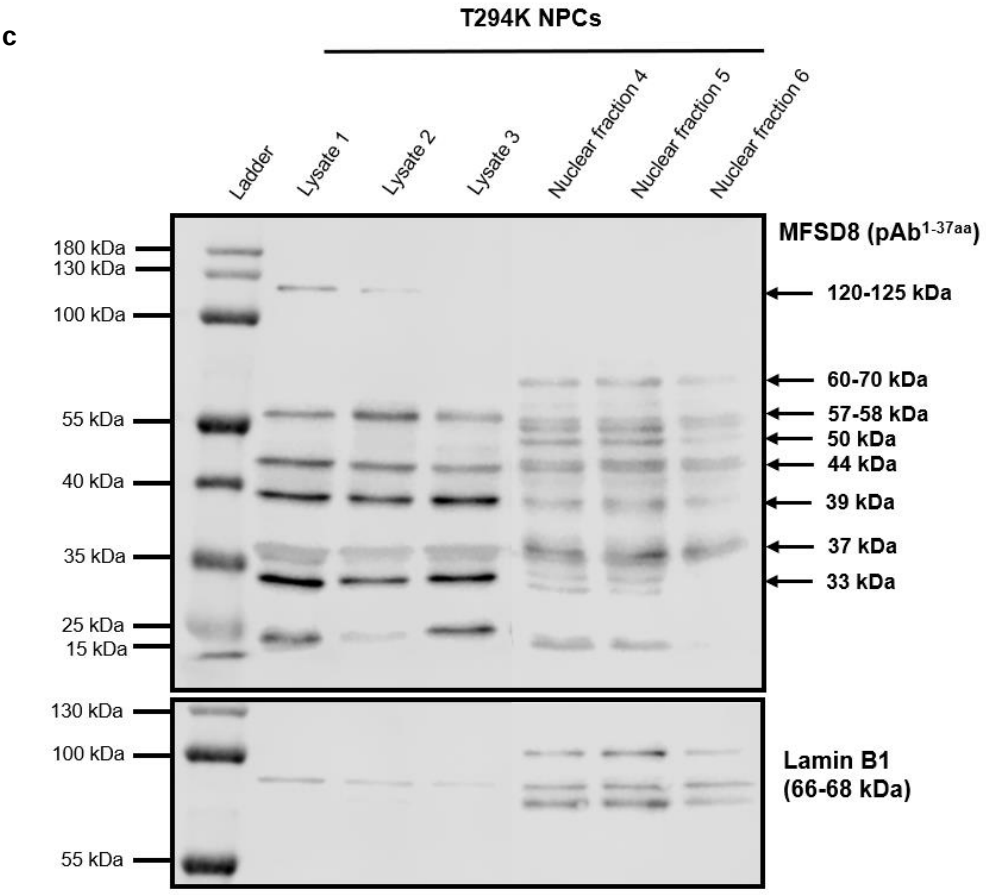
c
T294K NPCs
Ladder
Lysate 1
Lysate 2
Lysate 3
Nuclear fraction 4
Nuclear fraction 5
Nuclear fraction 6
180 kDa
130 kDa
100 kDa
55 kDa
40 kDa
35 kDa
25 kDa
15 kDa
MFSD8 (pAb1-37aa)
120-125 kDa
60-70 kDa
57-58 kDa
50 kDa
44 kDa
39 kDa
37 kDa
33 kDa
130 kDa
100 kDa
55 kDa
Lamin B1
(66-68 kDa)

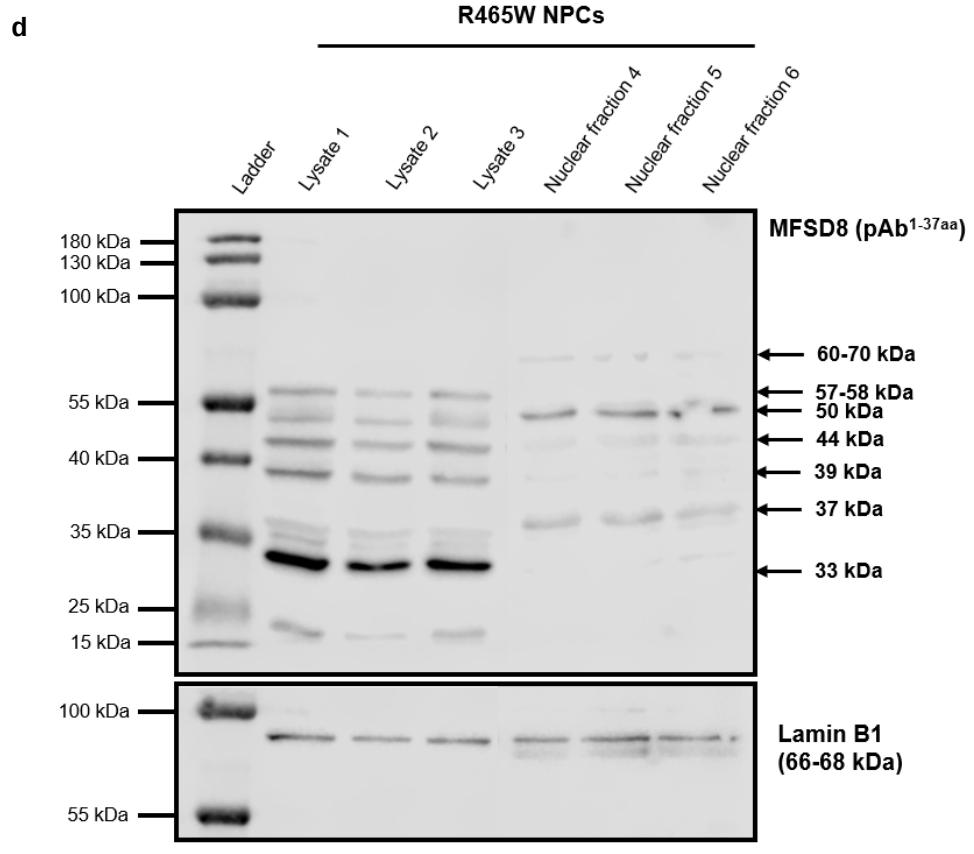
d
R465W NPCs
Ladder
Lysate 1
Lysate 2
Lysate 3
Nuclear fraction 4
Nuclear fraction 5
Nuclear fraction 6
180 kDa
130 kDa
100 kDa
55 kDa
40 kDa
35 kDa
25 kDa
15 kDa
MFSD8 (pAb1-37aa)
60-70 kDa
57-58 kDa
50 kDa
44 kDa
39 kDa
37 kDa
33 kDa
100 kDa
55 kDa
Lamin B1
(66-68 kDa)

Figure 5. 5. MFSD8 is expressed across different cell types. Representative blots of the expression of MFSD8 in HEK293T and SH-SY5Y cells, as well as WT and CLN7 (p.T294K and p.R465W) NPCs. (**a**) Immunoblotting of MFSD8 expression in HEK293T and SH-SY5Y cells. The primary antibody used to probe for MFSD8 was the anti-MFSD8 rabbit polyclonal (#PA5-60832, Invitrogen™) with an expected molecular weight of 57-58 kDa. (**b**) Nuclear fractionation of WT NPCs was performed to show the MFSD8 protein expression in the total cell lysate, cytoplasm and the nucleus of NPCs by immunoblotting. (**c**) Immunoblotting of the total cell lysate, cytoplasmic fraction, and nuclear fraction obtained from the CLN7 NPCs presenting the mutation p.T294K. (**d**) Immunoblotting of the total cell lysate, cytoplasmic fraction, and nuclear fraction obtained from the CLN7 NPCs presenting the mutation p.R465W. Lamin B1 was used to corroborate the nuclear fraction (66-68 kDa) (n = 3, biological replicates).

The differences in the expression of the potential MFSD8 isoforms observed in the nucleus of the different types of NPCs could shed light on the pathobiology of CLN7 disease. For instance, the 50 kDa form is predominantly expressed in the nucleus of WT NPCs, whereas the nuclear fraction of NPCs with the p.T294K mutation exhibited different bands, including the 60-70 kDa, 50 kDa, 44 kDa, 39 kDa, 37 kDa, and 33 kDa MFSD8 variants. Similarly, the NPCs with the p.R465W mutation presented the MFSD8 forms of 60-70 kDa, 50 kDa, 44 kDa, and 37 kDa in the nucleus (**Table 5.1**). These results suggest that some of the potential MFSD8 isoforms could lead to defective nuclear function, thus contributing to disease.

Table 5. 1. List of the proposed MFSD8 isoforms.

Size	HEK293T	SH-SY5Y	WT NPCs	T294K NPCs	R465W NPCs	Potential MFSD8 isoform
180 kDa	✓	✓				Oligomer or PTM
125-120 kDa	✓	✓		✓		Oligomer or PTM
60-70 kDa	✓	✓		✓ **(N)**	✓ **(N)**	Oligomer or PTM
57-58 kDa	✓	✓	✓	✓	✓	Full-length
50 kDa	✓		✓ **(N)**	✓ **(N)**	✓ **(N)**	Δex7/8
44 kDa	✓	✓	✓	✓ **(N)**	✓ **(N)**	Cys protease digested
39 kDa	✓	✓	✓	✓ **(N)**	✓	Undefined
37 kDa	✓	✓	✓	✓ **(N)**	✓ **(N)**	Δex7/8 + Cys protease digested
33 kDa		✓	✓	✓ **(N)**	✓	Undefined

N, nucleus (referring to the presence on the nuclear fraction of cell lysates).

Subsequently, a densitometry analysis of the two main bands found in the nucleus of NPCs, which included the 50 kDa ($CLN7^{\Delta ex7/8}$) and the 37 kDa band ($CLN7^{\Delta ex7/8\text{-}Cys}$), along with the 57 kDa band which seemed not present in the nuclear fraction on the blots but corresponds to the full-length, was conducted. These results revealed the presence of the three protein isoforms in the cytoplasm of the NPCs. However, there were no significant differences in the expression levels of the 57 kDa, 50 kDa, and 37 kDa bands among the cytoplasmic fraction of the three distinct NPCs (comparing WT and CLN7 NPCs) (**Figure 5.6a**). Nevertheless, the full-length 57 kDa MFSD8 form was absent from the nucleus of all NPCs (**Figure 5.6b**), corroborating its lysosomal localisation. Additionally, the densitometry results validate the observation that both the 50 kDa and 37 kDa isoforms localise to the nucleus, as seen in the previous blots (**Figures 5.5b-d**).

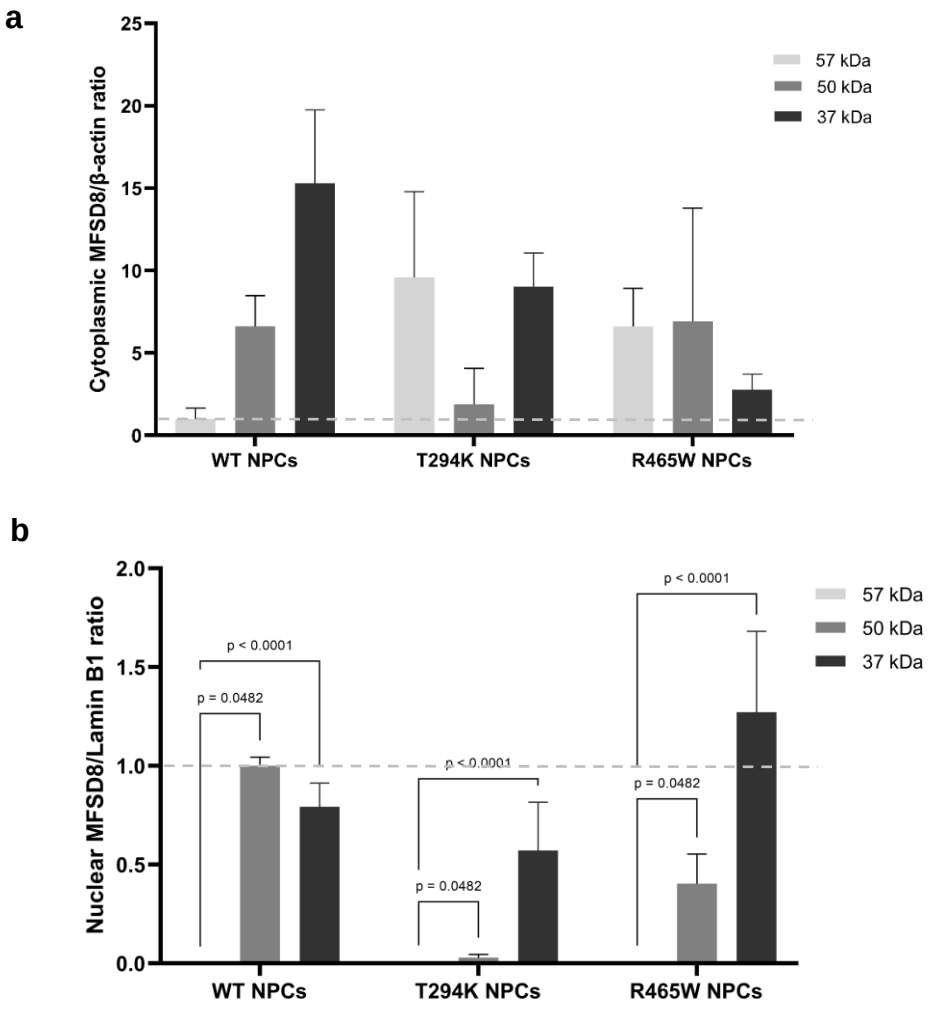

Figure 5. 6. MFSD8 is expressed in different isoforms within the cytoplasm and nucleus of WT and CLN7 NPCs. Quantification of the different MFSD8 protein bands in the blots of nuclear fractionation from WT and CLN7 (p.T294K and p.R465W) NPCs by densitometry. (**a**) Cytoplasmic expression of the different MFSD8 isoforms in WT and CLN7 NPCs. The data are presented as a ratio of nuclear MFSD8 and β-actin expression, which was used as a loading control. (**b**) Nuclear expression of the different MFSD8 isoforms in WT and CLN7 NPCs. The data are presented as a ratio of nuclear MFSD8 and Lamin B1 expression, which was used as a loading control. The cytoplasmic 57 kDa band was set as the control, with ratio = 1, and the rest of the bands/isoforms are relative to this one. The data were normally distributed, and a one-way ANOVA test was used for statistical analysis, followed by Tukey's post hoc test for multiple comparisons. Significant differences among the distinct MFSD8 bands are indicated with the corresponding *p*-value (n = 3, biological replicates).

Altogether, these findings are consistent and support the idea of the potential existence of different MFSD8 isoforms within NPCs, as well as the fact that the 50 kDa and 37 kDa variants are structurally different from the full-length MFSD8 (57 kDa). Specifically, the 50 kDa form could be a product of the deletion of exons 7 and 8, and the 37 kDa form could be a result of the deletion of those exons in addition to a protease cleavage at a cysteine residue.

5.5 MFSD8 is glycosylated and phosphorylated

After observing various bands of MFSD8 and verifying the specificity of the antibodies, the next objective was to determine the corresponding identity of each band. Given that MFSD8 is a transmembrane protein, it is plausible that it undergoes certain post-translational modifications before its translocation to the membrane. Before conducting any experiment, the expected PTMs for MFSD8 were examined. The PhosphoSitePlus® database (v6.7.1.1) was used to visualize a graphical representation of the predicted phosphorylation sites of the MFSD8 protein (**Figure 5.7**). The specific sites where these phosphorylation modifications occur may be at p.T17 (threonine at position 17), p.S54 (serine at position 54), p.Y63 (tyrosine at position 63), and p.Y134 (tyrosine at position 134). It was determined that this protein has the potential to undergo phosphorylation and glycosylation, as described by (Steenhuis et al., 2010). Therefore, a dephosphorylation experiment was conducted to assess the phosphorylation of MFSD8 using the Lambda Protein Phosphatase (Lambda PP). The dephosphorylation results revealed the presence of an extra band with a molecular weight of approximately 130 kDa when Lambda Protein Phosphatase was added (**Figure 5.8**). Considering that the removal of a phosphate molecule (MW = 94.97 Da) or four (which are the number of phosphorylation sites predicted, see **Figure 5.7**) cannot result in the reduction in weight of 50 kDa (observing that the largest form is about 180 kDa), this may be indicative of a structural change. Therefore, we suggest that the heavy MFSD8 bands could represent oligomeric MFSD8 forms, and phosphorylation might cause a specific oligomerisation event that can be reversed with dephosphorylation.

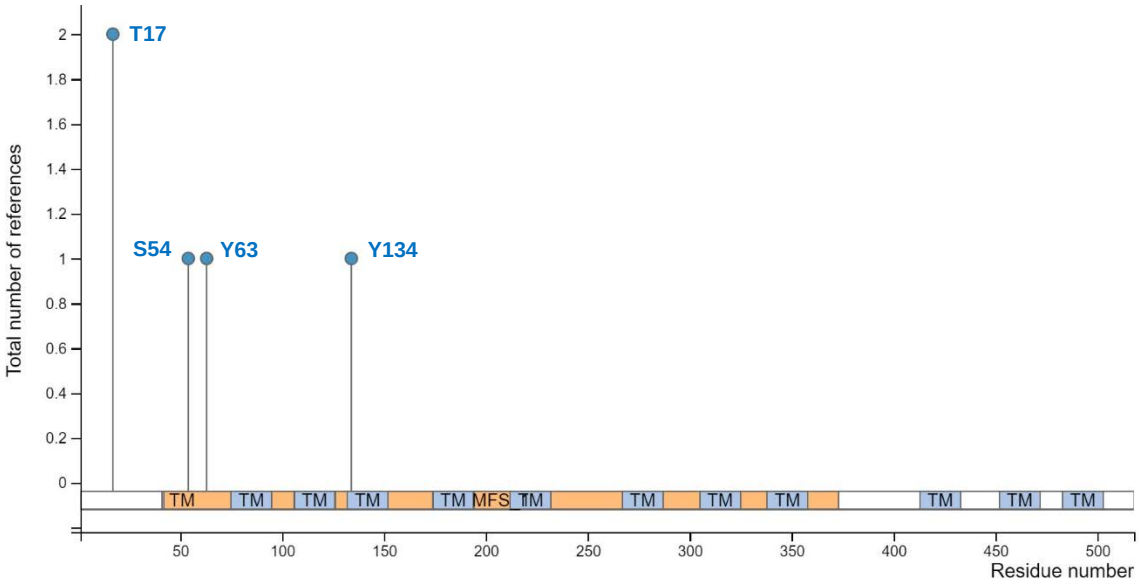

Figure 5. 7. Graphical representation of the predicted phosphorylated sites of MFSD8. The search for the predicted phosphorylation sites of MFSD8 using the PhosphoSitePlus® database (v6.7.1.1) indicated that this protein may exhibit phosphorylation residues at the position T17 (threonine 17), S54 (serine 54), Y63 (tyrosine 63), and T134 (tyrosine 134).

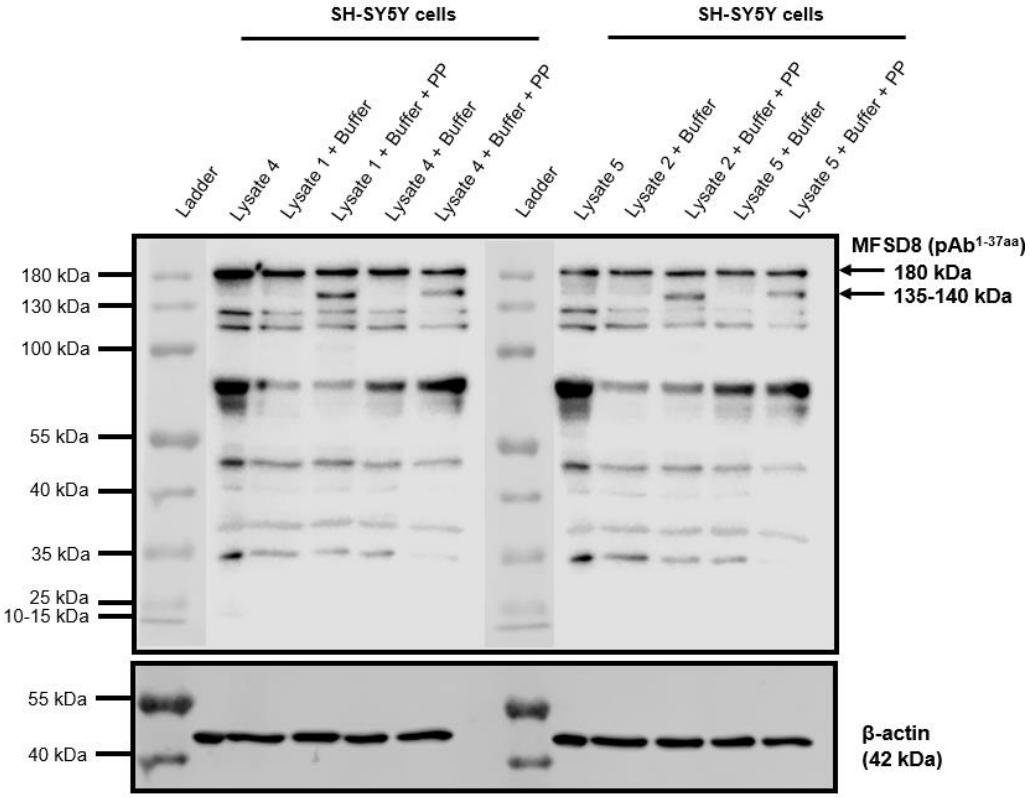

Figure 5. 8. Phosphorylation of MFSD8. Immunoblot of the MFSD8 phosphorylation using the Lambda Protein Phosphatase enzyme on SH-SY5Y cells. Cell lysates were treated with Lambda Protein Phosphatase or buffer as a negative control. The blots were probed with anti-MFSD8 rabbit polyclonal (#PA5-60832, Invitrogen™) with an expected molecular weight of 57-58 kDa. β-actin (42 kDa) was used as a loading control. (n = 3, biological replicates).

Subsequently, a deglycosylation experiment was performed by adding 5 ng of PNGase F to SH-SY5Y cells. The deglycosylation results revealed a shift in the band of the 60-70 kDa (where PNGase F was not utilised) to the 57-58 kDa band, which corresponds to the full-length MFSD8 (**Figure 5.9**). This suggests that the 60 kDa MFSD8 band corresponds to the form that has undergone glycosylation.

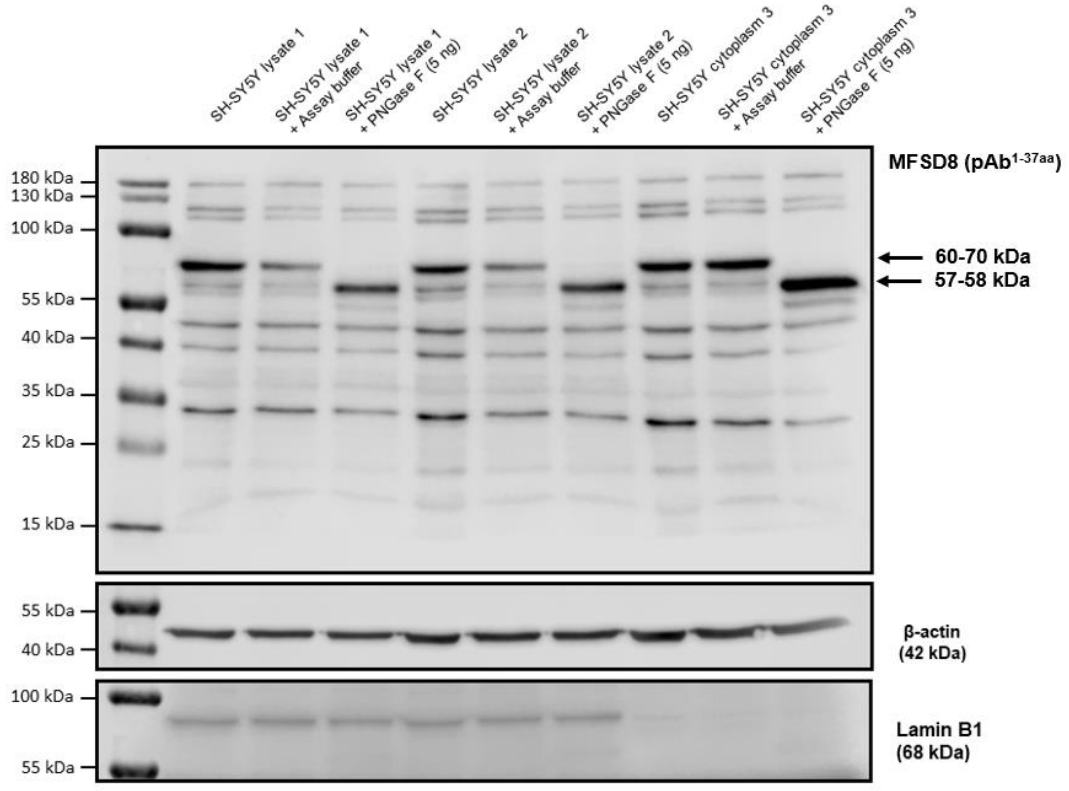

Figure 5. 9. Glycosylation of MFSD8. Immunoblot of MFSD8 glycosylation using the PNGase F enzyme on SH-SY5Y cells. Cell lysates and cytoplasmic fractions were treated with PNGase F for deglycosylation and assay buffer as a negative control. The blots were probed anti-MFSD8 rabbit polyclonal (#PA5-60832, Invitrogen™) with an expected molecular weight of 57-58 kDa. Lamin B1 was probed to demonstrate the cytoplasmic fraction of the samples, and β-actin was used as a loading control. (n = 3, biological replicates).

Despite the absence of any other predicted PTMs in the indicated databases, and not knowing what the heaviest bands represented, the investigation of another PTM called SUMOylation was conducted to explore the possibility of a larger molecular weight addition to the full-length MFSD8. To achieve this, an experiment was performed to remove the SUMO modification using a SUMOylase enzyme. The findings indicated that MFSD8 does not undergo SUMOylation, as there were no discernible variations in the bands of the blots at 1, 2, 4, and 6 h following treatment with the SUMO protease at a temperature of 30˚C (**Figure 5.10**).

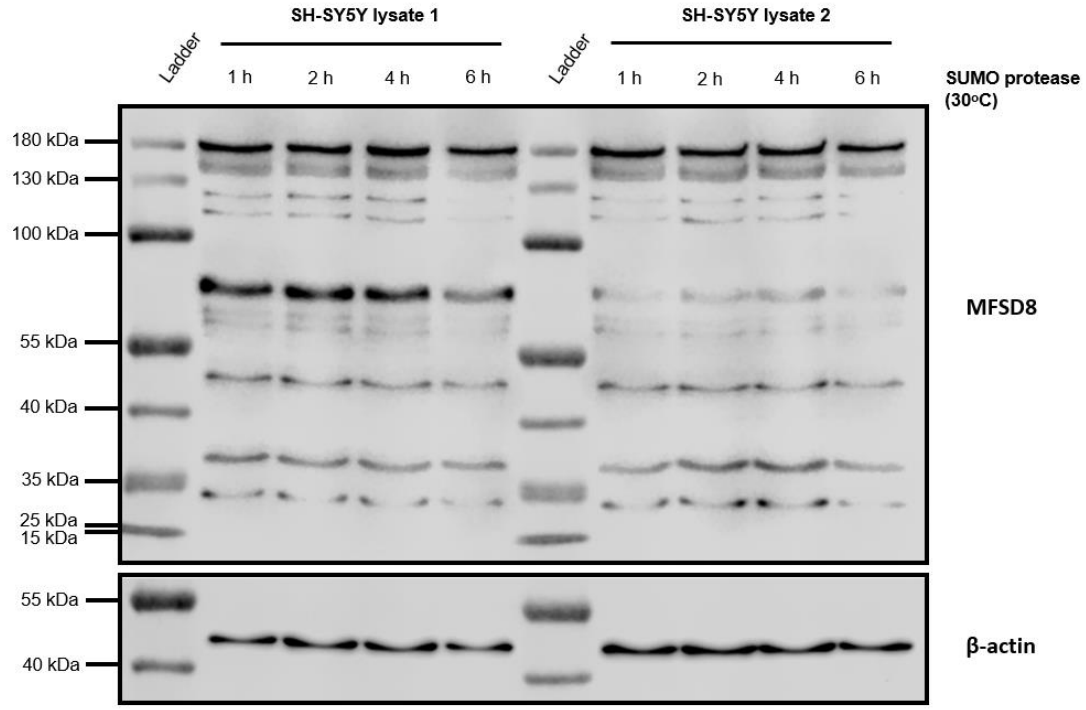

Figure 5. 10. SUMOylation study on MFSD8. Representative immunoblot using the SUMO protease to study SUMOylation on MFSD8 of SH-SY5Y cells. Cell lysates were subjected to SUMO protease for different periods (1, 2, 4, and 6 h) and incubated at 30ºC (n = 3, biological replicates). The blots were probed with the anti-MFSD8 rabbit polyclonal (#PA5-60832, Invitrogen™) with an expected molecular weight of 57-58 kDa. β-actin employed as a loading control. (n = 3, biological replicates).

Typically, Western blotting requires the application of heat to denature the samples before loading them onto a gel. Nevertheless, Tsuji (2020) conducted research on transmembrane iron transporter proteins, including the divalent metal transporter 1 (DMT1). The study revealed that only unheated samples, when loaded onto the gel, resulted in a clearer resolution of the DMT1 protein (Tsuji, 2020). Conversely, samples heated at 95˚C for 5 min led to a loss of resolution due to the formation of protein aggregates. Hence, to assess the heavy bands observed in most of the MFSD8 blots of this study and elucidate whether they could be protein aggregates, it was decided to perform immunoblotting on both heated and unheated samples using SH-SY5Y cells. These cells were used instead of NPCs, as they are neuroblastoma cells easy to maintain in cell culture and can offer a more comprehensive insight into the MFSD8 mechanism than HEK293T cells. However, once the immunoblotting was conducted, there were no discernible variations in the MFSD8 protein when samples were heated for 5-10 min at 95.5˚C (to be consistent with all the blots performed in this thesis) before being loaded onto the gel for subsequent protein transfer, compared to those that were not heated (**Figure 5.11**).

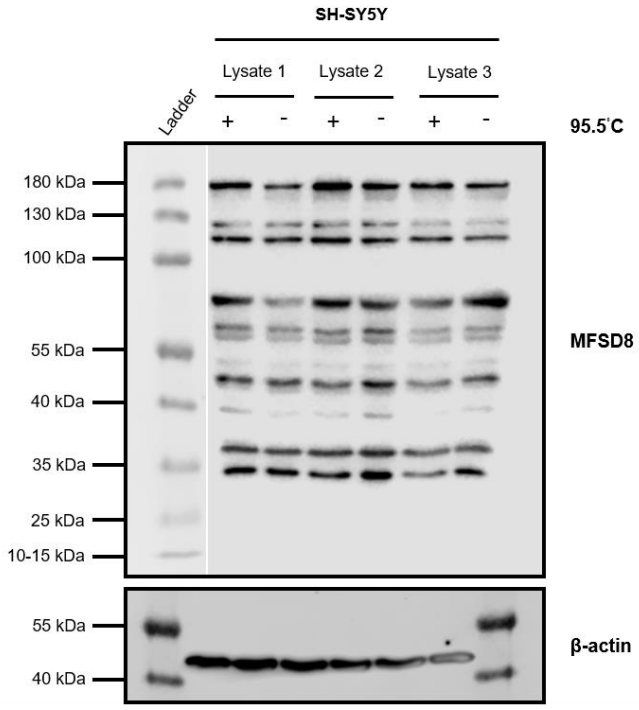

Figure 5. 11. Immunoblotting of MFSD8 using heated and non-heated samples. Cell lysates obtained from SH-SY5Y cells were prepared and a 5× loading buffer was added. Additionally, from the same biological replicates, a sample with the same amount of protein (10 μg) was taken and heated at 95.5˚C for 5-10 min and another sample with 10 μg of protein was not heated. The same procedure was conducted in samples from three biological replicates (n = 3), and they were loaded for gel electrophoresis. Then, protein transfer and Western blotting were carried out and the blots were probed with the primary anti-MFSD8 antibody. β-actin was used as a loading control (42 kDa).

Taken together, these results provide new insights into some of the MFSD8 forms considered oligomeric or subjected to PTMs. More precisely, the 60-70 kDa band was found to correspond to N-glycosylation of the MFSD8, consistent with previous studies by Steenhuis et al. (2010), and corroborating the N-glycosylation sites at positions 371 aa and 376 aa (Steenhuis et al., 2010). Additionally, the MFSD8 seems to be phosphorylated, which might cause structural events that lead to the formation of oligomers, resulting in heavier MFSD8 structures than the full-length. Therefore, the different proposed MFSD8 isoforms in this study are described in **Table 5.2**.

Table 5. 2. Potential MFSD8 isoforms proposed in this study.

Size	HEK293T	SH-SY5Y	WT NPCs	T294K NPCs	R465W NPCs	Potential MFSD8 isoform
180 kDa	✓	✓				Oligomer (phosphorylated)
125-120 kDa	✓	✓		✓		Oligomer or PTM
60-70 kDa	✓	✓		✓ (N)	✓ (N)	N-glycosylated
57-58 kDa	✓	✓	✓	✓	✓	Full-length
50 kDa	✓		✓ (N)	✓ (N)	✓ (N)	Δex7/8
44 kDa	✓	✓	✓	✓ (N)	✓ (N)	Cys protease digested
39 kDa	✓	✓	✓	✓ (N)	✓	Undefined
37 kDa	✓	✓	✓	✓ (N)	✓ (N)	Δex7/8 + Cys protease digested
33 kDa		✓	✓	✓ (N)	✓	Undefined

N, nucleus (referring to the presence on the nuclear fraction of cell lysates).

5.6 MFSD8 shows stability after protein synthesis inhibition and limited proteolysis

Previous results, along with the predicted protein structures indicate that MFSD8 can be expressed in the form of a transmembrane protein despite being truncated. To validate the results from the predicted MFSD8 structures (**Figure 5.8**), the subsequent aim was to conduct various experiments to evaluate protein stabilisation, including the use of Cycloheximide (CHX) to inhibit protein synthesis and limited proteolysis. Following the administration of 100 μM Cycloheximide treatment for 0 and 18 h, MFSD8 protein expression remained unchanged in SH-SY5Y cells, WT NPCs, CLN7$^{T294K/T294K}$ NPCs, and CLN7$^{R465W/R465W}$ NPCs. This was observed when comparing the absence of Cycloheximide treatment with its presence in the various cell types (**Figure 5.12**). These findings are in line with the observed protein stabilisation in the predicted MFSD8 structures using

AlphaFold (**section 5.3, Figure 5.4**), where the different MFSD8 seem to fold stably so that they might translocate to the membrane without being degraded.

Furthermore, the blot where protein stability was assessed with CHX treatment, shows the different profiles of MFSD8 in SH-SY5Y cells compared to NPCs (**Figure 5.12**). Interestingly, SH-SY5Y cells seem to exhibit predominantly the 57-58 kDa band, whereas in the NPCs the prevalent MFSD8 isoform appears to be the 50 kDa. Although, the underlying molecular biology that could explain this remains unknown, it is of interest to notice the different patterns comparing different cell lines for a better understanding of the potential cellular mechanisms explained by further experiments.

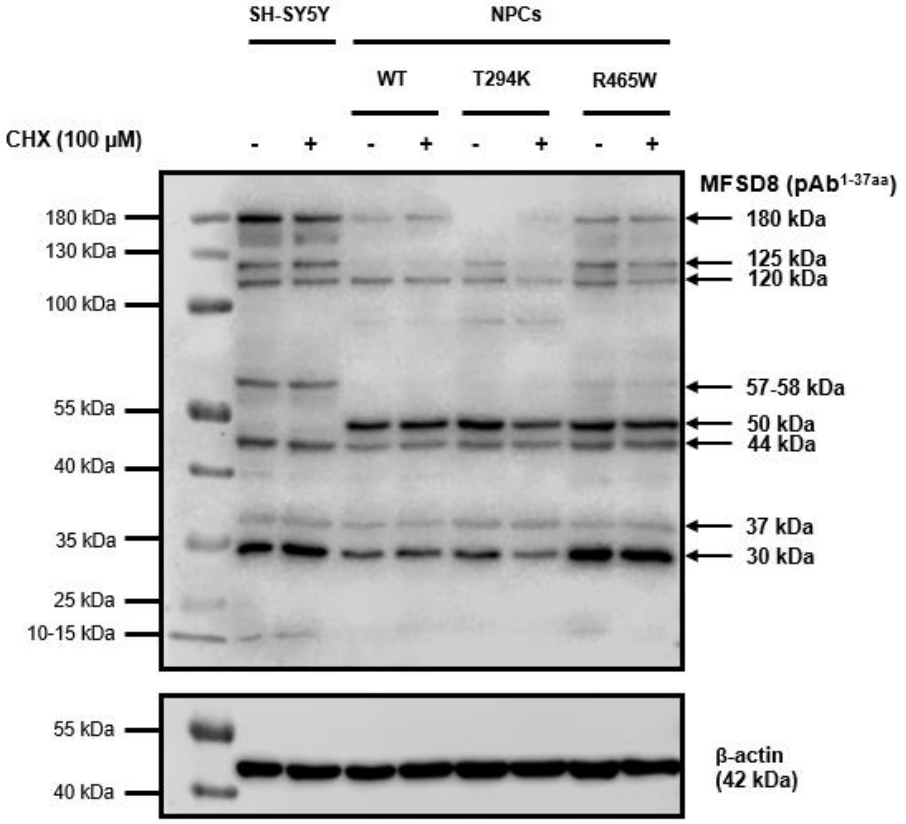

Figure 5. 12. MFSD8 protein stability after inhibition of protein biosynthesis. Protein synthesis was inhibited using 100 µM Cycloheximide (CHX) for 18 h in SH-SY5Y cells, WT NPCs, and CLN7-mutated NPCs. After cell harvesting and immunoblotting, the CLN7/MFSD8 protein showed no degradation (n = 3, biological replicates). β-actin was used as a loading control (42 kDa).

When subjecting the same cell types to limited proteolysis using varying concentrations of trypsin, the findings revealed that the full-length MFSD8 and its glycosylated form remained stable in the SH-SY5Y cells when treated with trypsin at most of the concentrations. The bands began to diminish in intensity, starting from 75-90 μg/mL trypsin (in the range of 0-125 μg/mL trypsin added) (**Figure 5.13**). This suggests that MFSD8 is highly stable in terms of structure, as the bands exhibited consistent patterns even when higher amounts of trypsin were added to the cell lysates. However, in the case of the NPCs, the protein bands of MFSD8 began to diminish after adding the lowest concentration of trypsin. The bands that remained unaffected were those representing the 44 and 37 kDa variants. Notably, the 37 kDa band demonstrated greater resistance to trypsin compared to the 44 kDa band. The differences between SH-SY5Y cells and NPCs may arise from the fact that SH-SY5Y cells are neuroblastoma cells, which possess distinct cellular machinery and protein stability as a result of their immortalised nature as a cell line. In contrast, NPCs more closely resemble primary cells, as they are differentiated, and cannot be continuously. Moreover, the differences observed among the NPCs in comparison to prior blots, where the complete MFSD8 and glycosylated MFSD8 were more apparent in the whole cell lysates, may be attributed to the cellular condition during harvesting or variations in the cell cycle.

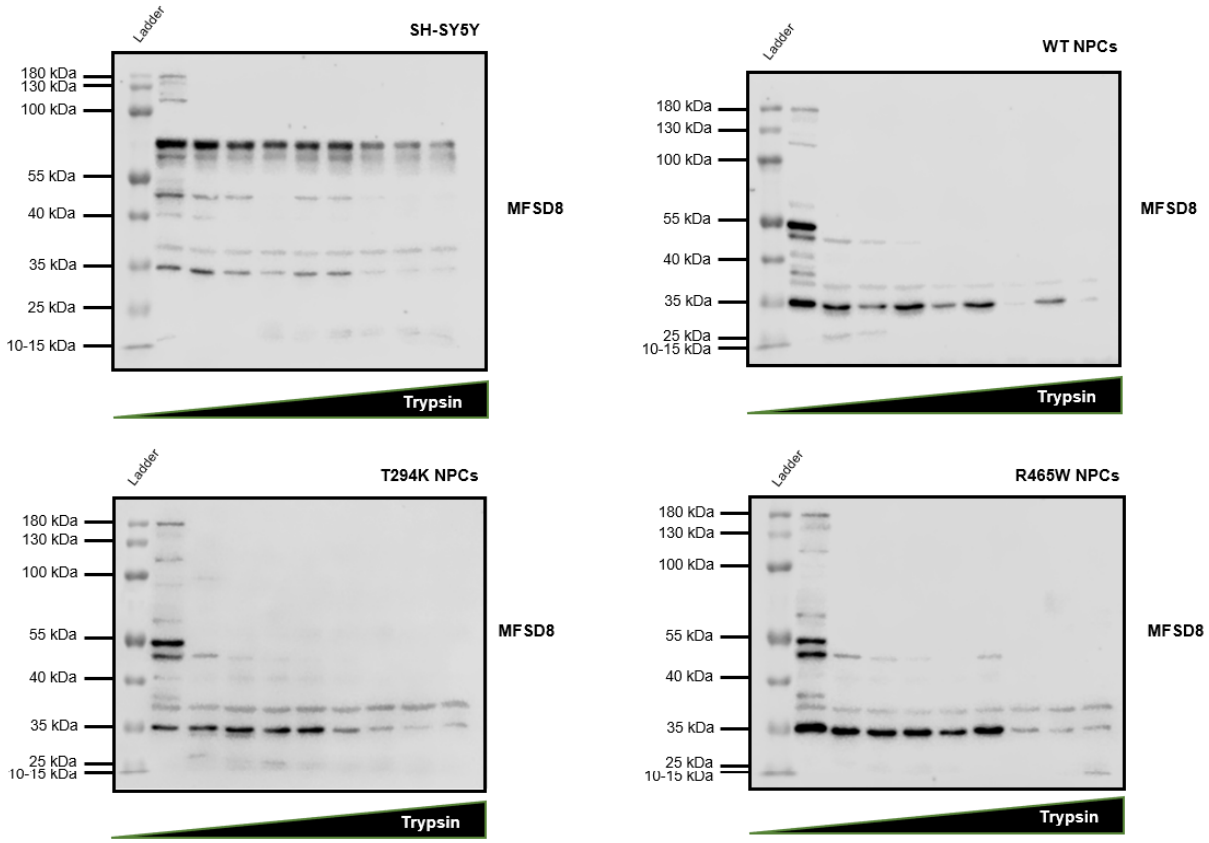

Figure 5. 13. Study of MFSD8 protein stability by limited proteolysis. SH-SY5Y cells, WT NPCs, and CLN7 patient-derived NPCs (with the mutations p.T294K and p.R465W) were treated with different concentrations (from 0 to 125 μg/mL) of trypsin to evaluate CLN7/MFSD8 protein stability.

Limitations

While this chapter aimed to examine the expression of MFSD8 and investigate its molecular biology, it is crucial to acknowledge its limitations. Initially, the process of nuclear fractionation was conducted in NPCs, as they were the main cells of interest for investigating the vLINCL CLN7. However, nuclear isolation could also have been carried out in SH-SY5Y cells and HEK293T cells to provide a comparison of the distinct bands expressed in each cellular fraction of other cell types as well. Additionally, to corroborate the specificity of the antibody, it would have been advantageous to use NPCs in addition to HEK293T or SH-SY5Y cells. However, the reason to just employ HEK293T and SH-SY5Y cells was based on their convenience in terms of growth and maintenance, as compared to NPCs. Moreover, the use of cell knockouts would have provided more rigorous evidence for the anti-MFSD8 antibodies' specificity. Despite numerous attempts to knockdown *MFSD8* using siRNAs and collaborating with another research group (from St George's, University of London) with expertise in knockout experiments, the complexity

of the MFSD8 protein prevented the obtention of knockouts during the development of this thesis. Ultimately, some experiments aimed to study the heaviest bands obtained in the blots using the anti-MFSD8 antibody. Nevertheless, it was overlooked to test various concentrations of the reducing agent DTT, which was present in the loading buffer for gel electrophoresis and subsequent immunoblotting. This oversight should have been taken into account when evaluating this aspect of the project.

Conclusions

The findings of this chapter provide evidence about specific biochemical characteristics of MFSD8, including glycosylation and phosphorylation. Additionally, the results of this study revealed the possible existence of many MFSD8 variants in both WT and CLN7 patient-derived NPCs, as well as in other types of cells (like HEK293T and SH-SY5Y cells) due to the ubiquitous expression of MFSD8. These novel insights indicate that the potential different MFSD8 isoforms may be localised in distinct cellular compartments, hence performing different activities inside the cell and being beneficial or detrimental for the cell. To obtain more robust results regarding the potential MFSD8 splice variants, further research would be required. Nevertheless, these findings offer valuable insights into the complexity of MFSD8's molecular biology and biochemistry. They also provide direction for future investigations into the vLINCL CLN7 and other diseases involving this protein, such as ALS, FTLD, and adult maculopathies and retinopathies.

Chapter 6

Protein binding partners of MFSD8

Summary

Acquiring knowledge of the cellular and molecular biology of MFSD8 in Chapters 4 and 5 was crucial for comprehending the molecular mechanisms that drive CLN7 disease. However, a better understanding of these mechanisms is essential for the development of novel therapeutic strategies to ameliorate or cure the vLINCL CLN7. Given that disease mechanisms are often mediated by interactions between proteins, the objective of this chapter was to explore the protein binding partners of MFSD8 to gain insight into the disease aetiology, progression, and pathogenesis to investigate potential druggable targets in the future. To accomplish this, co-immunoprecipitation (co-IP) experiments were conducted on SH-SY5Y cells, followed by mass spectrometry (MS) and DAVID analysis using Gene Ontology (GO). The findings indicated that cytoplasmic MFSD8 may play a role in perinuclear stress granules (SG), as evidenced by the identification of stress granules-associated proteins Caprin1 and G3BP1 in the co-IP and MS experiments. Furthermore, the results obtained from MS and the analysis using the DAVID tool indicated that MFSD8 may be a constituent of protein complexes responsible for the transportation of mRNA molecules from the nucleus. Additionally, these complexes may also have an impact on the regulation of translation, either by activating or inhibiting it.

Introduction

6.1 Protein-protein interactions (PPIs)

The human genome comprises approximately 20,000-30,000 genes that encode for more than 500,000 distinct proteins (International Human Genome Sequencing Consortium, 2004; Lander et al., 2001; Venter et al., 2001). Among these proteins, the cell can create over 10,000 at any given moment, collectively referred to as the cellular 'proteome'. It has been estimated that 80% of

proteins function in complexes forming protein-protein interactions (PPIs) rather than alone. Multiple processes regulate these interactions between proteins. For instance, the presence of metal-binding or PTMs might cause conformational alterations that modify the affinity, co-operativity, and kinetic properties of the interactions. The cellular network of PPI is constructed by protein nodes that are highly connected (known as 'hubs') and many nodes that are poorly connected. Significant protein complexes include the spliceosome, the ribosome, and the nuclear pore complex.

Previous studies have demonstrated that the elimination of a protein that plays a crucial role in several networks tends to result in lethality (Jeong et al., 2001). The prevailing perspective that the majority, if not all, of cellular processes are connected either directly or indirectly in a cellular PPI network has significant consequences for how we describe cellular pathways. Therefore, a specific pathway, such as vesicle trafficking, apoptosis, or cell cycle control, can be understood as a subgroup of interactions that present extensive interconnections with other pathways.

Several novel techniques for the identification and analysis of PPIs have been introduced and are widely used in laboratories worldwide. Over the past three decades, we have observed significant advancements in the development of some of these techniques, such as proteomics, especially mass spectrometry (MS), which has simplified the process of protein identification.

6.2 Co-immunoprecipitation

Co-immunoprecipitation (co-IP) is a widely employed technique for validating PPIs. In a standard experiment, bait proteins are isolated from a cell lysate by employing a particular antibody. The antibody is subsequently fixed by covalently binding it to Sepharose beads that have protein A or protein G linked to them, or magnetic beads (**Figure 6.1**). Following bead washing, the antibody, bait, and proteins bound to the bait are extracted, often through boiling, in the case of the Sepharose beads or using a magnetic rack for the magnetic beads (**Figure 6.1**). The proteins that are bound can subsequently be identified by immunoblotting and MS. Co-IP experiments typically produce substantial background noise, making it crucial to perform simultaneous negative control studies. Co-IP studies can be conducted using many methods. First, they can be performed using cell lines or tissues that express their native proteins, which have the benefit of studying endogenous protein complexes. Consequently, any artificial impacts caused by affinity tags or overexpression are prevented. An inherent drawback is the requirement of antibodies that are greatly specific. Another option is to utilise cells that have been transfected with a plasmid containing a labelled bait protein (Masters, 2004). In this case, an antibody targeting the tag (rather than the bait protein) can be employed. A benefit of this method is that it provides a high level of

confidence that the antibody targeting the tag is selective and does not have any unintended reactions with other proteins. Moreover, proteins labelled with epitope tags can frequently be separated by exposing them to competing peptides or other small molecules, rather than boiling them. Precise elution frequently decreases the quantity of contaminating proteins in the eluate. A third method is to conduct co-IP experiments by transfecting cells with genetically modified copies of two potential interacting proteins, which are labelled with tags.

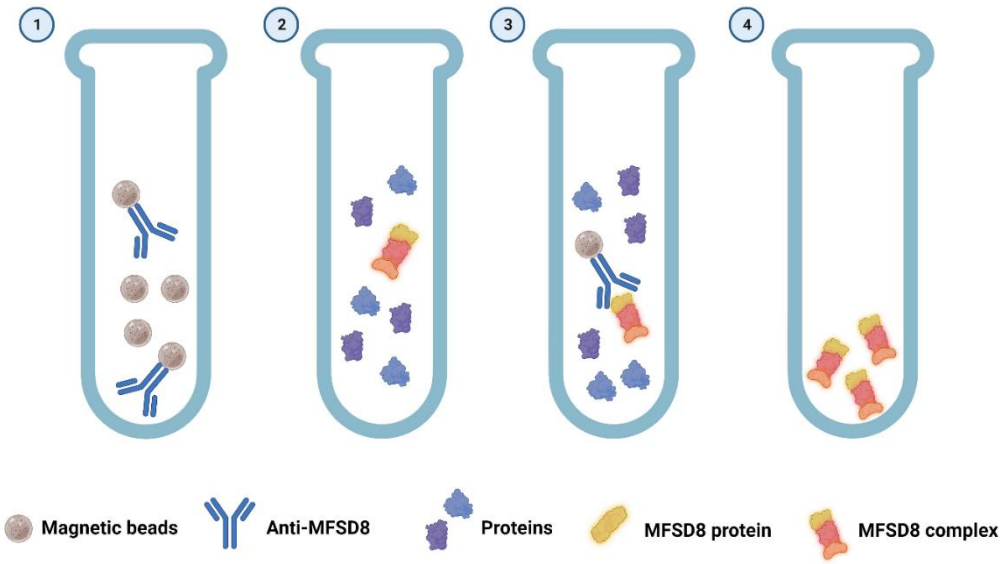

Figure 6. 1. Protein complex immunoprecipitation process using magnetic beads. (1) Coupling of beads and antibody. (2) Protein extract from cell lysates. (3) Incubation of cell lysate with the covalently coupled beads to select the bait protein and its interactors. (4) Elution of the proteins from the antibody-conjugated beads. This method is based on the published protocol by Lagundžin et al. (2022).

Interestingly, multiple commercial co-IP kits are accessible for mammalian protein expression systems, which enhance the effectiveness of different steps on the co-IP protocol, including washing steps and the formation of covalent bonds between antibodies and the protein A/G support. Thus, minimising antibody interference and facilitating elution.

6.3 Applying proteomics to PPI analysis

MS-based proteomics has made a substantial contribution to the study of protein complexes. Most proteins perform their activity by PPI and enzymes are often maintained in tightly restricted locations of the cell by such interactions. Thus, one of the first questions frequently addressed regarding a new protein is to what proteins it binds to. To examine this question by MS, the protein itself is used as an affinity reagent to isolate its binding partners.

Even though MS is a highly sensitive and specific technology, only a subset of the actual protein interactions will be detected by MS-based methods in a basic affinity experiment because many biologically significant interactions are low affinity, transient, and typically dependent on the particular cellular environment in which they occur. Direct connections and general architecture of multiprotein complexes can frequently be further clarified with the use of bioinformatics techniques, correlation of MS data with other methods' results, or repeated MS measurements combined with chemical crosslinking.

Significant insights into physiology have been derived by studying large protein complexes, organelles, and subcellular compartments. For instance, the first complex investigated using this approach was the spliceosome, a large RNA-protein complex that plays a crucial role in catalysing the removal of introns from nuclear pre-mRNA (Lamond, 1993; Neubauer et al., 1998, 1997). A subsequent re-evaluation of the spliceosome was conducted using improved equipment and more advanced databases. A study identified over 30 proteins, and further examination of their sequencing revealed a set of 55 unique proteins involved in splicing and RNA processing (Rappsilber et al., 2002).

Aims and objectives

The overall aim of this chapter was to explore the potential protein binding partners of MFSD8 to gain a better understanding of MFSD8's function after the identification of several possible protein forms. This was accomplished by the pursuit of the following objectives:

i) To visualise the predicted PPIs of MFSD8 that have been previously studied or reported, using the STRING database, to gain an initial understanding and facilitate further comparisons with experimental data.

ii) To pull down the endogenous MFSD8 from SH-SY5Y cells, which are neuroblastoma cells that are easy to maintain and provide enough material for co-IP assays.

iii) To analyse the samples acquired from the co-IP experiments using MS-based proteomics to uncover the potential interactors of MFSD8.

Results

6.4 Predicted MFSD8 protein-protein interactions

Before starting the co-IP experiments and studying the PPIs of MFSD8 using MS-based proteomics, the predicted MFSD8 protein interactions were queried on the STRING database (https://string-db.org/). This database systematically compiles and integrates protein-protein

interactions, encompassing both physical and functional interactions (Enright and Ouzounis, 2001; Guala et al., 2020; Snel et al., 2002). The data are obtained from several sources, such as automated text analysis of scientific literature, computational predictions of interactions based on co-expression, conserved genomic context, databases of experimental interactions, and established complexes/pathways from reviewed sources (Szklarczyk et al., 2023). Each of these interactions undergoes rigorous evaluation, scoring, and is then automatically translated to less extensively researched organisms based on hierarchical orthology information.

The interaction network of *MFSD8* on the STRING database mostly consisted of 11 nodes, which were associated with other NCL genes. The genes identified are the following: palmitoyl-protein thioesterase 1 (*PPT1* or *CLN1*), tripeptidyl peptidase 1 (*TPP1* or *CLN2*), *CLN3*, DnaJ heat shock protein family (Hsp40) member C5 (*DNAJC5* or *CLN4*), *CLN5*, *CLN6*, *CLN8*, cathepsin D (*CTSD* or *CLN10*), cathepsin F (*CTSF* or *CLN13*), and potassium channel tetramerization domain containing 7 (*KTCD7* or *CLN14*) (**Figure 6.2**). The STRING database suggests that NCL genes, such as *PPT1*, *TPP1*, *CLN3*, and *CLN5*, which encode either soluble or transmembrane lysosomal proteins, are potential interactors with MFSD8 (**Figure 6.2**). This finding aligns with the recent study by Wang *et al.* (2021) indicating that MFSD8 may function as a chloride channel within the lysosomes, underscoring the critical role of MFSD8 in lysosomal function.

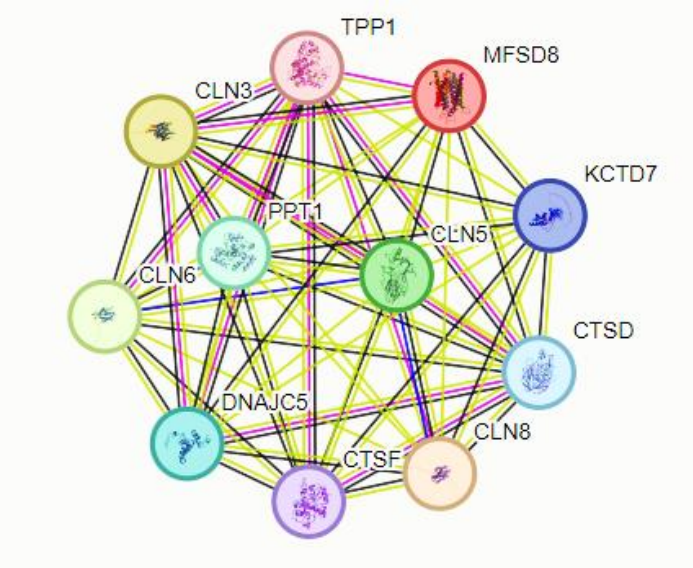

Major MFSD8 interactors	
Gene	**Function**
PPT1	Catalyses the cleavage of thioester-linked fatty acyl groups such as palmitate, from modified cysteine residues in proteins or peptides during lysosomal degradation.
TTP1	Lysosomal serine protease with tripeptidyl-peptidase I activity. May function as a non-specific lysosomal peptidase that produces tripeptides from the degradation products generated by lysosomal proteinases.
CLN3	Involved in microtubule-dependent, anterograde transport of late endosomes and lysosomes.
DNAJC5	Functions as a general chaperone in controlled exocytosis (by similarity). Functions as a co-chaperone for the SNARE protein SNAP-25 (by similarity). Participates in the calcium-dependent regulation of a late stage of exocytosis (by similarity). May play a crucial role in presynaptic function. May participate in the release of neurotransmitters at nerve endings, which is dependent on calcium (by similarity).
CLN5	Plays a role in influencing the retrograde trafficking of lysosomal sorting receptors SORT1 and IGF2R from the endosomes to the trans-Golgi network by controlling the recruitment of retromer complex to the endosomal membrane. Controls the localisation and activation of RAB7A, which is necessary for recruiting the retromer complex to the endosomal membrane.
CLN6	Facilitates the transfer of certain proteins and lipids from the endoplasmic reticulum to lysosomes.
CLN8	May contribute to cellular proliferation during neuronal differentiation and serve as a protective mechanism against cell death.
CTSD	Acid protease active in intracellular protein breakdown. Contributes to the processing of APP following cleavage and activation by ADAM30, resulting in the degradation of APP.
CTSF	Thiol protease which is believed to be involved in the intracellular degradation and turnover of proteins.
KTCD7	May play a role in regulating the excitability of cortical neurons.

Figure 6. 2. Predicted MFSD8 protein interactions obtained from the STRING database. The term 'MFSD8' (*Homo sapiens*) was searched on the STRING database (https://string-db.org/network/9606.ENSP00000296468) to visualize its potential protein-protein interaction network. The nodes (circles) represent proteins and the edges connect pairs of interacting proteins. The 11 nodes obtained in the PPI network of MFSD8 correspond to other NCL genes.

During the development of this thesis, the discovery of various potential isoforms of MFSD8 and their presence in both the cytoplasm and nucleus of cells prompts the question of whether this protein might also play a role in other cellular compartments and have additional functions. To investigate the potential binding partners of MFSD8 and understand its various activities depending on the isoform, co-IP experiments were conducted, followed by MS-based proteomics.

6.5 Co-IP optimisation

As abovementioned, co-IP is a widely used method for investigating protein-protein interactions by extracting protein complexes from cellular lysates. However, establishing accurate co-IP experiments often requires considerable optimisation. This study employed an initial protocol provided by Dr Richard Unwin (from the University of Manchester) (described in Chapter 2 Materials and Methods, **section 2.3.8**), which utilised Protein G-sepharose beads and SH-SY5Y cells. These cells were used since a substantial number of cells were needed to conduct four biological replicates, which were necessary to obtain statistically significant results in this experiment. The initial co-IP experiment was performed following a protocol that was previously established for the pull-down of another protein using different cells. In this case, the following modifications were introduced: (i) the use of the anti-MFSD8 polyclonal antibody (pAb) (#PA5-60832, ThermoFisher, and (ii) the addition of a negative control in which an irrelevant antibody was used (either anti-Lamin B1 or anti-SIRT1, both raised in rabbit, the same species as the anti-MFSD8 pAb). The anti-Lamin B1 was first chosen since it was one of the antibodies available to us that was produced in rabbit, as well as the anti-MFSD8 pAb. After completing all the steps for the co-IP, the samples with the bait protein – the MFSD8, in this case – were separated from the beads using heat. While monoclonal antibodies exhibit greater specificity than polyclonal antibodies as they recognise a single epitope on the target protein, the latter are more advantageous in co-IP experiments. This is due to the fact that co-IP assays aim to establish a stable complex between antibodies and proteins. As polyclonal antibodies can bind to multiple epitopes on the target protein, they form more tightly bound antibody-protein complexes compared to monoclonal antibodies.

The collected samples were subsequently processed and utilised for immunoblotting. The blots probed with anti-MFSD8 pAb (#PA5-60832) exhibited distinct bands in the lanes corresponding to the samples treated with the anti-MFSD8 pAb. One band displayed a molecular weight of approximately 120 kDa, consistent with our previous observations in blots containing SH-SY5Y cell lysates (**Figure 6.3a**). Another band, with high intensity, corresponded to a molecular weight of approximately 57-60 kDa, suggesting the presence of the full-length MFSD8 protein (**Figure 6.3a**). However, in the experimental samples where the anti-Lamin B1 antibody was used during

the co-IP, a consistent 57-60 kDa protein band was observed. This suggested that MFSD8 may potentially interact with Lamin B1, as shown in **Figure 6.3a**. Lamin B1 is expected to have a molecular weight of 66 kDa, although it usually appears as 70 kDa on blots. Even though the PPIs of MFSD8 are currently unidentified, the interaction of the anti-Lamin B1 antibody was unexpected. To gain a clearer understanding of the results obtained from this co-IP experiment, communication was established with Dr Jon Humphries from Manchester Metropolitan University. Subsequently, it was recommended to replace the secondary horseradish peroxidase (HRP) antibody with a light chain-specific secondary antibody. This is because the band observed at around 57-60 kDa might potentially have masked the MFSD8 protein band and also corresponded to the heavy chain of the antibody employed in the co-IP assay, as the heavy chain of an antibody typically has a molecular weight of 50 kDa. Consequently, when the same co-IP procedure was repeated using a light chain-specific HRP secondary antibody and an unrelated antibody, such as anti-SIRT1, the intensity of the 57-60 kDa band was reduced. This suggested that the 57-60 kDa band observed in the previous blot (**Figure 6.3a**) may not accurately represent a band associated with MFSD8. However, a distinct and strong band was observed at a molecular weight of 25 kDa in this instance, indicating that the light chain-specific secondary antibody picked the antibody's light chain instead of the heavy chain (**Figure 6.3b**). SIRT1 is a protein consisting of 747 aa with an estimated molecular weight of 82 kDa. However, in Western blots, its measured molecular weight ranges from 110 to 130 kDa. Based on these findings, the light chain-specific HRP secondary antibody was consistently employed for the subsequent co-IP blots. These blots were conducted to observe the results of the co-IP and determine if the obtained samples were appropriate for further analysis using MS-based proteomics.

a

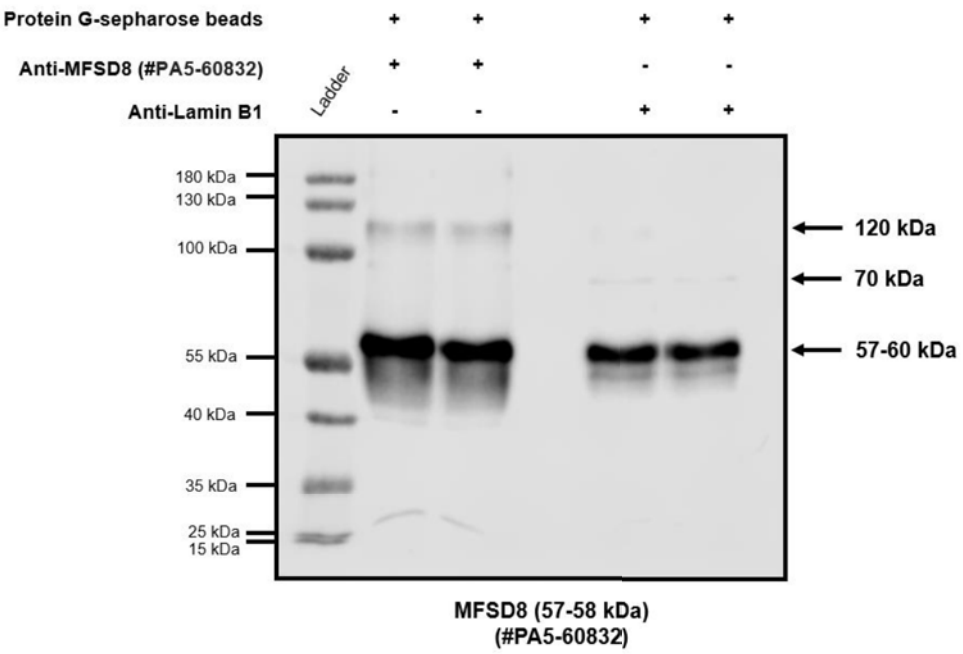
Protein G-sepharose beads
Anti-MFSD8 (#PA5-60832)
Anti-Lamin B1
Ladder
180 kDa
130 kDa
100 kDa
55 kDa
40 kDa
35 kDa
25 kDa
15 kDa
120 kDa
70 kDa
57-60 kDa
MFSD8 (57-58 kDa)
(#PA5-60832)

b

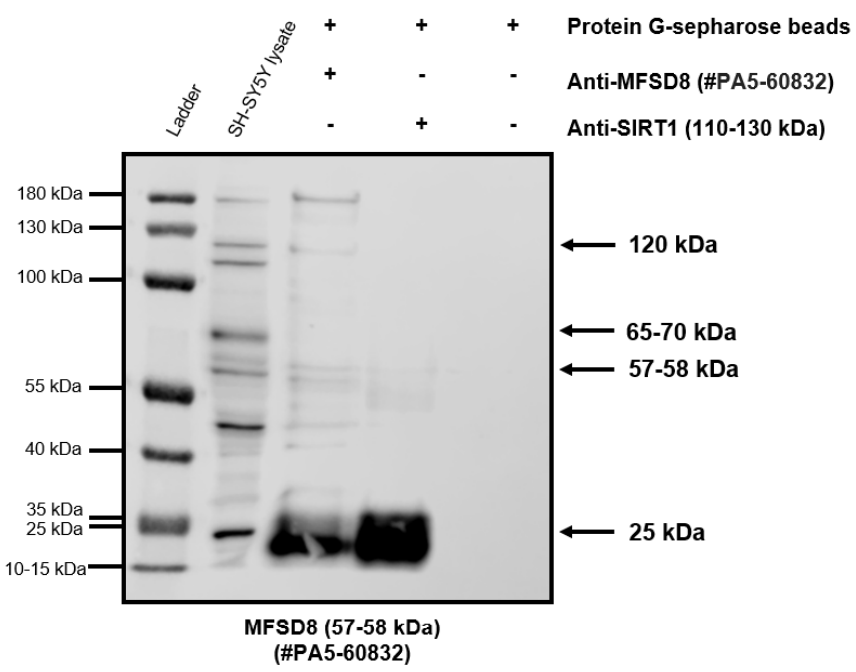
Protein G-sepharose beads
Anti-MFSD8 (#PA5-60832)
Anti-SIRT1 (110-130 kDa)
Ladder
SH-SY5Y lysate
180 kDa
130 kDa
100 kDa
55 kDa
40 kDa
35 kDa
25 kDa
10-15 kDa
120 kDa
65-70 kDa
57-58 kDa
25 kDa
MFSD8 (57-58 kDa)
(#PA5-60832)

Figure 6. 3. Immunoblots of MFSD8 co-IP using Protein G-sepharose beads. (**a**) In the process of this co-IP protein G-sepharose beads, as well as anti-MFSD8 pAb (#PA5-60832) to probe MFSD8, and anti-Lamin B1 as a negative control were used. A conventional secondary HRP antibody was used and intense bands were detected around the 57-60 kDa size area, which generated doubt in the results obtained. (**b**) To clarify those doubts, another co-IP following the same protocol (provided by Dr Richard Unwin from the University of Manchester) was conducted using an alternative irrelevant antibody, such as anti-SIRT1 and a secondary HRP antibody specific for the light chain to avoid the detection of the heavy chain of the antibody. These co-IP experiments were first performed with two biological replicates to avoid the waste of antibodies, due to the high amount of antibody needed for co-IP experiments.

While the previous co-IP experiments showed the presence of MFSD8 in the samples when the anti-MFSD8 pAb (#PA5-60832) was used along with a light chain-specific secondary antibody, the detection of certain bands with the irrelevant antibodies introduced some doubt regarding the reliability of the co-IP results. To obtain four replicates of samples using the anti-MFSD8 pAb (PA5-60832) and four control samples, a substantial quantity of antibodies would have been required. Due to these factors, it was decided to follow a recently published protocol by Lagundžin *et al.* (2022) based on the co-IP of endogenous proteins. In this new protocol, magnetic beads were employed as an alternative to Sepharose beads, potentially minimising the damage to the captured protein complexes and, thus, enhancing the accuracy of the co-IP results. Nevertheless, this protocol required a substantial amount of input material (SH-SY5Y cells) to obtain 2.5 mg of protein. Despite the need for several 10 mm cell culture dishes for four replicates of samples, the use of SH-SY5Y cells facilitated the process of obtaining the required amount of protein. Additionally, this approach needed a great amount of antibody. However, another commercially accessible anti-MFSD8 pAb, which is available at a higher concentration and volume compared to the anti-MFSD8 pAb (#PA5-60832) was used for conducting this new co-IP protocol. After performing the co-IP using Lagundžin's protocol, various modifications were made in comparison to the previous one involving Sepharose beads. In Lagundžin's protocol, magnetic beads and a magnetic rack were employed as an alternative to Sepharose beads and centrifugation steps, which were used in the previous co-IP method. In addition, the new anti-MFSD8 pAb (24298-1-AP, Poteintech®) was utilised, and its specificity was checked in Chapter 5, **section 5.5**. Furthermore, rabbit IgGs were used as a negative control instead of the use of an irrelevant antibody. Rabbit IgGs serve as an isotype control antibody, employed to assess the non-specific binding of target primary antibodies caused by Fc receptor binding or other protein-protein interactions.

After the first co-IP performed using this new protocol to pull down endogenous MFSD8 from SH-SY5Y cells, the antibody used to probe the MFSD8 by immunoblotting was the same one as

used in the co-IP, the new anti-MFSD8 pAb (24298-1-AP, Poteintech®) and as a secondary HRP antibody the light-chain specific antibody was also used. The results showed a similar heavy band of approximately 120-125 kDa, which is consistent with the findings from earlier co-IP experiments and immunoblots conducted using SH-SY5Y cells. However, in this instance, a prominent 65-70 kDa band was observed in both the lane containing the cell lysate and the lane containing the co-IP samples with the anti-MFSD8 pAb (24298-1-AP, Poteintech®) (**Figure 6.4**). This indicated that the new anti-MFSD8 antibody used effectively identified the MFSD8 protein and the co-IP experiment was successful. Two bands were detected in the lane containing the co-IP sample in which the rabbit IgGs were added instead of the anti-MFSD8 pAb. One band was observed at a molecular weight range of 57-60 kDa, likely indicating the heavy chain of the IgGs (50 kDa) (**Figure 6.4**). Another band, around 30 kDa in size, was also detected, representing the light chain of the IgGs (25 kDa). This band was also present in the sample in which the anti-MFSD8 pAb was added (**Figure 6.4**). More specifically, IgGs are macromolecules with a molecular weight of around 150 kDa, consisting of two distinct types of polypeptide chains. The heavy or H chain has a molecular weight of approximately 50 kDa, while the light or L chain has a molecular weight of 25 kDa. Altogether the results demonstrated an effective co-IP and pull-down of the protein of interest, specifically MFSD8. Consequently, the four replicates acquired by following Lagundžin's protocol were prepared and sent for MS-based proteomics, as outlined in the next section.

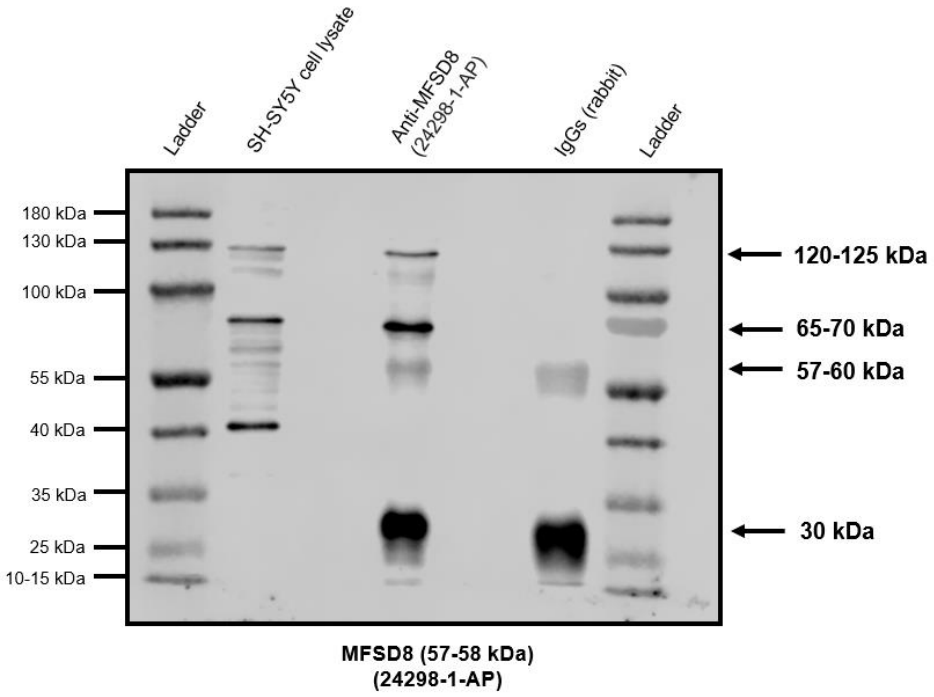

Figure 6. 4. Immunoblot of MFSD8 co-IP using magnetic beads. In this co-IP experiment, the protocol by Lagundžin et al. (2022) was followed, using magnetic beads, a different anti-MFSD8 pAb (24298-1-AP, Poteintech®), and a light chain-specific secondary HRP antibody. Rabbit IgGs were employed as a negative control and four biological replicates for each condition (four samples for the anti-MFSD8 pAb and four samples for the IgGs) were generated, which were used to produce the co-IP samples and sent for mass spectrometry and further proteomics analysis after the MFSD8 pull-down.

6.6 Gene ontology (GO) and KEGG pathway enrichment analysis using ShinyGO

To investigate the potential MFSD8 binding partners, from the co-IP control (IgGs) and MFSD8 (anti-MFSD8 antibody, 24298-1-AP, Proteintech®) samples in SH-SY5Y neuroblastoma cells, the pull-down of MFSD8 was first corroborated by immunoblotting with the other anti-MFSD8 primary antibody (#PA5-60832, ThermoFisher) (**Chapter 5, Figure 5.2b**). Subsequently, the same samples were sent for mass spectrometry to the Bio-MS facilities at the University of Manchester. Raw data were obtained from the Bio-MS facilities and they were analysed by Dr Jon Humphries (from Manchester Metropolitan University). Following raw data analysis (by Dr Jon Humphries), a total of 290 proteins were found to have an enrichment of at least >2-fold (with a Benjamini-corrected $p < 0.05$) for the MFSD8 pAb in comparison to the IgG control in SH-SH5Y cells. Following this, a Gene Ontology analysis was performed using the ShinyGO 0.77 (http://bioinformatics.sdstate.edu/go/) software and the DAVID web server

(https://david.ncifcrf.gov/). Out of the 290 proteins that were discovered, it is worth noting that 33 of them showed a substantial drop in $iNPC^{BD}$ compared to $iNPC^{WT}$ when cultured under normal conditions (see **Chapter 5, section 5.1**), which further corroborates the results obtained from the co-IP.

GO enrichment analysis of significant identified proteins from the MFSD8 pull-down was categorized into Biological Process (BP), Cellular Component (CC), and Molecular Function (MF) using ShinyGO 0.77 software. Among the 290 genes on our list, *translational initiation* (GO:0006413, indicating the accession number of the term at GO) was the most significantly enriched biological process considering that among the top three BPs with higher Fold Enrichment (FE), it was the GO term with a higher bubble (dot) size and a lower *p*-value (expressed as FDR, in this case) (FDR = 2.2×10^{-62}), which indicates higher significance. The *p*-values are expressed as false discovery rates (FDR), which are calculated based on nominal p-values from the hypergeometric test. An FDR of 5% indicates that, out of all the features identified as significant, 5% of them are null. Similar to how α is established as a threshold for the *p*-value in order to manage the false positive rate (FPR), it can also be established as a threshold for the *q*-value (corrected *p*-value), which serves as the FDR equivalent of the *p*-value. Other important BP terms associated with these identified genes in the co-IP were *cytoplasmic translation* (GO:0002181) (FDR = 8.1×10^{-57}), *nuclear-transcribed mRNA catabolic process* (GO:0000956) (FDR = 3.8×10^{-55}), and *mRNA catabolic process* (GO:0006402) (FDR = 8.5×10^{-60}) (**Figure 6.5**). Additionally, the most significantly enriched CC linked with the identified genes were *eukaryotic translation initiation factor complex 3* (GO:0005852) (FDR = 2.9×10^{-20}), *eukaryotic translation initiation factor complex 3* (eIF3m) (GO:0071541) (FDR = 7.7×10^{-13}), *eukaryotic 48S preinitiation complex* (GO:0033290) (FDR = 7.6×10^{-17}), *eukaryotic 43S preinitiation complex* (GO:0016282) (FDR = 4.6×10^{-18}), and *translation preinitiation complex* (GO:0070993) (FDR = 1.1×10^{-17}), all linked to translational initiation (**Figure 6.6**). However, among the 20 most enriched GO terms from the input gene list related to CC, other significantly enriched GO terms related to the localisation of the MFSD8 interactors with a lower FE than the abovementioned are *polysome* (GO:0005844), *cytoplasmic stress granule* (GO:0010494), *ribosome* (GO:0005840), *nucleolus* (GO:0005730), and *nuclear-protein-containing complex* (GO:0140513), among others. This could also corroborate the multifunctionality and different localisation of the distinct MFSD8 protein isoforms, even though these cellular compartments can also be related according to the biological processes enriched in these genes. Furthermore, the most significantly enriched GO terms for MF included *translation initiation factor activity* (GO:0003743) (FDR = 2.4×10^{-25}), *translation initiation factor binding* (GO:0031369) (FDR = 1.5×10^{-10}), *exoribonuclease activity producing 5′-phosphomonoesters*

(GO:0016896) (FDR = 1.3×10^{-8}), and *translation factor activity RNA binding* (GO:0008135) (FDR = 3.5×10^{-20}) (**Figure 6.7**).

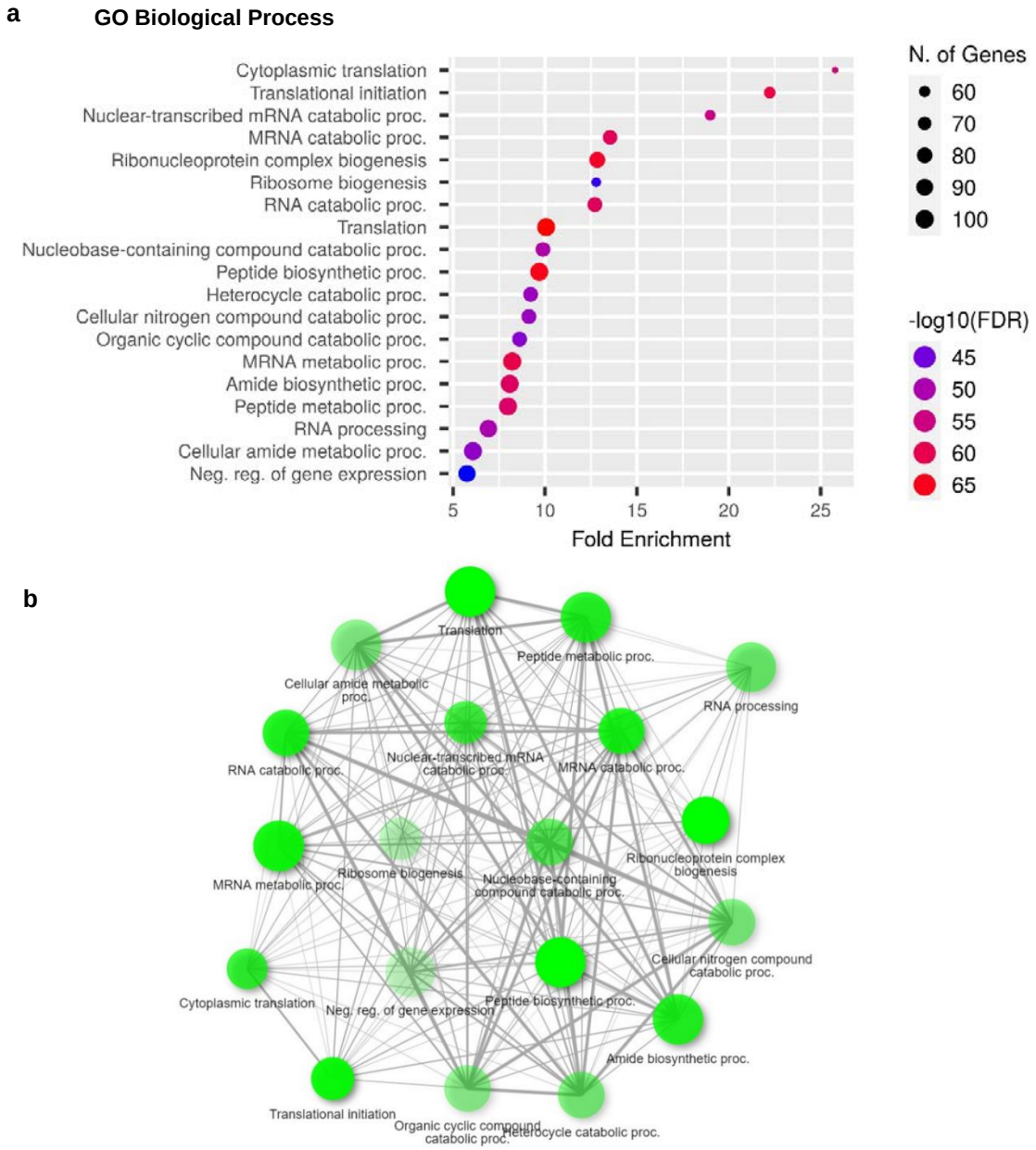

Figure 6. 5. Gene ontology analysis of the potential genes interacting with MFSD8 for the Biological Process category. (**a**) Fold enrichment of the top 20 enriched GO terms in the Biological Process (BP) category and (**b**) network analysis using ShinyGO 0.77. (**a**) FDR is the estimated probability that a gene set with a given enrichment score (normalised for gene set size) represents a false positive. It is calculated based on the nominal p-value from the hypergeometric test. Fold enrichment represents the percentage of genes in the list belonging to a pathway, divided by the corresponding percentage in the background. (**b**) The network diagram describes the link between enriched GO terms for the BP category. Two BPs (nodes) are connected if they share 20% (default) or more genes. Darker nodes represent more significantly enriched gene sets and bigger nodes describe larger gene sets. Thicker edges (lines) indicate more overlapped genes.

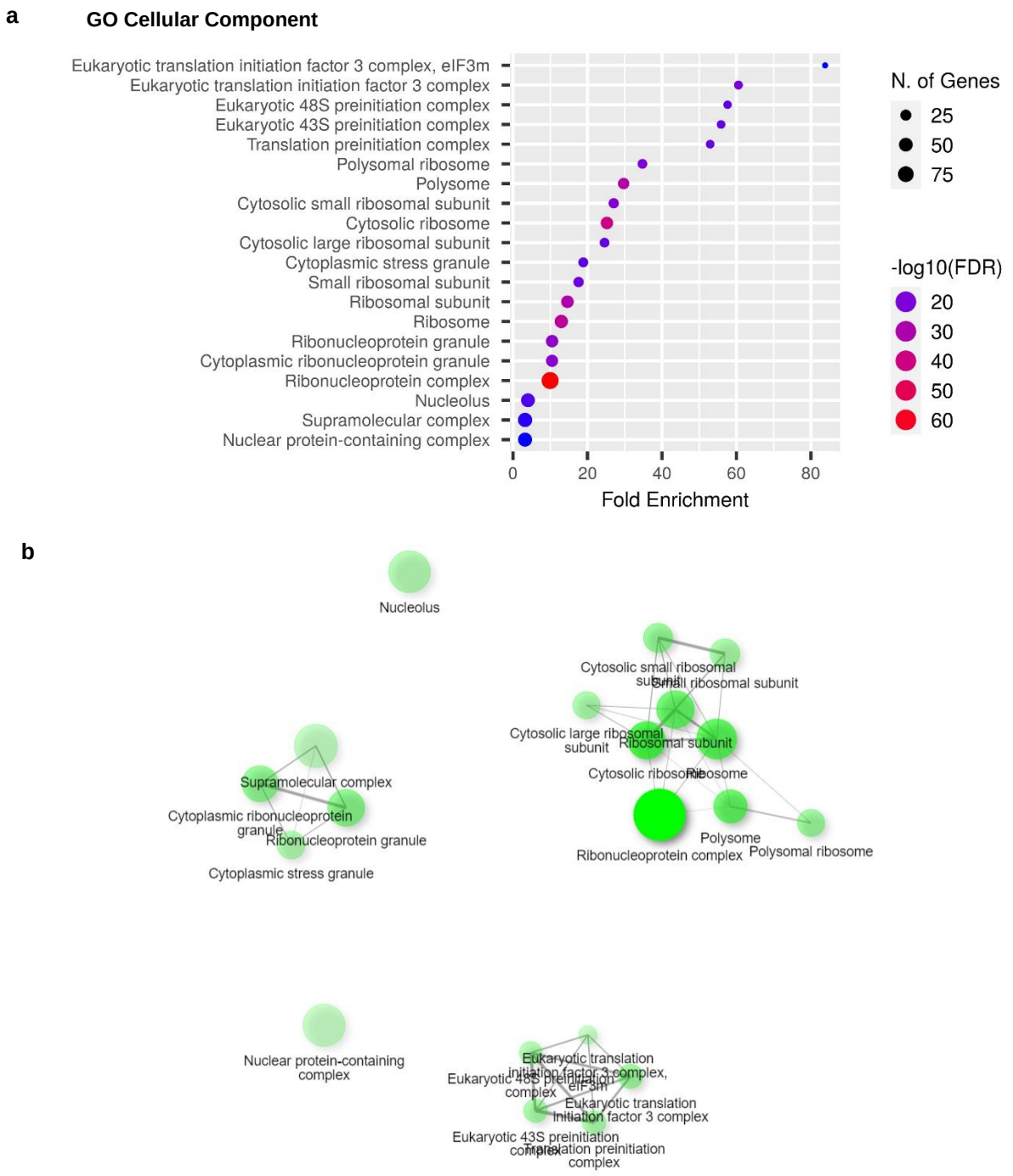

Figure 6. 6. Gene ontology analysis of the potential genes interacting with MFSD8 for the Cellular Component category. (**a**) Fold enrichment of the top 20 enriched GO terms in the Cellular Component (CC) category and (**b**) network analysis using ShinyGO 0.77. (**a**) FDR is the estimated probability that a gene set with a given enrichment score (normalised for gene set size) represents a false positive. It is calculated based on the nominal p-value from the hypergeometric test. Fold enrichment represents the percentage of genes in the list belonging to a pathway, divided by the corresponding percentage in the background. (**b**) The network diagram describes the link between enriched GO terms for the CC category. Two CCs (nodes) are connected if they share 20% (default) or more genes. Darker nodes represent more significantly enriched gene sets and bigger nodes describe larger gene sets. Thicker edges (lines) indicate more overlapped genes.

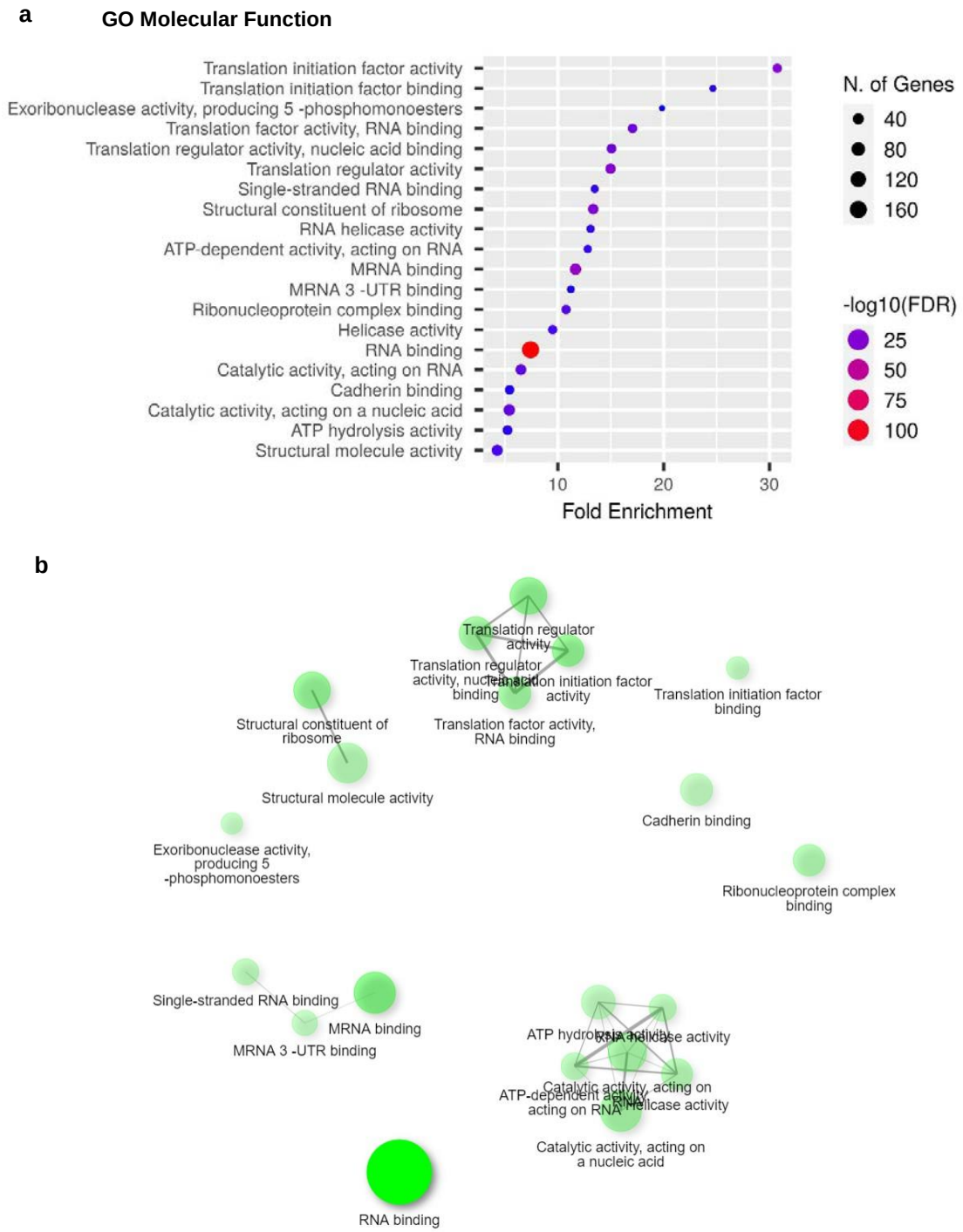

Figure 6. 7. Gene ontology analysis of the potential genes interacting with MFSD8 for the Molecular Function category. (**a**) Fold enrichment of the top 20 enriched GO terms in the Molecular Function (MF) category and (**b**) network analysis using ShinyGO 0.77. (**a**) FDR is the estimated probability that a gene set with a given enrichment score (normalised for gene set size) represents a false positive. It is calculated based on the nominal p-value from the hypergeometric test. Fold enrichment represents the percentage of genes in the list belonging to a pathway, divided by the corresponding percentage in the background. (**b**) The network diagram describes the link between enriched GO terms for the MF category. Two MFs (nodes) are connected if they share 20% (default) or more genes. Darker nodes represent more significantly enriched gene sets and bigger nodes describe larger gene sets. Thicker edges (lines) indicate more overlapped genes.

Following this, a KEGG pathway enrichment analysis was performed with the same gene list input using the ShinyGO software. Among the six most significantly enriched KEGG pathways, the terms related to *ribosome* and *RNA degradation* were the most remarkable, meaning that most of the MFSD8 interactors assessed by the KEGG pathway analysis might be involved in these two pathways (**Figure 6.8**). This correlates with the GO analysis, where *translation initiation* seemed to be the most enriched biological process in which MFSD8 interactors might be involved as translation occurs in the ribosomes. Additionally, consistent with the enriched RNA degradation pathway in KEGG, in the GO analysis, CC-enriched terms were linked to *RNA binding* and *catalytic activity acting on RNA*, with the latter having the highest number of genes as part of RNA binding (**Figure 6.6**). Even though the term *Coronavirus disease* was displayed in the KEGG pathway analysis (with a low FE of 11.6%), suggesting that some genes linked to this pathway might be interacting with MFSD8, the *Coronavirus disease* pathway (node) in the network analysis shows that this term is connected with mRNA surveillance in viral infection (**Figure 6.8b**). Specifically, the genes selected as the potential interactors of MFSD8 are the ribosome subunits 40S and 60S (80S ribosome) (see **Appendix, Supplementary Figure 6.4)**, which are not specific to Coronavirus disease nor viral infection. More precisely, the 40S and 60S genes constitute the 80S ribosome, which is consistent with the most significantly enriched pathway, the *Ribosome* (FE = 20%) (**Figure 6.8a**).

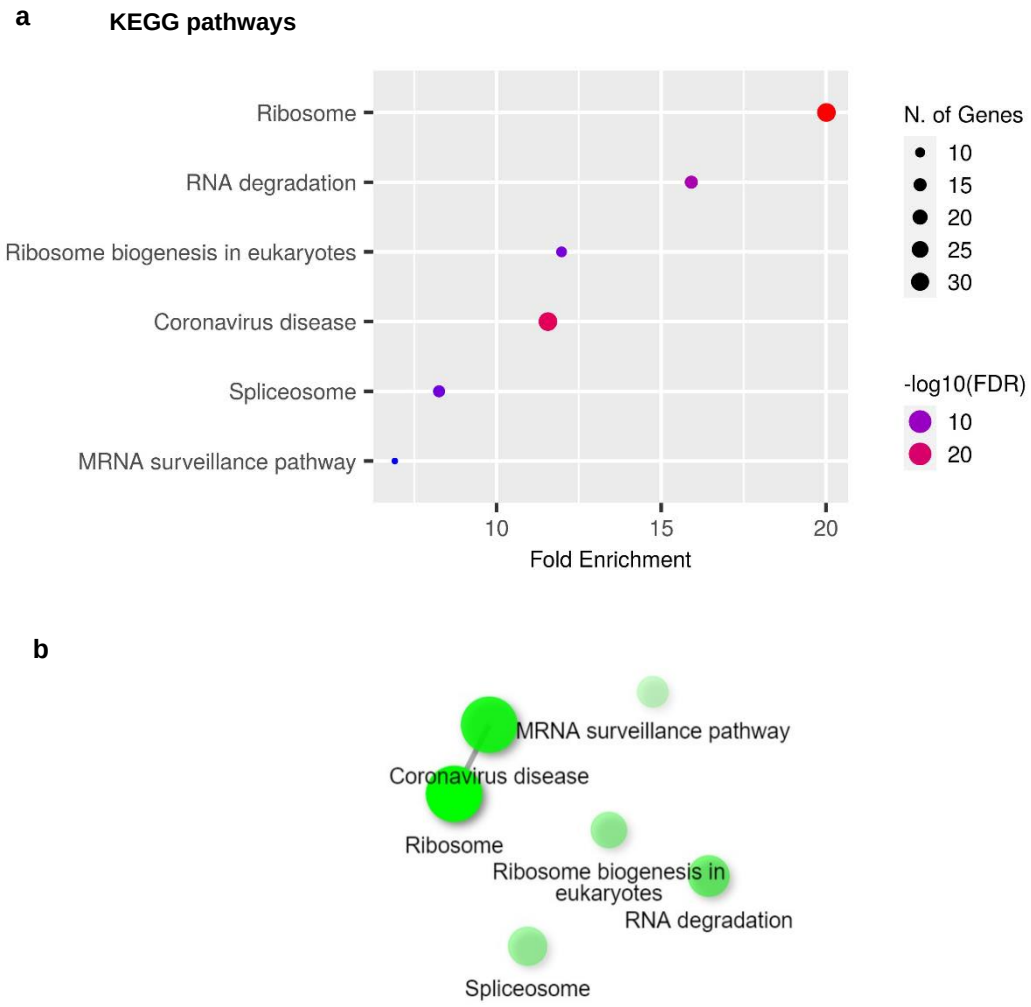

Figure 6. 8. KEGG pathway analysis of the potential genes interacting with MFSD8. (**a**) Fold enrichment of the top enriched KEGG pathways on the list of the genes and (**b**) network analysis using ShinyGO 0.77. (**a**) FDR is the estimated probability that a gene set with a given enrichment score (normalised for gene set size) represents a false positive. It is calculated based on the nominal p-value from the hypergeometric test. Fold enrichment represents the percentage of genes in the list belonging to a pathway, divided by the corresponding percentage in the background. (**b**) The network diagram describes the link between enriched KEGG pathways. Two pathways (nodes) are connected if they share 20% (default) or more genes. Darker nodes represent more significantly enriched gene sets and bigger nodes describe larger gene sets. Thicker edges (lines) indicate more overlapped genes.

6.7 GO Functional Annotation Clustering using DAVID

From the previous analysis, a lot of information was obtained about the possible biological processes, cellular components, and molecular functions that the MFSD8 might be part of. However, the abundance of terms can make it difficult to build a coherent idea about what is precisely occurring inside the cells. Therefore, in this section, the Functional Annotation Clustering tool from the DAVID server (https://david.ncifcrf.gov/tools.jsp) was utilised to get a more cohesive overview of the exact processes in which MFSD8 might be involved. This clustering tool consists of gathering all the terms that have been enriched in each block (BP, CC, and MF) and clustering them according to significance. For this, only the GOTERM_BP_DIRECT, GOTERM_CC_DIRECT, and GOTERM_MF_DIRECT from Gene Ontology were selected. Subsequently, a Functional Annotation Clustering was conducted and, as a result, 17 clusters were obtained with Enrichment scores ranging from 28.55% to 0.48%. In this case, only the three clusters with the highest scores were selected, as their Enrichment scores ranged from 28.55% to 15.69%, with the fourth having an Enrichment score of 4.45%, which is notably lower than the third cluster. The GO categories are presented with the number of genes, the *p*-value and the corrected *p*-value using FDR. This Functional Annotation Cluster was obtained considering 274-277 genes, as they were identified and annotated by the DAVID web server from the list of 290 genes uploaded.

In the first Functional Annotation Cluster, a total of 52 genes were associated with the same seven GO categories. These GO categories were *cytosolic ribosome* (36 genes, $p = 6.62\times10^{-42}$, FDR = 1.0×10^{-39}), *cytoplasmic translation* (36 genes, $p = 1.4\times10^{-41}$, FDR = 1.8×10^{-38}), *translation* (41 genes, $p = 8.9\times10^{-33}$, FDR = 3.9×10^{-30}), *structural constituent of ribosome* (33 genes, $p = 6.8\times10^{-25}$, FDR = 7.4×10^{-23}), *cytosolic small ribosomal subunit* (20 genes, $p = 6.4\times10^{-24}$, FDR = 5.1×10^{-22}), *ribosome* (30 genes, $p = 4.2\times10^{-23}$, FDR = 2.2×10^{-21}), and *cytosolic large ribosomal subunit* (17 genes, $p = 1.0\times10^{-16}$, FDR = 2.5×10^{-15}) (**Figure 6.9**).

In the second Functional Annotation Cluster, a total of 26 genes were attributed to the same three GO categories. These GO categories were *cytosolic small ribosomal subunit* (20 genes, $p = 6.4\times10^{-24}$, FDR = 5.1×10^{-22}), *ribosomal small subunit biogenesis* (20 genes, $p = 2.1\times10^{-16}$, FDR = 3.8×10^{-14}), *and small-subunit processome* (17 genes, $p = 2.8\times10^{-15}$, FDR = 5.9×10^{-14}) (**Figure 6.10**).

In the third Functional Annotation Cluster, a total of 29 genes were associated with nine GO categories. These GO categories were *translational initiation* (27 genes, $p = 4.8\times10^{-34}$, FDR = 3.1×10^{-31}), translation initiation factor activity (23 genes, p = 6.8×10^{-25}, FDR = 7.4×10^{-23}), *eukaryotic 43S preinitiation complex* (13 genes, $p = 1.2\times10^{-18}$, FDR = 3.4×10^{-17}), *formation of cytoplasmic translation*

initiation complex (12 genes, $p = 3.9\times10^{-18}$, FDR = 1.0×10^{-14}), *eukaryotic 48S preinitiation complex* (12 genes, $p = 5.8\times10^{-17}$, FDR = 1.5×10^{-15}), *eukaryotic translation initiation factor 3 complex* (11 genes, $p = 1.1\times10^{-15}$, FDR = 2.6×10^{-14}), *eukaryotic translation initiation factor 3 complex, eIF3m* (6 genes, $p = 8.4\times10^{-9}$, FDR = 1.2×10^{-7}), *viral translational terminating-reinitiation* (5 genes, $p = 1.9\times10^{-7}$, FDR = 1.7×10^{-5}), and *IRES-dependent viral translation initiation* (4 genes, $p = 4.1\times10^{-4}$, FDR = 1.3×10^{-2}) (**Figure 6.11**).

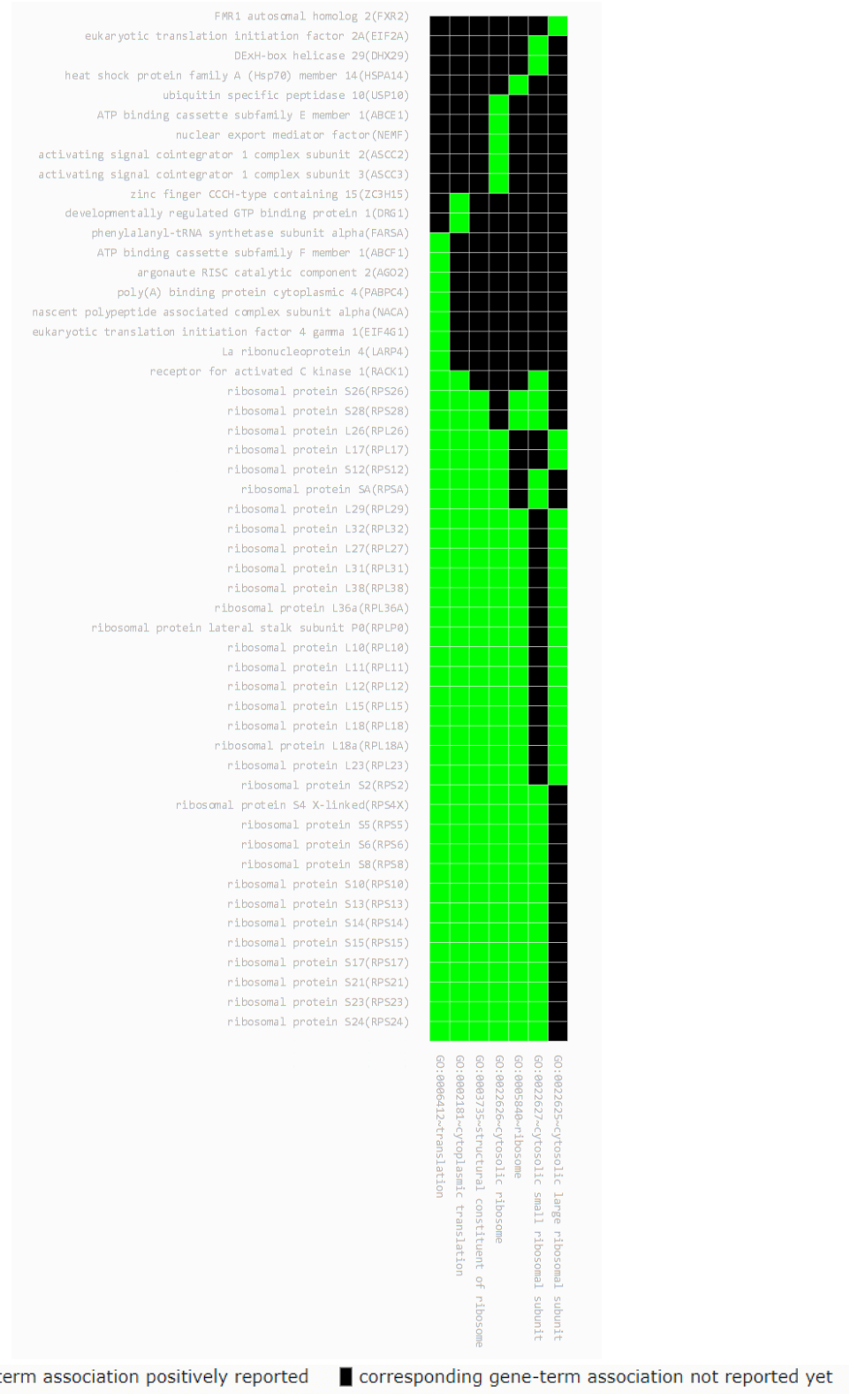

Figure 6. 9. Annotation cluster diagram 1 of the potential MFSD8 interactors. This annotation cluster diagram has an Enrichment score of 28.55% and was obtained using the Functional Annotation Tool from the DAVID web server by selecting the GOTERM_BP_DIRECT, GOTERM_CC_DIRECT, and GO_TERM_MF_DIRECT at Gene Ontology. Each row represents a different gene from the gene list run with the DAVID server, and each column indicates one of the different GO terms enriched for this specific cluster of genes. In this cluster, 52 genes were identified as related to seven GO categories.

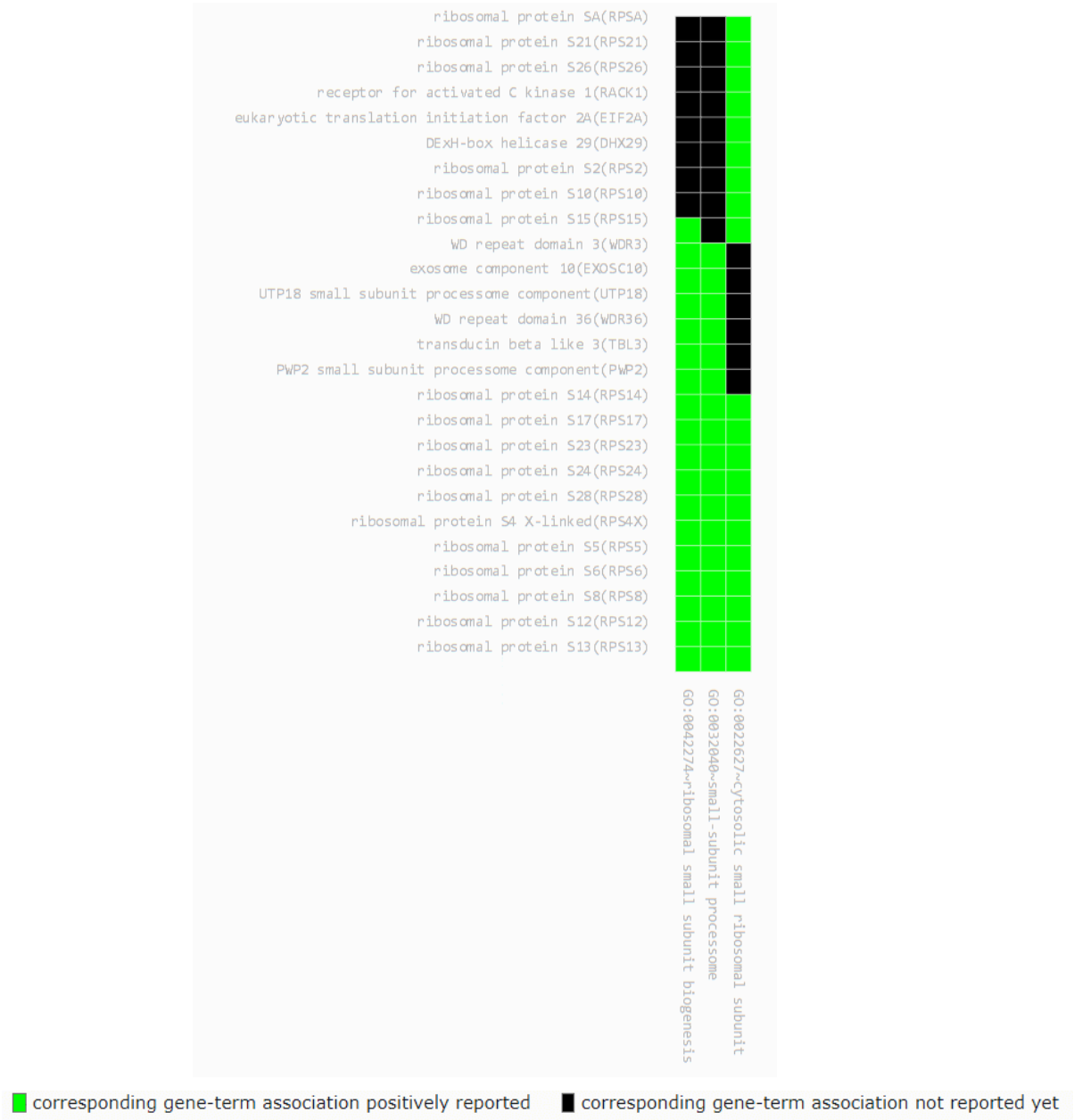

Figure 6. 10. Annotation cluster diagram 2 of the potential MFSD8 interactors. This annotation cluster diagram has an Enrichment score of 17.81% and was obtained using the Functional Annotation Tool from the DAVID web server by selecting the GOTERM_BP_DIRECT, GOTERM_CC_DIRECT, and GO_TERM_MF_DIRECT at Gene Ontology. Each row represents a different gene from the gene list run with the DAVID server, and each column indicates one of the different GO terms enriched for this specific cluster of genes. In this cluster, 26 genes were identified as related to three GO categories.

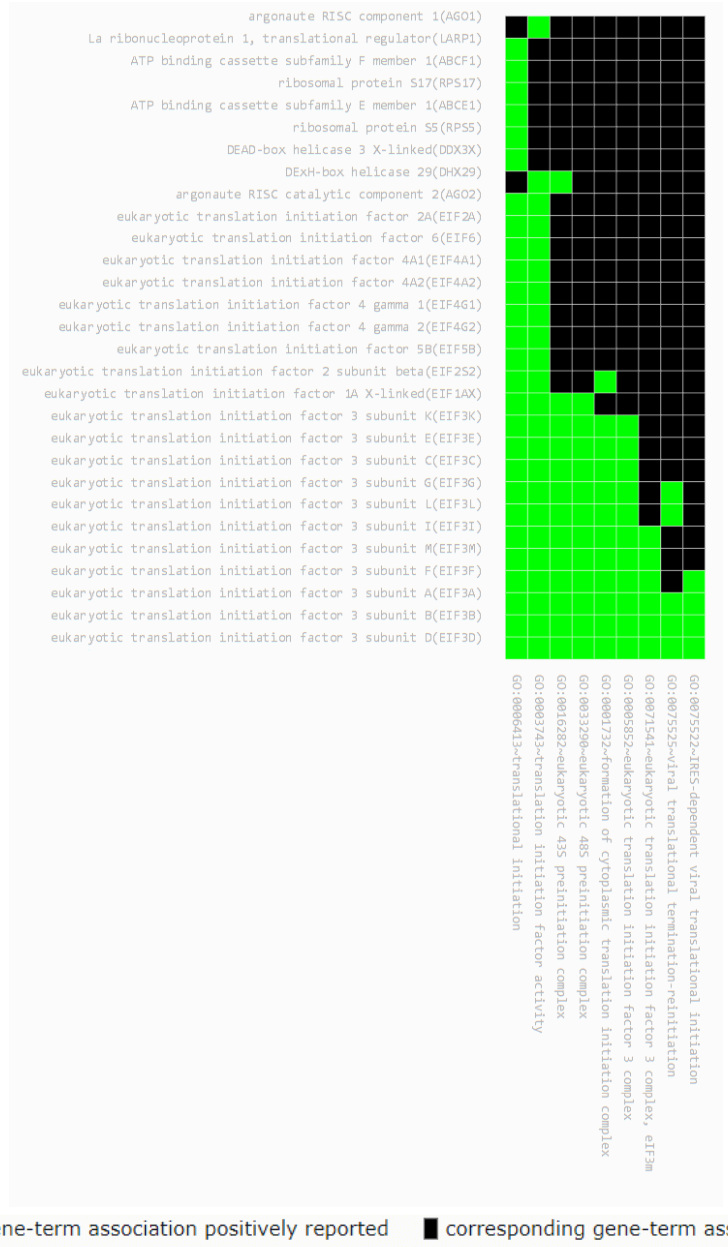

Figure 6. 11. Annotation cluster diagram 3 of the potential MFSD8 interactors. This annotation cluster diagram has an Enrichment score of 15.69% and was obtained using the Functional Annotation Tool from the DAVID web server by selecting the GOTERM_BP_DIRECT, GOTERM_CC_DIRECT, and GO_TERM_MF_DIRECT at Gene Ontology. Each row represents a different gene from the gene list run with the DAVID server, and each column indicates one of the different GO terms enriched for this specific cluster of genes. In this cluster, 29 genes were identified as related to nine GO categories.

Altogether, these results suggest that the most significant clusters of enriched genes (and therefore, with the highest Enrichment Score) as potential MFSD8 interactors, might primarily be associated with cytoplasmic translation, being ribosome constituents and involved in translation initiation. Additionally, other clusters with lower Enrichment Score, as less enriched genes are related to

those GO terms, that were also identified in the Functional Annotation Custer analysis were associated with chromosome segregation, spliceosome, RNA processing/cytoplasmic and nuclear exosome (RNase complex), dendritic spine and presynapse, as well as vesicle-mediated transport, lysosome and autophagy, among others. These findings suggest that MFSD8 might be also involved in the previous step of RNA processing and its nuclear/cytoplasmic export, as well as processes related to autophagy, which include the lysosome, as consistently demonstrated by previous studies, and the dogma of the MFSD8 being part of the lysosomal membrane.

6.8 BIOCARTA pathway enrichment analysis using DAVID

To gain further insights and explore all the potential pathways that can be enriched in our list of 290 genes, another pathway analysis was conducted using the DAVID web server. In this instance, the BIOCARTA pathway analysis was performed, where 42 out of the 280 DAVID IDs (*Homo sapiens* genes annotated on the DAVID web server from our list) were enriched for different potential pathways. In this case, the results indicated that some of these genes were related to four significantly enriched pathways in BIOCARTA, represented with their corresponding level of significance as *p*-value, and the adjusted *p*-value using FDR. Specifically, the most significantly enriched pathway in those 42 genes from the output was *eukaryotic protein translation* (8 genes, $p = 3.7\times10^{-8}$, FDR = 1.8×10^{-6}). Interestingly, the other three enriched pathways in BIOCARTA were the *mTOR signalling pathway* (8 genes, $p = 1.8\times10^{-6}$, FDR= 4.3×10^{-5}), the *internal ribosome entry pathway* (5 genes, $p = 1.2\times10^{-5}$, FDR = 1.9×10^{-4}), and the *regulation of eIF4e and p70 S6 kinase* (5 genes, $p = 1.8\times10^{-3}$, FDR = 3.1×10^{-2}) (**Table 6.1**). From these results, the *eukaryotic protein translation* and the *internal ribosome entry pathway* are consistent with the pathways obtained in the KEGG pathways analysis conducted using ShinyGO and the GO analysis in the DAVID web server. However, two novel pathways were identified utilising the BIOCARTA database in the DAVID server were the *mTOR signalling pathway* and the *regulation of eIF4e and p70 S6 kinase*, opening new avenues to constructing a unifying hypothesis of the MFSD8 interactome, considering that MFSD8 has been reported as a chloride channel in endosomal/lysosomal membranes.

Table 6. 1. Functional annotation chart of the enriched pathways associated with MFSD8 using BIOCARTA in DAVID analysis.

Category	Term (pathway)	Number of genes	Genes	*p*-value	FDR
BIOCARTA	Eukaryotic protein translation	8	EIF4A2, EIF4A1, EIF6, EIF1AX, EIF2S2, EIF3A, EIF4G2, EIF4G1	3.74E-08	1.8E-06
BIOCARTA	mTOR Signaling Pathway	8	EIF4A2, EIF4A1, RPS6, TSC2, TSC1, EIF3A, EIF4G2, EIF4G1	1.79E-06	4.3E-05
BIOCARTA	Internal Ribosome entry pathway	5	EIF4A2, EIF4A1, EIF3A, EIF4G2, EIF4G1	1.16E-05	1.90E-04
BIOCARTA	Regulation of eIF4e and p70 S6 Kinase	5	EIF4A2, EIF4A1, PABPC1, EIF4G2, EIF4G1	0.002586	0.031674
BIOCARTA	Spliceosomal Assembly	3	SNRPD1, SNRPD3, SNRPF	0.046774	0.458382
BIOCARTA	CDK Regulation of DNA Replication	3	MCM4, MCM6, MCM2	0.073823	0.602887

6.9 MFSD8 might be primarily involved in cytoplasmic stress granules, the mTOR signalling pathway, and translation

After conducting the functional annotation analysis using GO, KEGG, and BIOCARTA, the genes from our list participating in the different potential pathways, biological processes, cellular compartments, and molecular functions associated with MFSD8, were represented to obtain a general and more cohesive idea of the exact mechanisms MFSD8 could be involved in (**Figure 6.12**). The primary pathways of the MFSD8 interactome might be the following: cytoplasmic stress granule, ribosome (translation), RNA degradation, ribosome biogenesis, spliceosome, mRNA surveillance pathway, autophagy, eukaryotic protein translation, mTOR signalling pathway, and regulation of eIF4e and P70 S6 kinase. These pathways were identified with different significant levels and fold enrichment as explained in the previous sections of this Chapter. However, some of them seem to be interconnected even though the same significance level was not achieved and

it might be important to consider all of them, even if they exhibited a lower significance level, as it might depend on the cell cycle or cell state at the time of cell harvesting for the co-IP experiment, additionally to the impact of other factors throughout the development of this co-IP and MS-based proteomics.

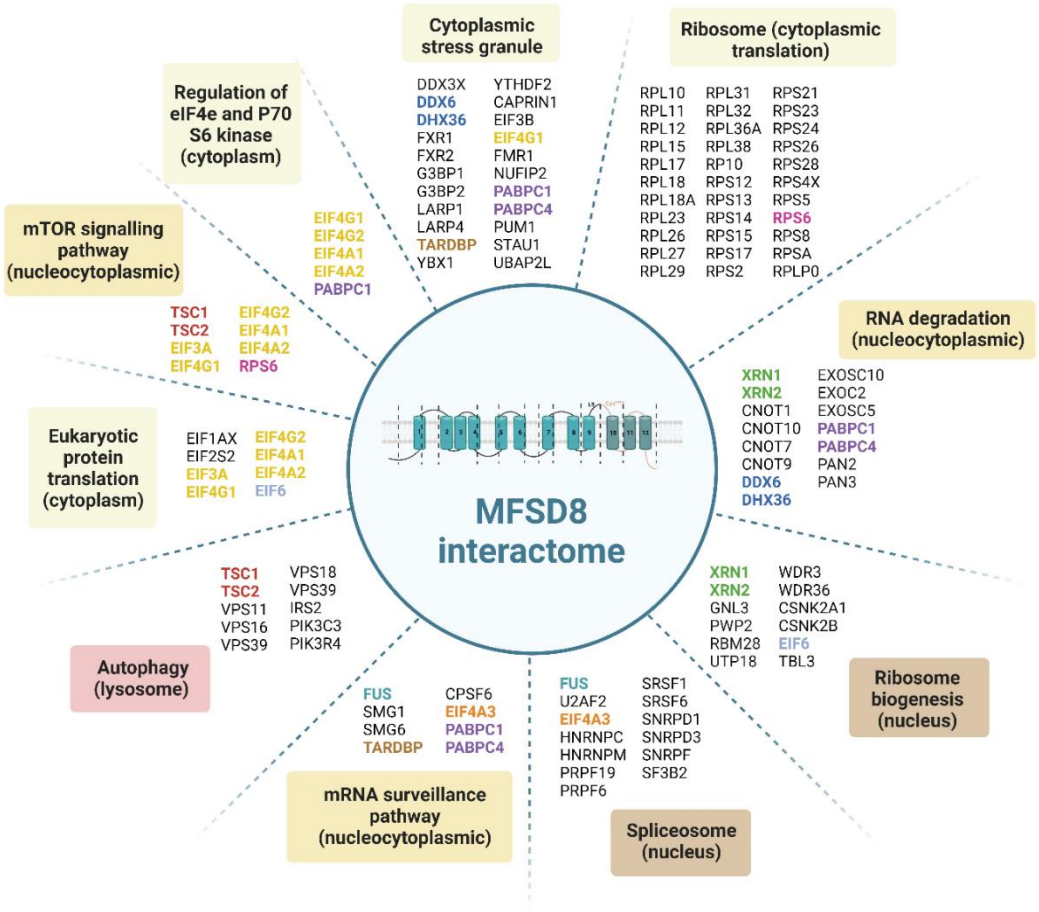

Figure 6. 12. Potential MFSD8 interactome obtained from MS-based proteomics and functional annotation analysis. Representation of the different genes involved in each enriched pathway obtained from the GO analysis, as well as KEGG and BIOCARTA pathway analysis, after MS-based proteomics analysis of the co-IP results (conducted by the Bio-MS facilities from the University of Manchester and raw data processing by Dr Jon Humphries from Manchester Metropolitan University). The genes that were present in different pathways are highlighted with the same colour. This might indicate that pathways sharing the same genes could be linked, which can help elucidate the exact pathways in which the MFSD8 protein may participate.

Interestingly, most of the molecular pathways and biological processes demonstrate a potentially significant involvement of MFSD8 around translation initiation and translation, involving eukaryotic initiation factors (eIFs) and ribosomal proteins (RPs), which occur in the cytoplasm of eukaryotic cells. Additionally, autophagy was also a mechanism present in the pathway analysis of the genes resulting from the co-IP experiment, which is consistent with the current dogma regarding the primary localisation and function of the MFSD8 protein as a chloride channel in the lysosomal membrane (Steenhuis et al., 2010; Yayu Wang et al., 2021). Another notable pathway that was enriched in the BIOCARTA pathway analysis was the mTOR signalling pathway, which is related to lysosomal and translation regulation (Puertollano, 2014; Yang et al., 2022), both in line with the results obtained in this study and the association of MFSD8 with the lysosomes. Furthermore, the regulation of eIF4e and p70 S6 kinase was enriched in BIOCARTA, corroborating its link with the mTOR pathway, as the eIF4e and p70 kinase experience phosphorylation in response to insulin or mitogen (an agent that induces mitosis) stimulation, which is partially hindered by rapamycin. Previous research has shown that the protein mTOR is the specific target that the rapamycin/FKB12 complex uses to remove phosphate groups and deactivate the p70 S6 kinase. Consequently, certain mTOR mutants that are unable to bind to the rapamycin/FKB12 complex can prevent the p70 S6 kinase from being dephosphorylated and deactivated by rapamycin (Hara et al., 1997). Finally, other significantly enriched cellular compartments where MFSD8 might be interacting with are stress granules. These cell components are structures without membranes located in the cytoplasm that consist of ribonucleoprotein (RNP) complexes. Their main role is to enhance cell survival by condensing mRNAs that are stuck in translation, as well as ribosomal elements, translation initiation factors, and RNA-binding proteins (RBPs), as a response to stress stimuli (Anderson and Kedersha, 2008). The phosphorylation of eukaryotic initiation factor 2 alpha (eIF2α) can be induced by cellular stress, and this is commonly believed to be the cause of stress granule assembly. The formation of stress granules can occur regardless of the phosphorylation of eIF2α and is instead initiated by eukaryotic translation initiation factor 4A (eiF4A), which was a protein present in our list of genes also related to mTOR and the regulation of the eIF4e and p70 SA kinase (Low et al., 2005; Mazroui et al., 2006). This demonstrates the part of the potential interconnection among the enriched pathways, which makes the results obtained more precise and coherent. Moreover, as previously reported, some of the main stress granules-associated proteins are Ras-GTPase-activating protein (GAP)-binding proteins (G3BPs) and cytoplasmic activation/proliferation-associated protein-1 (Caprin-1), which were also present in our list of genes and identified as stress granules components.

Altogether, the results of this work provide new insights into the potential MFSD8 interactome, indicating that MFSD8 cytosolic puncta could mostly consist of perinuclear stress granules and are rarely associated with endolysosomal vesicles (ELV). The co-IP MS data also suggest that MFSD8 forms an association with proteins involved in the transport of mRNA from the nucleus, as well as with complexes that have an impact on the initiation or suppression of translation.

Limitations

While this chapter provides novel insights on the potential different roles of MFSD8 within the cell considering the various interactors that may be involved, it is important to understand its limitations. One limitation of the co-IP technique in this study is the use of a capture antibody a detection antibody derived from the same species (rabbit, in this instance). The reason for using capture and detection antibodies from different species in co-IP assays is to prevent interference from the heavy and light chains of the capture antibody during the detection step using immunoblotting. However, during the co-IP optimisation, it was noticed that the band representing MFSD8 may have been masked by the detection of the heavy chain of the antibody, as they both exhibit similar molecular weights in the range of 50-58 kDa. Consequently, a resolution was proposed. This approach utilised an alternative secondary HRP antibody that specifically targeted the light chain. Another limitation is that subsequent experiments are required to validate the findings obtained using MS-based proteomics. These further experiments may involve transfecting SH-SY5Y cells with plasmids containing the sequences for Caprin-1 and G3BP1 proteins (with a GFP tag, for instance). The aim would be to evaluate the extent to which these proteins coexist with MFSD8 by conducting immunofluorescence staining of MFSD8. Additionally, it would be more accurate to conduct co-IP experiments, followed by MS-based proteomics, in both WT NPCs and CLN7 NPCs. This will allow for a comparison of the potential difference in the binding partners of MFSD8 between healthy and cells with disease-causing mutations, similar to the proteomics experiment previously conducted by Dr Aseel Sharaireh (see Chapter 5, **section 5.1**). By doing so, we can gain a deeper understanding of how the pathobiology of vLINCL CLN7 may impact the function of this protein.

Conclusions

Proteomics plays a crucial role in systems biology research as proteins contain abundant information that is highly relevant for describing biological processes. This chapter presents new and valuable information about putative binding partners of MFSD8. The main interactors of MFSD8 identified in this study are Caprin-1 and G3BP1, both of which are components of stress granules. This conclusion was further corroborated by the terms associated with mTOR signalling

and the regulation of p70 S6 Kinase. Caprin-1 is an mRNA-binding protein that functions as a regulator of mRNA transport, translation, and stability. It plays a role in synaptic plasticity in neurons and cell proliferation and migration in various cell types (T. H. Kim et al., 2019; Solomon et al., 2007). Furthermore, G3BP1 is a protein that binds to RNA and plays a role in the formation of stress granules. These granules are clusters that form in the cytoplasm in response to translational stress (Martin et al., 2013). Moreover, the results obtained from the MS (by Dr Jon Humphries) and DAVID analysis utilising GO, suggest that the interactors of MFSD8 may play a role in the transportation of mRNA molecules from the nucleus. Additionally, these interactors could potentially influence the regulation of translation, either by activating or suppressing it. The results obtained in this chapter, along with downstream studies for corroboration, have the potential to provide significant insights into the identification of targets for treatment to improve CLN7 disease.

Chapter 7

Discussion

The variant late-infantile NCL CLN7 is a progressive severe neurodegenerative disease that affects children from 2 to 7 years old, resulting in a life-restricting and fatal disorder. It is caused by biallelic mutations (in both copies of a gene) in the *MFSD8* gene and there is no current available cure or treatment. A thorough comprehension of the molecular biology of MFSD8, along with an understanding of how genetic mutations affect the functionality of this protein, is essential for the advancement of new treatments for CLN7 disease.

7.1 The use of iPSCs: a novel model to study CLN7 disease

The majority of research on CLN7 disease thus far has been carried out in animal models in which *Mfsd8* has been knocked out. Two *Mfsd8* knockout mice models have been published, including one with a deletion of exon 2 using Cre-mediated Floxed exon 2 deletion (*Mfsd8*$^{\Delta ex2}$) (Brandenstein et al., 2016), and another with a targeted deletion of a 3148 nt region from exons 4-6 using CRISPR-Cas9 (*Mfsd8*$^{\Delta ex4\text{-}6}$) (Yayu Wang et al., 2021). In both cases, these deletions lead to the absence of stable Mfsd8 expression. Both mouse models exhibit delayed and partial cerebral neurodegeneration (Jankowiak et al., 2016; Yayu Wang et al., 2021), but neither model completely replicates the severity of CLN7 disease in humans. There is limited evidence of neuroinflammation or cerebral atrophy. The modelling of disease using *Mfsd8* knockout mice implies that the loss of function is the unique mechanism of the disease, even though most CLN7 patients are expected to stable but structurally damaged MFSD8.

Therefore, for the development of this work, it was crucial to establish a relevant model to study the variant late-infantile NCL CLN7. Given the inaccessibility of acquiring neurons to investigate neurological disorders, as well as the limited availability and potential damage of post-mortem tissues derived from patients, it becomes difficult to effectively investigate the disease progression of this disorder. Moreover, acquiring post-mortem control donor samples poses significant

challenges. An additional disadvantage that requires the use of an accessible and reliable model to study CLN7 disease is the rareness of this genetic neurodegenerative disorder, along with other NCLs. These diseases typically result in a short lifespan for patients due to their early onset and rapid advancement, which presents a significant obstacle to the study of CLN7 phenotypes, particularly when attempting to address them through a more individualised approach. Nevertheless, the N-of-one approach, implemented by Kim *et al.* (2019) in a single patient with CLN7, challenged this belief and provided insights into the advancement and potential of employing such technologies for personalised medicine in CLN7 disease, with the opportunity for application in other genetic disorders as well. Although this clinical method was a significant breakthrough in the field of NCLs, there is currently no treatment or cure available for patients suffering from the variant late-infantile NCL CLN7.

Since the discovery of the reprogramming of iPSCs by Tahashi and Kamanaka (2006), these cells have been used in a wide range of studies, starting from the generation of iPSCs *in vitro* as disease models to investigate the pathogenesis and pathobiology of neurodegenerative diseases such as PD (Spathopoulou et al., 2022), through to the purification and injection of human-induced pluripotent stem cell-derived cardiomyocytes (iPS-CM) into the myocardium after myocardial infarction in mice, resulting in an improvement after four weeks (Jiang et al., 2020), or one of the first human trials employing clinical-grade hiPSC-CM patches to treat ischemic cardiomyopathy in humans (Miyagawa et al., 2022), among many other examples.

Considering the abovementioned reasons and the availability and feasibility of reprogramming somatic cells, such as epithelial cells, skin fibroblasts from CLN7 patients and aged-matched controls were previously obtained and reprogrammed by former members of McKay's group, followed by their genomic and pluripotency characterisation. These CLN7 patient-derived iPSCs and age-matched controls were the main cells used in this project to generate neuron-like cells, particularly NPCs, which facilitated the study of the MFSD8 protein. In this case, the generation of iPSCs from human fibroblasts was conducted through nucleofection of episomal vectors by previous members of McKay's group, which consists of non-integrating non-viral vectors. This technique has been created to produce iPSCs that are entirely free of viral contamination and reduce the risk of mutations caused by genomic integration (Belviso et al., 2020).

This study pioneered the use of patient-derived iPSCs to study the vLINCL CLN7 phenotype in differentiated neural cells *in vitro*. Specifically, this work aimed to assess the molecular pathobiology in neural cells produced from iPSCs of patients with two of the most prevalent MFSD8 mutations in the vLINCL CLN7. As described in **Chapter 3**, iPSC lines were derived from fibroblasts

obtained from a male patient with the p.R465W mutation and a female patient with the T294K, both of whom exhibited the usual age of onset and disease progression.

7.1.1 Relevance of NPCs as a model to study CLN7 disease

Instead of generating neurons from CLN7 patient-derived iPSCs, which is also possible, NPCs were generated as a previous stage to neurons. The reason for that was that the generation of neurons requires a longer time (from 2-3 months, in the case of the generation of motor neurons, for example) (Akter et al., 2022) and they are more difficult to maintain and expand in cell culture. Additionally, the purpose of this study was to study the cellular and molecular biology using a closer simulation of what could be occurring in the human body of the patients carrying the p.T294K and p.R465W mutations in homozygosity in CLN7 disease. This approach could provide a better understanding of the underlying molecular mechanism of MFSD8, due to the original endogenous CLN7 mutations in homozygosity, using cells from CLN7 patients. This strategy to study a neurodegenerative disease is consistent with what Schweitzer *et al.* (2020) used for investigating Parkinson's disease with a more clinical practice of the implantation of these cells in a patient, among other examples.

The cell culture of the iPSCs and the generation of NPCs were followed by their characterisation primarily using ICC of different markers for pluripotency and neural progenitor cells. The markers for pluripotency studied in the iPSCs were OCT3/4, SOX2, TRA-1-60, and NANOG, as they were also used by Adewumi *et al.* (2007) to corroborate the pluripotency of the cells they used. Consistently, when the NPCs were generated, they were characterised by ICC, using SOX2, Nestin, Pax6, and BLBP as neural markers. Despite not having conducted RT-qPCR, to corroborate the expression of these genes at the mRNA level, as other studies suggest (Kang et al., 2017; Rehakova et al., 2020), as well as flow cytometry for protein expression, or electrophysiology in the case of neurons generation, immunocytochemistry was the only technique used for characterisation in this case, as shown in other reports (Bell et al., 2019; Gunhanlar et al., 2018; Hu et al., 2010).

During hiPSCs and NPCs cell culture, plates and flasks were coated with Matrigel® Matrix to recapitulate the extracellular matrix (ECM), facilitating cell attachment and providing a growth factor reservoir. The use of Matrigel® Matrix was employed as a replacement of iMEFs once the iPSC colonies were stable and it was used routinely for NPCs culture. This synthetic Matrigel has been demonstrated to be an effective substitute for iMEFs due to its composition of many ECM components, including laminin, collagen IV, heparin sulphate proteoglycans, and nidogen. Even though Matrigel remains extensively utilised in research due to its well-documented efficacy, it is

not suitable to culture clinical-grade cells, as it is obtained from animals and can vary from batch to batch. To grow and maintain clinical-grade iPSCs for cell therapy, other protein- or peptide-based growth factors should be used, such as laminin-511, laminin-521, vitronectin, SynthemaxTM II, and cyclic RGD. However, the purpose of the use of WT and CLN7 patient-derived iPSCs and NPCs in this study was to investigate the molecular biology of MFSD8 associated with two specific mutations, with no clinical or cell therapy involvement. This led the investigation to be less strict in terms of regular genetic verification, as these cells were not required to be clinical grade because there were no clinical approaches involved in this project. If the purpose of these cells were for clinical practice, they would have undergone regular quality control and consistent documentation of biological material, culture, freezing, genetic testing and distribution following the current good manufacturing practices (cGMP), defined by the European Medicines Agency (EMA) in the European Union and by the US Food and Drug Administration (FDA) in the case of the US.

7.1.2 Future potential of the use of iPSCs in the study of neurodegenerative diseases

iPSCs have been employed in vitro to establish 2D cultures. However, these cultures fail to replicate the physiological three-dimensional cellular environment due to the absence of nutritional, waste, and oxygen gradients, as well as interactions between cells and the extracellular matrix (ECM). Therefore, several studies have developed 3D organoids using iPSCs to replicate the natural environment of living organisms (Chang et al., 2020). These organoids reproduce the interactions between cells and the extracellular matrix and demonstrate various cellular processes such as growth, proliferation, migration, protein production, and gene expression (Bott et al., 2010; Chang et al., 2020; Pineda et al., 2013; Zahumenska et al., 2020). The 3D organoids used to investigate neurodegenerative diseases consist of a diverse group of neural cells derived from iPSCs that have been differentiated into motor neurons, astrocytes, and oligodendrocytes (Lancaster et al., 2013; Pamies et al., 2017; Zahumenska et al., 2020). These 3D organoids show great potential as an alternative method for understanding the pathogenesis and progression of neurodegenerative disorders and can be used for the development of novel treatments for neurological disorders (Chang et al., 2020).

As abovementioned, there is compelling evidence that brain organoids represent a highly innovative scientific breakthrough due to the limited availability of generating human brain tissue and the complexity of neurological diseases. They have become an invaluable method for modelling characteristics of human brain development that are not accurately represented in animal models. However, the extensive usefulness of this approach can be reduced by several limitations that still need to be resolved. These limitations include the lack of accurate cell types,

limited growth, abnormal physiology, and the absence of optimal organisation, which may restrict their applicability for certain purposes (Andrews and Kriegstein, 2022), even though the overcoming of these limitations is constantly advancing (Adlakha, 2023).

7.2 Autophagy-lysosomal pathway as a potential therapeutic target in CLN7 disease

In **Chapter 4**, we demonstrated that the use of tamoxifen ameliorated the aberrant lysosomal phenotype observed in CLN7 NPCs produced by the accumulation of the Gb3 enzyme. In Chapter 4, the presence of the Gb3 and SCMAS accumulation in CLN7 iPSC-derived NPCs was observed, which is in line with what has been observed in $Cln7^{\Delta ex2}$ cortical neurons grown *in vitro*, demonstrating homologies and corroborating the conservation of MFSD8 across species (Connolly et al., 2019).

The pathophysiology underlying why CLN7 is predominantly a neurodegenerative disease remains unclear. However, the variant late-infantile CLN7 is commonly categorised as a lysosomal storage disease and the current dogma is that MFSD8 localises to the lysosomal membrane, where it may function as a chloride channel (Yayu Wang et al., 2021), and its loss of function leads to impaired lysosomal activity, which in turn causes neurodegeneration (Sharifi et al., 2010). However, the exact mechanism by which this occurs is not yet understood. The loss of function of Mfsd8 has been demonstrated to disrupt the normal activity of lysosomal enzymes, specifically Cln5 and Cln10 (Cathepsin D, CtsD) (Huber et al., 2020; von Kleist et al., 2019). This indicates a possible connection between different types of NCLs, which is in line with the STRING database analysis that was conducted in Chapter 6, showing the predicted MFSD8 interactors. Recent studies have revealed a broader range of intracellular localisation, encompassing late endosomes and autophagic vesicles (Yayu Wang et al., 2021).

In the experiments conducted under normal cell culture conditions, we observed that MFSD8 cytosolic puncta could interact with early endosomes (RAB5), autophagic (LC3, p62), and lysosomal (LAMP2) compartments in WT NPCs (see **Chapter 4**, **section 4.6**). However, we did not detect co-localisation of MFSD8 with endosomal, autophagic, or lysosomal markers in CLN7-derived NPCs, suggesting a potential alteration in the phenotype of CLN7 patients. The disease phenotype observed in CLN7 patient-derived NPCs was replicated in WT NPCs when lysosomal acidification was inhibited by suppressing vATPase activity with Baf A1 treatment. Baf A1 prevents the fusion between autophagosomes and lysosomes, possibly through a mechanism that is not solely dependent on vATPase but it is also influenced by calcium (Ca^{2+}), leading to a diversion in the autophagic process. Our findings suggest that the autophagic phenotype observed

in CLN7 disease is similar to the effects of Baf A1 treatment in NPCs. Accordingly, the pattern of increased ATG9A, Beclin-1, LC3B, and p62 caused by Baf A1 in WT NPCs aligns with the observations made by Wang *et al.* (2021) regarding the loss of function of MFSD8 protein. Specifically, Wang *et al.* (2021) described MFSD8 as a chloride channel located on endo-lysosomal vesicles (ELV) that controls the fusion of autophagosomes and lysosomes by regulating the release of Ca^{2+} from lysosomes through a Ca^{2+}/calmodulin-dependent mechanism (Wang et al., 2021). This funding could correlate with the role of Ca^{2+}/calmodulin-dependent protein kinase II (CAMK2) in promoting autophagic flux in response to short-term starvation as described by Zhan *et al.* (2022). However, further investigation into autophagic mechanisms in CLN7 disease, incorporating a larger number of replicates, is necessary to validate these preliminary observations.

The results obtained in **Chapter 4**, in collaboration with Prof Juan P Bolaños, regarding mitochondria condensation in the perinuclear region of CLN7 patient-derived NPCs, suggest a potential disruption in autophagy. However, the precise mechanism by which mitochondrial function becomes deregulated, resulting in aberrantly condensed mitochondria in the perinuclear region of NPCs, remains unclear.

7.3 Understanding the MFSD8 biology

In this study, we generated control (WT) and CLN7 patient-derived NPCs employing a pre-validated neural differentiation protocol from hiPSCs (FitzPatrick et al., 2018). The purpose of this thesis was to investigate the potential role of the MFSD8 gene within the nucleus of the cells and how MFSD8 mutations could contribute to CLN7 disease pathobiology. This work followed a preliminary transcriptomics study conducted by Dr Aseel Sharaireh (a former member of McKay's group), which was performed to compare the differences in the downregulated and upregulated genes in control and CLN7 patient-derived NPCs, as described in **Chapter 5** (see **section 5.1**). The unbiased iTRAQ proteomics analysis of NPCs from two unrelated individuals with CLN7 disease, each carrying a distinct missense mutation (p.T294K and p.R465W), compared to two unrelated age-matched controls, revealed strong evidence of a nuclear dysfunction specific to the vLINCL CLN7. Out of the 559 proteins that exhibited a decrease of more than 2-fold in CLN7 NPCs compared to WT NPCs, 442 of them, which accounts for 72%, were shown to have a nuclear role. This includes functions such as mitosis, DNA repair, RNA transcription, RNA processing, RNA splicing, and RNA export. The nuclear defect exhibited similar characteristics in terms of proteins that were deregulated, and the corresponding key GO terms, regardless of whether Baf A1 treatment was administered. This suggests that the defect is not worsened by Baf A1 and is therefore likely unrelated to autophagic diversion. Regarding downregulated proteins in

CLN7 NPCs, the most prevalent GO term was *mRNA splicing*. The results of these experiments revealed intriguing insights that lead to hypothesise that the MFSD8 protein is not only present in the lysosomes, as previously described (Sharifi et al., 2010; Steenhuis et al., 2010; Yayu Wang et al., 2021), but it could also localise to the nucleus, playing additional unknown roles. Moreover, previous studies have shown that mutations in *MFSD8* not only cause the variant late-infantile CLN7, but can also lead to other adult neurodegenerative diseases, such as ALS, FTLD, maculopathies, and retinopathies (Nagy et al., 2022; Ogonowski et al., 2023; Roosing et al., 2015). The *MFSD8* mutations that cause other neurodegenerative diseases consist of heterozygous mutations, opposite to what happens in CLN7 disease, where the majority of the mutations occur in a homozygous manner. Therefore, the study of *MFSD8* is of great relevance, especially in the NCL field, but also in adult dementias due to its incidence in other neurodegenerative disorders as mentioned above. Consequently, the discovery of potential therapeutic strategies targeting this gene or CLN7 disease, could also be translated in the mitigation or treatment for ALS and FTLD, as well as maculopathies and retinopathies.

Current understanding of MFSD8 biology has primarily been acquired from studying disease models in mice, *Drosophila melanogaster* (fly) (Connolly et al., 2019), *Dictyostelium discoideum* (amoeba) (Huber, 2016), and a Japanese macaque (McBride et al., 2018b). Additionally, the Chihuahua dog has been proposed as a potential animal model to study CLN7 disease after the identification of mutations in some NCL genes, including *MFSD8* (Faller et al., 2016; Guo et al., 2015; Katz et al., 2017). Our understanding of MFSD8 biology has also come from using ectopic gene expression of CLN7 cDNA in human and animal cell lines not similar to neurons (Sharifi et al., 2010; Steenhuis et al., 2012).

Mfsd8 knockout mice only replicate protein loss-of-function (LOF) (Brandenstein et al., 2016; Danyukova et al., 2018), while most of the *MFSD8* disease-causing mutations are missense or intronic, which are unlikely to hinder protein production or disrupt transport across the ER and Golgi apparatus. This is reflected in the protein stability assays performed in this study, as well as the predicted protein structures obtained using AlphaFold by Prof Sam Hay (University of Manchester). Our data suggest that MFSD8 carrying the p.T294K and p.R465W mutations preserved the stability after limited proteolysis and protein synthesis inhibition, compared to WT MFSD8.

7.3.1 Potential nuclear function and localisation of MFSD8

Siintola et al. reported the presence of transcript variations for both *CLN3* and *CLN7/MFSD8*. They specifically detailed a transcript that lacks exons 7 and 8. According to other studies, the

transmembrane loop 9 (L9) of MFSD8 can be cleaved by cysteine protease, however, the specific cleavage site has not yet been identified. We detected bands on the Western blot of NPC lysates that corresponded to the expected sizes of full-length MFSD8 (57 kDa), MFSD8$^{\Delta ex7/8}$ splice isoform (50 kDa), as well as the L9 protease cleaved 18 N-terminal product (44 kDa), and the MFSD8$^{\Delta ex7/8}$ splice isoform protease cleaved (37 kDa). The MFSD8$^{\Delta ex7/8}$ isoforms (50 and 37 kDa) were found in the nucleus, suggesting that they may play a role in nuclear processes. A defined nucleus localisation signal is not known to be present in MFSD8, but the nuclear fractionation experiment includes the membranous nuclear lamina (as shown by Lamin B1) and, based on the AlphaFold predicted structural models, it may be inferred that MFSD8$^{\Delta ex7/8}$ maintains a transmembrane protein structure.

One potentially interesting finding from this research was the observation of part of MFSD8 in the nucleus, detected through immunocytochemistry and immunoblotting of NPCs (**sections 4.5 and 5.4**). Our results suggested no significant differences in the nuclear expression of MFSD8 in CLN7-mutated NPCs compared to WT NPCs, though further investigation is needed to corroborate this. Interestingly, these observations appear to align with those of Geier *et al.* (2019), who also reported also the presence of MFSD8 in the nuclei of neurons in the middle frontal gyrus, as well as in cultured dermal fibroblasts from patients with *MFSD8* missense mutations associated with FTLD (Geier et al., 2019). However, it is important to not that Sharifi *et al.* (2010) previously detected nuclear MFSD8 but described it as artefactual, highlighting the need for further research to explore the potential presence and role of nuclear MFSD8.

7.4 Uncovering the MFSD8 interactome

Cells are highly dynamic structures, where organelles are interconnected by the process of vesicular transport and membrane contact sites, CLN3 has recently been identified as playing a role in the transportation of vesicles from the Golgi apparatus to the lysosome. The communication between the ELV network and the nucleus is effectively facilitated by the mTOR/TFEB network. To establish a connection between ELV and nuclear NCL characteristics, we conducted an MFSD8 co-immunoprecipitation (co-IP) experiment in SH-SY5Y cells to evaluate potential MFSD8 binding partners.

However, in the list of genes obtained from the raw data and downstream analysis comparing the co-IP samples with the anti-MFSD8 antibody to the control samples with IgGs, MFSD8 was not detected. Considering that the co-IP experiment was performed with a total of four replicates (n = 4), and in any of the raw data output the MFSD8 gene seemed to be detected, we assumed that this could be due to the unrecognition of the MFSD8 peptides by the databases used to obtain the

data from mass spectrometry. Additional reasons could have produced this, including different steps in the process of mass spectrometry, as the proteins are digested into small peptides, which could have generated troubles in the detection of MFSD8, as it is not the most commonly studied protein in the literature. Therefore, we decided to continue the analysis of the data, acknowledging these limitations for further conclusions.

We found MFSD8 interactors that are linked to the regulation of mTOR signalling and are located in the nucleus. Intriguingly, most of the potential MFSD8 interactors are related to the control of RNA translation at the stress granule. A stress granule is an intracellular structure located in the cytoplasm that lacks a membrane and consists of mRNAs and RNA-binding proteins. Its main function is to control the transport and translation of mRNA at the ribosome. Stress granules have recently been linked to Charcot-Marie-Tooth type 2 neuropathies (Cui et al., 2023; Zeng et al., 2023) and to CLN3 biology (Relton et al., 2023). In a similar manner to our investigation, Relton *et al.* (2023) demonstrated through co-immunoprecipitation that CLN3 also interacts with two crucial stress granule proteins G3BP1 and Caprin 1. In addition, Liao *et al.* (2019) have recently elucidated a new method of RNA transportation in neurons. They found that ANXA11 serves as a molecular tether, enabling the binding of RNA granules to lysosomes. This facilitates axonal transport and localised protein synthesis in specific regions. This research indicates that CLN7 and CLN3, in addition to their ELV function, are involved in stress granule function. However, the specific mechanism of their involvement remains unknown.

Chronic and aberrant stress granules that contain the G3BP protein are frequently observed in several neurodegenerative diseases characterised by the accumulation of proteins, including ALS, FTD, AD, PD, and HD (Sanchez et al., 2021; Shukla and Parker, 2016; Vanderweyde et al., 2016; Wolozin and Ivanov, 2019). Accumulating evidence suggests that abnormal stress granules play a role in the development of neurodegenerative disorders (Sanchez et al., 2021; Shukla and Parker, 2016; Vanderweyde et al., 2016; Wolozin and Ivanov, 2019). In ALS, the presence of disease-causing mutations can lead to the accumulation of these proteins within stress granules. Two such proteins, TDP-43 and FUS, have also been identified as potential interactors with MFSD8 in this study. At the genetic level, there is significant overlap between FTD and ALS (Gao et al., 2017), with also some shared disease-causing mutations in the MFSD8 gene in some cases. Additionally, ALS and FTD are regarded as two extremes of a spectrum disorder, sharing similar changes in essential biological processes, including stress granule assembly and disassembly (Gao et al., 2017). Therefore, considering that ALS and FTD also share disease-causing mutations in *MFSD8* in some cases, the common alterations occurring in these adult neurodegenerative disorders in stress granule dynamics may have a link with CLN7, which would need further investigation.

7.4.1 Potential novel hypothesis on the mechanism of MFSD8

Altogether, our data show strong evidence of the potential multifunctionality of MFSD8. This protein is known to act as a chloride channel on the outer surface of ELV membranes (Wang et al., 2021), and we have also discovered a novel nuclear function that was not previously reported. It is quite probable that this nuclear function relates to the transportation of RNA from the nucleus to the cytoplasm and its link with the regulatory stress granule. Essentially, this would lead to the integration of lysosomal and nuclear stress responses that go beyond or are connected to the mTOR/TFEB pathway. Our suggested new hypothesis is that MFSD8 is present in at least two protein isoforms: the full-length MFSD8 (57 kDa) and the MFSD8$^{\Delta ex7/8}$ isoform formed through alternative splicing (50 kDa). Some of the MFSD8 isoforms can undergo post-translational modifications, such as glycosylation and phosphorylation (as demonstrated in **Chapter 5, section 5.5**), as well as protease cleavage, which may generate further functional variants. Furthermore, the increasing similarities between the biology of *CLN7/MFSD8* and *CLN3* (Relton et al., 2023) may improve our understanding of how mutations in these two genes contribute to the pathogenesis of Batten disease. However, additional research is necessary, particularly focused on the interactions of MFSD8 protein and its structural characteristics, to further investigate and validate this hypothesis.

Future work

Acquiring a more detailed understanding of MFSD8 biology is crucial to developing novel therapies for CLN7 disease. In this work, we have shown some *in vitro* evidence of the intricacy and potential innovative mechanisms and signalling pathways that could be further assessed to develop novel therapies to treat CLN7 disease. However, it remains clear that there are many key questions still to be answered and the work conducted needs further corroboration with a higher number of replicates and subsequent experiments.

First, whilst these data demonstrate the possible existence of different MFSD8 variants due to mRNA splicing, which produces alternative transcripts with functional significance, it cannot be replicated by using cDNA constructs in gene therapy. It is crucial to note that the only advanced therapy that has demonstrated clinical effectiveness to date in treating CLN7 disease is Milasen, an N-of-1 therapy. Milasen is an antisense oligonucleotide specifically created to reverse an abnormal and distinct splicing event in the *MFSD8* mRNA of one specific patient (J. Kim et al., 2019).

We have not yet determined whether the CLN7 disease phenotype is caused by a decrease in the nuclear MFSD8$^{\Delta ex7/8}$ 50 kDa variant or an increase in the levels of its 37 kDa cleavage product.

Nevertheless, our results suggest that the ectopic expression of the full-length *MFSD8* cDNA will not completely ameliorate the vLINCL CLN7. Therefore, additional studies are required to fully recapitulate the cellular and molecular mechanisms of action of MFSD8 and its potential variants, to gain a deeper and fundamental understanding to generate an effective therapy to treat CLN7 patients. This further research and treatment development could help benefit patients not only suffering from the vLINCL CLN7 but also from other associated neurodegenerative diseases who carry the same disease-causing mutations as CLN7 patients. One such possible way to identify the MFSD8 isoforms, including the splicing variants, is to conduct long-read RNA sequencing using RNA or cDNA from WT and CLN7 patient-derived NPCs, with the addition of Baf A1 and a vehicle as a control. By conducting these experiments, the differences among the levels of *MFSD8* transcripts could be determined for each condition and *MFSD8* mutation, which would contribute to a better understanding of the underlying pathogenesis and pathobiology of CLN7 disease. Additionally, these potential *MFSD8* variants could be identified in control cells, followed by their corroboration in downstream experiments. These experiments would consist of the construction and transfection of the equivalent transcripts into NPCs and further assess how their overexpression could impact the different lysosomal and autophagy phenotypes that have been presented in this work, as well as to evaluate cellular apoptosis to elucidate whether these transcripts could be considered as therapeutic targets.

With strong evidence suggesting that calcium (Ca^{2+}) signalling is impaired in neurodegenerative diseases and considering its requirement in excitable cells like neuronal cells, it would be of great interest to study its potential defect in CLN7 disease (Pchitskaya et al., 2018). For this, calcium signalling could be assessed in WT and CLN7 NPCs carrying the p.T294K and p.R465W mutations to observe whether in the most severe disease-causing mutation (p.R465W) calcium signalling is presented as more defective. These findings could lead to the discovery of novel therapeutic strategies to ameliorate CLN7 disease by targeting Ca^{2+} entry pathways.

Furthermore, considering the MS-based proteomics data obtained in this project and accumulating evidence suggesting that defective stress granules are involved in the development of neurodegenerative disorders (Sanchez et al., 2021; Shukla and Parker, 2016; Vanderweyde et al., 2016; Wolozin and Ivanov, 2019), it could be of use to investigate this further. Therefore, additional experiments starting from the analysis of stress granule expression in WT and CLN7 NPCs could determine whether there are differences in distinct CLN7 genotypes that can be associated with stress granule dynamics. Additionally, co-localisation experiments of MFSD8 and G3BP1, G3BP2, or Caprin-1 proteins can lead to more robust results corroborating our findings. Experiments focused on stress granules can not only open new avenues of CLN7 research but

also shed light on the discovery of novel therapeutic strategies to ameliorate CLN7 disease and other adult neurodegenerative diseases.

Given that motor dysfunction is a cardinal manifestation of CLN7 disease, characterised by progressive ataxia (difficulty in coordinating movements), myoclonus (muscle twitches), and deteriorating motor skills (Simonati and Williams, 2022), the development of a CLN7 disease model utilizing differentiated motor neurons could be of significant consideration (Akter et al., 2022). This approach would complement the use of NPCs to study this disease. Additionally, the implementation of advanced functional assays, such as multielectrode array (MEA) recordings and quantitative neuromorphological analyses, could elucidate potential electrophysiological and morphological differences between WT and CLN7 patient-derived cellular phenotypes (Halliwell et al., 2021; Kapucu et al., 2022; Mossink et al., 2021). A crucial consideration is the potential to generate iPSC isogenic controls for further differentiation. This could be achieved through the use of CRISPR-Cas9 or other gene-editing technologies, enabling a clear comparison between healthy cells and those harbouring disease-causing mutations. This will ensure that any observed phenotypic differences can be attributed directly to the mutation rather than other genetic variations. Overall, these approaches may provide additional valuable insights into the pathophysiological mechanism underlying the motor deficits observed in CLN7 disease and potentially identify novel therapeutic targets.

General conclusion

In conclusion, this thesis has examined the molecular biology of MFSD8 associated with the most common disease-causing mutations (p.T294K and p.R465W). This has been achieved through the use of NPCs derived from iPSCs as a novel *in vitro* model to study the vLINCL CLN7 that can closely recapitulate the phenotype of neuronal cells in CLN7 disease. Significantly, these data demonstrate the inherent differences between CLN7 and healthy NPCs in MFSD8 expression and cellular localisation. Furthermore, these data suggest an autophagic-lysosomal deficiency, as well as mitochondria dysfunction, consistent with previous studies, potentially leading to the dysregulation of neuronal cells in CLN7 disease, causing pathological phenotypes and leading to the progression of this devastating disorder. Finally, through MS-based proteomics, this thesis opens new directions in the study of the CLN7 disease by focusing on potential novel MFSD8 interactors, which could lead to the discovery of more effective therapeutic modalities that prevent the failure of the development of CLN7 disease treatment.

Appendix

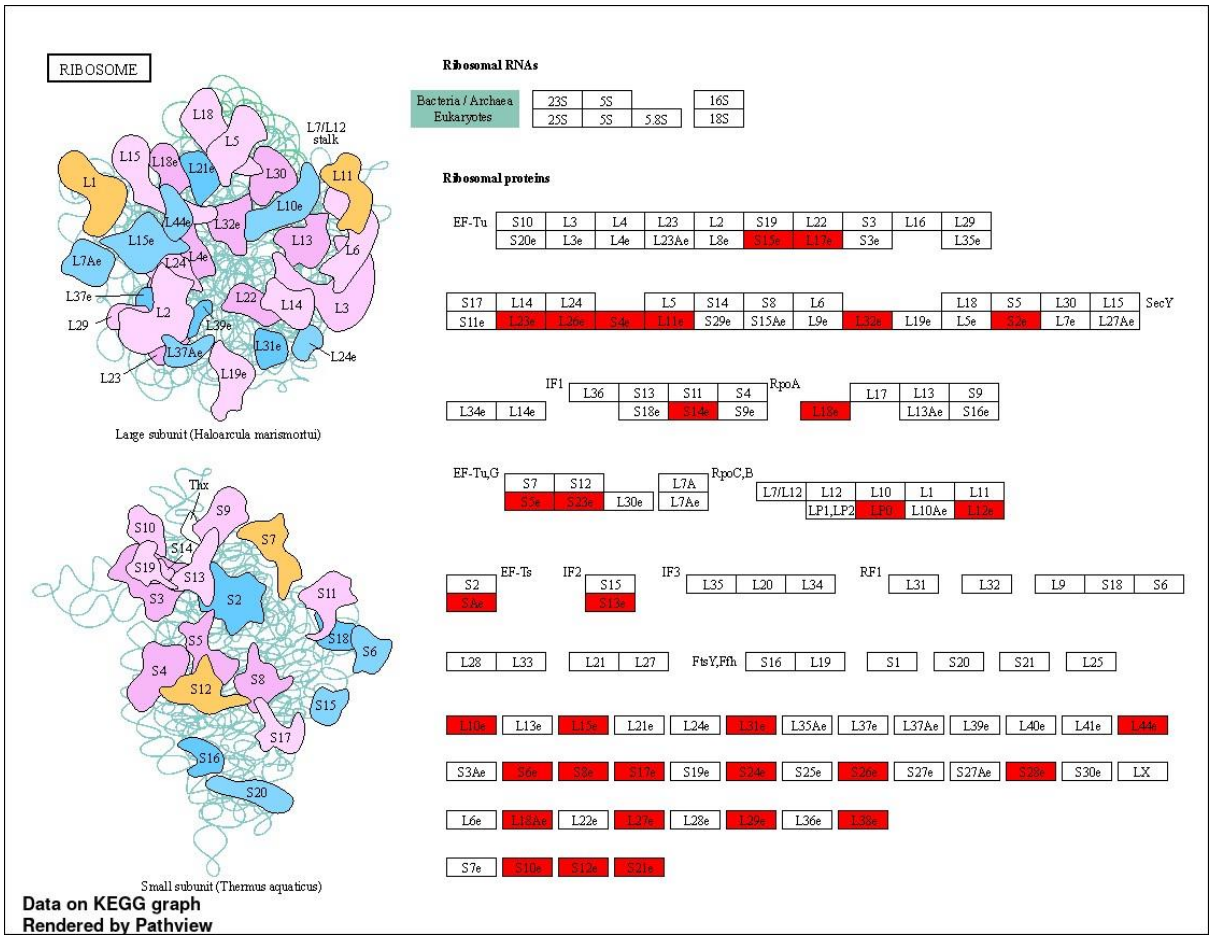

Supplementary Figure 6. 1. Ribosomal proteins from KEGG pathway analysis. Schematic representation of the proteins constituting the ribosomes obtained from the KEGG pathway analysis of the list of the potential genes interacting with MFSD8. The genes highlighted in red represent the identified genes from the co-IP and MS-based proteomics performed on SH-SY5Y cells to study the potential MFSD8 interactors.

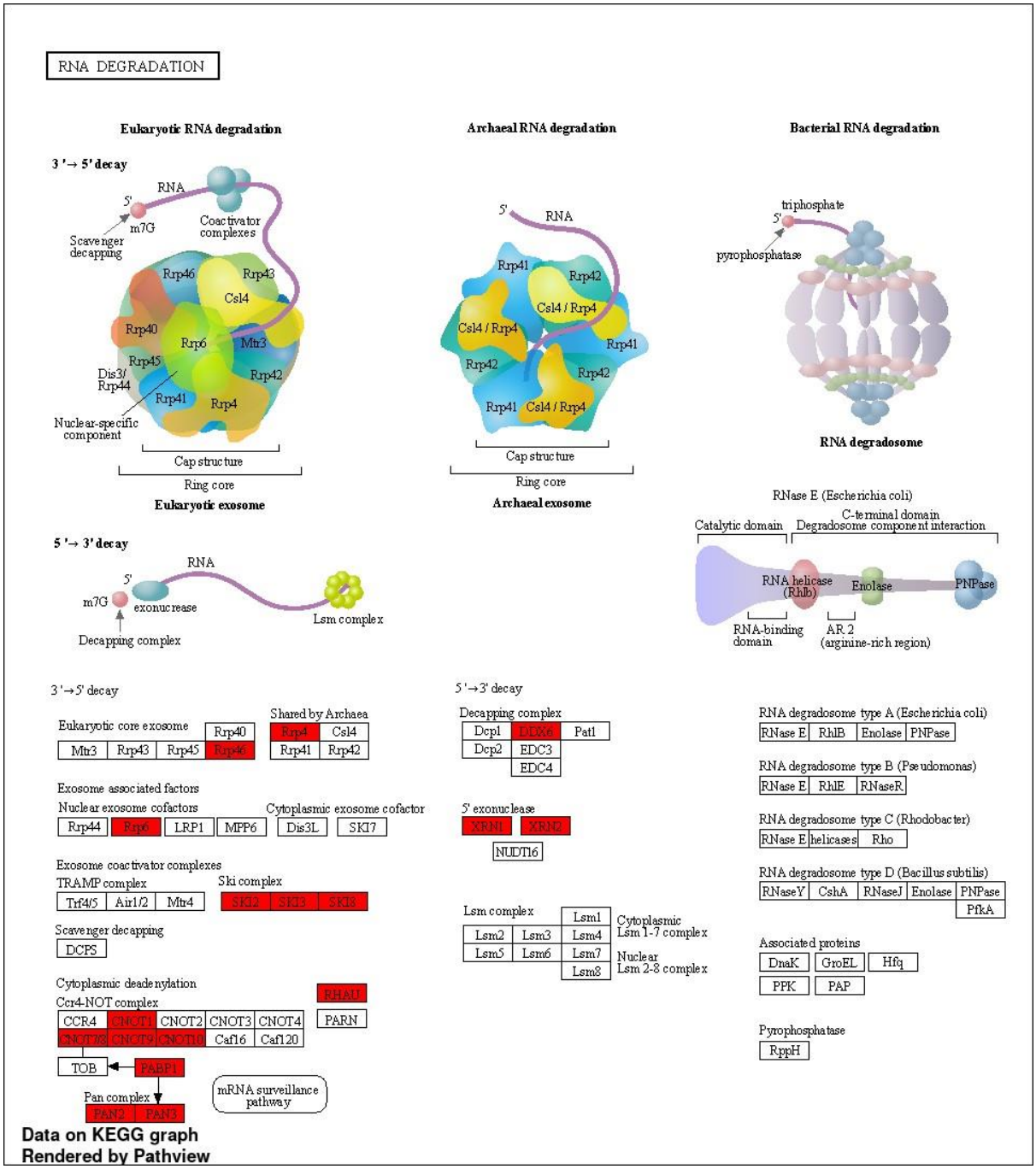

Supplementary Figure 6. 2. Proteins involved in RNA degradation from KEGG pathway analysis. Schematic representation of the proteins involved in RNA degradation obtained from the KEGG pathway analysis of the list of the potential genes interacting with MFSD8. The genes highlighted in red represent the identified genes from the co-IP and MS-based proteomics performed on SH-SY5Y cells to study the potential MFSD8 interactors.

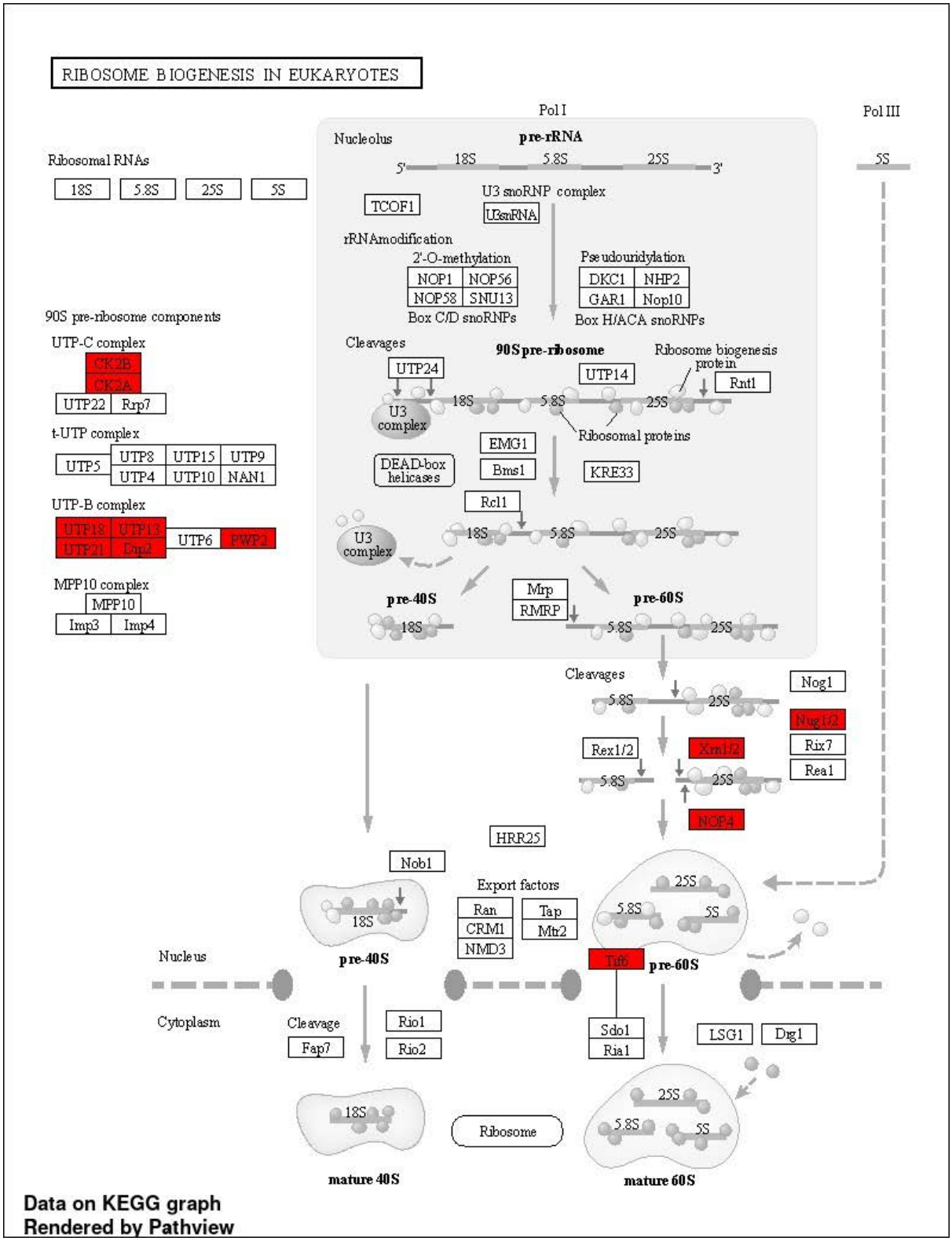

Supplementary Figure 6. 3. Proteins involved in ribosome biogenesis in eukaryotes from KEGG pathway analysis. Schematic representation of the proteins that play a role in ribosome biogenesis obtained from the KEGG pathway analysis of the list of the potential genes interacting with MFSD8. The genes highlighted in red represent the identified genes from the co-IP and MS-based proteomics performed on SH-SY5Y cells to study the potential MFSD8 interactors.

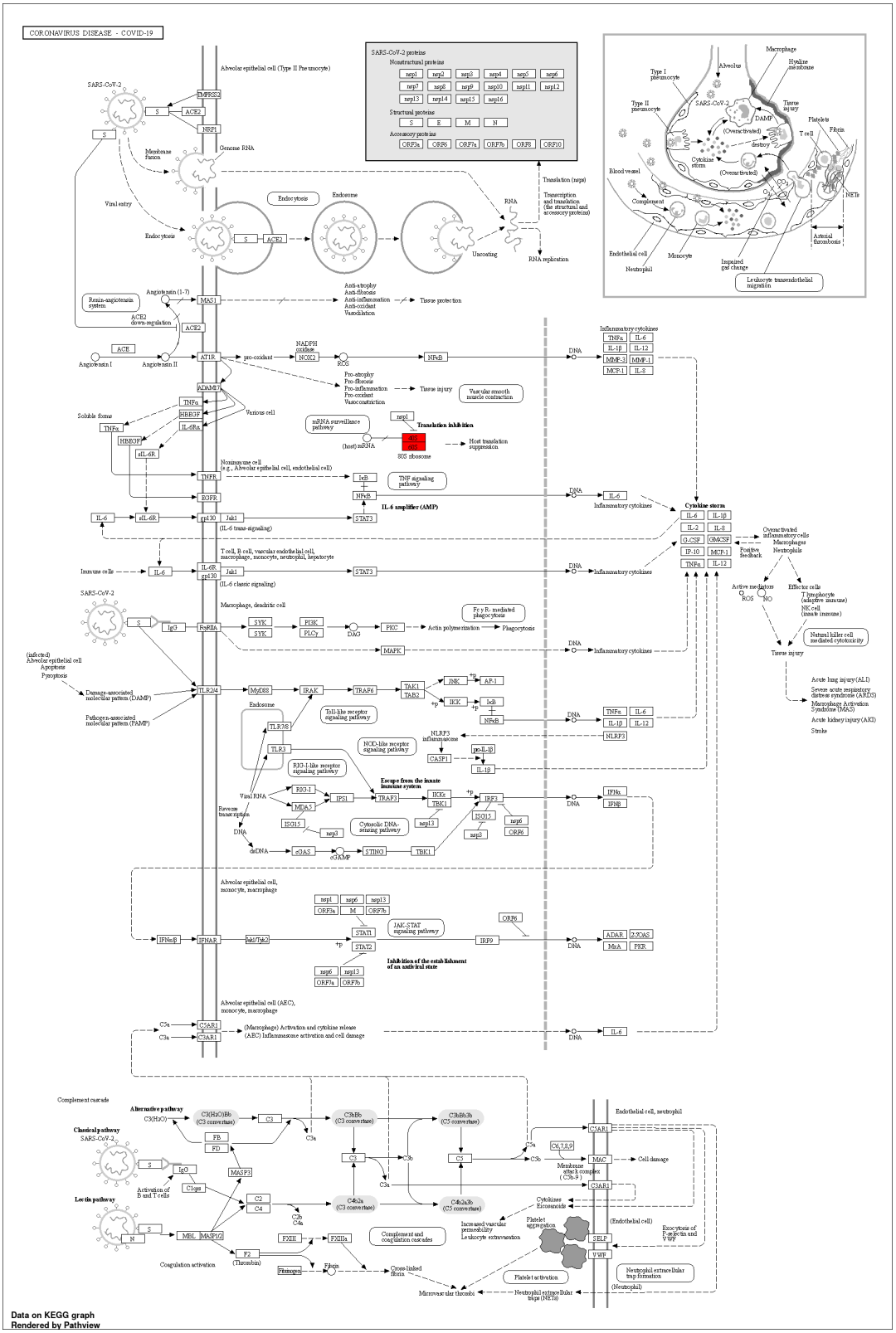

Supplementary Figure 6. 4. Proteins involved in Coronavirus disease from KEGG pathway analysis. Schematic representation of the proteins participating in Coronavirus infection obtained from the KEGG pathway analysis of the list of the potential genes interacting with MFSD8. The genes highlighted in red represent the identified genes from the co-IP and MS-based proteomics performed on SH-SY5Y cells to study the potential MFSD8 interactors.

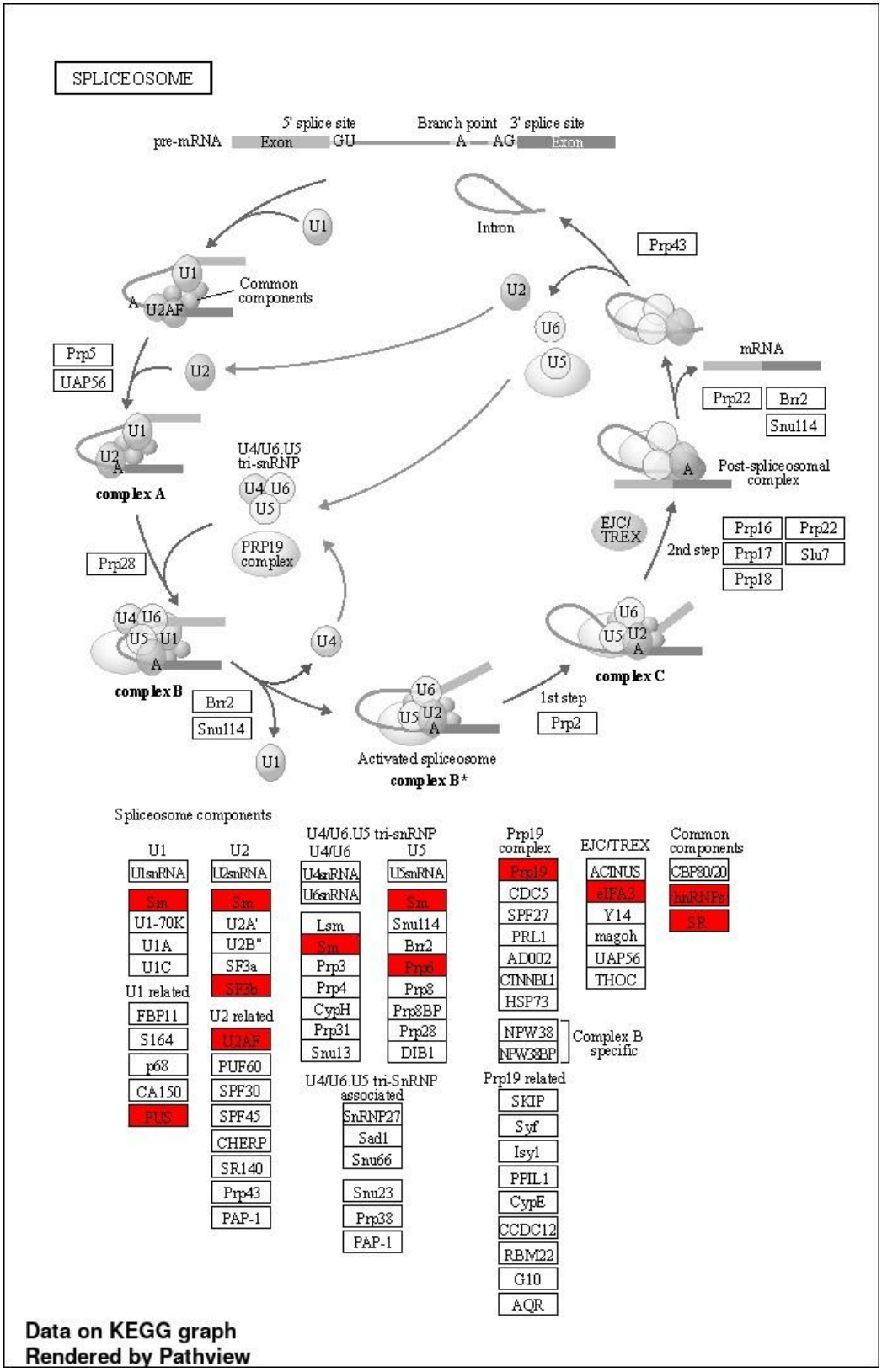

Supplementary Figure 6. 5. Spliceosome components from KEGG pathway analysis. Schematic representation of the proteins that form the spliceosome obtained from the KEGG pathway analysis of the list of the potential genes interacting with MFSD8. The genes highlighted in red represent the identified genes from the co-IP and MS-based proteomics performed on SH-SY5Y cells to study the potential MFSD8 interactors.

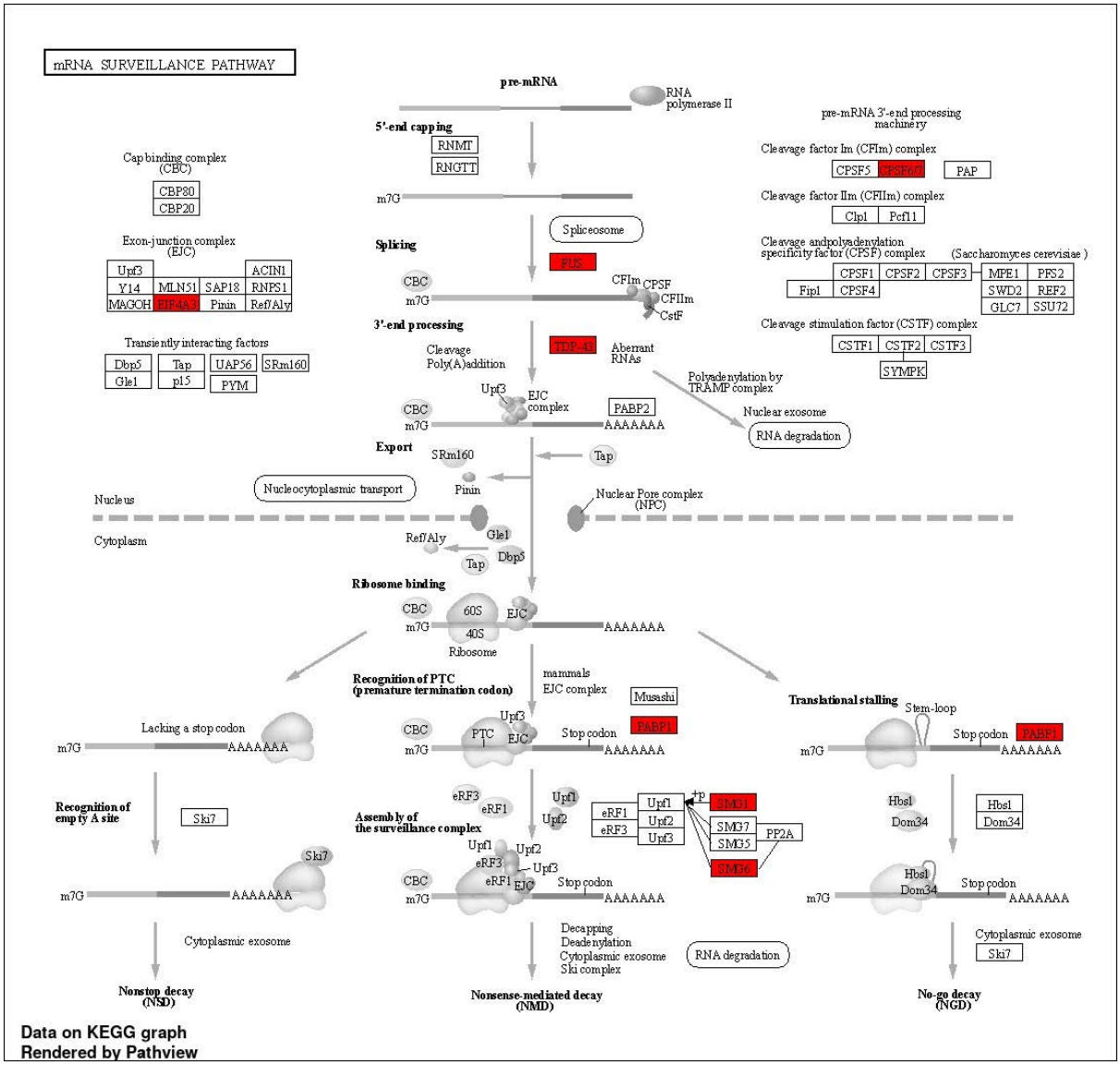

Supplementary Figure 6. 6. Proteins involved in mRNA surveillance from KEGG pathway analysis. Schematic representation of the proteins that participate in the mRNA surveillance pathway obtained from the KEGG pathway analysis of the list of the potential genes interacting with MFSD8. The genes highlighted in red represent the identified genes from the co-IP and MS-based proteomics performed on SH-SY5Y cells to study the potential MFSD8 interactors.

References

Åberg, L., Autti, T., Braulke, T., Cooper, J.D., van Diggelen, O.P., Jalanko, A., Kenrick, S., Kitzmüller, C., Kohlschütter, A., Kyttälä, A., Mitchison, H.M., Mole, S.E., Niezen-de Boer, R., Punkari, M.-L., Schulz, A., Talling, M., Williams, R.E., 2011a. CLN3, in: Mole, S., Williams, R., Goebel, H. (Eds.), The Neuronal Ceroid Lipofuscinoses (Batten Disease). Oxford University Press, p. 0. https://doi.org/10.1093/med/9780199590018.003.0008

Åberg, L., Autti, T., Cooper, J.D., Elleder, M., Haltia, M., Jalanko, A., Kitzmüller, C., Kopra, O., Mole, S.E., Nuutila, A., Peltonen, L., Punkari, M.-L., Rapola, J., Tyynelä, J., 2011b. CLN5, in: Mole, S., Williams, R., Goebel, H. (Eds.), The Neuronal Ceroid Lipofuscinoses (Batten Disease). Oxford University Press, p. 0. https://doi.org/10.1093/med/9780199590018.003.0009

Adewumi, O., Aflatoonian, B., Ahrlund-Richter, L., Amit, M., Andrews, P.W., Beighton, G., Bello, P.A., Benvenisty, N., Berry, L.S., Bevan, S., Blum, B., Brooking, J., Chen, K.G., Choo, A.B.H., Churchill, G.A., Corbel, M., Damjanov, I., Draper, J.S., Dvorak, P., Emanuelsson, K., Fleck, R.A., Ford, A., Gertow, K., Gertsenstein, M., Gokhale, P.J., Hamilton, R.S., Hampl, A., Healy, L.E., Hovatta, O., Hyllner, J., Imreh, M.P., Itskovitz-Eldor, J., Jackson, J., Johnson, J.L., Jones, M., Kee, K., King, B.L., Knowles, B.B., Lako, M., Lebrin, F., Mallon, B.S., Manning, D., Mayshar, Y., Mckay, R.D.G., Michalska, A.E., Mikkola, M., Mileikovsky, M., Minger, S.L., Moore, H.D., Mummery, C.L., Nagy, A., Nakatsuji, N., O'Brien, C.M., Oh, S.K.W., Olsson, C., Otonkoski, T., Park, K.-Y., Passier, R., Patel, H., Patel, M., Pedersen, R., Pera, M.F., Piekarczyk, M.S., Pera, R.A.R., Reubinoff, B.E., Robins, A.J., Rossant, J., Rugg-Gunn, P., Schulz, T.C., Semb, H., Sherrer, E.S., Siemen, H., Stacey, G.N., Stojkovic, M., Suemori, H., Szatkiewicz, J., Turetsky, T., Tuuri, T., van den Brink, S., Vintersten, K., Vuoristo, S., Ward, D., Weaver, T.A., Young, L.A., Zhang, W., Andrews, P.W., Gokhale, P.J., Healy, L.E., Andrews, P.W., Benvenisty, N., Mallon, B.S., Mckay, R.D.G., Pera, M.F., Rossant, J., Semb, H., Stacey, G.N., The International Stem Cell Initiative, Project coordination, Coordination of data collection and analysis, Coordination of material distribution and sample collection, The scientific management of the ISCI project was provided by a steering committee comprising, 2007. Characterization of human embryonic stem cell lines by the International Stem Cell Initiative. Nat. Biotechnol. 25, 803–816. https://doi.org/10.1038/nbt1318

Adlakha, Y.K., 2023. Human 3D brain organoids: steering the demolecularization of brain and neurological diseases. Cell Death Discov. 9, 1–17. https://doi.org/10.1038/s41420-023-01523-w

Agola, J., Jim, P., Ward, H., BasuRay, S., Wandinger-Ness, A., 2011. Rab GTPases as regulators of endocytosis, targets of disease and therapeutic opportunities. Clin. Genet. 80, 305–318. https://doi.org/10.1111/j.1399-0004.2011.01724.x

Akter, M., Cui, H., Sepehrimanesh, M., Hosain, M.A., Ding, B., 2022. Generation of highly pure motor neurons from human induced pluripotent stem cells. STAR Protoc. 3, 101223. https://doi.org/10.1016/j.xpro.2022.101223

Al Backer, N.B., 2015. Developmental regression in autism spectrum disorder. Sudan. J. Paediatr. 15, 21–26.

Alers, S., Löffler, A.S., Wesselborg, S., Stork, B., 2012. Role of AMPK-mTOR-Ulk1/2 in the Regulation of Autophagy: Cross Talk, Shortcuts, and Feedbacks. Mol. Cell. Biol. 32, 2–11. https://doi.org/10.1128/MCB.06159-11

Alirezaei, M., Kemball, C.C., Flynn, C.T., Wood, M.R., Whitton, J.L., Kiosses, W.B., 2010. Short-term fasting induces profound neuronal autophagy. Autophagy 6, 702–710. https://doi.org/10.4161/auto.6.6.12376

Almeida, A., Almeida, J., Bolaños, J.P., Moncada, S., 2001. Different responses of astrocytes and neurons to nitric oxide: The role of glycolytically generated ATP in astrocyte protection. Proc. Natl. Acad. Sci. 98, 15294–15299. https://doi.org/10.1073/pnas.261560998

Almeida, A., Moncada, S., Bolaños, J.P., 2004. Nitric oxide switches on glycolysis through the AMP protein kinase and 6-phosphofructo-2-kinase pathway. Nat. Cell Biol. 6, 45–51. https://doi.org/10.1038/ncb1080

Alroy, J., Braulke, T., Cismondi, I.A., Cooper, J.D., Creegan, D., Elleder, M., Kitzmüller, C., Kohan, R., Kohlschütter, A., Mole, S.E., Noher de Halac, I., Pfannl, R., Quitsch, A., Schulz, A., 2011. CLN6, in: Mole, S., Williams, R., Goebel, H. (Eds.), The Neuronal Ceroid Lipofuscinoses (Batten Disease). Oxford University Press, p. 0. https://doi.org/10.1093/med/9780199590018.003.0010

Anderson, P., Kedersha, N., 2008. Stress granules: the Tao of RNA triage. Trends Biochem. Sci. 33, 141–150. https://doi.org/10.1016/j.tibs.2007.12.003

Andrews, M.G., Kriegstein, A.R., 2022. Challenges of Organoid Research. Annu. Rev. Neurosci. 45, 23–39. https://doi.org/10.1146/annurev-neuro-111020-090812

Antonny, B., Bigay, J., Mesmin, B., 2018. The Oxysterol-Binding Protein Cycle: Burning Off PI(4)P to Transport Cholesterol. Annu. Rev. Biochem. 87, 809–837. https://doi.org/10.1146/annurev-biochem-061516-044924

Appelqvist, H., Wäster, P., Kågedal, K., Öllinger, K., 2013. The lysosome: from waste bag to potential therapeutic target. J. Mol. Cell Biol. 5, 214–226. https://doi.org/10.1093/jmcb/mjt022

Arsov, T., Smith, K.R., Damiano, J., Franceschetti, S., Canafoglia, L., Bromhead, C.J., Andermann, E., Vears, D.F., Cossette, P., Rajagopalan, S., McDougall, A., Sofia, V., Farrell, M., Aguglia, U., Zini, A., Meletti, S., Morbin, M., Mullen, S., Andermann, F., Mole, S.E., Bahlo, M., Berkovic, S.F., 2011. Kufs Disease, the Major Adult Form of Neuronal Ceroid Lipofuscinosis, Caused by Mutations in CLN6. Am. J. Hum. Genet. 88, 566–573. https://doi.org/10.1016/j.ajhg.2011.04.004

Audagnotto, M., Peraro, M.D., 2017. Protein post-translational modifications: In silico prediction tools and molecular modeling. Comput. Struct. Biotechnol. J. 15, 307–319. https://doi.org/10.1016/j.csbj.2017.03.004

Audo, I., Bujakowska, K., Orhan, E., Poloschek, C.M., Defoort-Dhellemmes, S., Drumare, I., Kohl, S., Luu, T.D., Lecompte, O., Zrenner, E., Lancelot, M.-E., Antonio, A., Germain, A., Michiels, C., Audier, C., Letexier, M., Saraiva, J.-P., Leroy, B.P., Munier, F.L., Mohand-Saïd, S., Lorenz, B., Friedburg, C., Preising, M., Kellner, U., Renner, A.B., Moskova-Doumanova, V., Berger, W., Wissinger, B., Hamel, C.P., Schorderet, D.F., De Baere, E., Sharon, D., Banin, E., Jacobson, S.G., Bonneau, D., Zanlonghi, X., Le Meur, G., Casteels, I., Koenekoop, R., Long, V.W., Meire, F., Prescott, K., de Ravel, T., Simmons, I., Nguyen, H., Dollfus, H., Poch, O., Léveillard, T., Nguyen-Ba-Charvet, K., Sahel, J.-A., Bhattacharya, S.S., Zeitz, C., 2012. Whole-Exome Sequencing Identifies Mutations in GPR179 Leading to Autosomal-Recessive Complete

Congenital Stationary Night Blindness. Am. J. Hum. Genet. 90, 321–330. https://doi.org/10.1016/j.ajhg.2011.12.007

Autti, T., Cooper, J.D., van Diggelen, O.P., Haltia, M., Jalanko, A., Kitzmüller, C., Kopra, O., Lönnqvist, T., Lyly, A., Mole, S.E., Rapola, J., Vanhanen, S.-L., 2011. CLN1, in: Mole, S., Williams, R., Goebel, H. (Eds.), The Neuronal Ceroid Lipofuscinoses (Batten Disease). Oxford University Press, p. 0. https://doi.org/10.1093/med/9780199590018.003.0006

Bains, M., Zaegel, V., Mize-Berge, J., Heidenreich, K.A., 2011. IGF-I stimulates Rab7-RILP interaction during neuronal autophagy. Neurosci. Lett. 488, 112–117. https://doi.org/10.1016/j.neulet.2010.09.018

Bajaj, L., Lotfi, P., Pal, R., Ronza, A. di, Sharma, J., Sardiello, M., 2019. Lysosome biogenesis in health and disease. J. Neurochem. 148, 573–589. https://doi.org/10.1111/jnc.14564

Baloyannis, S.J., 2006. Mitochondrial alterations in Alzheimer's disease. J. Alzheimers Dis. 9, 119–126. https://doi.org/10.3233/JAD-2006-9204

Barbero, P., Bittova, L., Pfeffer, S.R., 2002. Visualization of Rab9-mediated vesicle transport from endosomes to the trans-Golgi in living cells. J. Cell Biol. 156, 511–518. https://doi.org/10.1083/jcb.200109030

Barroca, N.C.B., Della Santa, G., Suchecki, D., García-Cairasco, N., Umeoka, E.H. de L., 2022. Challenges in the use of animal models and perspectives for a translational view of stress and psychopathologies. Neurosci. Biobehav. Rev. 140, 104771. https://doi.org/10.1016/j.neubiorev.2022.104771

Batten, F.E., Mayou, M.S., 1915. Family Cerebral Degeneration with Macular Changes. Proc. R. Soc. Med. 8, 70–90. https://doi.org/10.1177/003591571500801624

Bauwens, M., Storch, S., Weisschuh, N., Ceuterick-de Groote, C., De Rycke, R., Guillemyn, B., De Jaegere, S., Coppieters, F., Van Coster, R., Leroy, B.P., De Baere, E., 2020. Functional characterization of novel MFSD8 pathogenic variants anticipates neurological involvement in juvenile isolated maculopathy. Clin. Genet. 97, 426–436. https://doi.org/10.1111/cge.13673

Beal, M.F., 1998. Excitotoxicity and nitric oxide in parkinson's disease pathogenesis. Ann. Neurol. 44, S110–S114. https://doi.org/10.1002/ana.410440716

Beau, I., Mehrpour, M., Codogno, P., 2011. Autophagosomes and human diseases. Int. J. Biochem. Cell Biol. 43, 460–464. https://doi.org/10.1016/j.biocel.2011.01.006

Beauclair, G., Bridier-Nahmias, A., Zagury, J.-F., Saïb, A., Zamborlini, A., 2015. JASSA: a comprehensive tool for prediction of SUMOylation sites and SIMs. Bioinformatics 31, 3483–3491. https://doi.org/10.1093/bioinformatics/btv403

Bell, S., Hettige, N., Silveira, H., Peng, H., Wu, H., Jefri, M., Antonyan, L., Zhang, Y., Zhang, X., Ernst, C., 2019. Differentiation of Human Induced Pluripotent Stem Cells (iPSCs) into an Effective Model of Forebrain Neural Progenitor Cells and Mature Neurons. BIO-Protoc. 9. https://doi.org/10.21769/BioProtoc.3188

Belviso, I., Romano, V., Nurzynska, D., Castaldo, C., Meglio, F.D., Belviso, I., Romano, V., Nurzynska, D., Castaldo, C., Meglio, F.D., 2020. Non-integrating Methods to Produce Induced

Pluripotent Stem Cells for Regenerative Medicine: An Overview, in: Biomechanics and Functional Tissue Engineering. IntechOpen. https://doi.org/10.5772/intechopen.95070

Ben-Yoseph, O., Boxer, P.A., Ross, B.D., 1996. Assessment of the Role of the Glutathione and Pentose Phosphate Pathways in the Protection of Primary Cerebrocortical Cultures from Oxidative Stress. J. Neurochem. 66, 2329–2337. https://doi.org/10.1046/j.1471-4159.1996.66062329.x

Berkovic, S.F., Andermann, F., Andermann, E., Carpenter, S., Wolfe, L., Opitz, J.M., Reynolds, J.F., Pullarkat, R.K., 1988. Kufs disease: Clinical features and forms. Am. J. Med. Genet. 31, 105–109. https://doi.org/10.1002/ajmg.1320310614

Bernstein, B.E., Mikkelsen, T.S., Xie, X., Kamal, M., Huebert, D.J., Cuff, J., Fry, B., Meissner, A., Wernig, M., Plath, K., Jaenisch, R., Wagschal, A., Feil, R., Schreiber, S.L., Lander, E.S., 2006. A Bivalent Chromatin Structure Marks Key Developmental Genes in Embryonic Stem Cells. Cell 125, 315–326. https://doi.org/10.1016/j.cell.2006.02.041

Birtel, J., Gliem, M., Mangold, E., Müller, P.L., Holz, F.G., Neuhaus, C., Lenzner, S., Zahnleiter, D., Betz, C., Eisenberger, T., Bolz, H.J., Issa, P.C., 2018. Next-generation sequencing identifies unexpected genotype-phenotype correlations in patients with retinitis pigmentosa. PLOS ONE 13, e0207958. https://doi.org/10.1371/journal.pone.0207958

Bjørkøy, G., Lamark, T., Brech, A., Outzen, H., Perander, M., Øvervatn, A., Stenmark, H., Johansen, T., 2005. p62/SQSTM1 forms protein aggregates degraded by autophagy and has a protective effect on huntingtin-induced cell death. J. Cell Biol. 171, 603–614. https://doi.org/10.1083/jcb.200507002

Blesa, J., Przedborski, S., 2014. Parkinson's disease: animal models and dopaminergic cell vulnerability. Front. Neuroanat. 8.

Blom, N., Sicheritz-Pontén, T., Gupta, R., Gammeltoft, S., Brunak, S., 2004. Prediction of post-translational glycosylation and phosphorylation of proteins from the amino acid sequence. PROTEOMICS 4, 1633–1649. https://doi.org/10.1002/pmic.200300771

Bloom, F.E., Reilly, J.F., Redwine, J.M., Wu, C.-C., Young, W.G., Morrison, J.H., 2005. Mouse Models of Human Neurodegenerative Disorders: Requirements for Medication Development. Arch. Neurol. 62, 185–187. https://doi.org/10.1001/archneur.62.2.185

Bock, J.B., Matern, H.T., Peden, A.A., Scheller, R.H., 2001. A genomic perspective on membrane compartment organization. Nature 409, 839–841. https://doi.org/10.1038/35057024

Boland, B., Yu, W.H., Corti, O., Mollereau, B., Henriques, A., Bezard, E., Pastores, G.M., Rubinsztein, D.C., Nixon, R.A., Duchen, M.R., Mallucci, G.R., Kroemer, G., Levine, B., Eskelinen, E.-L., Mochel, F., Spedding, M., Louis, C., Martin, O.R., Millan, M.J., 2018. Promoting the clearance of neurotoxic proteins in neurodegenerative disorders of ageing. Nat. Rev. Drug Discov. 17, 660–688. https://doi.org/10.1038/nrd.2018.109

Bolaños, J.P., Almeida, A., Moncada, S., 2010. Glycolysis: a bioenergetic or a survival pathway? Trends Biochem. Sci. 35, 145–149. https://doi.org/10.1016/j.tibs.2009.10.006

Bolaños, J.P., Peuchen, S., Heales, S.J., Land, J.M., Clark, J.B., 1994. Nitric oxide-mediated inhibition of the mitochondrial respiratory chain in cultured astrocytes. J. Neurochem. 63, 910–916. https://doi.org/10.1046/j.1471-4159.1994.63030910.x

Bonifacino, J.S., Traub, L.M., 2003. Signals for Sorting of Transmembrane Proteins to Endosomes and Lysosomes. Annu. Rev. Biochem. 72, 395–447. https://doi.org/10.1146/annurev.biochem.72.121801.161800

Bott, K., Upton, Z., Schrobback, K., Ehrbar, M., Hubbell, J.A., Lutolf, M.P., Rizzi, S.C., 2010. The effect of matrix characteristics on fibroblast proliferation in 3D gels. Biomaterials 31, 8454–8464. https://doi.org/10.1016/j.biomaterials.2010.07.046

Boustany, R.-M.N., 2013. Lysosomal storage diseases—the horizon expands. Nat. Rev. Neurol. 9, 583–598. https://doi.org/10.1038/nrneurol.2013.163

Boyd, S., Brookfield, J.L., Critchlow, S.E., Cumming, I.A., Curtis, N.J., Debreczeni, J., Degorce, S.L., Donald, C., Evans, N.J., Groombridge, S., Hopcroft, P., Jones, N.P., Kettle, J.G., Lamont, S., Lewis, H.J., MacFaull, P., McLoughlin, S.B., Rigoreau, L.J.M., Smith, J.M., St-Gallay, S., Stock, J.K., Turnbull, A.P., Wheatley, E.R., Winter, J., Wingfield, J., 2015. Structure-Based Design of Potent and Selective Inhibitors of the Metabolic Kinase PFKFB3. J. Med. Chem. 58, 3611–3625. https://doi.org/10.1021/acs.jmedchem.5b00352

Boyer, L.A., Lee, T.I., Cole, M.F., Johnstone, S.E., Levine, S.S., Zucker, J.P., Guenther, M.G., Kumar, R.M., Murray, H.L., Jenner, R.G., Gifford, D.K., Melton, D.A., Jaenisch, R., Young, R.A., 2005. Core Transcriptional Regulatory Circuitry in Human Embryonic Stem Cells. Cell 122, 947–956. https://doi.org/10.1016/j.cell.2005.08.020

Bradley, A., Evans, M., Kaufman, M.H., Robertson, E., 1984. Formation of germ-line chimaeras from embryo-derived teratocarcinoma cell lines. Nature 309, 255–256. https://doi.org/10.1038/309255a0

Bradley, D.E., 1971. CHAPTER 7 - A Comparative Study of the Structure and Biological Properties of Bacteriophages, in: Maramorosch, K., Kurstak, E. (Eds.), Comparative Virology. Academic Press, pp. 207–253. https://doi.org/10.1016/B978-0-12-470260-8.50012-9

Brandenstein, L., Schweizer, M., Sedlacik, J., Fiehler, J., Storch, S., 2016. Lysosomal dysfunction and impaired autophagy in a novel mouse model deficient for the lysosomal membrane protein Cln7. Hum. Mol. Genet. 25, 777–791. https://doi.org/10.1093/hmg/ddv615

Bras, J., Verloes, A., Schneider, S.A., Mole, S.E., Guerreiro, R.J., 2012. Mutation of the parkinsonism gene ATP13A2 causes neuronal ceroid-lipofuscinosis. Hum. Mol. Genet. 21, 2646–2650. https://doi.org/10.1093/hmg/dds089

Braulke, T., Bonifacino, J.S., 2009. Sorting of lysosomal proteins. Biochim. Biophys. Acta BBA - Mol. Cell Res., Lysosomes 1793, 605–614. https://doi.org/10.1016/j.bbamcr.2008.10.016

Bright, N.A., Davis, L.J., Luzio, J.P., 2016. Endolysosomes Are the Principal Intracellular Sites of Acid Hydrolase Activity. Curr. Biol. 26, 2233–2245. https://doi.org/10.1016/j.cub.2016.06.046

Brimble, S.N., Sherrer, E.S., Uhl, E.W., Wang, E., Kelly, S., Merrill, A.H., Jr., Robins, A.J., Schulz, T.C., 2007. The Cell Surface Glycosphingolipids SSEA-3 and SSEA-4 Are Not Essential for Human ESC Pluripotency. Stem Cells 25, 54–62. https://doi.org/10.1634/stemcells.2006-0232

Bröcker, C., Engelbrecht-Vandré, S., Ungermann, C., 2010. Multisubunit Tethering Complexes and Their Role in Membrane Fusion. Curr. Biol. 20, R943–R952. https://doi.org/10.1016/j.cub.2010.09.015

Bröcker, C., Kuhlee, A., Gatsogiannis, C., kleine Balderhaar, H.J., Hönscher, C., Engelbrecht-Vandré, S., Ungermann, C., Raunser, S., 2012. Molecular architecture of the multisubunit homotypic fusion and vacuole protein sorting (HOPS) tethering complex. Proc. Natl. Acad. Sci. 109, 1991–1996. https://doi.org/10.1073/pnas.1117797109

Brudvig, J.J., Weimer, J.M., 2022. CLN7 gene therapy: hope for an ultra-rare condition. J. Clin. Invest. 132. https://doi.org/10.1172/JCI157820

Bucci, C., Parton, R.G., Mather, I.H., Stunnenberg, H., Simons, K., Hoflack, B., Zerial, M., n.d. The Small GTPase rab5 Functions as a Regulatory Factor in the Early Endocytic Pathway.

Bucci, C., Thomsen, P., Nicoziani, P., McCarthy, J., van Deurs, B., 2000. Rab7: A Key to Lysosome Biogenesis. Mol. Biol. Cell 11, 467–480. https://doi.org/10.1091/mbc.11.2.467

Büeler, H., 2021. Mitochondrial and Autophagic Regulation of Adult Neurogenesis in the Healthy and Diseased Brain. Int. J. Mol. Sci. 22, 3342. https://doi.org/10.3390/ijms22073342

Burmistrova, O., Olias-Arjona, A., Lapresa, R., Jimenez-Blasco, D., Eremeeva, T., Shishov, D., Romanov, S., Zakurdaeva, K., Almeida, A., Fedichev, P.O., Bolaños, J.P., 2019. Targeting PFKFB3 alleviates cerebral ischemia-reperfusion injury in mice. Sci. Rep. 9, 11670. https://doi.org/10.1038/s41598-019-48196-z

Campo, A. del, Jaimovich, E., Tevy, M.F., 2016. Mitochondria in the Aging Muscles of Flies and Mice: New Perspectives for Old Characters. Oxid. Med. Cell. Longev. 2016, e9057593. https://doi.org/10.1155/2016/9057593

Caragea, C., Sinapov, J., Silvescu, A., Dobbs, D., Honavar, V., 2007. Glycosylation site prediction using ensembles of Support Vector Machine classifiers. BMC Bioinformatics 8, 438. https://doi.org/10.1186/1471-2105-8-438

Casal, M., Paiva, S., Andrade, R.P., Gancedo, C., Leão, C., 1999. The Lactate-Proton Symport of Saccharomyces cerevisiae Is Encoded by JEN1. J. Bacteriol. 181, 2620–2623. https://doi.org/10.1128/jb.181.8.2620-2623.1999

Castro-Viñuelas, R., Sanjurjo-Rodríguez, C., Piñeiro-Ramil, M., Hermida-Gómez, T., Rodríguez-Fernández, S., Oreiro, N., de Toro, J., Fuentes, I., Blanco, F.J., Díaz-Prado, S., 2020. Generation and characterization of human induced pluripotent stem cells (iPSCs) from hand osteoarthritis patient-derived fibroblasts. Sci. Rep. 10, 4272. https://doi.org/10.1038/s41598-020-61071-6

Cecarini V, Bonfili L, Gogoi O, Lawrence S, Venanzi FM, Azevedo V, Mancha-Agresti P, Drumond MM, Rossi G, Berardi S, Galosi L, Cuccioloni M, Angeletti M, Suchodolski JS, Pilla R, Lidbury JA, Eleuteri AM. 2020. Neuroprotective effects of p62(SQSTM1)-engineered lactic acid bacteria in Alzheimer's disease: a pre-clinical study. Aging (Albany NY). 12(16):15995-16020. https://doi.org/10.18632/aging.103900

Cendelin, J., Cvetanovic, M., Gandelman, M., Hirai, H., Orr, H.T., Pulst, S.M., Strupp, M., Tichanek, F., Tuma, J., Manto, M., 2022. Consensus Paper: Strengths and Weaknesses of Animal Models of Spinocerebellar Ataxias and Their Clinical Implications. The Cerebellum 21, 452–481. https://doi.org/10.1007/s12311-021-01311-1

Chan, D.C., 2006. Mitochondria: Dynamic Organelles in Disease, Aging, and Development. Cell 125, 1241–1252. https://doi.org/10.1016/j.cell.2006.06.010

Chang, M., Cooper, J.D., Davidson, B.L., van Diggelen, O.P., Elleder, M., Goebel, H.H., Golabek, A.A., Kida, E., Kohlschütter, A., Lobel, P., Mole, S.E., Schulz, A., Sleat, D.E., Warburton, M., Wisniewski, K.E., 2011. CLN2, in: Mole, S., Williams, R., Goebel, H. (Eds.), The Neuronal Ceroid Lipofuscinoses (Batten Disease). Oxford University Press, p. 0. https://doi.org/10.1093/med/9780199590018.003.0007

Chang, Y., Kim, Junyeop, Park, H., Choi, H., Kim, Jongpil, 2020. Modelling neurodegenerative diseases with 3D brain organoids. Biol. Rev. 95, 1497–1509. https://doi.org/10.1111/brv.12626

Chen, D., Xiao, H., Zhang, K., Wang, B., Gao, Z., Jian, Y., Qi, X., Sun, J., Miao, L., Yang, C., 2010. Retromer Is Required for Apoptotic Cell Clearance by Phagocytic Receptor Recycling. Science 327, 1261–1264. https://doi.org/10.1126/science.1184840

Chen, X., Dong, T., Hu, Y., Shaffo, F.C., Belur, N.R., Mazzulli, J.R., Gray, S.J., 2022. AAV9/*MFSD8* gene therapy is effective in preclinical models of neuronal ceroid lipofuscinosis type 7 disease. J. Clin. Invest. 132. https://doi.org/10.1172/JCI146286

Chen, X., Shaffo, F., Dong, T., Hu, Y., Belur, N.R., Mazzulli, J.R., Gray, S.J., 2020. Preclinical efficacy and safety evaluation of scAAV9/CLN7 gene replacement therapy in rodents. Mol. Genet. Metab. 129, S40. https://doi.org/10.1016/j.ymgme.2019.11.079

Cheng L, Hu W, Qiu B, Zhao J, Yu Y, Guan W, Wang M, Yang W, Pei G. 2014. Generation of neural progenitor cells by chemical cocktails and hypoxia. Cell Res. 2014 Jun;24(6):665-79. https://doi.org/10.1038/cr.2014.32.

Cheng, X., Ma, X., Ding, X., Li, L., Jiang, X., Shen, Z., Chen, S., Liu, W., Gong, W., Sun, Q., 2017. Pacer Mediates the Function of Class III PI3K and HOPS Complexes in Autophagosome Maturation by Engaging Stx17. Mol. Cell 65, 1029-1043.e5. https://doi.org/10.1016/j.molcel.2017.02.010

Cheng, X.-T., Xie, Y.-X., Zhou, B., Huang, N., Farfel-Becker, T., Sheng, Z.-H., 2018. Revisiting LAMP1 as a marker for degradative autophagy-lysosomal organelles in the nervous system. Autophagy 14, 1472–1474. https://doi.org/10.1080/15548627.2018.1482147

Cherfils, J., Zeghouf, M., 2013. Regulation of Small GTPases by GEFs, GAPs, and GDIs. Physiol. Rev. 93, 269–309. https://doi.org/10.1152/physrev.00003.2012

Chew, J.-L., Loh, Y.-H., Zhang, W., Chen, X., Tam, W.-L., Yeap, L.-S., Li, P., Ang, Y.-S., Lim, B., Robson, P., Ng, H.-H., 2005. Reciprocal Transcriptional Regulation of Pou5f1 and Sox2 via the Oct4/Sox2 Complex in Embryonic Stem Cells. Mol. Cell. Biol. 25, 6031–6046. https://doi.org/10.1128/MCB.25.14.6031-6046.2005

Choi, J., Baek, K.-H., 2018. Cellular functions of stem cell factors mediated by the ubiquitin–proteasome system. Cell. Mol. Life Sci. 75, 1947–1957. https://doi.org/10.1007/s00018-018-2770-7

Chou, S.M., Norris, F.H., 1993. Issues & Opinions: Amyotrophic lateral sclerosis: Lower motor neuron disease spreading to upper motor neurons. Muscle Nerve 16, 864–869. https://doi.org/10.1002/mus.880160810

Chua, C.E.L., Gan, B.Q., Tang, B.L., 2011. Involvement of members of the Rab family and related small GTPases in autophagosome formation and maturation. Cell. Mol. Life Sci. 68, 3349–3358. https://doi.org/10.1007/s00018-011-0748-9

Cinque, L., De Leonibus, C., Iavazzo, M., Krahmer, N., Intartaglia, D., Salierno, F.G., De Cegli, R., Di Malta, C., Svelto, M., Lanzara, C., Maddaluno, M., Wanderlingh, L.G., Huebner, A.K., Cesana, M., Bonn, F., Polishchuk, E., Hübner, C.A., Conte, I., Dikic, I., Mann, M., Ballabio, A., Sacco, F., Grumati, P., Settembre, C., 2020. MiT/TFE factors control ER-phagy via transcriptional regulation of FAM134B. EMBO J. 39, e105696. https://doi.org/10.15252/embj.2020105696

Coding of Two Sphingolipid Activator Proteins (SAP-1 and SAP-2) by Same Genetic Locus | Science [WWW Document], n.d. URL https://www.science.org/doi/10.1126/science.2842863 (accessed 7.11.23).

Conner, S.D., Schmid, S.L., 2003. Regulated portals of entry into the cell. Nature 422, 37–44. https://doi.org/10.1038/nature01451

Connolly, K.J., O'Hare, M.B., Mohammed, A., Aitchison, K.M., Anthoney, N.C., Taylor, M.J., Stewart, B.A., Tuxworth, R.I., Tear, G., 2019. The neuronal ceroid lipofuscinosis protein Cln7 functions in the postsynaptic cell to regulate synapse development. Sci. Rep. 9, 15592. https://doi.org/10.1038/s41598-019-51588-w

Cooper, G.M., 2000. Lysosomes, in: The Cell: A Molecular Approach. 2nd Edition. Sinauer Associates.

Corti, O., Blomgren, K., Poletti, A., Beart, P.M., 2020. Autophagy in neurodegeneration: New insights underpinning therapy for neurological diseases. J. Neurochem. 154, 354–371. https://doi.org/10.1111/jnc.15002

Cox, T.M., Cachón-González, M.B., 2012. The cellular pathology of lysosomal diseases. J. Pathol. 226, 241–254. https://doi.org/10.1002/path.3021

Craiu, D., Dragostin, O., Dica, A., Hoffman-Zacharska, D., Gos, M., Bastian, A.E., Gherghiceanu, M., Rolfs, A., Nahavandi, N., Craiu, M., Iliescu, C., 2015. Rett-like onset in late-infantile neuronal ceroid lipofuscinosis (CLN7) caused by compound heterozygous mutation in the MFSD8 gene and review of the literature data on clinical onset signs. Eur. J. Paediatr. Neurol. 19, 78–86. https://doi.org/10.1016/j.ejpn.2014.07.008

Cudkowicz, M.E., McKenna-Yasek, D., Sapp, P.E., Chin, W., Geller, B., Hayden, D.L., Schoenfeld, D.A., Hosler, B.A., Horvitz, H.R., Brown, R.H., 1997. Epidemiology of mutations in superoxide dismutase in amyotrophic lateal sclerosis. Ann. Neurol. 41, 210–221. https://doi.org/10.1002/ana.410410212

Cuervo, A.M., Dice, J.F., 1998. Lysosomes, a meeting point of proteins, chaperones, and proteases. J. Mol. Med. 76, 6–12. https://doi.org/10.1007/s001090050185

Cuervo, A.M., Dice, J.F., 1996. A Receptor for the Selective Uptake and Degradation of Proteins by Lysosomes. Science 273, 501–503. https://doi.org/10.1126/science.273.5274.501

Cui, H., Kong, Y., Zhang, H., 2011. Oxidative Stress, Mitochondrial Dysfunction, and Aging. J. Signal Transduct. 2012, e646354. https://doi.org/10.1155/2012/646354

Cui, Q., Bi, H., Lv, Z., Wu, Q., Hua, J., Gu, B., Huo, C., Tang, M., Chen, Y., Chen, C., Chen, S., Zhang, X., Wu, Z., Lao, Z., Sheng, N., Shen, C., Zhang, Y., Wu, Z.-Y., Jin, Z., Yang, P., Liu, H., Li, J., Bai, G., 2023. Diverse CMT2 neuropathies are linked to aberrant G3BP interactions in stress granules. Cell 186, 803-820.e25. https://doi.org/10.1016/j.cell.2022.12.046

Cundy, T., Hegde, M., Naot, D., Chong, B., King, A., Wallace, R., Mulley, J., Love, D.R., Seidel, J., Fawkner, M., Banovic, T., Callon, K.E., Grey, A.B., Reid, I.R., Middleton-Hardie, C.A., Cornish, J., 2002. A mutation in the gene TNFRSF11B encoding osteoprotegerin causes an idiopathic hyperphosphatasia phenotype. Hum. Mol. Genet. 11, 2119–2127. https://doi.org/10.1093/hmg/11.18.2119

D'Angelo, G., Capasso, S., Sticco, L., Russo, D., 2013. Glycosphingolipids: synthesis and functions. FEBS J. 280, 6338–6353. https://doi.org/10.1111/febs.12559

Danyukova, T., Ariunbat, K., Thelen, M., Brocke-Ahmadinejad, N., Mole, S.E., Storch, S., 2018. Loss of CLN7 results in depletion of soluble lysosomal proteins and impaired mTOR reactivation. Hum. Mol. Genet. 27, 1711–1722. https://doi.org/10.1093/hmg/ddy076

Davis, P.C., Gearing, M., Gray, L., Mirra, S.S., Morris, J.C., Edland, S.D., Lin, T., Heyman, A., 1995. The CERAD experience, part VIII: Neuroimaging-neuropathology correlates of temporal lobe changes in Alzheimer's disease. Neurology 45, 178–179. https://doi.org/10.1212/WNL.45.1.178

Dawson, T.M., Golde, T.E., Lagier-Tourenne, C., 2018. Animal models of neurodegenerative diseases. Nat. Neurosci. 21, 1370–1379. https://doi.org/10.1038/s41593-018-0236-8

Deinhardt, K., Salinas, S., Verastegui, C., Watson, R., Worth, D., Hanrahan, S., Bucci, C., Schiavo, G., 2006. Rab5 and Rab7 Control Endocytic Sorting along the Axonal Retrograde Transport Pathway. Neuron 52, 293–305. https://doi.org/10.1016/j.neuron.2006.08.018

DeJesus-Hernandez, M., Mackenzie, I.R., Boeve, B.F., Boxer, A.L., Baker, M., Rutherford, N.J., Nicholson, A.M., Finch, N.A., Flynn, H., Adamson, J., Kouri, N., Wojtas, A., Sengdy, P., Hsiung, G.-Y.R., Karydas, A., Seeley, W.W., Josephs, K.A., Coppola, G., Geschwind, D.H., Wszolek, Z.K., Feldman, H., Knopman, D.S., Petersen, R.C., Miller, B.L., Dickson, D.W., Boylan, K.B., Graff-Radford, N.R., Rademakers, R., 2011. Expanded GGGGCC Hexanucleotide Repeat in Noncoding Region of C9ORF72 Causes Chromosome 9p-Linked FTD and ALS. Neuron 72, 245–256. https://doi.org/10.1016/j.neuron.2011.09.011

del Monte, F., Agnetti, G., 2014. Protein post-translational modifications and misfolding: New concepts in heart failure. PROTEOMICS – Clin. Appl. 8, 534–542. https://doi.org/10.1002/prca.201400037

Delgado-Esteban, M., Almeida, A., Bolaños, J.P., 2000. D-Glucose Prevents Glutathione Oxidation and Mitochondrial Damage After Glutamate Receptor Stimulation in Rat Cortical Primary Neurons. J. Neurochem. 75, 1618–1624. https://doi.org/10.1046/j.1471-4159.2000.0751618.x

Di Baldassarre A, Cimetta E, Bollini S, Gaggi G, Ghinassi B. Human-Induced Pluripotent Stem Cell Technology and Cardiomyocyte Generation: Progress and Clinical Applications. Cells. 2018 May 25;7(6):48. https://doi.org/10.3390/cells7060048

Doetschman, T., Gregg, R.G., Maeda, N., Hooper, M.L., Melton, D.W., Thompson, S., Smithies, O., 1987. Targetted correction of a mutant HPRT gene in mouse embryonic stem cells. Nature 330, 576–578. https://doi.org/10.1038/330576a0

Domenico, A. di, Carola, G., Calatayud, C., Pons-Espinal, M., Muñoz, J.P., Richaud-Patin, Y., Fernandez-Carasa, I., Gut, M., Faella, A., Parameswaran, J., Soriano, J., Ferrer, I., Tolosa, E., Zorzano, A., Cuervo, A.M., Raya, A., Consiglio, A., 2019. Patient-Specific iPSC-Derived

Astrocytes Contribute to Non-Cell-Autonomous Neurodegeneration in Parkinson's Disease. Stem Cell Rep. 12, 213–229. https://doi.org/10.1016/j.stemcr.2018.12.011

Dooley, H.C., Razi, M., Polson, H.E.J., Girardin, S.E., Wilson, M.I., Tooze, S.A., 2014. WIPI2 Links LC3 Conjugation with PI3P, Autophagosome Formation, and Pathogen Clearance by Recruiting Atg12–5-16L1. Mol. Cell 55, 238–252. https://doi.org/10.1016/j.molcel.2014.05.021

Dorszewska, J., Prendecki, M., Oczkowska, A., Dezor, M., Kozubski, W., 2016. Molecular Basis of Familial and Sporadic Alzheimer's Disease. Curr. Alzheimer Res. 13, 952–963. https://doi.org/10.2174/1567205013666160314150501

Duan, G., Walther, D., 2015. The Roles of Post-translational Modifications in the Context of Protein Interaction Networks. PLOS Comput. Biol. 11, e1004049. https://doi.org/10.1371/journal.pcbi.1004049

Duman, J.G., Forte, J.G., 2003. What is the role of SNARE proteins in membrane fusion? Am. J. Physiol.-Cell Physiol. 285, C237–C249. https://doi.org/10.1152/ajpcell.00091.2003

Dumont, M., Stack, C., Elipenahli, C., Jainuddin, S., Gerges, M., Starkova, N.N., Yang, L., Starkov, A.A., Beal, F., 2011. Behavioral deficit, oxidative stress, and mitochondrial dysfunction precede tau pathology in P301S transgenic mice. FASEB J. 25, 4063–4072. https://doi.org/10.1096/fj.11-186650

Edinger, A.L., Cinalli, R.M., Thompson, C.B., 2003. Rab7 Prevents Growth Factor-Independent Survival by Inhibiting Cell-Autonomous Nutrient Transporter Expression. Dev. Cell 5, 571–582. https://doi.org/10.1016/S1534-5807(03)00291-0

Edwards, A.S., Scott, J.D., 2000. A-kinase anchoring proteins: protein kinase A and beyond. Curr. Opin. Cell Biol. 12, 217–221. https://doi.org/10.1016/S0955-0674(99)00085-X

Egawa, N., Kitaoka, S., Tsukita, K., Naitoh, M., Takahashi, K., Yamamoto, T., Adachi, F., Kondo, T., Okita, K., Asaka, I., Aoi, T., Watanabe, A., Yamada, Y., Morizane, A., Takahashi, J., Ayaki, T., Ito, H., Yoshikawa, K., Yamawaki, S., Suzuki, S., Watanabe, D., Hioki, H., Kaneko, T., Makioka, K., Okamoto, K., Takuma, H., Tamaoka, A., Hasegawa, K., Nonaka, T., Hasegawa, M., Kawata, A., Yoshida, M., Nakahata, T., Takahashi, R., Marchetto, M.C.N., Gage, F.H., Yamanaka, S., Inoue, H., 2012. Drug Screening for ALS Using Patient-Specific Induced Pluripotent Stem Cells. Sci. Transl. Med. 4, 145ra104-145ra104. https://doi.org/10.1126/scitranslmed.3004052

Eifler, K., Vertegaal, A.C.O., 2015. Mapping the SUMOylated landscape. FEBS J. 282, 3669–3680. https://doi.org/10.1111/febs.13378

Elkabetz, Y., Panagiotakos, G., Al Shamy, G., Socci, N.D., Tabar, V., Studer, L., 2008. Human ES cell-derived neural rosettes reveal a functionally distinct early neural stem cell stage. Genes Dev. 22, 152–165. https://doi.org/10.1101/gad.1616208

Elleder, M., Kousi, M., Lehesjoki, A.-E., Mole, S.E., Siintola, E., Topçu, M., 2011. CLN7, in: Mole, S., Williams, R., Goebel, H. (Eds.), The Neuronal Ceroid Lipofuscinoses (Batten Disease). Oxford University Press, p. 0. https://doi.org/10.1093/med/9780199590018.003.0011

Elleder, M., Sokolová, J., Hřebíček, M., 1997. Follow-up study of subunit c of mitochondrial ATP synthase (SCMAS) in Batten disease and in unrelated lysosomal disorders. Acta Neuropathol. (Berl.) 93, 379–390. https://doi.org/10.1007/s004010050629

El-Maghrabi, M.R., Noto, F., Wu, N., Manes, N., 2001. 6-Phosphofructo-2-kinase/fructose-2,6-bisphosphatase: suiting structure to need, in a family of tissue-specific enzymes. Curr. Opin. Clin. Nutr. Metab. Care 4, 411.

Emini Veseli, B., Van Wielendaele, P., Delibegovic, M., Martinet, W., De Meyer, G.R.Y., 2021. The PFKFB3 Inhibitor AZ67 Inhibits Angiogenesis Independently of Glycolysis Inhibition. Int. J. Mol. Sci. 22, 5970. https://doi.org/10.3390/ijms22115970

Enright, A.J., Ouzounis, C.A., 2001. Functional associations of proteins in entire genomes by means of exhaustive detection of gene fusions. Genome Biol. 2, research0034.1. https://doi.org/10.1186/gb-2001-2-9-research0034

Enver, T., Soneji, S., Joshi, C., Brown, J., Iborra, F., Orntoft, T., Thykjaer, T., Maltby, E., Smith, K., Dawud, R.A., Jones, M., Matin, M., Gokhale, P., Draper, J., Andrews, P.W., 2005. Cellular differentiation hierarchies in normal and culture-adapted human embryonic stem cells. Hum. Mol. Genet. 14, 3129–3140. https://doi.org/10.1093/hmg/ddi345

Eskelinen, E.-L., 2006. Roles of LAMP-1 and LAMP-2 in lysosome biogenesis and autophagy. Mol. Aspects Med., Autophagy 27, 495–502. https://doi.org/10.1016/j.mam.2006.08.005

Eskelinen, E.-L., 2005. Maturation of Autophagic Vacuoles in Mammalian Cells. Autophagy 1, 1–10. https://doi.org/10.4161/auto.1.1.1270

Exner, N., Lutz, A.K., Haass, C., Winklhofer, K.F., 2012. Mitochondrial dysfunction in Parkinson's disease: molecular mechanisms and pathophysiological consequences. EMBO J. 31, 3038–3062. https://doi.org/10.1038/emboj.2012.170

Fader, C.M., Sánchez, D.G., Mestre, M.B., Colombo, M.I., 2009. TI-VAMP/VAMP7 and VAMP3/cellubrevin: two v-SNARE proteins involved in specific steps of the autophagy/multivesicular body pathways. Biochim. Biophys. Acta BBA - Mol. Cell Res. 1793, 1901–1916. https://doi.org/10.1016/j.bbamcr.2009.09.011

Faller, K.M.E., Bras, J., Sharpe, S.J., Anderson, G.W., Darwent, L., Kun-Rodrigues, C., Alroy, J., Penderis, J., Mole, S.E., Gutierrez-Quintana, R., Guerreiro, R.J., 2016. The Chihuahua dog: A new animal model for neuronal ceroid lipofuscinosis CLN7 disease? J. Neurosci. Res. 94, 339–347. https://doi.org/10.1002/jnr.23710

Feligioni, M., Nisticò, R., 2013. SUMO: a (Oxidative) Stressed Protein. NeuroMolecular Med. 15, 707–719. https://doi.org/10.1007/s12017-013-8266-6

Finkel, R.S., Chiriboga, C.A., Vajsar, J., Day, J.W., Montes, J., Vivo, D.C.D., Yamashita, M., Rigo, F., Hung, G., Schneider, E., Norris, D.A., Xia, S., Bennett, C.F., Bishop, K.M., 2016. Treatment of infantile-onset spinal muscular atrophy with nusinersen: a phase 2, open-label, dose-escalation study. The Lancet 388, 3017–3026. https://doi.org/10.1016/S0140-6736(16)31408-8

Fisher, E., Almaguer, C., Holic, R., Griac, P., Patton-Vogt, J., 2005. Glycerophosphocholine-dependent Growth Requires Gde1p (YPL110c) and Git1p in Saccharomyces cerevisiae*. J. Biol. Chem. 280, 36110–36117. https://doi.org/10.1074/jbc.M507051200

FitzPatrick, L.M., Hawkins, K.E., Delhove, J.M.K.M., Fernandez, E., Soldati, C., Bullen, L.F., Nohturfft, A., Waddington, S.N., Medina, D.L., Bolaños, J.P., McKay, T.R., 2018. NF-κB Activity Initiates Human ESC-Derived Neural Progenitor Cell Differentiation by Inducing a Metabolic

Maturation Program. Stem Cell Rep. 10, 1766–1781. https://doi.org/10.1016/j.stemcr.2018.03.015

Flotho, A., Melchior, F., 2013. Sumoylation: A Regulatory Protein Modification in Health and Disease. Annu. Rev. Biochem. 82, 357–385. https://doi.org/10.1146/annurev-biochem-061909-093311

Fong, H., Hohenstein, K.A., Donovan, P.J., 2008. Regulation of Self-Renewal and Pluripotency by Sox2 in Human Embryonic Stem Cells. Stem Cells 26, 1931–1938. https://doi.org/10.1634/stemcells.2007-1002

Forrest, A.R., Taylor, D.F., Fink, J.L., Gongora, M.M., Flegg, C., Teasdale, R.D., Suzuki, H., Kanamori, M., Kai, C., Hayashizaki, Y., Grimmond, S.M., 2006. PhosphoregDB: The tissue and sub-cellular distribution of mammalian protein kinases and phosphatases. BMC Bioinformatics 7, 82. https://doi.org/10.1186/1471-2105-7-82

Fraser, M.J., Smith, G.E., Summers, M.D., 1983. Acquisition of Host Cell DNA Sequences by Baculoviruses: Relationship Between Host DNA Insertions and FP Mutants of Autographa californica and Galleria mellonella Nuclear Polyhedrosis Viruses. J. Virol. 47, 287–300. https://doi.org/10.1128/jvi.47.2.287-300.1983

Fujikake, N., Shin, M., Shimizu, S., 2018. Association Between Autophagy and Neurodegenerative Diseases. Front. Neurosci. 12.

Fukuda, M., 1991. Lysosomal membrane glycoproteins. Structure, biosynthesis, and intracellular trafficking. J. Biol. Chem. 266, 21327–21330. https://doi.org/10.1016/S0021-9258(18)54636-6

Füllgrabe, J., Klionsky, D.J., Joseph, B., 2014. The return of the nucleus: transcriptional and epigenetic control of autophagy. Nat. Rev. Mol. Cell Biol. 15, 65–74. https://doi.org/10.1038/nrm3716

Fürst, W., Machleidt, W., Sandhoff, K., 1988. The Precursor of Sulfatide Activator Protein is Processed to Three Different Proteins 369, 317–328. https://doi.org/10.1515/bchm3.1988.369.1.317

Furuta, N., Amano, A., 2010. Cellular machinery to fuse antimicrobial autophagosome with lysosome. Commun. Integr. Biol. 3, 385–387. https://doi.org/10.4161/cib.3.4.12030

Furuta A, Kikuchi H, Fujita H, Yamada D, Fujiwara Y, Kabuta T, Nishino I, Wada K, Uchiyama Y. 2015. Property of lysosomal storage disease associated with midbrain pathology in the central nervous system of Lamp-2-deficient mice. Am J Pathol. 185(6):1713-23. https://doi.org/10.1016/j.ajpath.2015.02.015

Fusaki, N., Ban, H., Nishiyama, A., Saeki, K., Hasegawa, M., 2009. Efficient induction of transgene-free human pluripotent stem cells using a vector based on Sendai virus, an RNA virus that does not integrate into the host genome. Proc. Jpn. Acad. Ser. B 85, 348–362. https://doi.org/10.2183/pjab.85.348

Futerman, A.H., van Meer, G., 2004. The cell biology of lysosomal storage disorders. Nat. Rev. Mol. Cell Biol. 5, 554–565. https://doi.org/10.1038/nrm1423

Gallala, H.D., Sandhoff, K., 2011. Biological Function of the Cellular Lipid BMP—BMP as a Key Activator for Cholesterol Sorting and Membrane Digestion. Neurochem. Res. 36, 1594–1600. https://doi.org/10.1007/s11064-010-0337-6

Ganley, I.G., Wong, P.-M., Gammoh, N., Jiang, X., 2011. Distinct Autophagosomal-Lysosomal Fusion Mechanism Revealed by Thapsigargin-Induced Autophagy Arrest. Mol. Cell 42, 731–743. https://doi.org/10.1016/j.molcel.2011.04.024

Gao, F.-B., Almeida, S., Lopez-Gonzalez, R., 2017. Dysregulated molecular pathways in amyotrophic lateral sclerosis–frontotemporal dementia spectrum disorder. EMBO J. 36, 2931–2950. https://doi.org/10.15252/embj.201797568

García-Nogales, P., Almeida, A., Bolaños, J.P., 2003. Peroxynitrite Protects Neurons against Nitric Oxide-mediated Apoptosis: A KEY ROLE FOR GLUCOSE-6-PHOSPHATE DEHYDROGENASE ACTIVITY IN NEUROPROTECTION *. J. Biol. Chem. 278, 864–874. https://doi.org/10.1074/jbc.M206835200

Gardner, E., Mole, S.E., 2021. The Genetic Basis of Phenotypic Heterogeneity in the Neuronal Ceroid Lipofuscinoses. Front. Neurol. 12.

Gąsiorkiewicz BM, Koczurkiewicz-Adamczyk P, Piska K, Pękala E. 2021. Autophagy modulating agents as chemosensitizers for cisplatin therapy in cancer. Invest New Drugs. 39(2):538-563. https://doi.org/10.1007/s10637-020-01032-y

Gayi, E., Neff, L.A., Massana Muñoz, X., Ismail, H.M., Sierra, M., Mercier, T., Décosterd, L.A., Laporte, J., Cowling, B.S., Dorchies, O.M., Scapozza, L., 2018. Tamoxifen prolongs survival and alleviates symptoms in mice with fatal X-linked myotubular myopathy. Nat. Commun. 9, 4848. https://doi.org/10.1038/s41467-018-07058-4

Geier, E.G., Bourdenx, M., Storm, N.J., Cochran, J.N., Sirkis, D.W., Hwang, J.-H., Bonham, L.W., Ramos, E.M., Diaz, A., Van Berlo, V., Dokuru, D., Nana, A.L., Karydas, A., Balestra, M.E., Huang, Y., Russo, S.P., Spina, S., Grinberg, L.T., Seeley, W.W., Myers, R.M., Miller, B.L., Coppola, G., Lee, S.E., Cuervo, A.M., Yokoyama, J.S., 2019. Rare variants in the neuronal ceroid lipofuscinosis gene MFSD8 are candidate risk factors for frontotemporal dementia. Acta Neuropathol. (Berl.) 137, 71–88. https://doi.org/10.1007/s00401-018-1925-9

Germain, D.P., 2010. Fabry disease. Orphanet J. Rare Dis. 5, 30. https://doi.org/10.1186/1750-1172-5-30

Gibson, G.E., Sheu, K.-F.R., Blass, J.P., 1998. Abnormalities of mitochondrial enzymes in Alzheimer disease. J. Neural Transm. 105, 855–870. https://doi.org/10.1007/s007020050099

Gillooly, D.J., Morrow, I.C., Lindsay, M., Gould, R., Bryant, N.J., Gaullier, J.-M., Parton, R.G., Stenmark, H., 2000. Localization of phosphatidylinositol 3-phosphate in yeast and mammalian cells. EMBO J. 19, 4577–4588. https://doi.org/10.1093/emboj/19.17.4577

Gilyarov, A.V., 2008. Nestin in central nervous system cells. Neurosci. Behav. Physiol. 38, 165–169. https://doi.org/10.1007/s11055-008-0025-z

Girard, E., Chmiest, D., Fournier, N., Johannes, L., Paul, J.-L., Vedie, B., Lamaze, C., 2014. Rab7 Is Functionally Required for Selective Cargo Sorting at the Early Endosome. Traffic 15, 309–326. https://doi.org/10.1111/tra.12143

Glaser, T., Pollard, S.M., Smith, A., Brüstle, O., 2007. Tripotential Differentiation of Adherently Expandable Neural Stem (NS) Cells. PLoS ONE 2, e298. https://doi.org/10.1371/journal.pone.0000298

Glass, M., Dragunow, M., Faull, R.L.M., 2000. The pattern of neurodegeneration in Huntington's disease: a comparative study of cannabinoid, dopamine, adenosine and GABAA receptor alterations in the human basal ganglia in Huntington's disease. Neuroscience 97, 505–519. https://doi.org/10.1016/S0306-4522(00)00008-7

Goebel, H.H., 1995. Topical Review: The Neuronal Ceroid-Lipofuscinoses. J. Child Neurol. 10, 424–437. https://doi.org/10.1177/088307389501000602

Goldstein, L.J., Brown, S.M., 1977. The Low-Density Lipoprotein Pathway and its Relation to Atherosclerosis. Annu. Rev. Biochem. 46, 897–930. https://doi.org/10.1146/annurev.bi.46.070177.004341

Gong, W., Zhou, D., Ren, Y., Wang, Y., Zuo, Z., Shen, Y., Xiao, F., Zhu, Q., Hong, A., Zhou, X., Gao, X., Li, T., 2008. PepCyber:P∼PEP: a database of human protein–protein interactions mediated by phosphoprotein-binding domains. Nucleic Acids Res. 36, D679–D683. https://doi.org/10.1093/nar/gkm854

Gorno-Tempini, M.L., Hillis, A.E., Weintraub, S., Kertesz, A., Mendez, M., Cappa, S.F., Ogar, J.M., Rohrer, J.D., Black, S., Boeve, B.F., Manes, F., Dronkers, N.F., Vandenberghe, R., Rascovsky, K., Patterson, K., Miller, B.L., Knopman, D.S., Hodges, J.R., Mesulam, M.M., Grossman, M., 2011. Classification of primary progressive aphasia and its variants. Neurology 76, 1006–1014. https://doi.org/10.1212/WNL.0b013e31821103e6

Gorvel, J.-P., Chavrier, P., Zerial, M., Gruenberg, J., 1991. rab5 controls early endosome fusion in vitro. Cell 64, 915–925. https://doi.org/10.1016/0092-8674(91)90316-Q

Goulabchand, R., Vincent, T., Batteux, F., Eliaou, J., Guilpain, P., 2014. Impact of autoantibody glycosylation in autoimmune diseases. Autoimmun. Rev. 13, 742–750. https://doi.org/10.1016/j.autrev.2014.02.005

Granger, B.L., Green, S.A., Gabel, C.A., Howe, C.L., Mellman, I., Helenius, A., 1990. Characterization and cloning of lgp110, a lysosomal membrane glycoprotein from mouse and rat cells. J. Biol. Chem. 265, 12036–12043. https://doi.org/10.1016/S0021-9258(19)38504-7

Grskovic, M., Javaherian, A., Strulovici, B., Daley, G.Q., 2011. Induced pluripotent stem cells — opportunities for disease modelling and drug discovery. Nat. Rev. Drug Discov. 10, 915–929. https://doi.org/10.1038/nrd3577

Gruenberg, J., Maxfield, F.R., 1995. Membrane transport in the endocytic pathway. Curr. Opin. Cell Biol. 7, 552–563. https://doi.org/10.1016/0955-0674(95)80013-1

Guadagno NA, Progida C. 2019. Rab GTPases: Switching to Human Diseases. Cells. 8(8):909. https://doi.org/10.3390/cells8080909

Guala, D., Ogris, C., Müller, N., Sonnhammer, E.L.L., 2020. Genome-wide functional association networks: background, data & state-of-the-art resources. Brief. Bioinform. 21, 1224–1237. https://doi.org/10.1093/bib/bbz064

Gunhanlar, N., Shpak, G., van der Kroeg, M., Gouty-Colomer, L.A., Munshi, S.T., Lendemeijer, B., Ghazvini, M., Dupont, C., Hoogendijk, W.J.G., Gribnau, J., de Vrij, F.M.S., Kushner, S.A., 2018. A simplified protocol for differentiation of electrophysiologically mature neuronal networks from human induced pluripotent stem cells. Mol. Psychiatry 23, 1336–1344. https://doi.org/10.1038/mp.2017.56

Guo, J., O'Brien, D.P., Mhlanga-Mutangadura, T., Olby, N.J., Taylor, J.F., Schnabel, R.D., Katz, M.L., Johnson, G.S., 2015. A rare homozygous MFSD8 single-base-pair deletion and frameshift in the whole genome sequence of a Chinese Crested dog with neuronal ceroid lipofuscinosis. BMC Vet. Res. 10, 960. https://doi.org/10.1186/s12917-014-0181-z

Gurdon, J.B., 1962. The Developmental Capacity of Nuclei taken from Intestinal Epithelium Cells of Feeding Tadpoles. Development 10, 622–640. https://doi.org/10.1242/dev.10.4.622

Gurdon, J.B., Elsdale, T.R., Fischberg, M., 1958. Sexually Mature Individuals of Xenopus laevis from the Transplantation of Single Somatic Nuclei. Nature 182, 64–65. https://doi.org/10.1038/182064a0

Habersetzer, J., Ziani, W., Larrieu, I., Stines-Chaumeil, C., Giraud, M.-F., Brèthes, D., Dautant, A., Paumard, P., 2013. ATP synthase oligomerization: From the enzyme models to the mitochondrial morphology. Int. J. Biochem. Cell Biol., Directed Issue: Bioenergetic Dysfunction, Adaptation and Therapy 45, 99–105. https://doi.org/10.1016/j.biocel.2012.05.017

Hailey, D.W., Rambold, A.S., Satpute-Krishnan, P., Mitra, K., Sougrat, R., Kim, P.K., Lippincott-Schwartz, J., 2010. Mitochondria Supply Membranes for Autophagosome Biogenesis during Starvation. Cell 141, 656–667. https://doi.org/10.1016/j.cell.2010.04.009

Halliwell RF, Salmanzadeh H, Coyne L, Cao WS. An Electrophysiological and Pharmacological Study of the Properties of Human iPSC-Derived Neurons for Drug Discovery. Cells. 2021 Jul 31;10(8):1953. https://doi.org/10.3390/cells10081953

Haltia, M., 2003. The Neuronal Ceroid-Lipofuscinoses. J. Neuropathol. Exp. Neurol. 62, 1–13. https://doi.org/10.1093/jnen/62.1.1

Haltia, M., Rapola, J., Santavuori, P., Keränen, A., 1973. Infantile type of so-called neuronal ceroid-lipofuscinosis: Part 2. Morphological and biochemical studies. J. Neurol. Sci. 18, 269–285. https://doi.org/10.1016/0022-510X(73)90076-2

Haltiwanger, R.S., Lowe, J.B., 2004. Role of Glycosylation in Development. Annu. Rev. Biochem. 73, 491–537. https://doi.org/10.1146/annurev.biochem.73.011303.074043

Hamel, C., 2006. Retinitis pigmentosa. Orphanet J. Rare Dis. 1, 40. https://doi.org/10.1186/1750-1172-1-40

Hamel, C.P., 2007. Cone rod dystrophies. Orphanet J. Rare Dis. 2, 7. https://doi.org/10.1186/1750-1172-2-7

Han, J., Pluhackova, K., Böckmann, R.A., 2017. The Multifaceted Role of SNARE Proteins in Membrane Fusion. Front. Physiol. 8.

Han, X., Chen, M., Wang, F., Windrem, M., Wang, S., Shanz, S., Xu, Q., Oberheim, N.A., Bekar, L., Betstadt, S., Silva, A.J., Takano, T., Goldman, S.A., Nedergaard, M., 2013. Forebrain

Engraftment by Human Glial Progenitor Cells Enhances Synaptic Plasticity and Learning in Adult Mice. Cell Stem Cell 12, 342–353. https://doi.org/10.1016/j.stem.2012.12.015

Hanada, T., Noda, N.N., Satomi, Y., Ichimura, Y., Fujioka, Y., Takao, T., Inagaki, F., Ohsumi, Y., 2007. The Atg12-Atg5 Conjugate Has a Novel E3-like Activity for Protein Lipidation in Autophagy *. J. Biol. Chem. 282, 37298–37302. https://doi.org/10.1074/jbc.C700195200

Hara, K., Yonezawa, K., Kozlowski, M.T., Sugimoto, T., Andrabi, K., Weng, Q.-P., Kasuga, M., Nishimoto, I., Avruch, J., 1997. Regulation of eIF-4E BP1 Phosphorylation by mTOR *. J. Biol. Chem. 272, 26457–26463. https://doi.org/10.1074/jbc.272.42.26457

Hara, T., Nakamura, K., Matsui, M., Yamamoto, A., Nakahara, Y., Suzuki-Migishima, R., Yokoyama, M., Mishima, K., Saito, I., Okano, H., Mizushima, N., 2006. Suppression of basal autophagy in neural cells causes neurodegenerative disease in mice. Nature 441, 885–889. https://doi.org/10.1038/nature04724

Harrison, R.E., Bucci, C., Vieira, O.V., Schroer, T.A., Grinstein, S., 2003. Phagosomes Fuse with Late Endosomes and/or Lysosomes by Extension of Membrane Protrusions along Microtubules: Role of Rab7 and RILP. Mol. Cell. Biol. 23, 6494–6506. https://doi.org/10.1128/MCB.23.18.6494-6506.2003

Hartung, T., 2008. Thoughts on limitations of animal models. Parkinsonism Relat. Disord. 14, S81–S83. https://doi.org/10.1016/j.parkreldis.2008.04.003

Hay, D.C., Sutherland, L., Clark, J., Burdon, T., 2004. Oct-4 Knockdown Induces Similar Patterns of Endoderm and Trophoblast Differentiation Markers in Human and Mouse Embryonic Stem Cells. Stem Cells 22, 225–235. https://doi.org/10.1634/stemcells.22-2-225

Hayashi-Nishino, M., Fujita, N., Noda, T., Yamaguchi, A., Yoshimori, T., Yamamoto, A., 2009. A subdomain of the endoplasmic reticulum forms a cradle for autophagosome formation. Nat. Cell Biol. 11, 1433–1437. https://doi.org/10.1038/ncb1991

He, C., Levine, B., 2010. The Beclin 1 interactome. Curr. Opin. Cell Biol., Cell regulation 22, 140–149. https://doi.org/10.1016/j.ceb.2010.01.001

Heine, C., Koch, B., Storch, S., Kohlschütter, A., Palmer, D.N., Braulke, T., 2004. Defective Endoplasmic Reticulum-resident Membrane Protein CLN6 Affects Lysosomal Degradation of Endocytosed Arylsulfatase A *. J. Biol. Chem. 279, 22347–22352. https://doi.org/10.1074/jbc.M400643200

Hellsten, E., Vesa, J., Olkkonen, V.M., Jalanko, A., Peltonen, L., 1996. Human palmitoyl protein thioesterase: evidence for lysosomal targeting of the enzyme and disturbed cellular routing in infantile neuronal ceroid lipofuscinosis. EMBO J. 15, 5240–5245. https://doi.org/10.1002/j.1460-2075.1996.tb00909.x

Henderson, J.K., Draper, J.S., Baillie, H.S., Fishel, S., Thomson, J.A., Moore, H., Andrews, P.W., 2002. Preimplantation Human Embryos and Embryonic Stem Cells Show Comparable Expression of Stage-Specific Embryonic Antigens. Stem Cells 20, 329–337. https://doi.org/10.1634/stemcells.20-4-329

Herrero-Mendez, A., Almeida, A., Fernández, E., Maestre, C., Moncada, S., Bolaños, J.P., 2009. The bioenergetic and antioxidant status of neurons is controlled by continuous degradation of a

key glycolytic enzyme by APC/C–Cdh1. Nat. Cell Biol. 11, 747–752. https://doi.org/10.1038/ncb1881

Heurtier, V., Owens, N., Gonzalez, I., Mueller, F., Proux, C., Mornico, D., Clerc, P., Dubois, A., Navarro, P., 2019. The molecular logic of Nanog-induced self-renewal in mouse embryonic stem cells. Nat. Commun. 10, 1109. https://doi.org/10.1038/s41467-019-09041-z

Hiraiwa, M., Obrien, J.S., Kishimoto, Y., Galdzicka, M., Fluharty, A.L., Ginns, E.I., Martin, B.M., 1993. Isolation, Characterization, and Proteolysis of Human Prosaposin, the Precursor of Saposins (Sphingolipid Activator Proteins). Arch. Biochem. Biophys. 304, 110–116. https://doi.org/10.1006/abbi.1993.1328

Hiraiwa, M., Taylor, E.M., Campana, W.M., Darin, S.J., O'Brien, J.S., 1997. Cell death prevention, mitogen-activated protein kinase stimulation, and increased sulfatide concentrations in Schwann cells and oligodendrocytes by prosaposin and prosaptides. Proc. Natl. Acad. Sci. 94, 4778–4781. https://doi.org/10.1073/pnas.94.9.4778

Hobson, E.V., McDermott, C.J., 2016. Supportive and symptomatic management of amyotrophic lateral sclerosis. Nat. Rev. Neurol. 12, 526–538. https://doi.org/10.1038/nrneurol.2016.111

Hossain, M.I., Marcus, J.M., Lee, J.H., Garcia, P.L., Singh, V., Shacka, J.J., Zhang, J., Gropen, T.I., Falany, C.N., Andrabi, S.A., 2021. Restoration of CTSD (cathepsin D) and lysosomal function in stroke is neuroprotective. Autophagy 17, 1330–1348. https://doi.org/10.1080/15548627.2020.1761219

Hothersall, J.S., Baquer, N.Z., Greenbaum, A.L., McLean, P., 1979. Alternative pathways of glucose utilization in brain. Changes in the pattern of glucose utilization in brain during development and the effect of phenazine methosulfate on the integration of metabolic routes. Arch. Biochem. Biophys. 198, 478–492. https://doi.org/10.1016/0003-9861(79)90522-8

Hu, B.-Y., Weick, J.P., Yu, J., Ma, L.-X., Zhang, X.-Q., Thomson, J.A., Zhang, S.-C., 2010. Neural differentiation of human induced pluripotent stem cells follows developmental principles but with variable potency. Proc. Natl. Acad. Sci. 107, 4335–4340. https://doi.org/10.1073/pnas.0910012107

Huang, K.-Y., Lee, T.-Y., Kao, H.-J., Ma, C.-T., Lee, C.-C., Lin, T.-H., Chang, W.-C., Huang, H.-D., 2019. dbPTM in 2019: exploring disease association and cross-talk of post-translational modifications. Nucleic Acids Res. 47, D298–D308. https://doi.org/10.1093/nar/gky1074

Huber, R.J., 2016. Using the social amoeba Dictyostelium to study the functions of proteins linked to neuronal ceroid lipofuscinosis. J. Biomed. Sci. 23, 83. https://doi.org/10.1186/s12929-016-0301-0

Huber, R.J., Mathavarajah, S., Yap, S.Q., 2020. Mfsd8 localizes to endocytic compartments and influences the secretion of Cln5 and cathepsin D in Dictyostelium. Cell. Signal. 70, 109572. https://doi.org/10.1016/j.cellsig.2020.109572

Huotari, J., Helenius, A., 2011. Endosome maturation. EMBO J. 30, 3481–3500. https://doi.org/10.1038/emboj.2011.286

Hyslop, L., Stojkovic, M., Armstrong, L., Walter, T., Stojkovic, P., Przyborski, S., Herbert, M., Murdoch, A., Strachan, T., Lako, M., 2005. Downregulation of NANOG Induces Differentiation

of Human Embryonic Stem Cells to Extraembryonic Lineages. Stem Cells 23, 1035–1043. https://doi.org/10.1634/stemcells.2005-0080

Hyttinen, J.M.T., Niittykoski, M., Salminen, A., Kaarniranta, K., 2013. Maturation of autophagosomes and endosomes: A key role for Rab7. Biochim. Biophys. Acta BBA - Mol. Cell Res. 1833, 503–510. https://doi.org/10.1016/j.bbamcr.2012.11.018

Iberite F, Gruppioni E, Ricotti L. Skeletal muscle differentiation of human iPSCs meets bioengineering strategies: perspectives and challenges. NPJ Regen Med. 2022 Apr 7;7(1):23. https://doi.org/10.1038/s41536-022-00216-9

Ichimura, Y., Kirisako, T., Takao, T., Satomi, Y., Shimonishi, Y., Ishihara, N., Mizushima, N., Tanida, I., Kominami, E., Ohsumi, M., Noda, T., Ohsumi, Y., 2000. A ubiquitin-like system mediates protein lipidation. Nature 408, 488–492. https://doi.org/10.1038/35044114

International Human Genome Sequencing Consortium, 2004. Finishing the euchromatic sequence of the human genome. Nature 431, 931–945. https://doi.org/10.1038/nature03001

Isosomppi, J., Vesa, J., Jalanko, A., Peltonen, L., 2002. Lysosomal localization of the neuronal ceroid lipofuscinosis CLN5 protein. Hum. Mol. Genet. 11, 885–891. https://doi.org/10.1093/hmg/11.8.885

Iwata, R., Vanderhaeghen, P., 2021. Regulatory roles of mitochondria and metabolism in neurogenesis. Curr. Opin. Neurobiol., Molecular Neuroscience 69, 231–240. https://doi.org/10.1016/j.conb.2021.05.003

Jaeger PA, Wyss-Coray T. 2010. Beclin 1 complex in autophagy and Alzheimer disease. Arch Neurol. 67(10):1181-4. https://doi.org/10.1001/archneurol.2010.258

Jaenisch, R., Young, R., 2008. Stem Cells, the Molecular Circuitry of Pluripotency and Nuclear Reprogramming. Cell. https://doi.org/10.1016/j.cell.2008.01.015

Jalanko, A., Braulke, T., 2009. Neuronal ceroid lipofuscinoses. Biochim. Biophys. Acta BBA - Mol. Cell Res., Lysosomes 1793, 697–709. https://doi.org/10.1016/j.bbamcr.2008.11.004

James, M.N.G., 1999. Handbook of proteolytic enzymes, edited by A. J. Barrett, N. D. Rawlings, and J. F. Woessner. 1998. London: Academic Press. 1666 pp. \250.00. \90.00 for the CD-ROM. Protein Sci. 8, 693–694. https://doi.org/10.1110/ps.8.3.693

Jankowiak, W., Brandenstein, L., Dulz, S., Hagel, C., Storch, S., Bartsch, U., 2016. Retinal Degeneration in Mice Deficient in the Lysosomal Membrane Protein CLN7. Invest. Ophthalmol. Vis. Sci. 57, 4989–4998. https://doi.org/10.1167/iovs.16-20158

Jankowsky, J.L., Savonenko, A., Schilling, G., Wang, J., Xu, G., Borchelt, D.R., 2002. Transgenic mouse models of neurodegenerative disease: Opportunities for therapeutic development. Curr. Neurol. Neurosci. Rep. 2, 457–464. https://doi.org/10.1007/s11910-002-0073-7

Jankowsky, J.L., Zheng, H., 2017. Practical considerations for choosing a mouse model of Alzheimer's disease. Mol. Neurodegener. 12, 89. https://doi.org/10.1186/s13024-017-0231-7

Järvelä, I., Sainio, M., Rantamäki, T., Olkkonen, V.M., Carpén, O., Peltonen, L., Jalanko, A., 1998. Biosynthesis and Intracellular Targeting of the CLN3 Protein Defective in Batten Disease. Hum. Mol. Genet. 7, 85–90. https://doi.org/10.1093/hmg/7.1.85

Jentsch, S., Psakhye, I., 2013. Control of Nuclear Activities by Substrate-Selective and Protein-Group SUMOylation. Annu. Rev. Genet. 47, 167–186. https://doi.org/10.1146/annurev-genet-111212-133453

Jeong, H., Mason, S.P., Barabási, A.-L., Oltvai, Z.N., 2001. Lethality and centrality in protein networks. Nature 411, 41–42. https://doi.org/10.1038/35075138

Jiang, X., Yang, Z., Dong, M., 2020. Cardiac repair in a murine model of myocardial infarction with human induced pluripotent stem cell-derived cardiomyocytes. Stem Cell Res. Ther. 11, 297. https://doi.org/10.1186/s13287-020-01811-7

Jin, J., Liu, J., Chen, C., Liu, Z., Jiang, Cong, Chu, H., Pan, W., Wang, X., Zhang, L., Li, B., Jiang, Cizhong, Ge, X., Xie, X., Wang, P., 2016. The deubiquitinase USP21 maintains the stemness of mouse embryonic stem cells via stabilization of Nanog. Nat. Commun. 7, 13594. https://doi.org/10.1038/ncomms13594

Jin, J., Pawson, T., 2012. Modular evolution of phosphorylation-based signalling systems. Philos. Trans. R. Soc. B Biol. Sci. 367, 2540–2555. https://doi.org/10.1098/rstb.2012.0106

Jordan KL, Koss DJ, Outeiro TF, Giorgini F. 2022. Therapeutic Targeting of Rab GTPases: Relevance for Alzheimer's Disease. Biomedicines. 10(5):1141. https://doi.org/10.3390/biomedicines10051141

Joshi, A.U., Minhas, P.S., Liddelow, S.A., Haileselassie, B., Andreasson, K.I., Dorn, G.W., Mochly-Rosen, D., 2019. Fragmented mitochondria released from microglia trigger A1 astrocytic response and propagate inflammatory neurodegeneration. Nat. Neurosci. 22, 1635–1648. https://doi.org/10.1038/s41593-019-0486-0

Jovic, M., Sharma, M., Rahajeng, J., Caplan, S., 2010. The early endosome: a busy sorting station for proteins at the crossroads. Histol. Histopathol. 25, 99–112. https://doi.org/10.14670/HH-25.99

Kabeya, Y., Mizushima, N., Ueno, T., Yamamoto, A., Kirisako, T., Noda, T., Kominami, E., Ohsumi, Y., Yoshimori, T., 2000. LC3, a mammalian homologue of yeast Apg8p, is localized in autophagosome membranes after processing. EMBO J. 19, 5720–5728. https://doi.org/10.1093/emboj/19.21.5720

Kaji, K., Norrby, K., Paca, A., Mileikovsky, M., Mohseni, P., Woltjen, K., 2009. Virus-free induction of pluripotency and subsequent excision of reprogramming factors. Nature 458, 771–775. https://doi.org/10.1038/nature07864

Kang, R., Zeh, H.J., Lotze, M.T., Tang, D., 2011. The Beclin 1 network regulates autophagy and apoptosis. Cell Death Differ. 18, 571–580. https://doi.org/10.1038/cdd.2010.191

Kang, S., Chen, X., Gong, S., Yu, P., Yau, S., Su, Z., Zhou, L., Yu, J., Pan, G., Shi, L., 2017. Characteristic analyses of a neural differentiation model from iPSC-derived neuron according to morphology, physiology, and global gene expression pattern. Sci. Rep. 7, 12233. https://doi.org/10.1038/s41598-017-12452-x

Kannagi, R., Cochran, N. a., Ishigami, F., Hakomori, S., Andrews, P. w., Knowles, B. b., Solter, D., 1983. Stage-specific embryonic antigens (SSEA-3 and -4) are epitopes of a unique globo-series ganglioside isolated from human teratocarcinoma cells. EMBO J. 2, 2355–2361. https://doi.org/10.1002/j.1460-2075.1983.tb01746.x

Kapucu FE, Vinogradov A, Hyvärinen T, Ylä-Outinen L, Narkilahti S. 2022. Comparative microelectrode array data of the functional development of hPSC-derived and rat neuronal networks. Sci Data. 30;9(1):120. https://doi.org/10.1038/s41597-022-01242-4

Karagiannis, P., Takahashi, K., Saito, M., Yoshida, Y., Okita, K., Watanabe, A., Inoue, H., Yamashita, J.K., Todani, M., Nakagawa, M., Osawa, M., Yashiro, Y., Yamanaka, S., Osafune, K., 2019. Induced Pluripotent Stem Cells and Their Use in Human Models of Disease and Development. Physiol. Rev. 99, 79–114. https://doi.org/10.1152/physrev.00039.2017

Karve, T.M., Cheema, A.K., 2011. Small Changes Huge Impact: The Role of Protein Posttranslational Modifications in Cellular Homeostasis and Disease. J. Amino Acids 2011, e207691. https://doi.org/10.4061/2011/207691

Katz, M.L., Rustad, E., Robinson, G.O., Whiting, R.E.H., Student, J.T., Coates, J.R., Narfstrom, K., 2017. Canine neuronal ceroid lipofuscinoses: Promising models for preclinical testing of therapeutic interventions. Neurobiol. Dis. 108, 277–287. https://doi.org/10.1016/j.nbd.2017.08.017

Kaushik, S., Rodriguez-Navarro, J.A., Arias, E., Kiffin, R., Sahu, S., Schwartz, G.J., Cuervo, A.M., Singh, R., 2011. Autophagy in Hypothalamic AgRP Neurons Regulates Food Intake and Energy Balance. Cell Metab. 14, 173–183. https://doi.org/10.1016/j.cmet.2011.06.008

Khacho, M., Clark, A., Svoboda, D.S., MacLaurin, J.G., Lagace, D.C., Park, D.S., Slack, R.S., 2017. Mitochondrial dysfunction underlies cognitive defects as a result of neural stem cell depletion and impaired neurogenesis. Hum. Mol. Genet. 26, 3327–3341. https://doi.org/10.1093/hmg/ddx217

Khaminets, A., Heinrich, T., Mari, M., Grumati, P., Huebner, A.K., Akutsu, M., Liebmann, L., Stolz, A., Nietzsche, S., Koch, N., Mauthe, M., Katona, I., Qualmann, B., Weis, J., Reggiori, F., Kurth, I., Hübner, C.A., Dikic, I., 2015. Regulation of endoplasmic reticulum turnover by selective autophagy. Nature 522, 354–358. https://doi.org/10.1038/nature14498

Khan, K.N., El-Asrag, M.E., Ku, C.A., Holder, G.E., McKibbin, M., Arno, G., Poulter, J.A., Carss, K., Bommireddy, T., Bagheri, S., Bakall, B., Scholl, H.P., Raymond, F.L., Toomes, C., Inglehearn, C.F., Pennesi, M.E., Moore, A.T., Michaelides, M., Webster, A.R., Ali, M., for NIHR BioResource-Rare Diseases and UK Inherited Retinal Disease Consortium, 2017. Specific Alleles of CLN7/MFSD8, a Protein That Localizes to Photoreceptor Synaptic Terminals, Cause a Spectrum of Nonsyndromic Retinal Dystrophy. Invest. Ophthalmol. Vis. Sci. 58, 2906–2914. https://doi.org/10.1167/iovs.16-20608

Kim, D., Kim, C.-H., Moon, J.-I., Chung, Y.-G., Chang, M.-Y., Han, B.-S., Ko, S., Yang, E., Cha, K.Y., Lanza, R., Kim, K.-S., 2009. Generation of Human Induced Pluripotent Stem Cells by Direct Delivery of Reprogramming Proteins. Cell Stem Cell 4, 472–476. https://doi.org/10.1016/j.stem.2009.05.005

Kim, J., Hu, C., Moufawad El Achkar, C., Black, L.E., Douville, J., Larson, A., Pendergast, M.K., Goldkind, S.F., Lee, E.A., Kuniholm, A., Soucy, A., Vaze, J., Belur, N.R., Fredriksen, K., Stojkovska, I., Tsytsykova, A., Armant, M., DiDonato, R.L., Choi, J., Cornelissen, L., Pereira, L.M., Augustine, E.F., Genetti, C.A., Dies, K., Barton, B., Williams, L., Goodlett, B.D., Riley, B.L., Pasternak, A., Berry, E.R., Pflock, K.A., Chu, S., Reed, C., Tyndall, K., Agrawal, P.B., Beggs, A.H., Grant, P.E., Urion, D.K., Snyder, R.O., Waisbren, S.E., Poduri, A., Park, P.J., Patterson, A., Biffi, A., Mazzulli, J.R., Bodamer, O., Berde, C.B., Yu, T.W., 2019a. Patient-Customized Oligonucleotide

Therapy for a Rare Genetic Disease. N. Engl. J. Med. 381, 1644–1652. https://doi.org/10.1056/NEJMoa1813279

Kim, T.H., Tsang, B., Vernon, R.M., Sonenberg, N., Kay, L.E., Forman-Kay, J.D., 2019. Phospho-dependent phase separation of FMRP and CAPRIN1 recapitulates regulation of translation and deadenylation. Science 365, 825–829. https://doi.org/10.1126/science.aax4240

Kirkin, V., Lamark, T., Sou, Y.-S., Bjørkøy, G., Nunn, J.L., Bruun, J.-A., Shvets, E., McEwan, D.G., Clausen, T.H., Wild, P., Bilusic, I., Theurillat, J.-P., Øvervatn, A., Ishii, T., Elazar, Z., Komatsu, M., Dikic, I., Johansen, T., 2009. A role for NBR1 in autophagosomal degradation of ubiquitinated substrates. Mol. Cell 33, 505–516. https://doi.org/10.1016/j.molcel.2009.01.020

Kohl, S., Baumann, B., Broghammer, M., Jägle, H., Sieving, P., Kellner, U., Spegal, R., Anastasi, M., Zrenner, E., Sharpe, L.T., Wissinger, B., 2000. Mutations in the CNGB3 gene encoding the β-subunit of the cone photoreceptor cGMP-gated channel are responsible for achromatopsia (ACHM3) linked to chromosome 8q21. Hum. Mol. Genet. 9, 2107–2116. https://doi.org/10.1093/hmg/9.14.2107

Kokjohn, T.A., Roher, A.E., 2009. Amyloid precursor protein transgenic mouse models and Alzheimer's disease: Understanding the paradigms, limitations, and contributions. Alzheimers Dement. 5, 340–347. https://doi.org/10.1016/j.jalz.2009.03.002

Kolesnikova, M., Lima de Carvalho, J.R., Jr., Oh, J.K., Soucy, M., Demirkol, A., Kim, A.H., Tsang, S.H., Breazzano, M.P., 2023. Phenotypic Variability of Retinal Disease Among a Cohort of Patients With Variants in the CLN Genes. Invest. Ophthalmol. Vis. Sci. 64, 23. https://doi.org/10.1167/iovs.64.3.23

Komatsu, M., Waguri, S., Chiba, T., Murata, S., Iwata, J., Tanida, I., Ueno, T., Koike, M., Uchiyama, Y., Kominami, E., Tanaka, K., 2006. Loss of autophagy in the central nervous system causes neurodegeneration in mice. Nature 441, 880–884. https://doi.org/10.1038/nature04723

Koopman, W.J.H., Nijtmans, L.G.J., Dieteren, C.E.J., Roestenberg, P., Valsecchi, F., Smeitink, J.A.M., Willems, P.H.G.M., 2010. Mammalian Mitochondrial Complex I: Biogenesis, Regulation, and Reactive Oxygen Species Generation. Antioxid. Redox Signal. 12, 1431–1470. https://doi.org/10.1089/ars.2009.2743

Kornfeld, S., Mellman, I., 1989. The Biogenesis of Lysosomes. Annu. Rev. Cell Biol. 5, 483–525. https://doi.org/10.1146/annurev.cb.05.110189.002411

Korolchuk, V.I., Mansilla, A., Menzies, F.M., Rubinsztein, D.C., 2009. Autophagy Inhibition Compromises Degradation of Ubiquitin-Proteasome Pathway Substrates. Mol. Cell 33, 517–527. https://doi.org/10.1016/j.molcel.2009.01.021

Kousi, M., Lehesjoki, A.-E., Mole, S.E., 2012. Update of the mutation spectrum and clinical correlations of over 360 mutations in eight genes that underlie the neuronal ceroid lipofuscinoses. Hum. Mutat. 33, 42–63. https://doi.org/10.1002/humu.21624

Kousi, M., Siintola, E., Dvorakova, L., Vlaskova, H., Turnbull, J., Topcu, M., Yuksel, D., Gokben, S., Minassian, B.A., Elleder, M., Mole, S.E., Lehesjoki, A.-E., 2009a. Mutations in CLN7/MFSD8 are a common cause of variant late-infantile neuronal ceroid lipofuscinosis. Brain J. Neurol. 132, 810–819. https://doi.org/10.1093/brain/awn366

Krasnova, O.A., Gursky, V.V., Chabina, A.S., Kulakova, K.A., Alekseenko, L.L., Panova, A.V., Kiselev, S.L., Neganova, I.E., 2022. Prognostic Analysis of Human Pluripotent Stem Cells Based on Their Morphological Portrait and Expression of Pluripotent Markers. Int. J. Mol. Sci. 23, 12902. https://doi.org/10.3390/ijms232112902

Kubli, D.A., Gustafsson, Å.B., 2012. Mitochondria and Mitophagy. Circ. Res. 111, 1208–1221. https://doi.org/10.1161/CIRCRESAHA.112.265819

Kumar, A., Pareek, V., Faiq, M.A., Kumar, P., Kumari, C., Singh, H.N., Ghosh, S.K., 2020. Transcriptomic analysis of the signature of neurogenesis in human hippocampus suggests restricted progenitor cell progression post-childhood. IBRO Rep. 9, 224–232. https://doi.org/10.1016/j.ibror.2020.08.003

Kumar, A., Zhang, K.Y.J., 2015. Advances in the development of SUMO specific protease (SENP) inhibitors. Comput. Struct. Biotechnol. J. 13, 204–211. https://doi.org/10.1016/j.csbj.2015.03.001

Kyttälä, A., Lahtinen, U., Braulke, T., Hofmann, S.L., 2006. Functional biology of the neuronal ceroid lipofuscinoses (NCL) proteins. Biochim. Biophys. Acta BBA - Mol. Basis Dis., Molecular Basis of NCL 1762, 920–933. https://doi.org/10.1016/j.bbadis.2006.05.007

Lagundžin, D., Krieger, K.L., Law, H.C.-H., Woods, N.T., 2022a. An optimized co-immunoprecipitation protocol for the analysis of endogenous protein-protein interactions in cell lines using mass spectrometry. STAR Protoc. 3, 101234. https://doi.org/10.1016/j.xpro.2022.101234

Lagundžin, D., Krieger, K.L., Law, H.C.-H., Woods, N.T., 2022b. An optimized co-immunoprecipitation protocol for the analysis of endogenous protein-protein interactions in cell lines using mass spectrometry. STAR Protoc. 3, 101234. https://doi.org/10.1016/j.xpro.2022.101234

Lamond, A.I., 1993. The spliceosome. BioEssays News Rev. Mol. Cell. Dev. Biol. 15, 595–603. https://doi.org/10.1002/bies.950150905

Lancaster, M.A., Renner, M., Martin, C.-A., Wenzel, D., Bicknell, L.S., Hurles, M.E., Homfray, T., Penninger, J.M., Jackson, A.P., Knoblich, J.A., 2013. Cerebral organoids model human brain development and microcephaly. Nature 501, 373–379. https://doi.org/10.1038/nature12517

Land, P.W., Monaghan, A.P., 2003. Expression of the Transcription Factor, tailless, Is Required for Formation of Superficial Cortical Layers. Cereb. Cortex 13, 921–931. https://doi.org/10.1093/cercor/13.9.921

Lander, E.S., Linton, L.M., Birren, B., Nusbaum, C., Zody, M.C., Baldwin, J., Devon, K., Dewar, K., Doyle, M., FitzHugh, W., Funke, R., Gage, D., Harris, K., Heaford, A., Howland, J., Kann, L., Lehoczky, J., LeVine, R., McEwan, P., McKernan, K., Meldrim, J., Mesirov, J.P., Miranda, C., Morris, W., Naylor, J., Raymond, Christina, Rosetti, M., Santos, R., Sheridan, A., Sougnez, C., Stange-Thomann, N., Stojanovic, N., Subramanian, A., Wyman, D., Rogers, J., Sulston, J., Ainscough, R., Beck, S., Bentley, D., Burton, J., Clee, C., Carter, N., Coulson, A., Deadman, R., Deloukas, P., Dunham, A., Dunham, I., Durbin, R., French, L., Grafham, D., Gregory, S., Hubbard, T., Humphray, S., Hunt, A., Jones, M., Lloyd, C., McMurray, A., Matthews, L., Mercer, S., Milne, S., Mullikin, J.C., Mungall, A., Plumb, R., Ross, M., Shownkeen, R., Sims, S., Waterston, R.H., Wilson, R.K., Hillier, L.W., McPherson, J.D., Marra, M.A., Mardis, E.R., Fulton, L.A.,

Chinwalla, A.T., Pepin, K.H., Gish, W.R., Chissoe, S.L., Wendl, M.C., Delehaunty, K.D., Miner, T.L., Delehaunty, A., Kramer, J.B., Cook, L.L., Fulton, R.S., Johnson, D.L., Minx, P.J., Clifton, S.W., Hawkins, T., Branscomb, E., Predki, P., Richardson, P., Wenning, S., Slezak, T., Doggett, N., Cheng, J.-F., Olsen, A., Lucas, S., Elkin, C., Uberbacher, E., Frazier, M., Gibbs, R.A., Muzny, D.M., Scherer, S.E., Bouck, J.B., Sodergren, E.J., Worley, K.C., Rives, C.M., Gorrell, J.H., Metzker, M.L., Naylor, S.L., Kucherlapati, R.S., Nelson, D.L., Weinstock, G.M., Sakaki, Y., Fujiyama, A., Hattori, M., Yada, T., Toyoda, A., Itoh, T., Kawagoe, C., Watanabe, H., Totoki, Y., Taylor, T., Weissenbach, J., Heilig, R., Saurin, W., Artiguenave, F., Brottier, P., Bruls, T., Pelletier, E., Robert, C., Wincker, P., Rosenthal, A., Platzer, M., Nyakatura, G., Taudien, S., Rump, A., Smith, D.R., Doucette-Stamm, L., Rubenfield, M., Weinstock, K., Lee, H.M., Dubois, J., Yang, H., Yu, J., Wang, J., Huang, G., Gu, J., Hood, L., Rowen, L., Madan, A., Qin, S., Davis, R.W., Federspiel, N.A., Abola, A.P., Proctor, M.J., Roe, B.A., Chen, F., Pan, H., Ramser, J., Lehrach, H., Reinhardt, R., McCombie, W.R., de la Bastide, M., Dedhia, N., Blöcker, H., Hornischer, K., Nordsiek, G., Agarwala, R., Aravind, L., Bailey, J.A., Bateman, A., Batzoglou, S., Birney, E., Bork, P., Brown, D.G., Burge, C.B., Cerutti, L., Chen, H.-C., Church, D., Clamp, M., Copley, R.R., Doerks, T., Eddy, S.R., Eichler, E.E., Furey, T.S., Galagan, J., Gilbert, J.G.R., Harmon, C., Hayashizaki, Y., Haussler, D., Hermjakob, H., Hokamp, K., Jang, W., Johnson, L.S., Jones, T.A., Kasif, S., Kaspryzk, A., Kennedy, S., Kent, W.J., Kitts, P., Koonin, E.V., Korf, I., Kulp, D., Lancet, D., Lowe, T.M., McLysaght, A., Mikkelsen, T., Moran, J.V., Mulder, N., Pollara, V.J., Ponting, C.P., Schuler, G., Schultz, J., Slater, G., Smit, A.F.A., Stupka, E., Szustakowki, J., Thierry-Mieg, D., Thierry-Mieg, J., Wagner, L., Wallis, J., Wheeler, R., Williams, A., Wolf, Y.I., Wolfe, K.H., Yang, S.-P., Yeh, R.-F., Collins, F., Guyer, M.S., Peterson, J., Felsenfeld, A., Wetterstrand, K.A., Myers, R.M., Schmutz, J., Dickson, M., Grimwood, J., Cox, D.R., Olson, M.V., Kaul, R., Raymond, Christopher, Shimizu, N., Kawasaki, K., Minoshima, S., Evans, G.A., Athanasiou, M., Schultz, R., Patrinos, A., Morgan, M.J., International Human Genome Sequencing Consortium, Whitehead Institute for Biomedical Research, C. for G.R., The Sanger Centre:, Washington University Genome Sequencing Center, US DOE Joint Genome Institute:, Baylor College of Medicine Human Genome Sequencing Center:, RIKEN Genomic Sciences Center:, Genoscope and CNRS UMR-8030:, Department of Genome Analysis, I. of M.B., GTC Sequencing Center:, Beijing Genomics Institute/Human Genome Center:, Multimegabase Sequencing Center, T.I. for S.B., Stanford Genome Technology Center:, University of Oklahoma's Advanced Center for Genome Technology:, Max Planck Institute for Molecular Genetics:, Cold Spring Harbor Laboratory, L.A.H.G.C., GBF—German Research Centre for Biotechnology:, *Genome Analysis Group (listed in alphabetical order, also includes individuals listed under other headings):, Scientific management: National Human Genome Research Institute, U.N.I. of H., Stanford Human Genome Center:, University of Washington Genome Center:, Department of Molecular Biology, K.U.S. of M., University of Texas Southwestern Medical Center at Dallas:, Office of Science, U.D. of E., The Wellcome Trust:, 2001. Initial sequencing and analysis of the human genome. Nature 409, 860–921. https://doi.org/10.1038/35057062

Lebrun, A.-H., Moll-Khosrawi, P., Pohl, S., Makrypidi, G., Storch, S., Kilian, D., Streichert, T., Otto, B., Mole, S.E., Ullrich, K., Cotman, S., Kohlschütter, A., Braulke, T., Schulz, A., 2011. Analysis of Potential Biomarkers and Modifier Genes Affecting the Clinical Course of CLN3 Disease. Mol. Med. 17, 1253–1261. https://doi.org/10.2119/molmed.2010.00241

Lebrun, A.-H., Storch, S., Rüschendorf, F., Schmiedt, M.-L., Kyttälä, A., Mole, S.E., Kitzmüller, C., Saar, K., Mewasingh, L.D., Boda, V., Kohlschütter, A., Ullrich, K., Braulke, T., Schulz, A., 2009. Retention of lysosomal protein CLN5 in the endoplasmic reticulum causes neuronal ceroid lipofuscinosis in Asian Sibship. Hum. Mutat. 30, E651–E661. https://doi.org/10.1002/humu.21010

Lei, H., Oh, S.P., Okano, M., Jüttermann, R., Goss, K.A., Jaenisch, R., Li, E., 1996. De novo DNA cytosine methyltransferase activities in mouse embryonic stem cells. Development 122, 3195–3205.

Lendahl, U., Zimmerman, L.B., McKay, R.D.G., 1990. CNS stem cells express a new class of intermediate filament protein. Cell 60, 585–595. https://doi.org/10.1016/0092-8674(90)90662-X

Lerou, P.H., Yabuuchi, A., Huo, H., Miller, J.D., Boyer, L.F., Schlaeger, T.M., Daley, G.Q., 2008. Derivation and maintenance of human embryonic stem cells from poor-quality in vitro fertilization embryos. Nat. Protoc. 3, 923–933. https://doi.org/10.1038/nprot.2008.60

Liao YC, Fernandopulle MS, Wang G, Choi H, Hao L, Drerup CM, Patel R, Qamar S, Nixon-Abell J, Shen Y, Meadows W, Vendruscolo M, Knowles TPJ, Nelson M, Czekalska MA, Musteikyte G, Gachechiladze MA, Stephens CA, Pasolli HA, Forrest LR, St George-Hyslop P, Lippincott-Schwartz J, Ward ME. 2019. RNA Granules Hitchhike on Lysosomes for Long-Distance Transport, Using Annexin A11 as a Molecular Tether. Cell. 179(1):147-164.e20. https://doi.org/10.1016/j.cell.2019.08.050

Lippincott-Schwartz, J., Fambrough, D.M., 1987. Cycling of the integral membrane glycoprotein, LEP100, between plasma membrane and lysosomes: Kinetic and morphological analysis. Cell 49, 669–677. https://doi.org/10.1016/0092-8674(87)90543-5

Lisowski, P., Kannan, P., Mlody, B., Prigione, A., 2018. Mitochondria and the dynamic control of stem cell homeostasis. EMBO Rep. 19, e45432. https://doi.org/10.15252/embr.201745432

Liu, W.J., Ye, L., Huang, W.F., Guo, L.J., Xu, Z.G., Wu, H.L., Yang, C., Liu, H.F., 2016. p62 links the autophagy pathway and the ubiqutin–proteasome system upon ubiquitinated protein degradation. Cell. Mol. Biol. Lett. 21, 29. https://doi.org/10.1186/s11658-016-0031-z

Liu, Y., Edwards, R.H., 1997. The Role of Vesicular Transport Proteins in Synaptic Transmission and Neural Degeneration. Annu. Rev. Neurosci. 20, 125–156. https://doi.org/10.1146/annurev.neuro.20.1.125

Liu, Y., Levine, B., 2015. Autosis and autophagic cell death: the dark side of autophagy. Cell Death Differ. 22, 367–376. https://doi.org/10.1038/cdd.2014.143

Lloyd, J.B., Forster, S., 1986. The lysosome membrane. Trends Biochem. Sci. 11, 365–368. https://doi.org/10.1016/0968-0004(86)90205-7

Lonka, L., Kyttälä, A., Ranta, S., Jalanko, A., Lehesjoki, A.-E., 2000. The neuronal ceroid lipofuscinosis CLN8 membrane protein is a resident of the endoplasmic reticulum. Hum. Mol. Genet. 9, 1691–1697. https://doi.org/10.1093/hmg/9.11.1691

Lopez-Fabuel, I., Garcia-Macia, M., Buondelmonte, C., Burmistrova, O., Bonora, N., Alonso-Batan, P., Morant-Ferrando, B., Vicente-Gutierrez, C., Jimenez-Blasco, D., Quintana-Cabrera, R., Fernandez, E., Llop, J., Ramos-Cabrer, P., Sharaireh, A., Guevara-Ferrer, M., Fitzpatrick, L., Thompton, C.D., McKay, T.R., Storch, S., Medina, D.L., Mole, S.E., Fedichev, P.O., Almeida, A., Bolaños, J.P., 2022. Aberrant upregulation of the glycolytic enzyme PFKFB3 in CLN7 neuronal ceroid lipofuscinosis. Nat. Commun. 13, 536. https://doi.org/10.1038/s41467-022-28191-1

Low, W.-K., Dang, Y., Schneider-Poetsch, T., Shi, Z., Choi, N.S., Merrick, W.C., Romo, D., Liu, J.O., 2005. Inhibition of eukaryotic translation initiation by the marine natural product pateamine A. Mol. Cell 20, 709–722. https://doi.org/10.1016/j.molcel.2005.10.008

Lürick, A., Kümmel, D., Ungermann, C., 2018. Multisubunit tethers in membrane fusion. Curr. Biol. 28, R417–R420. https://doi.org/10.1016/j.cub.2017.12.012

Luzio, J.P., Gray, S.R., Bright, N.A., 2010. Endosome–lysosome fusion. Biochem. Soc. Trans. 38, 1413–1416. https://doi.org/10.1042/BST0381413

Luzio, J.P., Hackmann, Y., Dieckmann, N.M.G., Griffiths, G.M., 2014. The Biogenesis of Lysosomes and Lysosome-Related Organelles. Cold Spring Harb. Perspect. Biol. 6, a016840. https://doi.org/10.1101/cshperspect.a016840

Ma S, Attarwala IY, Xie XQ. 2019. SQSTM1/p62: A Potential Target for Neurodegenerative Disease. ACS Chem Neurosci. 10(5):2094-2114. https://doi.org/10.1021/acschemneuro.8b00516

MacDonald, M.E., Ambrose, C.M., Duyao, M.P., Myers, R.H., Lin, C., Srinidhi, L., Barnes, G., Taylor, S.A., James, M., Groot, N., MacFarlane, H., Jenkins, B., Anderson, M.A., Wexler, N.S., Gusella, J.F., Bates, G.P., Baxendale, S., Hummerich, H., Kirby, S., North, M., Youngman, S., Mott, R., Zehetner, G., Sedlacek, Z., Poustka, A., Frischauf, A.-M., Lehrach, H., Buckler, A.J., Church, D., Doucette-Stamm, L., O'Donovan, M.C., Riba-Ramirez, L., Shah, M., Stanton, V.P., Strobel, S.A., Draths, K.M., Wales, J.L., Dervan, P., Housman, D.E., Altherr, M., Shiang, R., Thompson, L., Fielder, T., Wasmuth, J.J., Tagle, D., Valdes, J., Elmer, L., Allard, M., Castilla, L., Swaroop, M., Blanchard, K., Collins, F.S., Snell, R., Holloway, T., Gillespie, K., Datson, N., Shaw, D., Harper, P.S., 1993. A novel gene containing a trinucleotide repeat that is expanded and unstable on Huntington's disease chromosomes. Cell 72, 971–983. https://doi.org/10.1016/0092-8674(93)90585-E

Maday, S., Wallace, K.E., Holzbaur, E.L.F., 2012. Autophagosomes initiate distally and mature during transport toward the cell soma in primary neurons. J. Cell Biol. 196, 407–417. https://doi.org/10.1083/jcb.201106120

Maejima, I., Takahashi, A., Omori, H., Kimura, T., Takabatake, Y., Saitoh, T., Yamamoto, A., Hamasaki, M., Noda, T., Isaka, Y., Yoshimori, T., 2013. Autophagy sequesters damaged lysosomes to control lysosomal biogenesis and kidney injury. EMBO J. 32, 2336–2347. https://doi.org/10.1038/emboj.2013.171

Maestre, C., Delgado-Esteban, M., Gomez-Sanchez, J.C., Bolaños, J.P., Almeida, A., 2008. Cdk5 phosphorylates Cdh1 and modulates cyclin B1 stability in excitotoxicity. EMBO J. 27, 2736–2745. https://doi.org/10.1038/emboj.2008.195

Maherali, N., Ahfeldt, T., Rigamonti, A., Utikal, J., Cowan, C., Hochedlinger, K., 2008. A High-Efficiency System for the Generation and Study of Human Induced Pluripotent Stem Cells. Cell Stem Cell 3, 340–345. https://doi.org/10.1016/j.stem.2008.08.003

Maherali, N., Sridharan, R., Xie, W., Utikal, J., Eminli, S., Arnold, K., Stadtfeld, M., Yachechko, R., Tchieu, J., Jaenisch, R., Plath, K., Hochedlinger, K., 2007. Directly Reprogrammed Fibroblasts Show Global Epigenetic Remodeling and Widespread Tissue Contribution. Cell Stem Cell 1, 55–70. https://doi.org/10.1016/j.stem.2007.05.014

Malatesta, P., Hartfuss, E., Götz, M., 2000. Isolation of radial glial cells by fluorescent-activated cell sorting reveals a neural lineage. Development 127, 5253–5263.

Marshall, C.J., 1993. Protein Prenylation: a Mediator of Protein-Protein Interactions. Science 259, 1865–1866. https://doi.org/10.1126/science.8456312

Marshansky, V., Futai, M., 2008. The V-type H+-ATPase in vesicular trafficking: targeting, regulation and function. Curr. Opin. Cell Biol. 20, 415–426. https://doi.org/10.1016/j.ceb.2008.03.015

Martin, S., Zekri, L., Metz, A., Maurice, T., Chebli, K., Vignes, M., Tazi, J., 2013. Deficiency of G3BP1, the stress granules assembly factor, results in abnormal synaptic plasticity and calcium homeostasis in neurons. J. Neurochem. 125, 175–184. https://doi.org/10.1111/jnc.12189

Martínez-Reyes, I., Cuezva, J.M., 2014. The H+-ATP synthase: A gate to ROS-mediated cell death or cell survival. Biochim. Biophys. Acta BBA - Bioenerg., 18th European Bioenergetics Conference 2014 Lisbon, Portugal 1837, 1099–1112. https://doi.org/10.1016/j.bbabio.2014.03.010

Masters, S.C., 2004. Co-Immunoprecipitation from Transfected Cells, in: Fu, H. (Ed.), Protein-Protein Interactions: Methods and Applications, Methods in Molecular Biology. Humana Press, Totowa, NJ, pp. 337–348. https://doi.org/10.1385/1-59259-762-9:337

Masui, S., Nakatake, Y., Toyooka, Y., Shimosato, D., Yagi, R., Takahashi, K., Okochi, H., Okuda, A., Matoba, R., Sharov, A.A., Ko, M.S.H., Niwa, H., 2007. Pluripotency governed by Sox2 via regulation of Oct3/4 expression in mouse embryonic stem cells. Nat. Cell Biol. 9, 625–635. https://doi.org/10.1038/ncb1589

Mauvezin, C., Nagy, P., Juhász, G., Neufeld, T.P., 2015. Autophagosome–lysosome fusion is independent of V-ATPase-mediated acidification. Nat. Commun. 6, 7007. https://doi.org/10.1038/ncomms8007

Mazroui, R., Sukarieh, R., Bordeleau, M.-E., Kaufman, R.J., Northcote, P., Tanaka, J., Gallouzi, I., Pelletier, J., 2006. Inhibition of Ribosome Recruitment Induces Stress Granule Formation Independently of Eukaryotic Initiation Factor 2α Phosphorylation. Mol. Biol. Cell 17, 4212–4219. https://doi.org/10.1091/mbc.e06-04-0318

McBride, J.L., Neuringer, M., Ferguson, B., Kohama, S.G., Tagge, I.J., Zweig, R.C., Renner, L.M., McGill, T.J., Stoddard, J., Peterson, S., Su, W., Sherman, L.S., Domire, J.S., Ducore, R.M., Colgin, L.M., Lewis, A.D., 2018a. Discovery of a CLN7 model of Batten disease in non-human primates. Neurobiol. Dis. 119, 65–78. https://doi.org/10.1016/j.nbd.2018.07.013

McBride, J.L., Neuringer, M., Ferguson, B., Kohama, S.G., Tagge, I.J., Zweig, R.C., Renner, L.M., McGill, T.J., Stoddard, J., Peterson, S., Su, W., Sherman, L.S., Domire, J.S., Ducore, R.M., Colgin, L.M., Lewis, A.D., 2018b. Discovery of a CLN7 model of Batten disease in non-human primates. Neurobiol. Dis. 119, 65–78. https://doi.org/10.1016/j.nbd.2018.07.013

McGowan, E., Eriksen, J., Hutton, M., 2006. A decade of modeling Alzheimer's disease in transgenic mice. Trends Genet. 22, 281–289. https://doi.org/10.1016/j.tig.2006.03.007

McHugh, D., Gil, J., 2017. Senescence and aging: Causes, consequences, and therapeutic avenues. J. Cell Biol. 217, 65–77. https://doi.org/10.1083/jcb.201708092

McNally, K.E., Cullen, P.J., 2018. Endosomal Retrieval of Cargo: Retromer Is Not Alone. Trends Cell Biol. 28, 807–822. https://doi.org/10.1016/j.tcb.2018.06.005

Mehta, M.M., Weinberg, S.E., Chandel, N.S., 2017. Mitochondrial control of immunity: beyond ATP. Nat. Rev. Immunol. 17, 608–620. https://doi.org/10.1038/nri.2017.66

Mellman, I., 1996. Endocytosis and Molecular Sorting. Annu. Rev. Cell Dev. Biol. 12, 575–625. https://doi.org/10.1146/annurev.cellbio.12.1.575

Meng T, Lin S, Zhuang H, Huang H, He Z, Hu Y, Gong Q, Feng D. 2019. Recent progress in the role of autophagy in neurological diseases. Cell Stress. 29;3(5):141-161. https://doi.org/10.15698/cst2019.05.186

Menzies, F., Fleming, A., Rubinsztein, D., 2015. Compromised autophagy and neurodegenerative diseases. Nat. Rev. Neurosci. 16, 345–57. https://doi.org/10.1038/nrn3961

Menzies, F.M., Fleming, A., Caricasole, A., Bento, C.F., Andrews, S.P., Ashkenazi, A., Füllgrabe, J., Jackson, A., Sanchez, M.J., Karabiyik, C., Licitra, F., Ramirez, A.L., Pavel, M., Puri, C., Renna, M., Ricketts, T., Schlotawa, L., Vicinanza, M., Won, H., Zhu, Y., Skidmore, J., Rubinsztein, D.C., 2017b. Autophagy and Neurodegeneration: Pathogenic Mechanisms and Therapeutic Opportunities. Neuron 93, 1015–1034. https://doi.org/10.1016/j.neuron.2017.01.022

Mercy, L., Hodges, J.R., Dawson, K., Barker, R.A., Brayne, C., 2008. Incidence of early-onset dementias in Cambridgeshire, United Kingdom. Neurology 71, 1496–1499. https://doi.org/10.1212/01.wnl.0000334277.16896.fa

Merkle, F.T., Tramontin, A.D., García-Verdugo, J.M., Alvarez-Buylla, A., 2004. Radial glia give rise to adult neural stem cells in the subventricular zone. Proc. Natl. Acad. Sci. U. S. A. 101, 17528–17532. https://doi.org/10.1073/pnas.0407893101

Miaczynska, M., Christoforidis, S., Giner, A., Shevchenko, A., Uttenweiler-Joseph, S., Habermann, B., Wilm, M., Parton, R.G., Zerial, M., 2004. APPL Proteins Link Rab5 to Nuclear Signal Transduction via an Endosomal Compartment. Cell 116, 445–456. https://doi.org/10.1016/S0092-8674(04)00117-5

Michaelides, M., Hunt, D.M., Moore, A.T., 2004. The cone dysfunction syndromes. Br. J. Ophthalmol. 88, 291–297. https://doi.org/10.1136/bjo.2003.027102

Miranda-Negrón, Y., García-Arrarás, J.E., 2022. Radial glia and radial glia-like cells: Their role in neurogenesis and regeneration. Front. Neurosci. 16.

Mishra, E., Thakur, M.K., 2022. Alterations in hippocampal mitochondrial dynamics are associated with neurodegeneration and recognition memory decline in old male mice. Biogerontology 23, 251–271. https://doi.org/10.1007/s10522-022-09960-3

Misrani, A., Tabassum, S., Yang, L., 2021. Mitochondrial Dysfunction and Oxidative Stress in Alzheimer's Disease. Front. Aging Neurosci. 13.

Mitsui, K., Tokuzawa, Y., Itoh, H., Segawa, K., Murakami, M., Takahashi, K., Maruyama, M., Maeda, M., Yamanaka, S., 2003. The Homeoprotein Nanog Is Required for Maintenance of Pluripotency in Mouse Epiblast and ES Cells. Cell 113, 631–642. https://doi.org/10.1016/S0092-8674(03)00393-3

Miyagawa, S., Kainuma, S., Kawamura, T., Suzuki, K., Ito, Y., Iseoka, H., Ito, E., Takeda, M., Sasai, M., Mochizuki-Oda, N., Shimamoto, T., Nitta, Y., Dohi, H., Watabe, T., Sakata, Y., Toda, K., Sawa, Y., 2022. Transplantation of IPSC-Derived Cardiomyocyte Patches for Ischemic Cardiomyopathy. https://doi.org/10.1101/2021.12.27.21268295

Mizushima, N., Levine, B., Cuervo, A.M., Klionsky, D.J., 2008. Autophagy fights disease through cellular self-digestion. Nature 451, 1069–1075. https://doi.org/10.1038/nature06639

Mizushima, N., Yoshimori, T., Ohsumi, Y., 2011. The Role of Atg Proteins in Autophagosome Formation. Annu. Rev. Cell Dev. Biol. 27, 107–132. https://doi.org/10.1146/annurev-cellbio-092910-154005

Mohamad O, Drury-Stewart D, Song M, Faulkner B, Chen D, Yu SP, Wei L. 2013. Vector-free and transgene-free human iPS cells differentiate into functional neurons and enhance functional recovery after ischemic stroke in mice. PLoS One. 8(5):e64160. https://doi.org/10.1371/journal.pone.0064160

Mole, S.E., Cotman, S.L., 2015. Genetics of the Neuronal Ceroid Lipofuscinoses (Batten disease). Biochim. Biophys. Acta 1852, 2237–2241. https://doi.org/10.1016/j.bbadis.2015.05.011

Mole, S.E., Michaux, G., Codlin, S., Wheeler, R.B., Sharp, J.D., Cutler, D.F., 2004. CLN6, which is associated with a lysosomal storage disease, is an endoplasmic reticulum protein. Exp. Cell Res. 298, 399–406. https://doi.org/10.1016/j.yexcr.2004.04.042

Morselli, E., Shen, S., Ruckenstuhl, C., Bauer, M.A., Mariño, G., Galluzzi, L., Criollo, A., Michaud, M., Maiuri, M.C., Chano, T., Madeo, F., Kroemer, G., 2011. p53 inhibits autophagy by interacting with the human ortholog of yeast Atg17, RB1CC1/FIP200. Cell Cycle 10, 2763–2769. https://doi.org/10.4161/cc.10.16.16868

Mossink B, Verboven AHA, van Hugte EJH, Klein Gunnewiek TM, Parodi G, Linda K, Schoenmaker C, Kleefstra T, Kozicz T, van Bokhoven H, Schubert D, Nadif Kasri N, Frega M. 2021. Human neuronal networks on micro-electrode arrays are a highly robust tool to study disease-specific genotype-phenotype correlations in vitro. Stem Cell Reports. 14;16(9):2182-2196. https://doi.org/10.1016/j.stemcr.2021.07.001

Muhr, J., Arbor, T.C., Ackerman, K.M., 2023. Embryology, Gastrulation, in: StatPearls. StatPearls Publishing, Treasure Island (FL).

Mukherjee, A.B., Appu, A.P., Sadhukhan, T., Casey, S., Mondal, A., Zhang, Z., Bagh, M.B., 2019. Emerging new roles of the lysosome and neuronal ceroid lipofuscinoses. Mol. Neurodegener. 14, 4. https://doi.org/10.1186/s13024-018-0300-6

Mustfa, S.A., Singh, M., Suhail, A., Mohapatra, G., Verma, S., Chakravorty, D., Rana, S., Rampal, R., Dhar, A., Saha, S., Ahuja, V., Srikanth, C.V., 2017. SUMOylation pathway alteration coupled with downregulation of SUMO E2 enzyme at mucosal epithelium modulates inflammation in inflammatory bowel disease. Open Biol. 7, 170024. https://doi.org/10.1098/rsob.170024

Nagy, Z.F., Pál, M., Salamon, A., Kafui Esi Zodanu, G., Füstös, D., Klivényi, P., Széll, M., 2022. Re-analysis of the Hungarian amyotrophic lateral sclerosis population and evaluation of novel ALS genetic risk variants. Neurobiol. Aging 116, 1–11. https://doi.org/10.1016/j.neurobiolaging.2022.04.002

Nakano, T., Sandhoff, K., Stumper, J., Christomanou, H., Suzuki, K., 1989. Structure of Full-Length cDNA Coding for Sulfatide Activator, a Co-β-Glucosidase and Two Other Homologous Proteins: Two Alternate Forms of the Sulfatide Activator1. J. Biochem. (Tokyo) 105, 152–154. https://doi.org/10.1093/oxfordjournals.jbchem.a122629

Navarro, A., López-Cepero, J.M., Bández, M.J., Sánchez-Pino, M.-J., Gómez, C., Cadenas, E., Boveris, A., 2008. Hippocampal mitochondrial dysfunction in rat aging. Am. J. Physiol.-Regul. Integr. Comp. Physiol. 294, R501–R509. https://doi.org/10.1152/ajpregu.00492.2007

Netsrithong R, Garcia-Perez L, Themeli M. Engineered T cells from induced pluripotent stem cells: from research towards clinical implementation. Front Immunol. 2024 Jan 12;14:1325209. https://doi.org/10.3389/fimmu.2023.1325209

Neubauer, G., Gottschalk, A., Fabrizio, P., Séraphin, B., Lührmann, R., Mann, M., 1997. Identification of the proteins of the yeast U1 small nuclear ribonucleoprotein complex by mass spectrometry. Proc. Natl. Acad. Sci. 94, 385–390. https://doi.org/10.1073/pnas.94.2.385

Neubauer, G., King, A., Rappsilber, J., Calvio, C., Watson, M., Ajuh, P., Sleeman, J., Lamond, A., Mann, M., 1998. Mass spectrometry and EST-database searching allows characterization of the multi-protein spliceosome complex. Nat. Genet. 20, 46–50. https://doi.org/10.1038/1700

Nickerson, D.P., Brett, C.L., Merz, A.J., 2009. Vps-C complexes: gatekeepers of endolysosomal traffic. Curr. Opin. Cell Biol. 21, 543–551. https://doi.org/10.1016/j.ceb.2009.05.007

Nielsen, E., Severin, F., Backer, J.M., Hyman, A.A., Zerial, M., 1999. Rab5 regulates motility of early endosomes on microtubules. Nat. Cell Biol. 1, 376–382. https://doi.org/10.1038/14075

Nikoletopoulou, V., Papandreou, M.-E., Tavernarakis, N., 2015. Autophagy in the physiology and pathology of the central nervous system. Cell Death Differ. 22, 398–407. https://doi.org/10.1038/cdd.2014.204

Nishimura, K., Sano, M., Ohtaka, M., Furuta, B., Umemura, Y., Nakajima, Y., Ikehara, Y., Kobayashi, T., Segawa, H., Takayasu, S., Sato, H., Motomura, K., Uchida, E., Kanayasu-Toyoda, T., Asashima, M., Nakauchi, H., Yamaguchi, T., Nakanishi, M., 2011. Development of defective and persistent Sendai virus vector: a unique gene delivery/expression system ideal for cell reprogramming. J. Biol. Chem. 286, 4760–4771. https://doi.org/10.1074/jbc.M110.183780

Nixon, R.A., Yang, D.-S., Lee, J.-H., 2008. Neurodegenerative lysosomal disorders: A continuum from development to late age. Autophagy 4, 590–599. https://doi.org/10.4161/auto.6259

Noctor, S.C., Flint, A.C., Weissman, T.A., Dammerman, R.S., Kriegstein, A.R., 2001. Neurons derived from radial glial cells establish radial units in neocortex. Nature 409, 714–720. https://doi.org/10.1038/35055553

Noda, N.N., Fujioka, Y., Hanada, T., Ohsumi, Y., Inagaki, F., 2013. Structure of the Atg12-Atg5 conjugate reveals a platform for stimulating Atg8-PE conjugation. EMBO Rep. 14, 206–211. https://doi.org/10.1038/embor.2012.208

Noda, N.N., Inagaki, F., 2015. Mechanisms of Autophagy. Annu. Rev. Biophys. 44, 101–122. https://doi.org/10.1146/annurev-biophys-060414-034248

Nosková, L., Stránecký, V., Hartmannová, H., Přistoupilová, A., Barešová, V., Ivánek, R., Hůlková, H., Jahnová, H., van der Zee, J., Staropoli, J.F., Sims, K.B., Tyynelä, J., Van Broeckhoven, C., Nijssen, P.C.G., Mole, S.E., Elleder, M., Kmoch, S., 2011a. Mutations in DNAJC5, Encoding Cysteine-String Protein Alpha, Cause Autosomal-Dominant Adult-Onset Neuronal Ceroid Lipofuscinosis. Am. J. Hum. Genet. 89, 241–252. https://doi.org/10.1016/j.ajhg.2011.07.003

Nosková, L., Stránecký, V., Hartmannová, H., Přistoupilová, A., Barešová, V., Ivánek, R., Hůlková, H., Jahnová, H., van der Zee, J., Staropoli, J.F., Sims, K.B., Tyynelä, J., Van Broeckhoven, C., Nijssen, P.C.G., Mole, S.E., Elleder, M., Kmoch, S., 2011b. Mutations in DNAJC5, Encoding Cysteine-String Protein Alpha, Cause Autosomal-Dominant Adult-Onset Neuronal Ceroid Lipofuscinosis. Am. J. Hum. Genet. 89, 241–252. https://doi.org/10.1016/j.ajhg.2011.07.003

Oberheim, N.A., Takano, T., Han, X., He, W., Lin, J.H.C., Wang, F., Xu, Q., Wyatt, J.D., Pilcher, W., Ojemann, J.G., Ransom, B.R., Goldman, S.A., Nedergaard, M., 2009. Uniquely Hominid Features of Adult Human Astrocytes. J. Neurosci. 29, 3276–3287. https://doi.org/10.1523/JNEUROSCI.4707-08.2009

Ogonowski, N., Santamaria-Garcia, H., Baez, S., Lopez, A., Laserna, A., Garcia-Cifuentes, E., Ayala-Ramirez, P., Zarante, I., Suarez-Obando, F., Reyes, P., Kauffman, M., Cochran, N., Schulte, M., Sirkis, D.W., Spina, S., Yokoyama, J.S., Miller, B.L., Kosik, K.S., Matallana, D., Ibáñez, A., 2023. Frontotemporal dementia presentation in patients with heterozygous p.H157Y variant of TREM2. J. Med. Genet. https://doi.org/10.1136/jmg-2022-108627

Ohtsubo, K., Marth, J.D., 2006. Glycosylation in Cellular Mechanisms of Health and Disease. Cell 126, 855–867. https://doi.org/10.1016/j.cell.2006.08.019

Okano, H., Yamanaka, S., 2014. iPS cell technologies: significance and applications to CNS regeneration and disease. Mol. Brain 7, 22. https://doi.org/10.1186/1756-6606-7-22

Okita, K., Ichisaka, T., Yamanaka, S., 2007. Generation of germline-competent induced pluripotent stem cells. Nature 448, 313–317. https://doi.org/10.1038/nature05934

Okita, K., Nakagawa, M., Hyenjong, H., Ichisaka, T., Yamanaka, S., 2008. Generation of Mouse Induced Pluripotent Stem Cells Without Viral Vectors. Science 322, 949–953. https://doi.org/10.1126/science.1164270

Olszewska, D.A., Lonergan, R., Fallon, E.M., Lynch, T., 2016. Genetics of Frontotemporal Dementia. Curr. Neurol. Neurosci. Rep. 16, 107. https://doi.org/10.1007/s11910-016-0707-9

Onyike, C.U., Diehl-Schmid, J., 2013. The epidemiology of frontotemporal dementia. Int. Rev. Psychiatry 25, 130–137. https://doi.org/10.3109/09540261.2013.776523

Ostrowicz, C.W., Bröcker, C., Ahnert, F., Nordmann, M., Lachmann, J., Peplowska, K., Perz, A., Auffarth, K., Engelbrecht-Vandré, S., Ungermann, C., 2010. Defined Subunit Arrangement and Rab Interactions Are Required for Functionality of the HOPS Tethering Complex. Traffic 11, 1334–1346. https://doi.org/10.1111/j.1600-0854.2010.01097.x

Ozgen, S., Krigman, J., Zhang, R., Sun, N., 2022. Significance of mitochondrial activity in neurogenesis and neurodegenerative diseases. Neural Regen. Res. 17, 741. https://doi.org/10.4103/1673-5374.322429

Palmer, D.N., 2015. The relevance of the storage of subunit c of ATP synthase in different forms and models of Batten disease (NCLs). Biochim. Biophys. Acta BBA - Mol. Basis Dis., Current Research on the Neuronal Ceroid Lipofuscinoses (Batten Disease) 1852, 2287–2291. https://doi.org/10.1016/j.bbadis.2015.06.014

Palmer, D.N., Fearnley, I.M., Walker, J.E., Hall, N.A., Lake, B.D., Wolfe, L.S., Haltia, M., Martinus, R.D., Jolly, R.D., 1992. Mitochondrial ATP synthase subunit c storage in the ceroid-lipofuscinoses (Batten disease). Am. J. Med. Genet. 42, 561–567. https://doi.org/10.1002/ajmg.1320420428

Pamies, D., Barreras, P., Block, K., Makri, G., Kumar, A., Wiersma, D., Smirnova, L., Zhang, C., Bressler, J., Christian, K.M., Harris, G., Ming, G., Berlinicke, C.J., Kyro, K., Song, H., Pardo, C.A., Hartung, T., Hogberg, H.T., 2017. A human brain microphysiological system derived from induced pluripotent stem cells to study neurological diseases and toxicity. ALTEX - Altern. Anim. Exp. 34, 362–376. https://doi.org/10.14573/altex.1609122

Pankiv, S., Clausen, T.H., Lamark, T., Brech, A., Bruun, J.-A., Outzen, H., Øvervatn, A., Bjørkøy, G., Johansen, T., 2007. p62/SQSTM1 Binds Directly to Atg8/LC3 to Facilitate Degradation of Ubiquitinated Protein Aggregates by Autophagy *. J. Biol. Chem. 282, 24131–24145. https://doi.org/10.1074/jbc.M702824200

Panni, S., 2019. Phospho-peptide binding domains in S. cerevisiae model organism. Biochimie 163, 117–127. https://doi.org/10.1016/j.biochi.2019.06.005

Pao, S.S., Paulsen, I.T., Saier, M.H., 1998. Major Facilitator Superfamily. Microbiol. Mol. Biol. Rev. 62, 1–34. https://doi.org/10.1128/mmbr.62.1.1-34.1998

Park, D., Xiang, A.P., Mao, F.F., Zhang, L., Di, C.-G., Liu, X.-M., Shao, Y., Ma, B.-F., Lee, J.-H., Ha, K.-S., Walton, N., Lahn, B.T., 2010. Nestin Is Required for the Proper Self-Renewal of Neural Stem Cells. STEM CELLS 28, 2162–2171. https://doi.org/10.1002/stem.541

Park, H., Kang, J.-H., Lee, S., 2020. Autophagy in Neurodegenerative Diseases: A Hunter for Aggregates. Int. J. Mol. Sci. 21, 3369. https://doi.org/10.3390/ijms21093369

Parrotta, E.I., Scalise, S., Scaramuzzino, L., Cuda, G., 2019. Stem Cells: The Game Changers of Human Cardiac Disease Modelling and Regenerative Medicine. Int. J. Mol. Sci. 20, 5760. https://doi.org/10.3390/ijms20225760

Patiño, L.C., Battu, R., Ortega-Recalde, O., Nallathambi, J., Anandula, V.R., Renukaradhya, U., Laissue, P., 2014. Exome Sequencing Is an Efficient Tool for Variant Late-Infantile Neuronal Ceroid Lipofuscinosis Molecular Diagnosis. PLOS ONE 9, e109576. https://doi.org/10.1371/journal.pone.0109576

Patton-Vogt, J.L., Henry, S.A., 1998. GIT1, a Gene Encoding a Novel Transporter for Glycerophosphoinositol in Saccharomyces cerevisiae. Genetics 149, 1707–1715. https://doi.org/10.1093/genetics/149.4.1707

Pchitskaya, E., Popugaeva, E., Bezprozvanny, I., 2018. Calcium signaling and molecular mechanisms underlying neurodegenerative diseases. Cell Calcium, The role of Ca2+ signals in the regulation of cell death & survival processes in health, disease and therapy 70, 87–94. https://doi.org/10.1016/j.ceca.2017.06.008

Pelkmans, L., Helenius, A., 2003. Insider information: what viruses tell us about endocytosis. Curr. Opin. Cell Biol. 15, 414–422. https://doi.org/10.1016/S0955-0674(03)00081-4

Peng, C., Ye, J., Yan, S., Kong, S., Shen, Y., Li, C., Li, Q., Zheng, Y., Deng, K., Xu, T., Tao, W., 2012. Ablation of Vacuole Protein Sorting 18 (Vps18) Gene Leads to Neurodegeneration and Impaired Neuronal Migration by Disrupting Multiple Vesicle Transport Pathways to Lysosomes. J. Biol. Chem. 287, 32861–32873. https://doi.org/10.1074/jbc.M112.384305

Pera, M.F., Reubinoff, B., Trounson, A., 2000. Human embryonic stem cells. J. Cell Sci. 113, 5–10. https://doi.org/10.1242/jcs.113.1.5

Pescosolido, M.F., Stein, D.M., Schmidt, M., El Achkar, C.M., Sabbagh, M., Rogg, J.M., Tantravahi, U., McLean, R.L., Liu, J.S., Poduri, A., Morrow, E.M., 2014. Genetic and phenotypic diversity of NHE6 mutations in Christianson syndrome. Ann. Neurol. 76, 581–593. https://doi.org/10.1002/ana.24225

Peters, C., von Figura, K., 1994. Biogenesis of lysosomal membranes. FEBS Lett. 346, 108–114. https://doi.org/10.1016/0014-5793(94)00499-4

Pezzini F, Fiorini M, Doccini S, Santorelli FM, Zanusso G, Simonati A. 2023. Enhanced expression of the autophagosomal marker LC3-II in detergent-resistant protein lysates from a CLN3 patient's post-mortem brain. Biochim Biophys Acta Mol Basis Dis. 1869(6):166756. https://doi.org/10.1016/j.bbadis.2023.166756

Pickles, S., Vigié, P., Youle, R.J., 2018. Mitophagy and Quality Control Mechanisms in Mitochondrial Maintenance. Curr. Biol. 28, R170–R185. https://doi.org/10.1016/j.cub.2018.01.004

Pineda, E.T., Nerem, R.M., Ahsan, T., 2013. Differentiation Patterns of Embryonic Stem Cells in Two- versus Three-Dimensional Culture. Cells Tissues Organs 197, 399–410. https://doi.org/10.1159/000346166

Platt, F.M., Boland, B., van der Spoel, A.C., 2012. Lysosomal storage disorders: The cellular impact of lysosomal dysfunction. J. Cell Biol. 199, 723–734. https://doi.org/10.1083/jcb.201208152

Poët, M., Kornak, U., Schweizer, M., Zdebik, A.A., Scheel, O., Hoelter, S., Wurst, W., Schmitt, A., Fuhrmann, J.C., Planells-Cases, R., Mole, S.E., Hübner, C.A., Jentsch, T.J., 2006. Lysosomal storage disease upon disruption of the neuronal chloride transport protein ClC-6. Proc. Natl. Acad. Sci. 103, 13854–13859. https://doi.org/10.1073/pnas.0606137103

Pollard, S.M., Conti, L., Sun, Y., Goffredo, D., Smith, A., 2006. Adherent Neural Stem (NS) Cells from Fetal and Adult Forebrain. Cereb. Cortex 16, i112–i120. https://doi.org/10.1093/cercor/bhj167

Polovitskaya, M.M., Barbini, C., Martinelli, D., Harms, F.L., Cole, F.S., Calligari, P., Bocchinfuso, G., Stella, L., Ciolfi, A., Niceta, M., Rizza, T., Shinawi, M., Sisco, K., Johannsen, J., Denecke, J., Carrozzo, R., Wegner, D.J., Kutsche, K., Tartaglia, M., Jentsch, T.J., 2020. A Recurrent Gain-of-Function Mutation in CLCN6, Encoding the ClC-6 Cl−/H+-Exchanger, Causes Early-Onset Neurodegeneration. Am. J. Hum. Genet. 107, 1062–1077. https://doi.org/10.1016/j.ajhg.2020.11.004

Poncet, A.F., Grunewald, O., Vaclavik, V., Meunier, I., Drumare, I., Pelletier, V., Bocquet, B., Todorova, M.G., Le Moing, A.-G., Devos, A., Schorderet, D.F., Jobic, F., Defoort-Dhellemmes, S., Dollfus, H., Smirnov, V.M., Dhaenens, C.-M., 2022. Contribution of Whole-Genome Sequencing and Transcript Analysis to Decipher Retinal Diseases Associated with MFSD8 Variants. Int. J. Mol. Sci. 23, 4294. https://doi.org/10.3390/ijms23084294

Press, E.M., Porter, R.R., Cebra, J., 1960. The isolation and properties of a proteolytic enzyme, cathepsin D, from bovine spleen. Biochem. J. 74, 501–514. https://doi.org/10.1042/bj0740501

Pressey, S.N.R., O'Donnell, K.J., Stauber, T., Fuhrmann, J.C., Tyynelä, J., Jentsch, T.J., Cooper, J.D., 2010. Distinct Neuropathologic Phenotypes After Disrupting the Chloride Transport Proteins ClC-6 or ClC-7/Ostm1. J. Neuropathol. Exp. Neurol. 69, 1228–1246. https://doi.org/10.1097/NEN.0b013e3181ffe742

Progida, C., Cogli, L., Piro, F., De Luca, A., Bakke, O., Bucci, C., 2010. Rab7b controls trafficking from endosomes to the TGN. J. Cell Sci. 123, 1480–1491. https://doi.org/10.1242/jcs.051474

Progida, C., Nielsen, M.S., Koster, G., Bucci, C., Bakke, O., 2012. Dynamics of Rab7b-Dependent Transport of Sorting Receptors. Traffic 13, 1273–1285. https://doi.org/10.1111/j.1600-0854.2012.01388.x

Puertollano, R., 2014. mTOR and lysosome regulation. F1000Prime Rep 6.

Raffaello, A., Mammucari, C., Gherardi, G., Rizzuto, R., 2016. Calcium at the Center of Cell Signaling: Interplay between Endoplasmic Reticulum, Mitochondria, and Lysosomes. Trends Biochem. Sci. 41, 1035–1049. https://doi.org/10.1016/j.tibs.2016.09.001

Rahman, M.M., Fatema, K., 2021. Genetic Diagnosis in Children with Epilepsy and Developmental Disorders by Targeted Gene Panel Analysis in a Developing Country. J. Epilepsy Res. 11, 22–31. https://doi.org/10.14581/jer.21004

Ramadan, H., Al-Din, A.S., Ismail, A., Balen, F., Varma, A., Twomey, A., Watts, R., Jackson, M., Anderson, G., Green, E., Mole, S.E., 2007. Adult neuronal ceroid lipofuscinosis caused by deficiency in palmitoyl protein thioesterase 1. Neurology 68, 387–388. https://doi.org/10.1212/01.wnl.0000252825.85947.2f

Ramazi, S., Allahverdi, A., Zahiri, J., 2020. Evaluation of post-translational modifications in histone proteins: A review on histone modification defects in developmental and neurological disorders. J. Biosci. 45, 135. https://doi.org/10.1007/s12038-020-00099-2

Ranta, S., Topcu, M., Tegelberg, S., Tan, H., Ustübütün, A., Saatci, I., Dufke, A., Enders, H., Pohl, K., Alembik, Y., Mitchell, W.A., Mole, S.E., Lehesjoki, A.-E., 2004. Variant late infantile neuronal ceroid lipofuscinosis in a subset of Turkish patients is allelic to Northern epilepsy. Hum. Mutat. 23, 300–305. https://doi.org/10.1002/humu.20018

Rappsilber, J., Ryder, U., Lamond, A.I., Mann, M., 2002. Large-scale proteomic analysis of the human spliceosome. Genome Res. 12, 1231–1245. https://doi.org/10.1101/gr.473902

Rascovsky, K., Hodges, J.R., Kipps, C.M., Johnson, J.K., Seeley, W.W., Mendez, M.F., Knopman, D., Kertesz, A., Mesulam, M., Salmon, D.P., Galasko, D., Chow, T.W., DeCarli, C., Hillis, A., Josephs, K., Kramer, J.H., Weintraub, S., Grossman, M., Gorno-Tempini, M.-L., Miller, B.M., 2007. Diagnostic Criteria for the Behavioral Variant of Frontotemporal Dementia (bvFTD): Current Limitations and Future Directions. Alzheimer Dis. Assoc. Disord. 21, S14. https://doi.org/10.1097/WAD.0b013e31815c3445

Ravikumar, B., Moreau, K., Jahreiss, L., Puri, C., Rubinsztein, D.C., 2010. Plasma membrane contributes to the formation of pre-autophagosomal structures. Nat. Cell Biol. 12, 747–757. https://doi.org/10.1038/ncb2078

Rayon, T., Stamataki, D., Perez-Carrasco, R., Garcia-Perez, L., Barrington, C., Melchionda, M., Exelby, K., Lazaro, J., Tybulewicz, V.L.J., Fisher, E.M.C., Briscoe, J., 2020. Species-specific pace of development is associated with differences in protein stability. Science 369, eaba7667. https://doi.org/10.1126/science.aba7667

Reece, M., Prawitt, D., Landers, J., Kast, C., Gros, P., Housman, D., Zabel, B.U., Pelletier, J., 1998. Functional characterization of ORCTL2 - an organic cation transporter expressed in the renal proximal tubules. FEBS Lett. 433, 245–250. https://doi.org/10.1016/S0014-5793(98)00907-7

Rehakova, D., Souralova, T., Koutna, I., 2020. Clinical-Grade Human Pluripotent Stem Cells for Cell Therapy: Characterization Strategy. Int. J. Mol. Sci. 21, 2435. https://doi.org/10.3390/ijms21072435

Relton EL, Roth NJ, Yasa S, Kaleem A, Hermey G, Minnis CJ, Mole SE, Shelkovnikova T, Lefrancois S, McCormick PJ, Locker N. 2023. The Batten disease protein CLN3 is important for stress granules dynamics and translational activity. J Biol Chem. 299(5):104649. https://doi.org/10.1016/j.jbc.2023.104649

Renton, A.E., Majounie, E., Waite, A., Simón-Sánchez, J., Rollinson, S., Gibbs, J.R., Schymick, J.C., Laaksovirta, H., van Swieten, J.C., Myllykangas, L., Kalimo, H., Paetau, A., Abramzon, Y., Remes, A.M., Kaganovich, A., Scholz, S.W., Duckworth, J., Ding, J., Harmer, D.W., Hernandez, D.G., Johnson, J.O., Mok, K., Ryten, M., Trabzuni, D., Guerreiro, R.J., Orrell, R.W., Neal, J., Murray, A., Pearson, J., Jansen, I.E., Sondervan, D., Seelaar, H., Blake, D., Young, K., Halliwell, N., Callister, J.B., Toulson, G., Richardson, A., Gerhard, A., Snowden, J., Mann, D., Neary, D., Nalls, M.A., Peuralinna, T., Jansson, L., Isoviita, V.-M., Kaivorinne, A.-L., Hölttä-Vuori, M., Ikonen, E., Sulkava, R., Benatar, M., Wuu, J., Chiò, A., Restagno, G., Borghero, G., Sabatelli, M., Heckerman, D., Rogaeva, E., Zinman, L., Rothstein, J.D., Sendtner, M., Drepper, C., Eichler, E.E., Alkan, C., Abdullaev, Z., Pack, S.D., Dutra, A., Pak, E., Hardy, J., Singleton, A., Williams, N.M., Heutink, P., Pickering-Brown, S., Morris, H.R., Tienari, P.J., Traynor, B.J., 2011. A Hexanucleotide Repeat Expansion in C9ORF72 Is the Cause of Chromosome 9p21-Linked ALS-FTD. Neuron 72, 257–268. https://doi.org/10.1016/j.neuron.2011.09.010

Reubinoff, B.E., Pera, M.F., Fong, C.-Y., Trounson, A., Bongso, A., 2000. Embryonic stem cell lines from human blastocysts: somatic differentiation in vitro. Nat. Biotechnol. 18, 399–404. https://doi.org/10.1038/74447

Rideout, W.M., Eggan, K., Jaenisch, R., 2001. Nuclear cloning and epigenetic reprogramming of the genome. Science. https://doi.org/10.1126/science.1063206

RIDER, M.H., BERTRAND, L., VERTOMMEN, D., MICHELS, P.A., ROUSSEAU, G.G., HUE, L., 2004. 6-Phosphofructo-2-kinase/fructose-2,6-bisphosphatase: head-to-head with a bifunctional enzyme that controls glycolysis. Biochem. J. 381, 561–579. https://doi.org/10.1042/BJ20040752

Ring, K.L., Tong, L.M., Balestra, M.E., Javier, R., Andrews-Zwilling, Y., Li, G., Walker, D., Zhang, W.R., Kreitzer, A.C., Huang, Y., 2012. Direct Reprogramming of Mouse and Human Fibroblasts into Multipotent Neural Stem Cells with a Single Factor. Cell Stem Cell 11, 100–109. https://doi.org/10.1016/j.stem.2012.05.018

Robinton, D.A., Daley, G.Q., 2012a. The promise of induced pluripotent stem cells in research and therapy. Nature. https://doi.org/10.1038/nature10761

Robinton, D.A., Daley, G.Q., 2012b. The promise of induced pluripotent stem cells in research and therapy. Nature 481, 295–305. https://doi.org/10.1038/nature10761

Rodriguez-Rodriguez, P., Fernandez, E., Almeida, A., Bolaños, J.P., 2012. Excitotoxic stimulus stabilizes PFKFB3 causing pentose-phosphate pathway to glycolysis switch and neurodegeneration. Cell Death Differ. 19, 1582–1589. https://doi.org/10.1038/cdd.2012.33

Rodriguez-Rodriguez, P., Fernandez, E., Bolaños, J.P., 2013. Underestimation of the Pentose–Phosphate Pathway in Intact Primary Neurons as Revealed by Metabolic Flux Analysis. J. Cereb. Blood Flow Metab. 33, 1843–1845. https://doi.org/10.1038/jcbfm.2013.168

Rogers, L.D., Overall, C.M., 2013. Proteolytic Post-translational Modification of Proteins: Proteomic Tools and Methodology *. Mol. Cell. Proteomics 12, 3532–3542. https://doi.org/10.1074/mcp.M113.031310

Rogov, V., Dötsch, V., Johansen, T., Kirkin, V., 2014. Interactions between Autophagy Receptors and Ubiquitin-like Proteins Form the Molecular Basis for Selective Autophagy. Mol. Cell 53, 167–178. https://doi.org/10.1016/j.molcel.2013.12.014

Roosing, S., Rohrschneider, K., Beryozkin, A., Sharon, D., Weisschuh, N., Staller, J., Kohl, S., Zelinger, L., Peters, T.A., Neveling, K., Strom, T.M., van den Born, L.I., Hoyng, C.B., Klaver, C.C.W., Roepman, R., Wissinger, B., Banin, E., Cremers, F.P.M., den Hollander, A.I., 2013. Mutations in RAB28, Encoding a Farnesylated Small GTPase, Are Associated with Autosomal-Recessive Cone-Rod Dystrophy. Am. J. Hum. Genet. 93, 110–117. https://doi.org/10.1016/j.ajhg.2013.05.005

Roosing, S., van den Born, L.I., Sangermano, R., Banfi, S., Koenekoop, R.K., Zonneveld-Vrieling, M.N., Klaver, C.C.W., van Lith-Verhoeven, J.J.C., Cremers, F.P.M., den Hollander, A.I., Hoyng, C.B., 2015. Mutations in MFSD8, Encoding a Lysosomal Membrane Protein, Are Associated with Nonsyndromic Autosomal Recessive Macular Dystrophy. Ophthalmology 122, 170–179. https://doi.org/10.1016/j.ophtha.2014.07.040

Rosen, D.R., Siddique, T., Patterson, D., Figlewicz, D.A., Sapp, P., Hentati, A., Donaldson, D., Goto, J., O'Regan, J.P., Deng, H.-X., Rahmani, Z., Krizus, A., McKenna-Yasek, D., Cayabyab, A., Gaston, S.M., Berger, R., Tanzi, R.E., Halperin, J.J., Herzfeldt, B., Van den Bergh, R., Hung, W.-Y., Bird, T., Deng, G., Mulder, D.W., Smyth, C., Laing, N.G., Soriano, E., Pericak–Vance, M.A., Haines, J., Rouleau, G.A., Gusella, J.S., Horvitz, H.R., Brown, R.H., 1993a. Mutations in Cu/Zn superoxide dismutase gene are associated with familial amyotrophic lateral sclerosis. Nature 362, 59–62. https://doi.org/10.1038/362059a0

Rosen, D.R., Siddique, T., Patterson, D., Figlewicz, D.A., Sapp, P., Hentati, A., Donaldson, D., Goto, J., O'Regan, J.P., Deng, H.-X., Rahmani, Z., Krizus, A., McKenna-Yasek, D., Cayabyab, A., Gaston, S.M., Berger, R., Tanzi, R.E., Halperin, J.J., Herzfeldt, B., Van den Bergh, R., Hung, W.-Y., Bird, T., Deng, G., Mulder, D.W., Smyth, C., Laing, N.G., Soriano, E., Pericak–Vance, M.A., Haines, J., Rouleau, G.A., Gusella, J.S., Horvitz, H.R., Brown, R.H., 1993b. Mutations in Cu/Zn superoxide dismutase gene are associated with familial amyotrophic lateral sclerosis. Nature 362, 59–62. https://doi.org/10.1038/362059a0

Rothman, J.E., Söllner, T.H., 1997. Throttles and Dampers: Controlling the Engine of Membrane Fusion. Science 276, 1212–1212. https://doi.org/10.1126/science.276.5316.1212

Rothstein, J.D., 2009. Current hypotheses for the underlying biology of amyotrophic lateral sclerosis. Ann. Neurol. 65, S3–S9. https://doi.org/10.1002/ana.21543

Rowe, A.A., Chen, X., Nettesheim, E.R., Issioui, Y., Dong, T., Hu, Y., Messahel, S., Kayani, S.N., Gray, S.J., Wert, K.J., 2022. Long-term progression of retinal degeneration in a preclinical model of CLN7 Batten disease as a baseline for testing clinical therapeutics. EBioMedicine 85, 104314. https://doi.org/10.1016/j.ebiom.2022.104314

Russell, R.C., Tian, Y., Yuan, H., Park, H.W., Chang, Y.-Y., Kim, J., Kim, H., Neufeld, T.P., Dillin, A., Guan, K.-L., 2013. ULK1 induces autophagy by phosphorylating Beclin-1 and activating VPS34 lipid kinase. Nat. Cell Biol. 15, 741–750. https://doi.org/10.1038/ncb2757

Russell, W.M.S., Burch, R.L., 1959. The principles of humane experimental technique. Methuen, London.

Ryan, C.L., Baranowski, D.C., Chitramuthu, B.P., Malik, S., Li, Z., Cao, M., Minotti, S., Durham, H.D., Kay, D.G., Shaw, C.A., Bennett, H.P., Bateman, A., 2009. Progranulin is expressed within motor neurons and promotes neuronal cell survival. BMC Neurosci. 10, 130. https://doi.org/10.1186/1471-2202-10-130

Ryšlavá, H., Doubnerová, V., Kavan, D., Vaněk, O., 2013. Effect of posttranslational modifications on enzyme function and assembly. J. Proteomics, Special Issue: Posttranslational Protein Modifications in Biology and Medicine 92, 80–109. https://doi.org/10.1016/j.jprot.2013.03.025

Saftig, P., Klumperman, J., 2009. Lysosome biogenesis and lysosomal membrane proteins: trafficking meets function. Nat. Rev. Mol. Cell Biol. 10, 623–635. https://doi.org/10.1038/nrm2745

Saha, K., Jaenisch, R., 2009. Technical Challenges in Using Human Induced Pluripotent Stem Cells to Model Disease. Cell Stem Cell. https://doi.org/10.1016/j.stem.2009.11.009

Salmaninejad, A., Motaee, J., Farjami, M., Alimardani, M., Esmaeilie, A., Pasdar, A., 2019. Next-generation sequencing and its application in diagnosis of retinitis pigmentosa. Ophthalmic Genet. 40, 393–402. https://doi.org/10.1080/13816810.2019.1675178

Sanchez, I.I., Nguyen, T.B., England, W.E., Lim, R.G., Vu, A.Q., Miramontes, R., Byrne, L.M., Markmiller, S., Lau, A.L., Orellana, I., Curtis, M.A., Faull, R.L.M., Yeo, G.W., Fowler, C.D., Reidling, J.C., Wild, E.J., Spitale, R.C., Thompson, L.M., 2021. Huntington's disease mice and human brain tissue exhibit increased G3BP1 granules and TDP43 mislocalization. J. Clin. Invest. 131. https://doi.org/10.1172/JCI140723

Sano, A., Matsuda, S., Wen, T.C., Kotani, Y., Kondoh, K., Ueno, S., Kakimoto, Y., Yoshimura, H., Sakanaka, M., 1994. Protection by Prosaposin Against Ischemia-Induced Learning Disability and Neuronal Loss. Biochem. Biophys. Res. Commun. 204, 994–1000. https://doi.org/10.1006/bbrc.1994.2558

Santavuori, P., 1988. Neuronal ceroid-lipofuscinoses in childhood. Brain Dev. 10, 80–83. https://doi.org/10.1016/S0387-7604(88)80075-5

Santavuori, P., Haltia, M., Rapola, J., Raitta, C., 1973. Infantile type of so-called neuronal ceroid-lipofuscinosis: Part 1. A clinical study of 15 patients. J. Neurol. Sci. 18, 257–267. https://doi.org/10.1016/0022-510X(73)90075-0

Santavuori, P., Vanhanen, S.-L., Sainio, K., Nieminen, M., Wallden, T., Launes, J., Raininko, R., 1993. Infantile neuronal ceroid-lipofuscinosis (INCL): Diagnostic criteria. J. Inherit. Metab. Dis. 16, 227–229. https://doi.org/10.1007/BF00710250

Savukoski, M., Klockars, T., Holmberg, V., Santavuori, P., Lander, E.S., Peltonen, L., 1998. CLN5, a novel gene encoding a putative transmembrane protein mutated in Finnish variant late infantile neuronal ceroid lipofuscinosis. Nat. Genet. 19, 286–288. https://doi.org/10.1038/975

Saxena, S., Bucci, C., Weis, J., Kruttgen, A., 2005. The Small GTPase Rab7 Controls the Endosomal Trafficking and Neuritogenic Signaling of the Nerve Growth Factor Receptor TrkA. J. Neurosci. 25, 10930–10940. https://doi.org/10.1523/JNEUROSCI.2029-05.2005

Schink, K.O., Tan, K.-W., Stenmark, H., 2016. Phosphoinositides in Control of Membrane Dynamics. Annu. Rev. Cell Dev. Biol. 32, 143–171. https://doi.org/10.1146/annurev-cellbio-111315-125349

Schnabel, D., Schröder, M., Fürst, W., Klein, A., Hurwitz, R., Zenk, T., Weber, J., Harzer, K., Paton, B.C., Poulos, A., 1992. Simultaneous deficiency of sphingolipid activator proteins 1 and 2 is caused by a mutation in the initiation codon of their common gene. J. Biol. Chem. 267, 3312–3315. https://doi.org/10.1016/S0021-9258(19)50733-5

Schroeder, T., 2008. Imaging stem-cell-driven regeneration in mammals. Nature 453, 345–351. https://doi.org/10.1038/nature07043

Schubert, U., Antón, L.C., Gibbs, J., Norbury, C.C., Yewdell, J.W., Bennink, J.R., 2000. Rapid degradation of a large fraction of newly synthesized proteins by proteasomes. Nature 404, 770–774. https://doi.org/10.1038/35008096

Schulz, A., Dhar, S., Rylova, S., Dbaibo, G., Alroy, J., Hagel, C., Artacho, I., Kohlschütter, A., Lin, S., Boustany, R.-M., 2004. Impaired cell adhesion and apoptosis in a novel CLN9 Batten disease variant. Ann. Neurol. 56, 342–350. https://doi.org/10.1002/ana.20187

Schulze, H., Sandhoff, K., 2014. Sphingolipids and lysosomal pathologies. Biochim. Biophys. Acta BBA - Mol. Cell Biol. Lipids, New frontiers in sphingolipid biology 1841, 799–810. https://doi.org/10.1016/j.bbalip.2013.10.015

Schweitzer, J.S., Song, B., Herrington, T.M., Park, T.-Y., Lee, N., Ko, S., Jeon, J., Cha, Y., Kim, K., Li, Q., Henchcliffe, C., Kaplitt, M., Neff, C., Rapalino, O., Seo, H., Lee, I.-H., Kim, J., Kim, T., Petsko, G.A., Ritz, J., Cohen, B.M., Kong, S.-W., Leblanc, P., Carter, B.S., Kim, K.-S., 2020. Personalized iPSC-Derived Dopamine Progenitor Cells for Parkinson's Disease. N. Engl. J. Med. 382, 1926–1932. https://doi.org/10.1056/NEJMoa1915872

Sedek, M., Strous, G.J., 2013. SUMOylation is a regulator of the translocation of Jak2 between nucleus and cytosol. Biochem. J. 453, 231–239. https://doi.org/10.1042/BJ20121375

Sharaireh, A.M., Guevara-Ferrer, M., Herranz-Martin, S., Garcia-Macia, M., Phillips, A., Tierney, A., Hughes, M.P., Coombe-Tennant, O., Nelvagel, H., Burrows, A.E., Fielding, S., FitzPatrick, L.M., Thornton, C.D., Storch, S., Mole, S.E., Dowsey, A., Unwin, R., Bolanos, J.P., Rahim, A.A., McKay, T.R., 2022. CLN7 mutation causes aberrant redistribution of protein isoforms and contributes to Batten disease pathobiology. https://doi.org/10.1101/2022.04.21.488782

Sharifi, A., Kousi, M., Sagné, C., Bellenchi, G.C., Morel, L., Darmon, M., Hůlková, H., Ruivo, R., Debacker, C., El Mestikawy, S., Elleder, M., Lehesjoki, A.-E., Jalanko, A., Gasnier, B., Kyttälä, A., 2010. Expression and lysosomal targeting of CLN7, a major facilitator superfamily transporter associated with variant late-infantile neuronal ceroid lipofuscinosis. Hum. Mol. Genet. 19, 4497–4514. https://doi.org/10.1093/hmg/ddq381

Sheff, D.R., Daro, E.A., Hull, M., Mellman, I., 1999. The Receptor Recycling Pathway Contains Two Distinct Populations of Early Endosomes with Different Sorting Functions. J. Cell Biol. 145, 123–139. https://doi.org/10.1083/jcb.145.1.123

Shimobayashi, M., Hall, M.N., 2014. Making new contacts: the mTOR network in metabolism and signalling crosstalk. Nat. Rev. Mol. Cell Biol. 15, 155–162. https://doi.org/10.1038/nrm3757

Shin, W.J., Seo, J., Choi, H.W., Hong, Y.J., Lee, W.J., Chae, J. Il, Kim, S.J., Lee, J.W., Hong, K., Song, H., Park, C., Do, J.T., 2019. Derivation of primitive neural stem cells from human-induced pluripotent stem cells. J. Comp. Neurol. 527, 3023–3033. https://doi.org/10.1002/cne.24727

Shukla, S., Parker, R., 2016. Hypo- and Hyper-Assembly Diseases of RNA–Protein Complexes. Trends Mol. Med. 22, 615–628. https://doi.org/10.1016/j.molmed.2016.05.005

Sidoryk-Wegrzynowicz, M., Wegrzynowicz, M., Lee, E., Bowman, A.B., Aschner, M., 2011. Role of Astrocytes in Brain Function and Disease. Toxicol. Pathol. 39, 115–123. https://doi.org/10.1177/0192623310385254

Siintola, E., Partanen, S., Strömme, P., Haapanen, A., Haltia, M., Maehlen, J., Lehesjoki, A.-E., Tyynelä, J., 2006. Cathepsin D deficiency underlies congenital human neuronal ceroid-lipofuscinosis. Brain 129, 1438–1445. https://doi.org/10.1093/brain/awl107

Siintola, E., Topcu, M., Aula, N., Lohi, H., Minassian, B.A., Paterson, A.D., Liu, X.-Q., Wilson, C., Lahtinen, U., Anttonen, A.-K., Lehesjoki, A.-E., 2007. The Novel Neuronal Ceroid Lipofuscinosis Gene MFSD8 Encodes a Putative Lysosomal Transporter. Am. J. Hum. Genet. 81, 136–146. https://doi.org/10.1086/518902

Siintola, E., Topcu, M., Kohlschütter, A., Salonen, T., Joensuu, T., Anttonen, A.-K., Lehesjoki, A.-E., 2005. Two novel CLN6 mutations in variant late-infantile neuronal ceroid lipofuscinosis patients of Turkish origin. Clin. Genet. 68, 167–173. https://doi.org/10.1111/j.1399-0004.2005.00471.x

Simonati A, Williams RE. Neuronal Ceroid Lipofuscinosis: The Multifaceted Approach to the Clinical Issues, an Overview. Front Neurol. 2022 Mar 11;13:811686. https://doi.org/10.3389/fneur.2022.811686

Singh, V.K., Kalsan, M., Kumar, N., Saini, A., Chandra, R., 2015. Induced pluripotent stem cells: applications in regenerative medicine, disease modeling, and drug discovery. Front. Cell Dev. Biol. 3.

Skamnaki, V.T., Owen, D.J., Noble, M.E.M., Lowe, E.D., Lowe, G., Oikonomakos, N.G., Johnson, L.N., 1999. Catalytic Mechanism of Phosphorylase Kinase Probed by Mutational Studies,. Biochemistry 38, 14718–14730. https://doi.org/10.1021/bi991454f

Skibinski, G., Nakamura, K., Cookson, M.R., Finkbeiner, S., 2014. Mutant LRRK2 Toxicity in Neurons Depends on LRRK2 Levels and Synuclein But Not Kinase Activity or Inclusion Bodies. J. Neurosci. 34, 418–433. https://doi.org/10.1523/JNEUROSCI.2712-13.2014

Sleat, D.E., Ding, L., Wang, S., Zhao, C., Wang, Y., Xin, W., Zheng, H., Moore, D.F., Sims, K.B., 2009. Mass Spectrometry-based Protein Profiling to Determine the Cause of Lysosomal Storage Diseases of Unknown Etiology *. Mol. Cell. Proteomics 8, 1708–1718. https://doi.org/10.1074/mcp.M900122-MCP200

Sleat, D.E., Donnelly, R.J., Lackland, H., Liu, C.-G., Sohar, I., Pullarkat, R.K., Lobel, P., 1997. Association of Mutations in a Lysosomal Protein with Classical Late-Infantile Neuronal Ceroid Lipofuscinosis. Science 277, 1802–1805. https://doi.org/10.1126/science.277.5333.1802

Smith, K.R., Dahl, H.-H.M., Canafoglia, L., Andermann, E., Damiano, J., Morbin, M., Bruni, A.C., Giaccone, G., Cossette, P., Saftig, P., Grötzinger, J., Schwake, M., Andermann, F., Staropoli, J.F., Sims, K.B., Mole, S.E., Franceschetti, S., Alexander, N.A., Cooper, J.D., Chapman, H.A.,

Carpenter, S., Berkovic, S.F., Bahlo, M., 2013. Cathepsin F mutations cause Type B Kufs disease, an adult-onset neuronal ceroid lipofuscinosis. Hum. Mol. Genet. 22, 1417–1423. https://doi.org/10.1093/hmg/dds558

Smith, K.R., Damiano, J., Franceschetti, S., Carpenter, S., Canafoglia, L., Morbin, M., Rossi, G., Pareyson, D., Mole, S.E., Staropoli, J.F., Sims, K.B., Lewis, J., Lin, W.-L., Dickson, D.W., Dahl, H.-H., Bahlo, M., Berkovic, S.F., 2012. Strikingly Different Clinicopathological Phenotypes Determined by Progranulin-Mutation Dosage. Am. J. Hum. Genet. 90, 1102–1107. https://doi.org/10.1016/j.ajhg.2012.04.021

Snel, B., Bork, P., Huynen, M.A., 2002. The identification of functional modules from the genomic association of genes. Proc. Natl. Acad. Sci. 99, 5890–5895. https://doi.org/10.1073/pnas.092632599

Snowden, J.S., Craufurd, D., Griffiths, H.L., Neary, D., 1998. Awareness of Involuntary Movements in Huntington Disease. Arch. Neurol. 55, 801–805. https://doi.org/10.1001/archneur.55.6.801

SOARES-SILVA, I., SCHULLER, D., ANDRADE, R.P., BALTAZAR, F., CÁSSIO, F., CASAL, M., 2003. Functional expression of the lactate permease Jen1p of Saccharomyces cerevisiae in Pichia pastoris. Biochem. J. 376, 781–787. https://doi.org/10.1042/bj20031180

Soldati, C., Lopez-Fabuel, I., Wanderlingh, L.G., Garcia-Macia, M., Monfregola, J., Esposito, A., Napolitano, G., Guevara-Ferrer, M., Scotto Rosato, A., Krogsaeter, E.K., Paquet, D., Grimm, C.M., Montefusco, S., Braulke, T., Storch, S., Mole, S.E., De Matteis, M.A., Ballabio, A., Sampaio, J.L., McKay, T., Johannes, L., Bolaños, J.P., Medina, D.L., 2021. Repurposing of tamoxifen ameliorates CLN3 and CLN7 disease phenotype. EMBO Mol. Med. 13, e13742. https://doi.org/10.15252/emmm.202013742

Söllner, T., Whiteheart, S.W., Brunner, M., Erdjument-Bromage, H., Geromanos, S., Tempst, P., Rothman, J.E., 1993. SNAP receptors implicated in vesicle targeting and fusion. Nature 362, 318–324. https://doi.org/10.1038/362318a0

Solomon, S., Xu, Y., Wang, B., David, M.D., Schubert, P., Kennedy, D., Schrader, J.W., 2007. Distinct Structural Features ofCaprin-1 Mediate Its Interaction with G3BP-1 and Its Induction of Phosphorylation of Eukaryotic Translation InitiationFactor 2α, Entry to Cytoplasmic Stress Granules, and Selective Interaction with a Subset of mRNAs. Mol. Cell. Biol. 27, 2324–2342. https://doi.org/10.1128/MCB.02300-06

Sönnichsen, B., De Renzis, S., Nielsen, E., Rietdorf, J., Zerial, M., 2000. Distinct Membrane Domains on Endosomes in the Recycling Pathway Visualized by Multicolor Imaging of Rab4, Rab5, and Rab11. J. Cell Biol. 149, 901–914. https://doi.org/10.1083/jcb.149.4.901

Spathopoulou, A., Edenhofer, F., Fellner, L., 2022. Targeting α-Synuclein in Parkinson's Disease by Induced Pluripotent Stem Cell Models. Front. Neurol. 12.

Spencer B, Potkar R, Trejo M, Rockenstein E, Patrick C, Gindi R, Adame A, Wyss-Coray T, Masliah E. 2009. Beclin 1 gene transfer activates autophagy and ameliorates the neurodegenerative pathology in alpha-synuclein models of Parkinson's and Lewy body diseases. J Neurosci. 28;29(43):13578-88. https://doi.org/10.1523/JNEUROSCI.4390-09.2009

Sphingolipid Activator Proteins [WWW Document], n.d. . McGraw Hill Med. URL https://ommbid.mhmedical.com/content.aspx?bookId=2709&sectionId=225543732 (accessed 7.11.23).

Spinelli, J.B., Haigis, M.C., 2018. The multifaceted contributions of mitochondria to cellular metabolism. Nat. Cell Biol. 20, 745–754. https://doi.org/10.1038/s41556-018-0124-1

Sreedharan, J., Blair, I.P., Tripathi, V.B., Hu, X., Vance, C., Rogelj, B., Ackerley, S., Durnall, J.C., Williams, K.L., Buratti, E., Baralle, F., de Belleroche, J., Mitchell, J.D., Leigh, P.N., Al-Chalabi, A., Miller, C.C., Nicholson, G., Shaw, C.E., 2008. TDP-43 Mutations in Familial and Sporadic Amyotrophic Lateral Sclerosis. Science 319, 1668–1672. https://doi.org/10.1126/science.1154584

Stadtfeld, M., Nagaya, M., Utikal, J., Weir, G., Hochedlinger, K., 2008. Induced Pluripotent Stem Cells Generated Without Viral Integration. Science 322, 945–949. https://doi.org/10.1126/science.1162494

Staropoli, J.F., Karaa, A., Lim, E.T., Kirby, A., Elbalalesy, N., Romansky, S.G., Leydiker, K.B., Coppel, S.H., Barone, R., Xin, W., MacDonald, M.E., Abdenur, J.E., Daly, M.J., Sims, K.B., Cotman, S.L., 2012. A Homozygous Mutation in KCTD7 Links Neuronal Ceroid Lipofuscinosis to the Ubiquitin-Proteasome System. Am. J. Hum. Genet. 91, 202–208. https://doi.org/10.1016/j.ajhg.2012.05.023

Steenhuis, P., Froemming, J., Reinheckel, T., Storch, S., 2012. Proteolytic cleavage of the disease-related lysosomal membrane glycoprotein CLN7. Biochim. Biophys. Acta BBA - Mol. Basis Dis. 1822, 1617–1628. https://doi.org/10.1016/j.bbadis.2012.05.015

Steenhuis, P., Herder, S., Gelis, S., Braulke, T., Storch, S., 2010. Lysosomal Targeting of the CLN7 Membrane Glycoprotein and Transport Via the Plasma Membrane Require a Dileucine Motif. Traffic 11, 987–1000. https://doi.org/10.1111/j.1600-0854.2010.01073.x

Steinfeld, R., Reinhardt, K., Schreiber, K., Hillebrand, M., Kraetzner, R., Brück, W., Saftig, P., Gärtner, J., 2006. Cathepsin D Deficiency Is Associated with a Human Neurodegenerative Disorder. Am. J. Hum. Genet. 78, 988–998. https://doi.org/10.1086/504159

Stolz, A., Ernst, A., Dikic, I., 2014. Cargo recognition and trafficking in selective autophagy. Nat. Cell Biol. 16, 495–501. https://doi.org/10.1038/ncb2979

Strumillo, M., Beltrao, P., 2015. Towards the computational design of protein post-translational regulation. Bioorg. Med. Chem., Chemistry and Biology of Protein and Inositol Phosphorylation 23, 2877–2882. https://doi.org/10.1016/j.bmc.2015.04.056

Suzuki, K., Kirisako, T., Kamada, Y., Mizushima, N., Noda, T., Ohsumi, Y., 2001. The pre-autophagosomal structure organized by concerted functions of APG genes is essential for autophagosome formation. EMBO J. 20, 5971–5981. https://doi.org/10.1093/emboj/20.21.5971

Suzuki, K., Kubota, Y., Sekito, T., Ohsumi, Y., 2007. Hierarchy of Atg proteins in pre-autophagosomal structure organization. Genes Cells 12, 209–218. https://doi.org/10.1111/j.1365-2443.2007.01050.x

Szklarczyk, D., Kirsch, R., Koutrouli, M., Nastou, K., Mehryary, F., Hachilif, R., Gable, A.L., Fang, T., Doncheva, N.T., Pyysalo, S., Bork, P., Jensen, L.J., von Mering, C., 2023. The STRING database in 2023: protein–protein association networks and functional enrichment analyses for any

sequenced genome of interest. Nucleic Acids Res. 51, D638–D646. https://doi.org/10.1093/nar/gkac1000

Takahashi, K., Tanabe, K., Ohnuki, M., Narita, M., Ichisaka, T., Tomoda, K., Yamanaka, S., 2007. Induction of Pluripotent Stem Cells from Adult Human Fibroblasts by Defined Factors. Cell 131, 861–872. https://doi.org/10.1016/j.cell.2007.11.019

Takahashi, K., Yamanaka, S., 2006. Induction of Pluripotent Stem Cells from Mouse Embryonic and Adult Fibroblast Cultures by Defined Factors. Cell 126, 663–676. https://doi.org/10.1016/j.cell.2006.07.024

Takáts, S., Nagy, P., Varga, Á., Pircs, K., Kárpáti, M., Varga, K., Kovács, A.L., Hegedűs, K., Juhász, G., 2013. Autophagosomal Syntaxin17-dependent lysosomal degradation maintains neuronal function in Drosophila. J. Cell Biol. 201, 531–539. https://doi.org/10.1083/jcb.201211160

Tamamaki, N., Nakamura, K., Okamoto, K., Kaneko, T., 2001. Radial glia is a progenitor of neocortical neurons in the developing cerebral cortex. Neurosci. Res. 41, 51–60. https://doi.org/10.1016/S0168-0102(01)00259-0

Tamura, Y., Endo, T., 2017. Role of Intra- and Inter-mitochondrial Membrane Contact Sites in Yeast Phospholipid Biogenesis, in: Tagaya, M., Simmen, T. (Eds.), Organelle Contact Sites: From Molecular Mechanism to Disease, Advances in Experimental Medicine and Biology. Springer, Singapore, pp. 121–133. https://doi.org/10.1007/978-981-10-4567-7_9

Tan, C.-C., Yu, J.-T., Tan, M.-S., Jiang, T., Zhu, X.-C., Tan, L., 2014. Autophagy in aging and neurodegenerative diseases: implications for pathogenesis and therapy. Neurobiol. Aging 35, 941–957. https://doi.org/10.1016/j.neurobiolaging.2013.11.019

Tanabe, K., Nakamura, M., Narita, M., Takahashi, K., Yamanaka, S., 2013. Maturation, not initiation, is the major roadblock during reprogramming toward pluripotency from human fibroblasts. Proc. Natl. Acad. Sci. 110, 12172–12179. https://doi.org/10.1073/pnas.1310291110

Tanaka, Y., Guhde, G., Suter, A., Eskelinen, E.-L., Hartmann, D., Lüllmann-Rauch, R., Janssen, P.M.L., Blanz, J., von Figura, K., Saftig, P., 2000. Accumulation of autophagic vacuoles and cardiomyopathy in LAMP-2-deficient mice. Nature 406, 902–906. https://doi.org/10.1038/35022595

Tanida, I., 2011. Autophagosome Formation and Molecular Mechanism of Autophagy. Antioxid. Redox Signal. 14, 2201–2214. https://doi.org/10.1089/ars.2010.3482

Tanida, I., Ueno, T., Kominami, E., 2008. LC3 and Autophagy, in: Deretic, V. (Ed.), Autophagosome and Phagosome, Methods in Molecular Biology™. Humana Press, Totowa, NJ, pp. 77–88. https://doi.org/10.1007/978-1-59745-157-4_4

Tanzi, R.E., Bertram, L., 2005. Twenty Years of the Alzheimer's Disease Amyloid Hypothesis: A Genetic Perspective. Cell 120, 545–555. https://doi.org/10.1016/j.cell.2005.02.008

Tarabykin, V., Stoykova, A., Usman, N., Gruss, P., 2001. Cortical upper layer neurons derive from the subventricular zone as indicated by Svet1 gene expression. Development 128, 1983–1993. https://doi.org/10.1242/dev.128.11.1983

Thiadens, A.A.H.J., Slingerland, N.W.R., Roosing, S., Schooneveld, M.J. van, Lith-Verhoeven, J.J.C. van, Moll-Ramirez, N. van, Born, L.I. van den, Hoyng, C.B., Cremers, F.P.M., Klaver,

C.C.W., 2009. Genetic Etiology and Clinical Consequences of Complete and Incomplete Achromatopsia. Ophthalmology 116, 1984-1989.e1. https://doi.org/10.1016/j.ophtha.2009.03.053

Thiadens, A.A.H.J., Somervuo, V., van den Born, L.I., Roosing, S., van Schooneveld, M.J., Kuijpers, R.W.A.M., van Moll-Ramirez, N., Cremers, F.P.M., Hoyng, C.B., Klaver, C.C.W., 2010. Progressive Loss of Cones in Achromatopsia: An Imaging Study Using Spectral-Domain Optical Coherence Tomography. Invest. Ophthalmol. Vis. Sci. 51, 5952–5957. https://doi.org/10.1167/iovs.10-5680

Thomson, J.A., Itskovitz-Eldor, J., Shapiro, S.S., Waknitz, M.A., Swiergiel, J.J., Marshall, V.S., Jones, J.M., 1998. Embryonic Stem Cell Lines Derived from Human Blastocysts. Science 282, 1145–1147. https://doi.org/10.1126/science.282.5391.1145

Tillement, L., Lecanu, L., Papadopoulos, V., 2011. Alzheimer's disease: Effects of β-amyloid on mitochondria. Mitochondrion 11, 13–21. https://doi.org/10.1016/j.mito.2010.08.009

Trancikova, A., Ramonet, D., Moore, D.J., 2011. Chapter 11 - Genetic Mouse Models of Neurodegenerative Diseases, in: Chang, K.T., Min, K.-T. (Eds.), Progress in Molecular Biology and Translational Science, Animal Models of Human Disease. Academic Press, pp. 419–482. https://doi.org/10.1016/B978-0-12-384878-9.00012-1

Tsuji, Y., 2020. Transmembrane protein western blotting: Impact of sample preparation on detection of SLC11A2 (DMT1) and SLC40A1 (ferroportin). PLOS ONE 15, e0235563. https://doi.org/10.1371/journal.pone.0235563

Tsukada, M., Ohsumi, Y., 1993. Isolation and characterization of autophagy-defective mutants of Saccharomyces cerevisiae. FEBS Lett. 333, 169–174. https://doi.org/10.1016/0014-5793(93)80398-E

Tyynelä, J., Palmer, D.N., Baumann, M., Haltia, M., 1993. Storage of saposins A and D in infantile neuronal ceroid-lipofuscinosis. FEBS Lett. 330, 8–12. https://doi.org/10.1016/0014-5793(93)80908-D

Vanderweyde, T., Apicco, D.J., Youmans-Kidder, K., Ash, P.E.A., Cook, C., Rocha, E.L. da, Jansen-West, K., Frame, A.A., Citro, A., Leszyk, J.D., Ivanov, P., Abisambra, J.F., Steffen, M., Li, H., Petrucelli, L., Wolozin, B., 2016. Interaction of tau with the RNA-Binding Protein TIA1 Regulates tau Pathophysiology and Toxicity. Cell Rep. 15, 1455–1466. https://doi.org/10.1016/j.celrep.2016.04.045

Vantaggiato, C., Redaelli, F., Falcone, S., Perrotta, C., Tonelli, A., Bondioni, S., Morbin, M., Riva, D., Saletti, V., Bonaglia, M.C., Giorda, R., Bresolin, N., Clementi, E., Bassi, M.T., 2009. A novel CLN8 mutation in late-infantile-onset neuronal ceroid lipofuscinosis (LINCL) reveals aspects of CLN8 neurobiological function. Hum. Mutat. 30, 1104–1116. https://doi.org/10.1002/humu.21012

Varki, A., 1993. Biological roles of oligosaccharides: all of the theories are correct. Glycobiology 3, 97–130. https://doi.org/10.1093/glycob/3.2.97

Vaughn, A.E., Deshmukh, M., 2008. Glucose metabolism inhibits apoptosis in neurons and cancer cells by redox inactivation of cytochrome c. Nat. Cell Biol. 10, 1477–1483. https://doi.org/10.1038/ncb1807

Venter, J.C., Adams, M.D., Myers, E.W., Li, P.W., Mural, R.J., Sutton, G.G., Smith, H.O., Yandell, M., Evans, C.A., Holt, R.A., Gocayne, J.D., Amanatides, P., Ballew, R.M., Huson, D.H., Wortman, J.R., Zhang, Q., Kodira, C.D., Zheng, X.H., Chen, L., Skupski, M., Subramanian, G., Thomas, P.D., Zhang, J., Gabor Miklos, G.L., Nelson, C., Broder, S., Clark, A.G., Nadeau, J., McKusick, V.A., Zinder, N., Levine, A.J., Roberts, R.J., Simon, M., Slayman, C., Hunkapiller, M., Bolanos, R., Delcher, A., Dew, I., Fasulo, D., Flanigan, M., Florea, L., Halpern, A., Hannenhalli, S., Kravitz, S., Levy, S., Mobarry, C., Reinert, K., Remington, K., Abu-Threideh, J., Beasley, E., Biddick, K., Bonazzi, V., Brandon, R., Cargill, M., Chandramouliswaran, I., Charlab, R., Chaturvedi, K., Deng, Z., Francesco, V.D., Dunn, P., Eilbeck, K., Evangelista, C., Gabrielian, A.E., Gan, W., Ge, W., Gong, F., Gu, Z., Guan, P., Heiman, T.J., Higgins, M.E., Ji, R.-R., Ke, Z., Ketchum, K.A., Lai, Z., Lei, Y., Li, Z., Li, J., Liang, Y., Lin, X., Lu, F., Merkulov, G.V., Milshina, N., Moore, H.M., Naik, A.K., Narayan, V.A., Neelam, B., Nusskern, D., Rusch, D.B., Salzberg, S., Shao, W., Shue, B., Sun, J., Wang, Z.Y., Wang, A., Wang, X., Wang, J., Wei, M.-H., Wides, R., Xiao, C., Yan, C., Yao, A., Ye, J., Zhan, M., Zhang, W., Zhang, H., Zhao, Q., Zheng, L., Zhong, F., Zhong, W., Zhu, S.C., Zhao, S., Gilbert, D., Baumhueter, S., Spier, G., Carter, C., Cravchik, A., Woodage, T., Ali, F., An, H., Awe, A., Baldwin, D., Baden, H., Barnstead, M., Barrow, I., Beeson, K., Busam, D., Carver, A., Center, A., Cheng, M.L., Curry, L., Danaher, S., Davenport, L., Desilets, R., Dietz, S., Dodson, K., Doup, L., Ferriera, S., Garg, N., Gluecksmann, A., Hart, B., Haynes, J., Haynes, C., Heiner, C., Hladun, S., Hostin, D., Houck, J., Howland, T., Ibegwam, C., Johnson, J., Kalush, F., Kline, L., Koduru, S., Love, A., Mann, F., May, D., McCawley, S., McIntosh, T., McMullen, I., Moy, M., Moy, L., Murphy, B., Nelson, K., Pfannkoch, C., Pratts, E., Puri, V., Qureshi, H., Reardon, M., Rodriguez, R., Rogers, Y.-H., Romblad, D., Ruhfel, B., Scott, R., Sitter, C., Smallwood, M., Stewart, E., Strong, R., Suh, E., Thomas, R., Tint, N.N., Tse, S., Vech, C., Wang, G., Wetter, J., Williams, S., Williams, M., Windsor, S., Winn-Deen, E., Wolfe, K., Zaveri, J., Zaveri, K., Abril, J.F., Guigó, R., Campbell, M.J., Sjolander, K.V., Karlak, B., Kejariwal, A., Mi, H., Lazareva, B., Hatton, T., Narechania, A., Diemer, K., Muruganujan, A., Guo, N., Sato, S., Bafna, V., Istrail, S., Lippert, R., Schwartz, R., Walenz, B., Yooseph, S., Allen, D., Basu, A., Baxendale, J., Blick, L., Caminha, M., Carnes-Stine, J., Caulk, P., Chiang, Y.-H., Coyne, M., Dahlke, C., Mays, A.D., Dombroski, M., Donnelly, M., Ely, D., Esparham, S., Fosler, C., Gire, H., Glanowski, S., Glasser, K., Glodek, A., Gorokhov, M., Graham, K., Gropman, B., Harris, M., Heil, J., Henderson, S., Hoover, J., Jennings, D., Jordan, C., Jordan, J., Kasha, J., Kagan, L., Kraft, C., Levitsky, A., Lewis, M., Liu, X., Lopez, J., Ma, D., Majoros, W., McDaniel, J., Murphy, S., Newman, M., Nguyen, T., Nguyen, N., Nodell, M., Pan, S., Peck, J., Peterson, M., Rowe, W., Sanders, R., Scott, J., Simpson, M., Smith, T., Sprague, A., Stockwell, T., Turner, R., Venter, E., Wang, M., Wen, M., Wu, D., Wu, M., Xia, A., Zandieh, A., Zhu, X., 2001. The Sequence of the Human Genome. Science 291, 1304–1351. https://doi.org/10.1126/science.1058040

Verkruyse, L.A., Hofmann, S.L., 1996. Lysosomal Targeting of Palmitoyl-protein Thioesterase *. J. Biol. Chem. 271, 15831–15836. https://doi.org/10.1074/jbc.271.26.15831

Vesa, J., Hellsten, E., Verkruyse, L.A., Camp, L.A., Rapola, J., Santavuori, P., Hofmann, S.L., Peltonen, L., 1995. Mutations in the palmitoyl protein thioesterase gene causing infantile neuronal ceroid lipofuscinosis. Nature 376, 584–587. https://doi.org/10.1038/376584a0

Völgyi, K., Gulyássy, P., Háden, K., Kis, V., Badics, K., Kékesi, K.A., Simor, A., Györffy, B., Tóth, E.A., Lubec, G., Juhász, G., Dobolyi, A., 2015. Synaptic mitochondria: A brain mitochondria cluster with a specific proteome. J. Proteomics 120, 142–157. https://doi.org/10.1016/j.jprot.2015.03.005

von Kleist, L., Ariunbat, K., Braren, I., Stauber, T., Storch, S., Danyukova, T., 2019. A newly generated neuronal cell model of CLN7 disease reveals aberrant lysosome motility and impaired

cell survival. Mol. Genet. Metab., Special Issue of Molecular Genetics and Metabolism on The Lysosome 126, 196–205. https://doi.org/10.1016/j.ymgme.2018.09.009

Wakao, S., Kitada, M., Kuroda, Y., Ogura, F., Murakami, T., Niwa, A., Dezawa, M., 2012. Morphologic and Gene Expression Criteria for Identifying Human Induced Pluripotent Stem Cells. PLoS ONE 7, 48677. https://doi.org/10.1371/journal.pone.0048677

Walker, J.E., 2013. The ATP synthase: the understood, the uncertain and the unknown. Biochem. Soc. Trans. 41, 1–16. https://doi.org/10.1042/BST20110773

Wang, C., Najm, R., Xu, Q., Jeong, D., Walker, D., Balestra, M.E., Yoon, S.Y., Yuan, H., Li, G., Miller, Z.A., Miller, B.L., Malloy, M.J., Huang, Y., 2018. Gain of toxic apolipoprotein E4 effects in human iPSC-derived neurons is ameliorated by a small-molecule structure corrector. Nat. Med. 24, 647–657. https://doi.org/10.1038/s41591-018-0004-z

Wang, M., Jiang, Y., Xu, X., 2015. A novel method for predicting post-translational modifications on serine and threonine sites by using site-modification network profiles. Mol. Biosyst. 11, 3092–3100. https://doi.org/10.1039/C5MB00384A

Wang, W., Gopal, S., Pocock, R., Xiao, Z., 2019. Glycan Mimetics from Natural Products: New Therapeutic Opportunities for Neurodegenerative Disease. Molecules 24, 4604. https://doi.org/10.3390/molecules24244604

Wang, W., Zhao, F., Ma, X., Perry, G., Zhu, X., 2020. Mitochondria dysfunction in the pathogenesis of Alzheimer's disease: recent advances. Mol. Neurodegener. 15, 30. https://doi.org/10.1186/s13024-020-00376-6

Wang, X., Yang, C., 2016. Programmed cell death and clearance of cell corpses in Caenorhabditis elegans. Cell. Mol. Life Sci. 73, 2221–2236. https://doi.org/10.1007/s00018-016-2196-z

Wang, Yihui, Teng, Y., Liang, D., Li, Z., Wu, L., 2021. Simultaneous Identification of Both MFSD8 and RDH12 Pathogenic Variants in a Chinese Family Affected With Retinitis Pigmentosa. Front. Genet. 12.

Wang, Yayu, Zeng, W., Lin, B., Yao, Y., Li, C., Hu, W., Wu, H., Huang, J., Zhang, M., Xue, T., Ren, D., Qu, L., Cang, C., 2021. CLN7 is an organellar chloride channel regulating lysosomal function. Sci. Adv. 7, eabj9608. https://doi.org/10.1126/sciadv.abj9608

Warren, L., Manos, P.D., Ahfeldt, T., Loh, Y.-H., Li, H., Lau, F., Ebina, W., Mandal, P.K., Smith, Z.D., Meissner, A., Daley, G.Q., Brack, A.S., Collins, J.J., Cowan, C., Schlaeger, T.M., Rossi, D.J., 2010. Highly Efficient Reprogramming to Pluripotency and Directed Differentiation of Human Cells with Synthetic Modified mRNA. Cell Stem Cell 7, 618–630. https://doi.org/10.1016/j.stem.2010.08.012

Wei, L., Xing, P., Shi, G., Ji, Z., Zou, Q., 2019. Fast Prediction of Protein Methylation Sites Using a Sequence-Based Feature Selection Technique. IEEE/ACM Trans. Comput. Biol. Bioinform. 16, 1264–1273. https://doi.org/10.1109/TCBB.2017.2670558

Wernig, M., Lengner, C.J., Hanna, J., Lodato, M.A., Steine, E., Foreman, R., Staerk, J., Markoulaki, S., Jaenisch, R., 2008. A drug-inducible transgenic system for direct reprogramming of multiple somatic cell types. Nat. Biotechnol. 26, 916–924. https://doi.org/10.1038/nbt1483

Wernig, M., Meissner, A., Foreman, R., Brambrink, T., Ku, M., Hochedlinger, K., Bernstein, B.E., Jaenisch, R., 2007. In vitro reprogramming of fibroblasts into a pluripotent ES-cell-like state. Nature 448, 318–324. https://doi.org/10.1038/nature05944

Wilk-Blaszczak, M., n.d. Posttranslational modifications of proteins.

Williams, R.E., Mole, S.E., 2012. New nomenclature and classification scheme for the neuronal ceroid lipofuscinoses. Neurology 79, 183–191. https://doi.org/10.1212/WNL.0b013e31825f0547

Wolf, D., Goff, S.P., 2007. TRIM28 Mediates Primer Binding Site-Targeted Silencing of Murine Leukemia Virus in Embryonic Cells. Cell 131, 46–57. https://doi.org/10.1016/j.cell.2007.07.026

Wolozin, B., Ivanov, P., 2019. Stress granules and neurodegeneration. Nat. Rev. Neurosci. 20, 649–666. https://doi.org/10.1038/s41583-019-0222-5

Woltjen, K., Michael, I.P., Mohseni, P., Desai, R., Mileikovsky, M., Hämäläinen, R., Cowling, R., Wang, W., Liu, P., Gertsenstein, M., Kaji, K., Sung, H.-K., Nagy, A., 2009. piggyBac transposition reprograms fibroblasts to induced pluripotent stem cells. Nature 458, 766–770. https://doi.org/10.1038/nature07863

Wong, H.-S., Dighe, P.A., Mezera, V., Monternier, P.-A., Brand, M.D., 2017. Production of superoxide and hydrogen peroxide from specific mitochondrial sites under different bioenergetic conditions. J. Biol. Chem. 292, 16804–16809. https://doi.org/10.1074/jbc.R117.789271

Wong, P., Cai, H., Borchelt, D., Price, D., 2002. Genetically engineered mouse models of neurodegenerative diseases. Nat. Neurosci. 5, 633–9. https://doi.org/10.1038/nn0702-633

Wright, A.J., Andrews, P.W., 2009. Surface marker antigens in the characterization of human embryonic stem cells. Stem Cell Res. 3, 3–11. https://doi.org/10.1016/j.scr.2009.04.001

Xu W, Fang F, Ding J, Wu C. 2018. Dysregulation of Rab5-mediated endocytic pathways in Alzheimer's disease. Traffic. 19(4):253-262. https://doi.org/10.1111/tra.12547

Yamamoto H, Zhang S, Mizushima N. Autophagy genes in biology and disease. 2023. Nat Rev Genet. 24(6):382-400. https://doi.org/10.1038/s41576-022-00562-w.

Yamano, K., Fogel, A.I., Wang, C., van der Bliek, A.M., Youle, R.J., 2014. Mitochondrial Rab GAPs govern autophagosome biogenesis during mitophagy. eLife 3, e01612. https://doi.org/10.7554/eLife.01612

Yang, C., Wang, X., 2021. Lysosome biogenesis: Regulation and functions. J. Cell Biol. 220, e202102001. https://doi.org/10.1083/jcb.202102001

Yang, M., Lu, Y., Piao, W., Jin, H., 2022. The Translational Regulation in mTOR Pathway. Biomolecules 12, 802. https://doi.org/10.3390/biom12060802

Yasuda, T., Mochizuki, H., 2010. The regulatory role of α-synuclein and parkin in neuronal cell apoptosis; possible implications for the pathogenesis of Parkinson's disease. Apoptosis 15, 1312–1321. https://doi.org/10.1007/s10495-010-0486-8

Yasui R, Sekine K, Taniguchi H. Clever Experimental Designs: Shortcuts for Better iPSC Differentiation. Cells. 2021 Dec 15;10(12):3540. https://doi.org/10.3390/cells10123540

Yen, W.-L., Shintani, T., Nair, U., Cao, Y., Richardson, B.C., Li, Z., Hughson, F.M., Baba, M., Klionsky, D.J., 2010. The conserved oligomeric Golgi complex is involved in double-membrane vesicle formation during autophagy. J. Cell Biol. 188, 101–114. https://doi.org/10.1083/jcb.200904075

Ylä-Anttila, P., Vihinen, H., Jokitalo, E., Eskelinen, E.-L., 2009. 3D tomography reveals connections between the phagophore and endoplasmic reticulum. Autophagy 5, 1180–1185. https://doi.org/10.4161/auto.5.8.10274

Yokoseki, A., Shiga, A., Tan, C.-F., Tagawa, A., Kaneko, H., Koyama, A., Eguchi, H., Tsujino, A., Ikeuchi, T., Kakita, A., Okamoto, K., Nishizawa, M., Takahashi, H., Onodera, O., 2008. TDP-43 mutation in familial amyotrophic lateral sclerosis. Ann. Neurol. 63, 538–542. https://doi.org/10.1002/ana.21392

Yoshida, M., Muneyuki, E., Hisabori, T., 2001. ATP synthase — a marvellous rotary engine of the cell. Nat. Rev. Mol. Cell Biol. 2, 669–677. https://doi.org/10.1038/35089509

Yoshimori, T., Yamamoto, A., Moriyama, Y., Futai, M., Tashiro, Y., 1991. Bafilomycin A1, a specific inhibitor of vacuolar-type H(+)-ATPase, inhibits acidification and protein degradation in lysosomes of cultured cells. J. Biol. Chem. 266, 17707–17712. https://doi.org/10.1016/S0021-9258(19)47429-2

Yu, J., Hu, K., Smuga-Otto, K., Tian, S., Stewart, R., Slukvin, I.I., Thomson, J.A., 2009. Human Induced Pluripotent Stem Cells Free of Vector and Transgene Sequences. Science 324, 797–801. https://doi.org/10.1126/science.1172482

Yu, J., Vodyanik, M.A., Smuga-Otto, K., Antosiewicz-Bourget, J., Frane, J.L., Tian, S., Nie, J., Jonsdottir, G.A., Ruotti, V., Stewart, R., Slukvin, I.I., Thomson, J.A., 2007. Induced Pluripotent Stem Cell Lines Derived from Human Somatic Cells. Science 318, 1917–1920. https://doi.org/10.1126/science.1151526

Zahiri, J., 2016. Computational Prediction of Proteins Sumoylation: A Review on the Methods and Databases. J. Nanomedicine Res. 3. https://doi.org/10.15406/jnmr.2016.03.00068

Zahumenska, R., Nosal, V., Smolar, M., Okajcekova, T., Skovierova, H., Strnadel, J., Halasova, E., 2020. Induced Pluripotency: A Powerful Tool for In Vitro Modeling. Int. J. Mol. Sci. 21, 8910. https://doi.org/10.3390/ijms21238910

Zare-Abdollahi, D., Bushehri, A., Alavi, A., Dehghani, A., Mousavi-Mirkala, M., Effati, J., Miratashi, S.A.M., Dehani, M., Jamali, P., Khorram Khorshid, H.R., 2019. MFSD8 gene mutations; evidence for phenotypic heterogeneity. Ophthalmic Genet. 40, 141–145. https://doi.org/10.1080/13816810.2019.1592200

Zeitz, C., Jacobson, S.G., Hamel, C.P., Bujakowska, K., Neuillé, M., Orhan, E., Zanlonghi, X., Lancelot, M.-E., Michiels, C., Schwartz, S.B., Bocquet, B., Antonio, A., Audier, C., Letexier, M., Saraiva, J.-P., Luu, T.D., Sennlaub, F., Nguyen, H., Poch, O., Dollfus, H., Lecompte, O., Kohl, S., Sahel, J.-A., Bhattacharya, S.S., Audo, I., 2013. Whole-Exome Sequencing Identifies LRIT3 Mutations as a Cause of Autosomal-Recessive Complete Congenital Stationary Night Blindness. Am. J. Hum. Genet. 92, 67–75. https://doi.org/10.1016/j.ajhg.2012.10.023

Zeng, W., Wang, M., Xiong, Z., Huang, Z., Jiang, Y., 2023. Aberrant stress granule network is involved in CMT2 neuropathies. Innov. Med. 1, 100021–2. https://doi.org/10.59717/j.xinn-med.2023.100021

Zerial, M., McBride, H., 2001. Rab proteins as membrane organizers. Nat. Rev. Mol. Cell Biol. 2, 107–117. https://doi.org/10.1038/35052055

Zhan, Q., Jeon, J., Li, Ying, Huang, Y., Xiong, J., Wang, Q., Xu, T.-L., Li, Yong, Ji, F.-H., Du, G., Zhu, M.X., 2022. CAMK2/CaMKII activates MLKL in short-term starvation to facilitate autophagic flux. Autophagy 18, 726–744. https://doi.org/10.1080/15548627.2021.1954348

Zhang, J., Feng, Y., Forgac, M., 1994. Proton conduction and bafilomycin binding by the V0 domain of the coated vesicle V-ATPase. J. Biol. Chem. 269, 23518–23523. https://doi.org/10.1016/S0021-9258(17)31546-6

Zhang, L., Pitcher, L.E., Yousefzadeh, M.J., Niedernhofer, L.J., Robbins, P.D., Zhu, Y., 2022. Cellular senescence: a key therapeutic target in aging and diseases. J. Clin. Invest. 132. https://doi.org/10.1172/JCI158450

Zhang, N., An, M.C., Montoro, D., Ellerby, L.M., 2010. Characterization of Human Huntington's Disease Cell Model from Induced Pluripotent Stem Cells. PLoS Curr. 2, RRN1193. https://doi.org/10.1371/currents.RRN1193

Zhang, S., Cui, W., 2014. Sox2, a key factor in the regulation of pluripotency and neural differentiation. World J. Stem Cells 6, 305–311. https://doi.org/10.4252/wjsc.v6.i3.305

Zhang, X., Huang, C.T., Chen, J., Pankratz, M.T., Xi, J., Li, J., Yang, Y., LaVaute, T.M., Li, X.-J., Ayala, M., Bondarenko, G.I., Du, Z.-W., Jin, Y., Golos, T.G., Zhang, S.-C., 2010. Pax6 Is a Human Neuroectoderm Cell Fate Determinant. Cell Stem Cell 7, 90–100. https://doi.org/10.1016/j.stem.2010.04.017

Zhang, Y., Sloan, S.A., Clarke, L.E., Caneda, C., Plaza, C.A., Blumenthal, P.D., Vogel, H., Steinberg, G.K., Edwards, M.S.B., Li, G., Duncan, J.A., Cheshier, S.H., Shuer, L.M., Chang, E.F., Grant, G.A., Gephart, M.G.H., Barres, B.A., 2016. Purification and Characterization of Progenitor and Mature Human Astrocytes Reveals Transcriptional and Functional Differences with Mouse. Neuron 89, 37–53. https://doi.org/10.1016/j.neuron.2015.11.013

Zhao, H., Zhao, Y.G., Wang, X., Xu, L., Miao, L., Feng, D., Chen, Q., Kovács, A.L., Fan, D., Zhang, H., 2013. Mice deficient in Epg5 exhibit selective neuronal vulnerability to degeneration. J. Cell Biol. 200, 731–741. https://doi.org/10.1083/jcb.201211014

Zhao, Y.G., Zhang, H., 2018. Autophagosome maturation: An epic journey from the ER to lysosomes. J. Cell Biol. 218, 757–770. https://doi.org/10.1083/jcb.201810099

Zhu Y, Runwal G, Obrocki P, Rubinsztein DC. 2019. Autophagy in childhood neurological disorders. Dev Med Child Neurol. 2019 Jun;61(6):639-645. doi: 10.1111/dmcn.14092. Dev Med Child Neurol. 61(7):852. https://doi.org/10.1111/dmcn.14276